CAWTHRON
The power of science®

REPORT NO. 3076

PELAGIC BIOPHYSICAL ASSESSMENT: PORT PEGASUS / PIKIHATITI

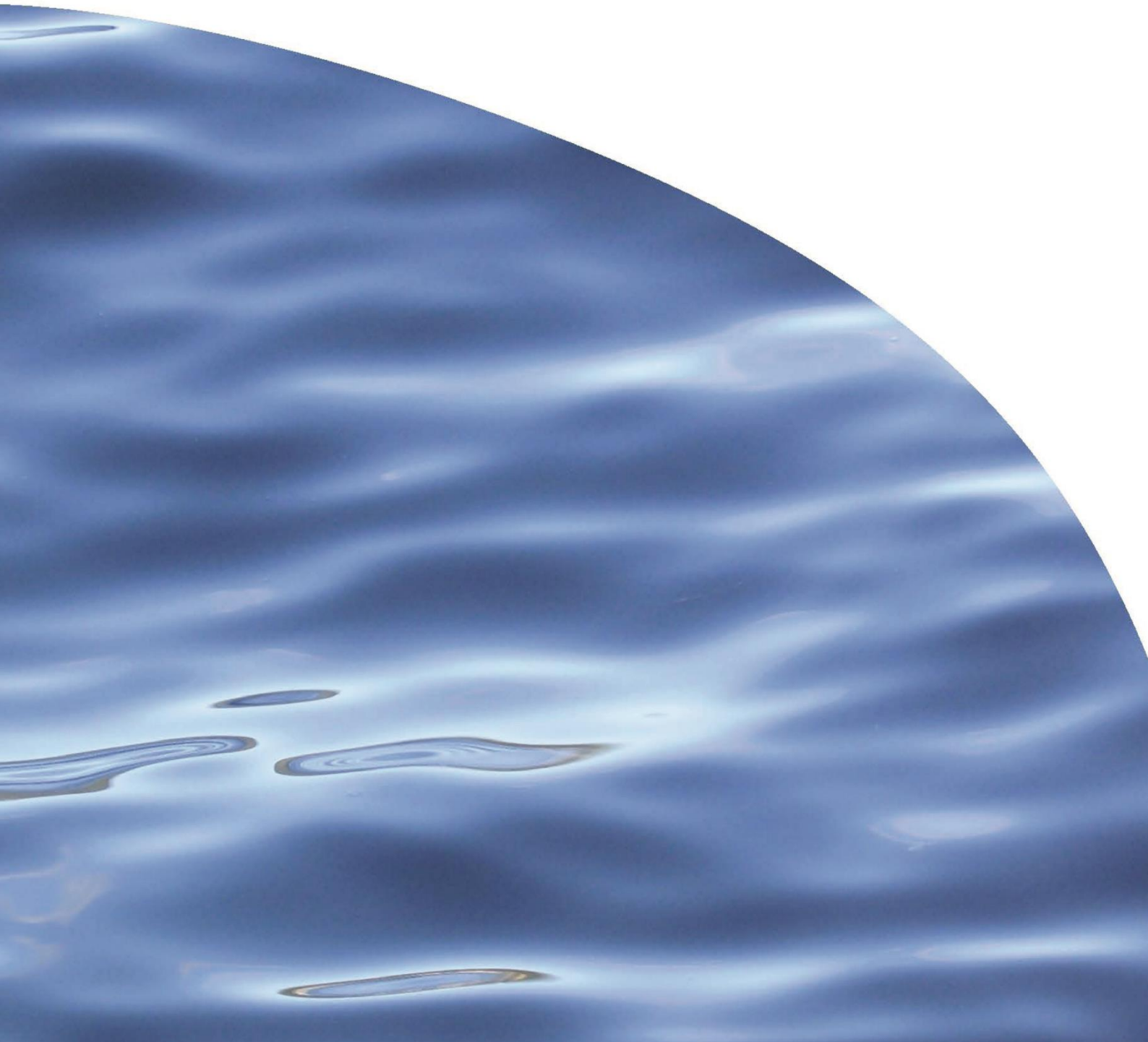

PELAGIC BIOPHYSICAL ASSESSMENT: PORT PEGASUS / PIKIHATITI

BEN KNIGHT, ROSS VENNELL, LINCOLN MACKENZIE

Prepared for Ministry of Primary Industries

CAWTHRON INSTITUTE
98 Halifax Street East, Nelson 7010 | Private Bag 2, Nelson 7042 | New Zealand
Ph. +64 3 548 2319 | Fax. +64 3 546 9464
www.cawthron.org.nz

REVIEWED BY:
Deanna Elvines

APPROVED FOR RELEASE BY:
Grant Hopkins

ISSUE DATE:09 October 2017

RECOMMENDED CITATION: Knight B, Vennell R, MacKenzie L 2017. Pelagic biophysical assessment: Port Pegasus / Pikihatiti. Prepared for Ministry for Primary Industries. Cawthron Report No. 3076. 81 p. plus appendices.

EXECUTIVE SUMMARY

The Southland Regional Development Strategy (SoRDS) has identified opportunities for economic and social development within the Southland region. The strategy identifies aquaculture, in particular finfish aquaculture, as a leading opportunity for regional development. This report constitutes a Stage 2 assessment of the pelagic environment for the North Arm of Port Pegasus, a region identified as a potential farming area based on initial scoping assessments. A combination of modelling exercises as well as instrument measurements, and sampling carried out within the period April to May 2017 have helped to provide further information on the area.

Analysis of measured and modelled currents within North Arm shows that it offers low current flows which are not ideal for finfish aquaculture due to the reduced capacity for dissolved and organic waste dispersion and subsequently, higher benthic accumulation. Frequent episodic wave energy in the southern entrance to North Arm (Big Ship Passage) could present operational constraints to the use of this area and also act to reduce benthic accumulation of organic waste under net pens placed here. However, there are key differences between midwater tidal currents (used to define 'low' and 'high' flow sites) and benthic wave-driven currents. Tidally-driven currents occur daily over long time periods of several hours, whereas peak wave-driven currents occur for short periods of time (seconds) and rapidly change direction. Consequently the magnitude of any benthic effect from wave-driven currents could not be determined for this assessment.

In terms of pelagic effects, the hydraulic residence time of dissolved wastes is an important consideration. Models simulating the release of dissolved nitrogen from potential aquaculture sites in North Arm suggest residence times to be about 18 days within the Arm. This result implies there is the potential for dissolved finfish wastes to be retained longer in comparison to a similar farmed area in Big Glory Bay (BGB), which also has low flows and an estimated residence time of 10–13 days under light winds. The BGB farm has a thirty-year salmon production history with recent production estimated at about 3,500 ton per annum (tpa) of salmon. Given this long farming history without record of significant pelagic effects in BGB, and considering the longer residence time of North Arm, we have suggested an initial production limit of 2,200 tpa for North Arm. The feasibility of an initial 2,200 tpa production level would be determined following Stage 3 aquaculture assessments. Subsequent increases would only follow stable and acceptable water quality results over a period of time.

The modelled increase in total nitrogen (TN) from an initial 'low' production level (2,200 tpa) show that mean summer increases in TN of about 10% over North Arm are possible. The effects from modelled higher production scenarios (> 2,200 tpa) show that larger increases (about 31% at 6,000 tpa) could occur. A phytoplankton bloom that occurred in 1989 in BGB led to large mortalities of salmon. Bloom events could also occur naturally in North Arm, and modelling shows waste nitrogen from salmon farming has the potential to exacerbate bloom intensity from 20% to 70% depending on the production scenario considered (i.e. 2,200 to

6,000 tpa, respectively). However it is difficult to assess the ecological relevance of these rare large bloom events, because in the case of the BGB bloom there were no reported wider-ranging ecological effects.

Although we recognise the potential for significant pelagic water quality effects at high production scenarios, we note that nutrient-induced effects in the pelagic environment are extremely complex. Without surety of effects it is difficult to translate a 'large' change in nitrogen or chlorophyll-*a* into a 'good', 'bad' or 'significant' ecological change. Consequently, if high production scenarios (i.e. up to 6,000 tpa) are considered for this area, staged development from initially low production levels (e.g. 2,200 tpa) should be implemented cautiously and in combination with appropriate monitoring, to manage potential risks to the environment.

TABLE OF CONTENTS

LIST OF FIGURES

LIST OF TABLES

LIST OF APPENDICES

GLOSSARY

ADCP	Acoustic Doppler Current Profiler
CTD	Conductivity Temperature Depth instrument
PAR	Photosynthetically Active Radiation
Significant wave height	The mean height of the highest one third of waves
Hindcast	Historical modelling of a period of time, typically more accurate than a forecast which relies on information which has not been compared to observations
Residence time	The length of time water remains within the boundaries of an aquatic system
Sea waves	Waves with a period less than 9 seconds
Swell	Waves with a period greater than 9 seconds
Tidal prism	The volume of water displaced over a tide. If intertidal areas do not form a large component in the area of interest, it is typically calculated as the tidal range multiplied by the surface area

1. INTRODUCTION

1.1. Background

The Southland Regional Development Strategy (SoRDS) has identified opportunities for economic and social development within the Southland region. The strategy identifies aquaculture, in particular finfish aquaculture, as a leading opportunity for regional development. As such, the Ministry for Primary Industries (MPI) is conducting a three-stage process to investigate this opportunity.

1.1.1. Three stage site assessment process

Preliminary scoping investigations, conducted by Cawthron Institute (Cawthron) as part of Stage 1, suggested that the North Arm of Port Pegasus/Pikihatiti (see Figure 1) may be suitable for finfish farming from a bio-physical and ecological perspective (Clark et al. 2015; Elvines et al. 2015; Elvines et al. 2016). In addition to the North Arm, 12 sites[1] along the eastern coastline of Stewart Island/Rakiura were investigated. However, all 12 of these sites presented a number of limitations with regards to one or more of the following factors: water depth, wave exposure or the presence of sensitive benthic habitats.

In March 2017, MPI and the Ministry of Business, Innovation and Employment (MBIE) contracted Cawthron to undertake further investigations as part of a Stage 2 assessment within the North Arm region of Port Pegasus/Pikihatiti. The purpose was to assess the potential environmental sustainability for finfish aquaculture in this area. Stage 2 thus includes more comprehensive assessments of both benthic habitat and pelagic environmental components. However, only the results relating to the pelagic environment are presented here; results of the benthic habitat assessment are presented separately, in Fletcher et al. (2017).

Information provided from the Stage 2 assessments[2] will be considered[3] to decide whether or not the third and final stage of assessment will proceed. Stage 3 assessments would involve additional site-specific survey and research work necessary for an assessment of environmental effects (AEE) under the Resource Management Act 1991.

[1] Port Adventure, Paterson Inlet, Big Glory Bay (2 sites), South Arm of Port Pegasus/Pikihatiti, Tikitahi, Owen Island, Weka Island, Chew Tobacco Bay, Horseshoe Bay, Lee Bay and Lords River.
[2] Including assessments on pelagic and benthic effects, economic considerations, and natural character, landscape and visual amenity.
[3] By MPI, MBIE, Department of Conservation, Ministry for the Environment, SoRDS and Southland Regional Council.

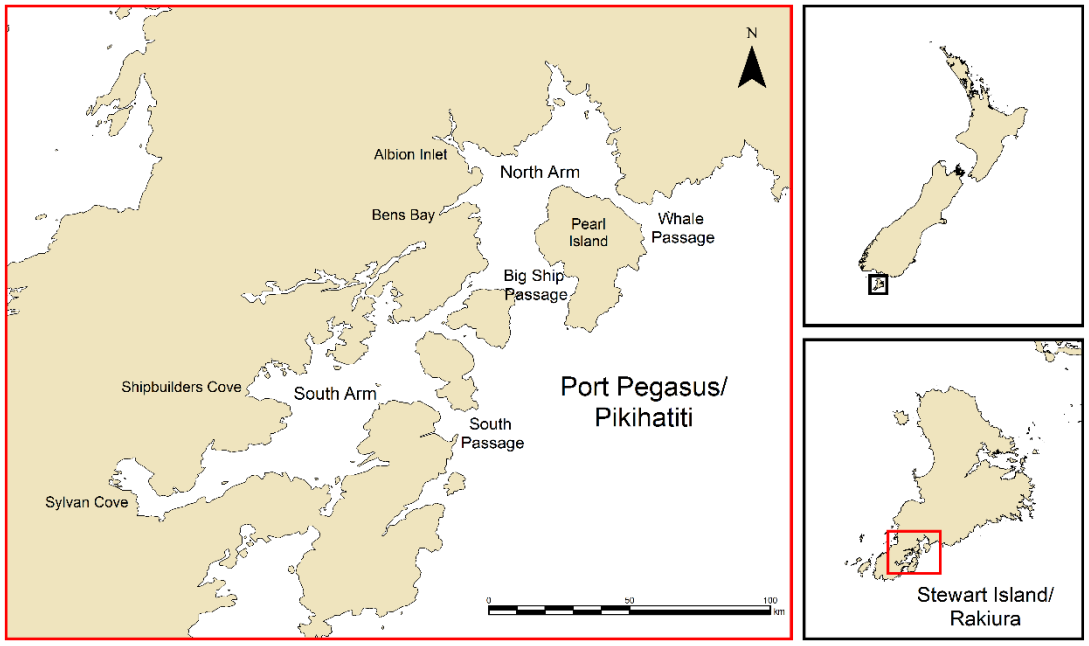

Figure 1. Map of Port Pegasus/Pikihatiti showing the North Arm and South Arm regions, as well as oceanic connections and key features of the area. The location at the southern end of Stewart Island/Rakiura is indicated.

1.2. Project scope

North Arm is the focus of proposed aquaculture developments considered in this report. This pelagic environmental assessment focussed on physical and biological characterisation of the area. The scope included the following:

1. A field component, including two separate trips to the study area over the period 28 March–6 April and 9–11 May 2017. Field data collection included:
    - measurements of hydrodynamic features (water currents and waves) at key locations relevant to hydrodynamic and wave modelling in the region
    - physical measurements of key water column properties (temperature and salinity)
    - measurements of the biological and chemical properties potentially relevant to finfish aquaculture and water quality in the region (phytoplankton communities and biomass, chlorophyll-*a*, dissolved oxygen, turbidity, and key nutrients).
2. Development and application of models to (a) characterise the physical pelagic environment, and (b) help predict the effects of several finfish aquaculture scenarios.
3. An assessment of potential effects to the pelagic environment from finfish aquaculture in the North Arm.

1.2.1. Report structure

The report firstly summarises the aquaculture scenarios considered for Port Pegasus. The physical data collected in the field are then presented along with a basic description of the results. In conjunction with modelling, physical data are then used to describe the wider area in terms of hydrodynamics including connectivity, water residence times, and wave characteristics. The presentation and description of the biological and chemical field results is then provided along with context from existing literature.

The above information is then is drawn together with further existing literature to provide an assessment, or estimate, of:

- an initial production level for North Arm
- potential pelagic changes resulting from initial, and higher production scenarios.

Model specifications and limitations of the assessment are also described.

1.3. Site description

Port Pegasus/Pikihatiti is located near the southern tip of Stewart Island/Rakiura (Figure 1). The area comprises two relatively sheltered water bodies: North Arm and the larger South Arm of Port Pegasus (hereafter referred to as 'North Arm' and 'South Arm'). Both water bodies are joined by the narrow Pegasus Passage, but each has at least one independent connection to the open ocean. The North Arm is connected to the ocean either side of Pearl Island; at the south through Big Ship Passage and at the east by the narrower Whale Passage. The main oceanic connection to South Arm is through South Passage.

North Arm has steep drop-offs along much of the coastline and has relatively deep water (mean depth of 29 m, maximum depth c. 50 m; Figure 2) when compared to other embayments around Stewart Island/Rakiura. The greatest water depth is found to the northwest of Pearl Island. The remainder of the mid-channel waters are between 30–40 m deep. North Arm has a surface area of about 1,120 ha and encompasses a volume of about 320 million m^3. The area is relatively exposed to wave action through the southern entrance, Big Ship Passage; however, Pearl Island in the east provides shelter from the easterly and south-easterly swells.

South Arm has a slightly larger surface area than North Arm at 1,410 ha although it is shallower, with a mean depth of about 18 m, and encompasses a volume of about 285 million m^3 (Figure 1). Its surface waters are also more sheltered from southerly and westerly weather compared to North Arm, due to the topography surrounding

South Arm. Due to the landscape and low currents in South Arm it was not considered suitable for future aquaculture development.

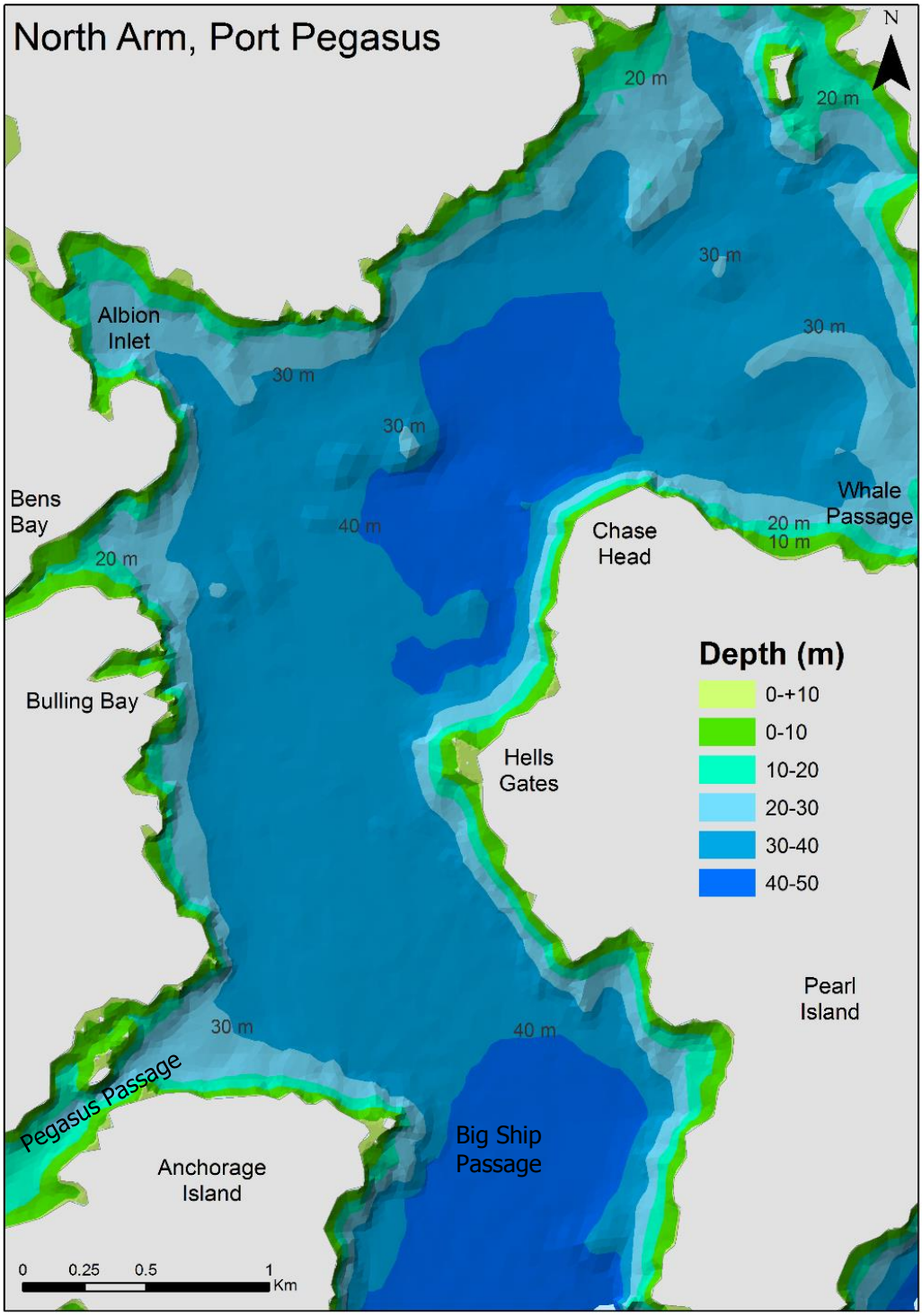

Figure 2. Bathymetry (in metres, relative to mean sea level) of North Arm, Port Pegasus/Pikihatiti. Based on Stage 1 (Elvines et al. 2016) and Stage 2 sonar data (Fletcher et al. 2017) with additional LINZ data used where available. GPS positioning was accurate to ± 5 m.

2. AQUACULTURE SCENARIOS

Due to benthic and flow limitations, the area considered for finfish aquaculture is mainly confined to the southern entrance of the North Arm, Big Ship Passage. A detailed discussion around the siting considerations for aquaculture is found in Fletcher et al. (2017). In summary, there are five 'farm areas' considered (Figure 3); four of these are grow-out sites (f1–f4), and one is a smolt-only site (s1).

For each farm area as above, several production scenarios were modelled to determine varying levels of benthic waste deposition at varying production rates. The estimated 'acceptable' benthic enrichment levels for these scenarios are discussed in detail in Fletcher et al. (2017).

Four fish-production scenarios (combining feed loads and cage sizes) were considered for the pelagic assessment (Table 1; scenarios 1a–4a), matching the scenarios presented in Fletcher et al. (2017). The total salmon production across all scenarios ranges from 2,801 tons per annum (tpa) to 6,000 tpa and assumes a salmon feed conversion ratio[4] (FCR) of 1.7 based on the performance of Big Glory Bay salmon farms (Jaco Swart, Sanford Farm manager pers. comm.). This FCR is also used to estimate the associated feed loads, and on this basis the total feed inputs for the four scenarios range from 5,001 tpa to 10,710 tpa (Table 1). Only a small amount of feed (about 1%; Table 1) is added to the smolt farm area.

[4] a ratio of dry weight feed to wet weight fish production

Table 1. Farm production scenarios used in models. Farming locations (f1–f4 and s1) are shown in Figure 3. All scenarios show feed input levels that are estimated to result in conditions of Enrichment State ≤ 5 at the pen edge assuming farms operate like low-flow sites. This table is adapted from Fletcher et al. (2017) and does not include all benthic scenarios that were assessed. A feed conversion efficiency of 1.7 was used to estimate production for all scenarios. (tpa: tonnes per annum).

Scenario	Input parameters	Farming area				Grow-out totals	Smolt totals (s1)
		f1	f2	f3	f4		
1a	Feed per pen (tpa)	**131**	**131**	**150**	**225**		64
	Number pens	16	16	16	16	64	8
	Total feed (tpa)	2100	2100	2400	3600	10200	510
	Total production (tpa)	1235	1235	1412	2118	6000	
2a	Feed per pen (tpa)	**131**	**131**	**150**	**225**		63
	Number pens	8	10	14	14	46	6
	Total feed (tpa)	1050	1312.5	2100	3150	7613	381
	Total production (tpa)	618	772	1235	1853	4478	
3a	Feed per pen (tpa)	**131**	**131**	**150**	**225**		79
	Number pens	6	8	12	12	38	4
	Total feed (tpa)	787.5	1050	1800	2700	6338	317
	Total production (tpa)	463	618	1059	1588	3728	
4a	Feed per pen (tpa)	**131**	**131**	**150**	**225**		60
	Number pens	4	6	8	10	28	4
	Total feed (tpa)	525	787.5	1200	2250	4763	238
	Total production (tpa)	309	463	706	1324	2801	

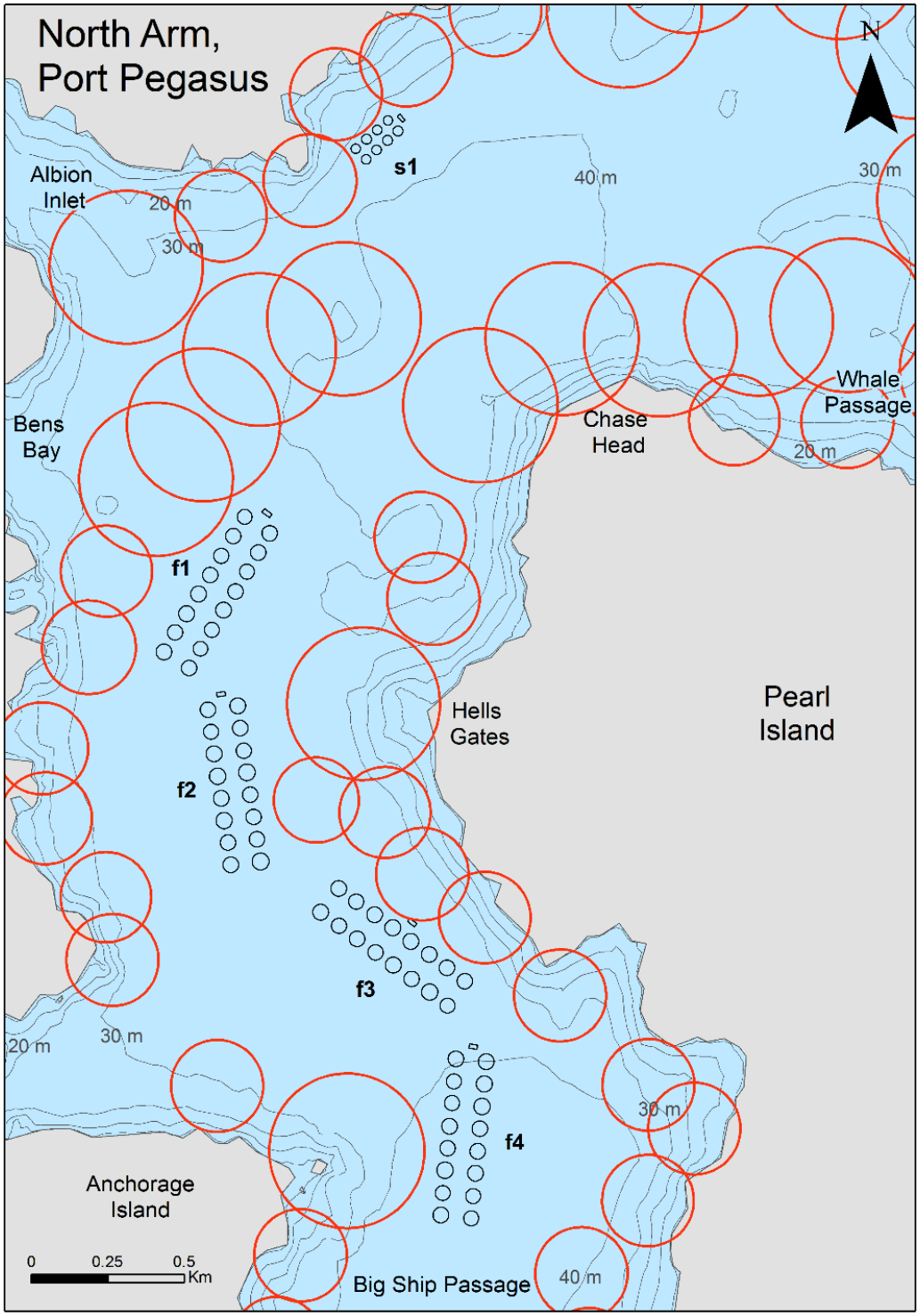

Figure 3. Proposed grow-out farm areas (f1–f4) and smolt farm area (s1) within North Arm, Port Pegasus/Pikihatiti. Net pen areas are denoted with small black circles. Pen sizes are 160 m radius for grow-out, and 100 m radius for smolt. Red circles indicate areas that were excluded due to benthic constraints as discussed in Fletcher et al. (2017).

3. PHYSICAL CHARACTERISTICS

3.1. Field measurements

3.1.1. Hydrographic data—CTD

Data collection

Temperature and salinity[5] profiles within the North Arm of Port Pegasus were measured using a Conductivity Temperature and Depth (CTD) instrument. These data were collected to indicate water column stratification and variation across North Arm. As such, the locations of CTD profiling (Figure 4) create a vertical cross-section of water properties along the main axis of North Arm.

Profiles were taken during two sampling periods in Port Pegasus (30 March–3 April 2017 and on 30 May 2017), with the majority of profile measurements collected during the first sampling period.

[5] In conjunction with other water profile characteristics, presented in Section 4.

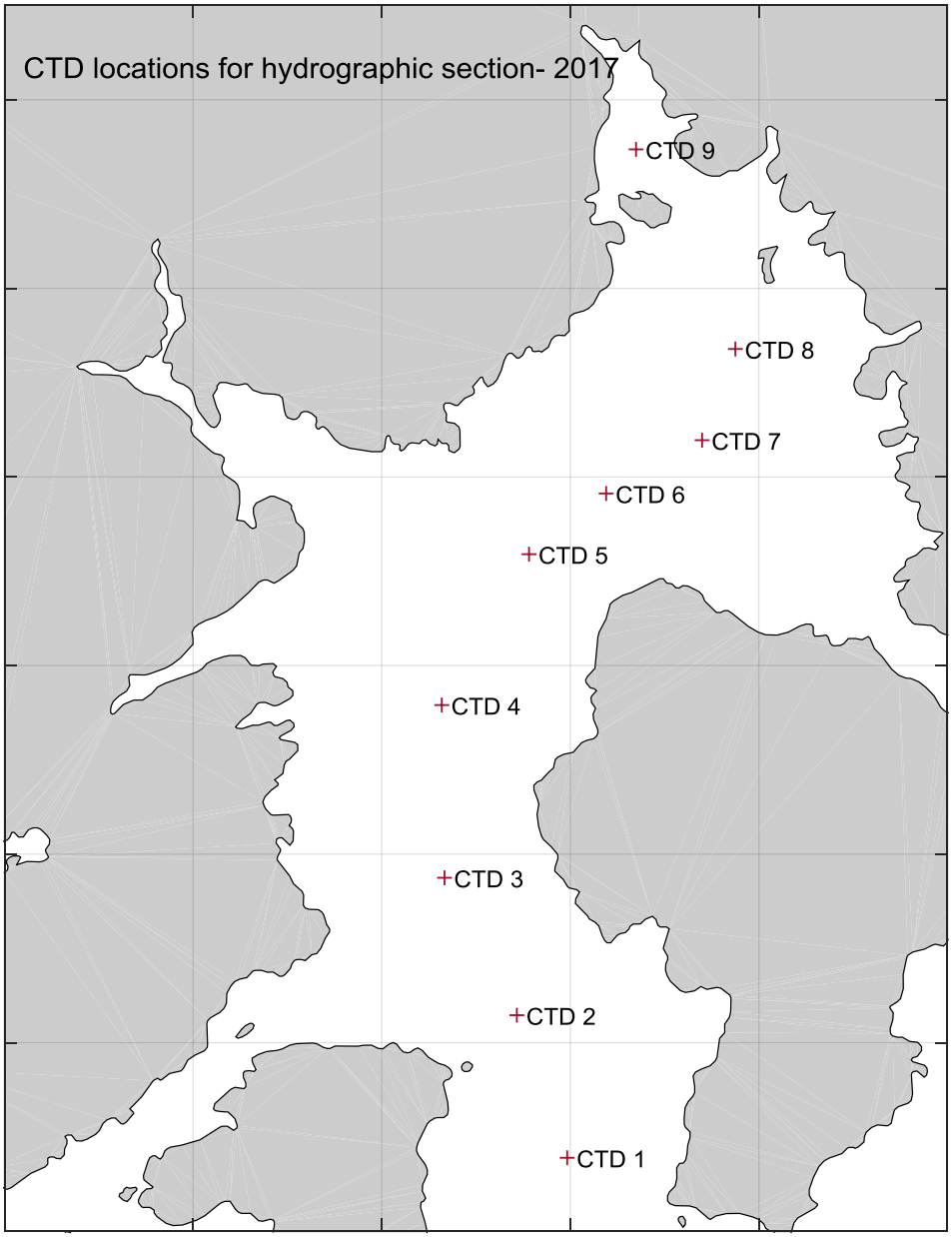

Figure 4. Map of CTD profile locations used to create vertical cross-section in the North Arm of Port Pegasus.

Results

The cross-section for 30 March 2017 (Figure 5) shows that North Arm is vertically well mixed. Temperatures vary by less than 0.25°C over the cross-section. Below 5 m, salinities vary by less than 0.1 parts per thousand (PPT). A thin, slightly fresher layer of water in the upper 2 m of the profile at CTD 8 is marginally apparent, with salinities 0.1 PPT lower than deeper waters. This freshening may be due to river flows. However, overall the profiles showed the measured water properties to be almost uniform during this sampling period. Water properties for the profiles from

10 May 2017 (Figure 6) show similar uniformity. Thus during autumn and early winter, winds and currents appear to keep North Arm vertically well mixed.

These data represent only a snapshot (i.e. during the sampling periods only) of conditions that this site experiences. For example, in mid-summer, thermal stratification of the water column is more likely, as surface water can be warmer than the underlying water.

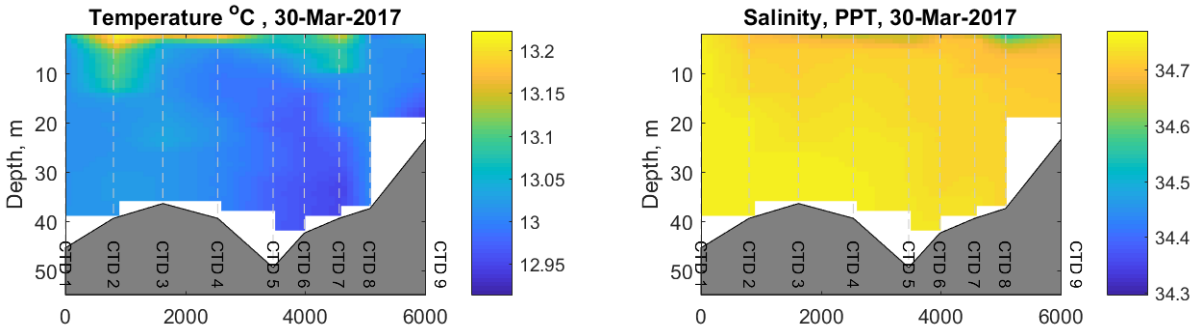

Figure 5. Vertical cross-section of water properties from the south end (CTD 1) to the north end (CTD 9) of North Arm on 30 March 2017. Sites are shown in Figure 4.

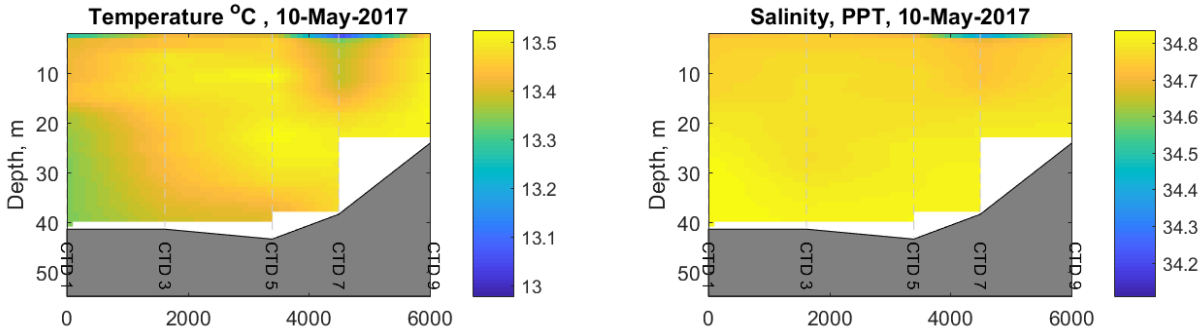

Figure 6. Vertical cross-section of water properties from the south end of North Arm (CTD 1) to the north end of North Arm (CTD 9) on 10 May 2017. Sites are shown in Figure 4. Note, only a sub-selection of sites in Figure 4 were resampled on this date.

3.1.2. Current measurements–moored ADCPs

Data collection

Four bottom-mounted Teledyne RD Instruments (RDI) ADCPs were deployed to measure current speed and direction throughout the water column profile at the locations shown in Figure 7. One deployment was in 2016 for 42 days, the other three were in 2017 for 41 days (see Table 2 for dates).

The instruments were mounted in frames with the ADCP head approximately 0.4 m above the seabed (Table 2). A 40 m ground line from the ADCP frame connected it to a weight with a vertical line to a surface buoy above. An RBR wave sensor was installed on a separate vertical line with a subsurface buoy, data from which are presented in Section 5.3. At the end of the deployments the data were downloaded and processed using the Matlab™ software package.

Figure 7. Locations of bottom-mounted ADCPs deployed in 2016 and 2017.

Table 2. North Arm ADCP instrument configurations for deployment in 2016 and 2017.

Location	Deployment date range	ADCP type	Water depth	First depth cell above bottom	Depth cell size
Mid Bay-2017	29-Mar-2017 to 10-May-2017	RDI-Workhorse	47 m	2.5 m	1.0 m
Whale Passage-2017	29-Mar-2017 to 10-May-2017	RDI V-series	16 m	1.5 m	0.5 m
Pegasus Passage-2017	29-Mar-2017 to 10-May-2017	RDI V-series	19 m	1.5 m	0.5 m
West Side-2016	07-Aug-2016 to 18-Sep-2016	RDI-Workhorse	36 m	3.5 m	2.0 m

Current speed results

Time series results of the measured ADCP current are given in Appendix 1. The average and maximum near-bottom and mid-water current speeds for each location are given in Table 3.

Maximum current speeds within North Arm, at the Mid Bay and West Side locations were 0.12 m/s to 0.19 m/s (Table 3). However, these speeds occured very rarely, as reflected in the mid-water current 'roses' (Figure 8) which show speeds less than 0.1 m/s almost 100% of the time at these sites (yellow bars) (also see time series of currents plotted in Figure A1.1 and Figure A1.4 in Appendix 1).

As expected, the two entrances to North Arm (Whale and Pegasus passages) typically have much stronger currents than the Mid Bay and West Side locations, exceeding 0.3 m/s 7-10% of the time, with maximum flows greater than 0.45 m/s (Figure 8 and Appendix 1). The mean mid-water current speeds were 0.14 and 0.15 m/s for the Whale and Pegasus passage sites, respectively.

Table 3. Near-bottom and mid-water mean and maximum current speeds (m/s) for each ADCP deployment. Water depths are also shown.

Location		Near-bottom		Mid-water		
	Total water Depth (m)	Mean (m/s)	Max. (m/s)	Mid-water Depth (m)	Mean (m/s)	Max (m/s)
Mid Bay-2017	47	0.05	0.19	22	0.04	0.20
Whale Passage-2017	16	0.15	0.45	8	0.15	0.71
Pegasus Passage-2017	19	0.12	0.49	9	0.14	0.63
West Side-2016	36	0.04	0.12	16	0.04	0.14

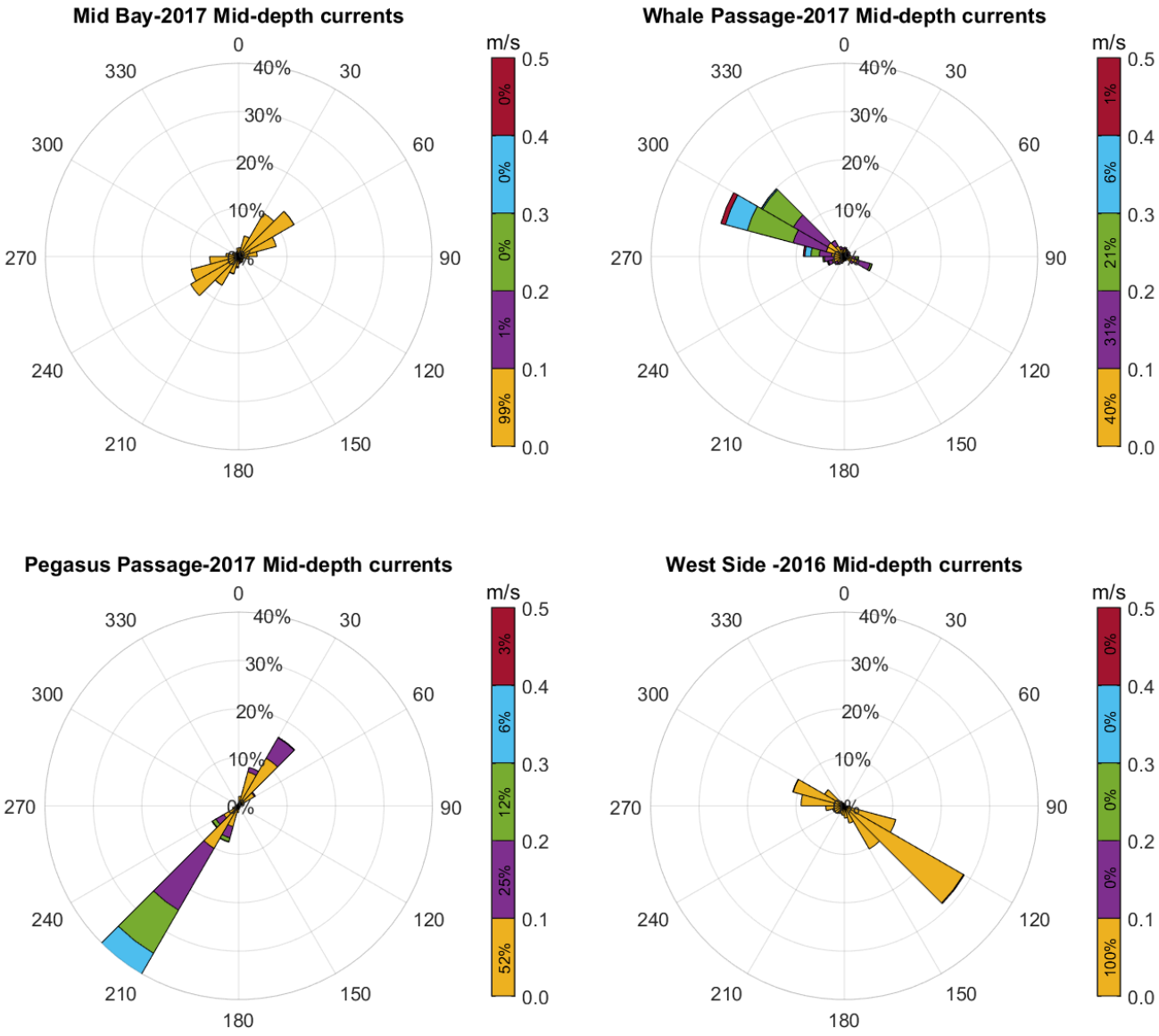

Figure 8. Current 'roses' showing frequency of ADCP measured currents in given directions at mid-water depth. Numbers within coloured legend show percentage of measurements in each speed band.

Net drift

The water current time series (Appendix 1, Figures A1.1 to A1.4) shows that the measured currents are mainly tidal in character, with oscillating tidal flows of up to 0.1 to 0.5 m/s. However, the ebb and flood tidal currents are not always the same, and differences between the ebb and flood currents means there may be a gradual 'net' drift over time. This net drift, or residual motion is poorly represented in the rose diagrams of the previous section. As such, net drift is shown for each site in Figure 9 using progressive vector diagrams. These diagrams represent the cumulative displacement of a water particle (starting at the ADCP location) due to the measured current at that site.

To give a sense of scale, the circles in each diagram show how far particles with a steady velocity of 0.05 m/s would move in a straight line away from the starting point, during the time the ADCP was deployed. The lines are coloured depending on which of the three depth ranges the particles originated from. Depth ranges were split in to upper, mid and lower thirds of the water column.

For the Mid Bay and West Side sites, the net motion is very small, equivalent to less than 0.02 m/s or less (for the duration of the deployment), much smaller than the 0.1 to 0.2 m/s peak tidal flows. At both sites, the upper third of the water column shows almost no net drift, suggesting that currents driven by winds blowing over North Arm do not cause significant net transport. Interestingly, the currents in the lower third of the water column at both sites show some northward drift. This weak northward drift into North Arm may be the result of a weak estuarine circulation driven by river water flowing out in a thin surface layer which can't be measured by the ADCPs due to acoustic interference effects by the sea surface.

The Pegasus Passage location showed a net drift towards the southwest, implying salmon wastes released from North Arm could migrate into South Arm. However, this may not be truly representative of a mean, or residual, flow through the Passage into South Arm. This is because the water current patterns within the passage are complex, influenced by the depth contours and constrictions. In particular, a narrow gap exists between a small island north east of the ADCP, which likely causes accelerated flows, creating a narrow 'jet' extending well beyond the gap itself. This jet impinged on the ADCP's readings and resulted in strong southwest flows showing during the first half of the tidal cycle. During the second half of the tidal cycle, the ADCP's location was upstream of the constriction, where northeast flows were spread more widely over the width of the channel, resulting in weaker velocities during the second half of the tidal cycle at this location. Thus, the strong mean southwest flow indicated from the Pegasus Passage ADCP data may instead be a reflection of difference in flow distribution across the channel between the two halves of the tidal cycle.

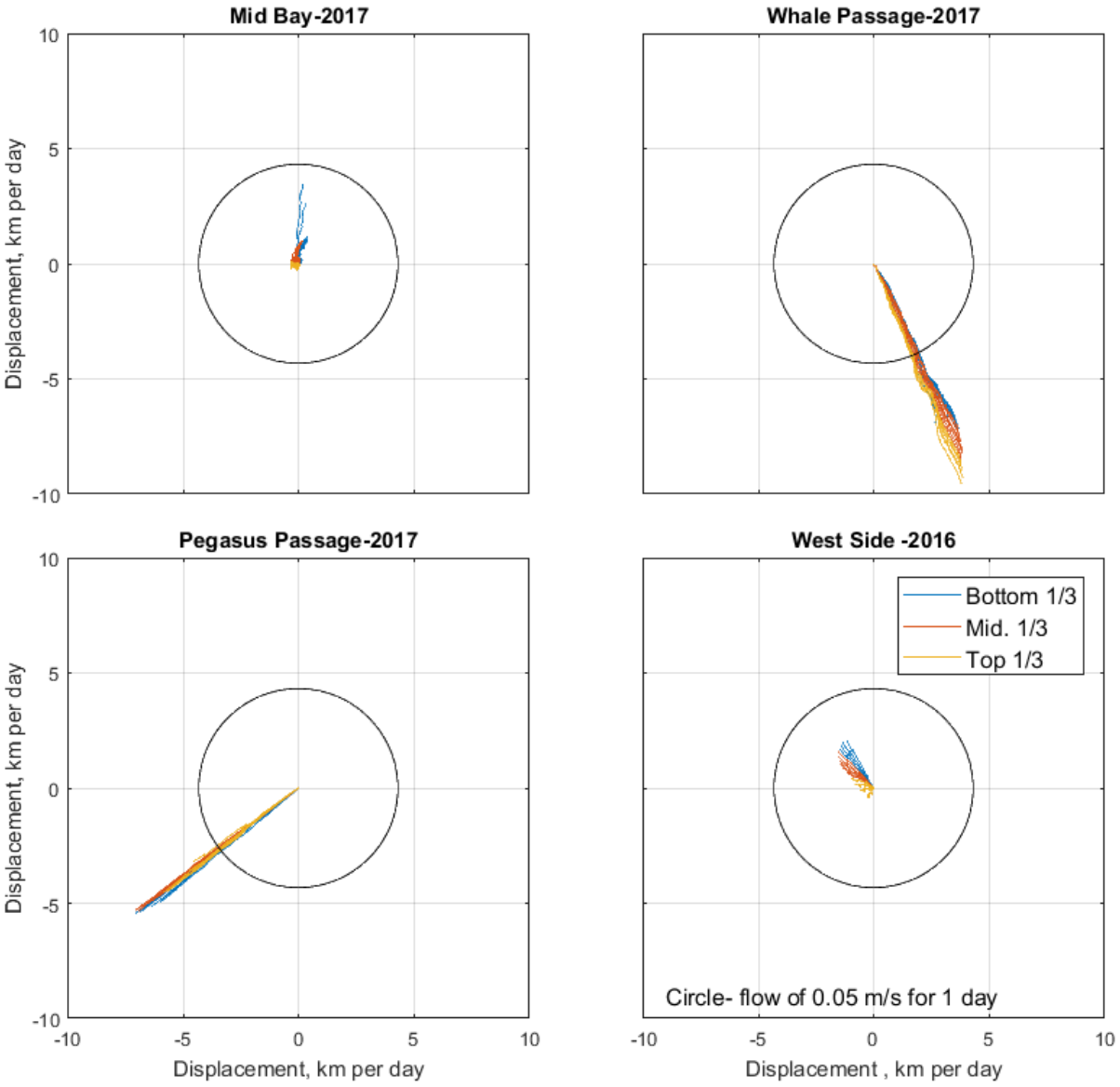

Figure 9. Progressive vector diagrams showing net drift, or residual motion, in km per day, at four ADCP locations for three depth ranges (bottom, mid and top thirds of the water column).

3.1.3. Wave measurements

Data collection

Wave height measurements were made over five weeks, between 29 March 2017 and 10 May 2017. Data were collected using RBR[6] wave sensors deployed directly adjacent to each of the three 2017 ADCP locations, as well as in Big Ship Passage (Figure 10). For context, data from the two 2016 deployments between 7 August 2016 to 18 September 2016 (West and North; Figure 10) are provided in this assessment.

Measurements were made in c. 4 minute bursts[7], every 10 minutes for the duration of the deployment. The RBRs were moored on floats at the average depths below the surface (Table 4). Though strongly buoyed, the RBRs can move vertically due to swell action, affecting the measured wave heights; an RBR deployed lower down the buoy line would be less effective at capturing the shorter period waves. Thus the 10–15 m deployment depth below a subsurface float was a compromise between being able to resolve shorter period waves and the effects of wave motion on the buoyed RBR. Recorded wave heights were adjusted for their attenuation at these depths using the RBR manufacturer's supplied Ruskin software.

Results

A standard wave statistic is 'significant wave height'. Significant wave height is calculated by averaging the highest third of the waves recorded during a c. 4 minute burst of measurements. The measured significant wave heights during the 5-week periods in 2017 were small; less than 0.7 m at all sites (Table 4). At some sites (Mid Bay-2017 and Big Ship Passage-2017), the maximum wave height was about twice the significant wave height (Table 4).

The largest significant wave heights in 2017 were measured in Big Ship Passage. These occurred for short periods of time (e.g. up to a day, Figure 11). Within North Arm in 2017, the largest measured significant wave heights were 2.2 m, in Big Ship Passage with the next largest site, Whale Passage, recording about 5 times lower waves. In 2016, measured wave heights at the North-2016 site were also generally low, under 0.3 m (Elvines et al. 2016). However, the largest measured waves recorded were at the West-2016 site and had significant heights up to 1.9 m (Figure 11). The West-2016 results were similar to the Big Ship Passage-2017 results, however given the more sheltered location, the West-2016 was likely associated with a larger winter wave event than was observed in the autumn 2017 deployment period.

As would be expected, the 2017 wave measurements show the highest waves were seen in the more exposed southern part of North Arm (i.e. Big Ship Passage-2017). There were still low wave heights (< 0.1 m) in the more sheltered Whale and Pegasus

[6] RBRs can measure wave heights, but not wave directions.
[7] 1024 measurements were taken at 4 Hz sampling frequency.

Passage (2017) sites, which were most likely swell waves refracted around the Arm's topography.

The wave measurements only covered about 5 weeks in each of 2016 and 2017 at specific sites, therefore were unlikely to capture the complete range of heights at these locations. The long-term wave modelling given later in this chapter will provide more comprehensive information on wave heights within North Arm.

Figure 10. Locations of 41- to 42-day RBR wave sensor deployments in North Arm 2016 and 2017.

Table 4. Maximum measured significant wave heights in Port Pegasus at locations given in Figure 10. H_S is the significant wave height (the average height of the highest 1/3 of waves in each c. 4-min burst).

Location	Instrument mean depth below sea surface	Maximum measured 'significant wave height' H_S	Maximum wave height
Mid Bay-2017	4.4 m	0.5 m	1.1 m
Whale Passage-2017	9.7 m	0.4 m	0.6 m
Pegasus Passage-2017	9.0 m	0.7 m	0.8 m
Big Ship Passage-2017	9.6 m	2.2 m	4.3 m
West-2016	7.1 m	1.9 m	2.7 m
North-2016	6.8 m	0.3 m	0.5 m

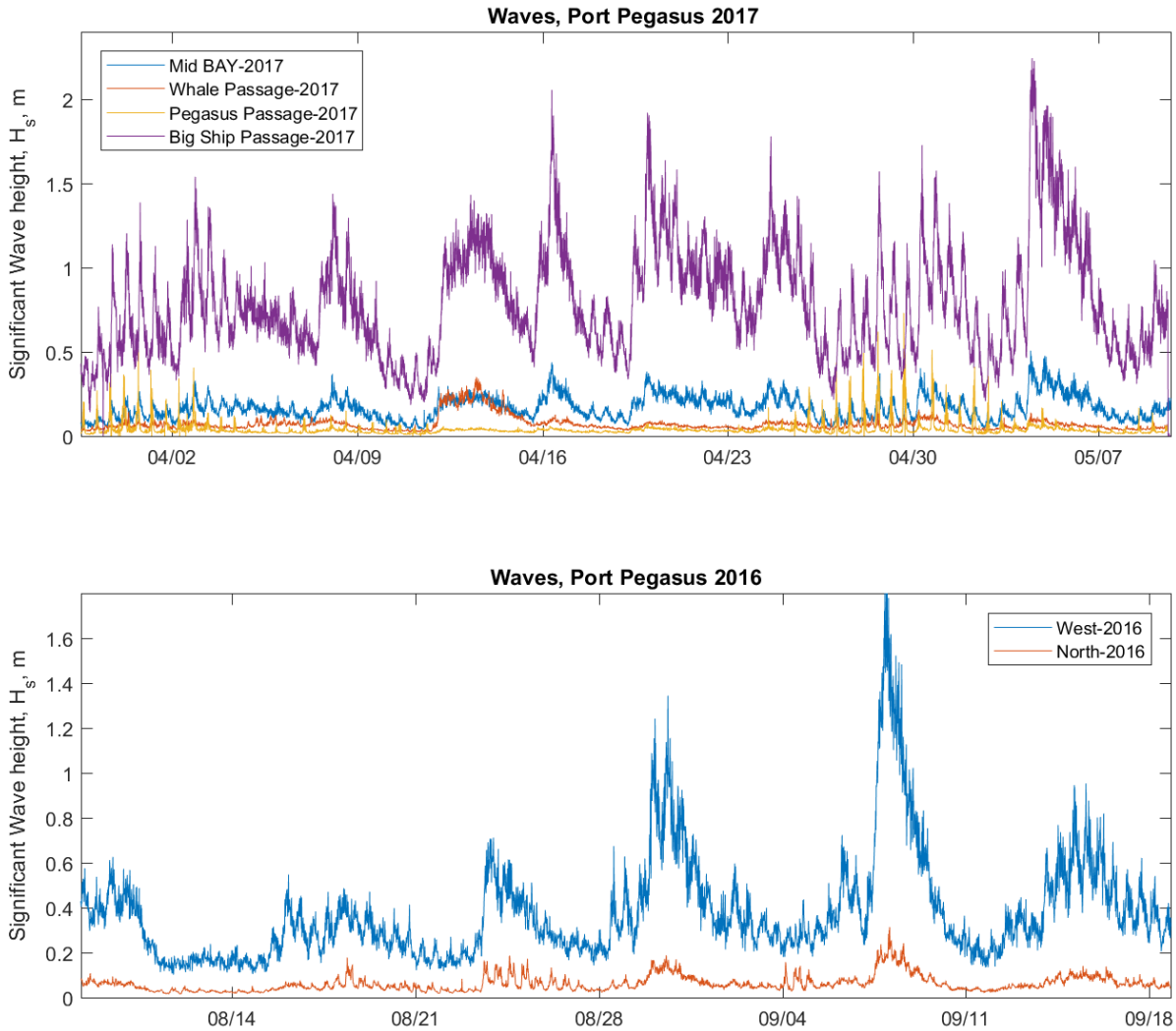

Figure 11. Measured significant wave heights in 2017 (top) and 2016 (bottom). H_S is the significant wave height calculated from each c. 4-min. burst of measurements. Locations are given in Figure 10. Note different scales used for the two years.

3.2. Physical modelling

3.2.1. Overview

Three types of models were used to characterise the physical environment of Port Pegasus; a hydrodynamic model, a wave model, and a particle tracking model (which uses the hydrodynamic model developed by MetOcean). MetOcean Solutions Ltd. (MSL) have constructed and produced the outputs of the hydrodynamic and wave models. Detailed descriptions of the models as well as additional output plots are located in the appendices (refer next section), however a summarised description of the models are provided below.

Hydrodynamic model

The 3D hydrodynamics of Port Pegasus and surrounds were modelled using the open-sourced hydrodynamic model SCHISM by MSL. The horizontal resolution of the model grid ranged from 100 m at the boundary to 10 m in shallow water and near the coast, with grid refinement in the main passages (i.e. Whale Passage, Pegasus Passage). The triangular elements of the model domain meshes are shown in Figure 12 and the water depths used are given in Figure 13. More detail about the model and its implementation in Port Pegasus can be seen in Appendix 2.

The hydrodynamic model estimates water mass movements through tracking changes in small volumes throughout the volume of Port Pegasus. This model has enabled water current time series to be constructed for any point in Port Pegasus. Depth-averaged current maps were also created and used to derive the 'index of suitable location' (ISL) presented in Fletcher et al. (2017). The key objectives of the hydrodynamic modelling were to:

- Indicate current speeds specific to the farming areas
- Provide a base on which the particle tracking model could be run.

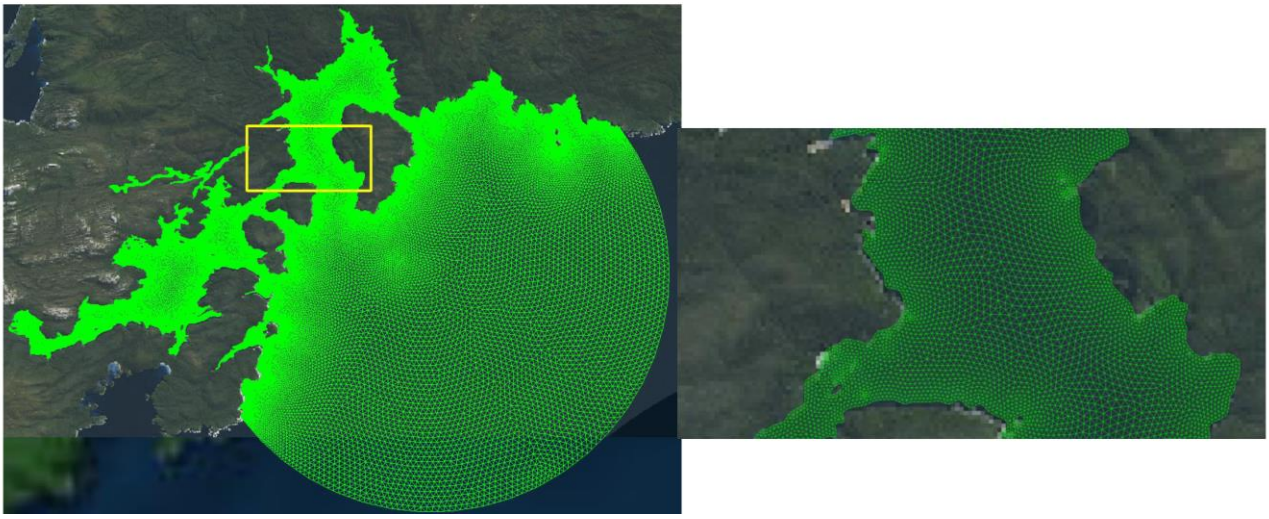

Figure 12. Triangular model mesh defined for Pegasus Bay. Left image shows the whole domain used in this study, right image shows a zoomed view over the Pegasus passage and the entrance of North Arm. Sourced from MetOcean Solutions Ltd.

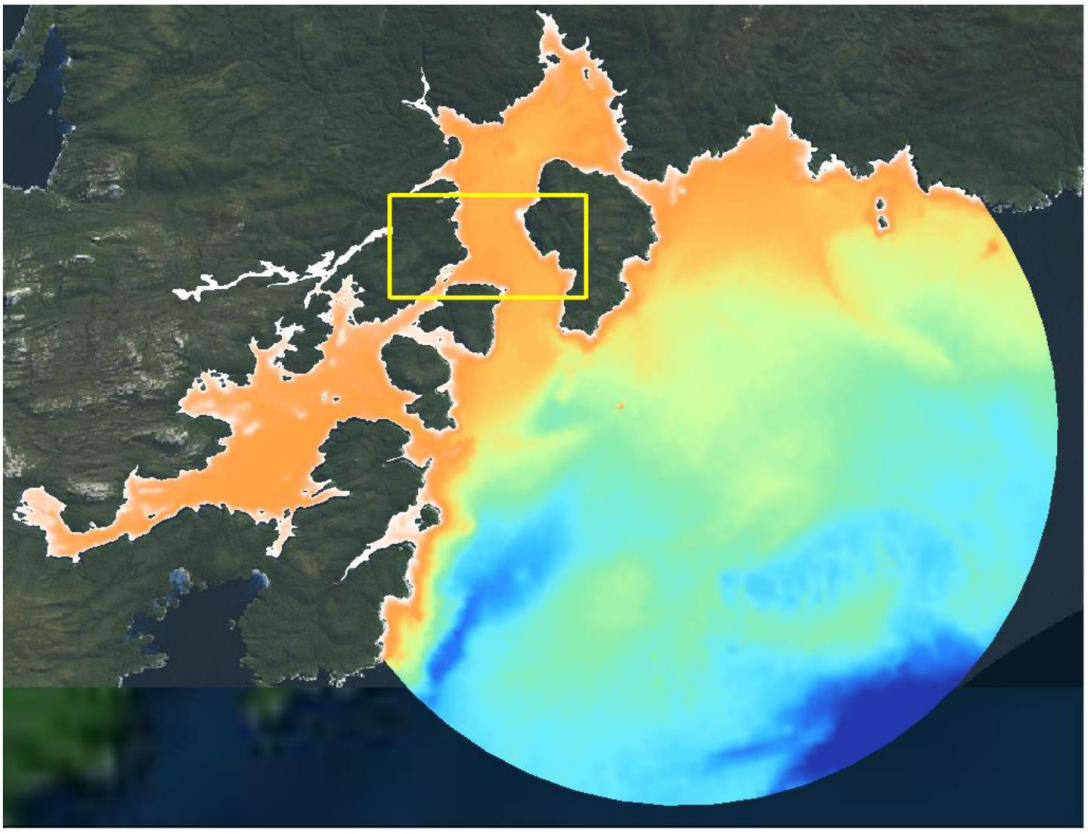

Figure 13. Bathymetry of model domains showing the water depth variation from blue (more than 100 m deep) to red (50 m depth, or less). Local hydrographic fare sheets were digitised to provide depth data. Sourced from MetOcean Solutions Ltd. Yellow box highlights area with detailed bathymetric gridding shown in Figure 12.

Particle tracking

The platform of the hydrodynamic model allowed us to assess the fate of dissolved wastes that could be released from proposed salmon farming in the region, using particle tracking; for example, to assess the likelihood that water (and waste) from farm areas in North Arm will enter South Arm (connectivity). It also allows an estimate of how long water parcels (and wastes) will be retained within a certain region (flushing or retention time).

Specifically, particle tracking modelling traces the path of virtual particles released from a point source as they are moved by the currents produced by the hydrodynamic model. The particles therefore describe the movement of neutrally buoyant material, or non-swimming organisms, which may be contained within parcels of water. It is the analysis of the path of these thousands of virtual particles that allows us to calculate (a) the fraction of particles that will pass from one release area to another within a given timeframe (connectivity) and (b) how long the particles typically reside within an inlet (retention times). In addition, the model aided in estimating changes in pelagic properties from the release of dissolved aquaculture wastes (discussed in Chapter 5).

The particle tracking tool used is ERCore[8], developed by MSL. The particle tracking spanned 79 days in 2017; from 15 April to 29 June, and used a 79-day long 'hindcast' of currents from the MSL hydrodynamic model to move virtual particles around the inlets.

Wave model

A wave model was also constructed to provide important information on wave heights and periods. This information is important for assessing the feasibility of securing aquaculture structures in high energy environments. As well as this structural effect, waves can also episodically influence the currents observed on the seabed and can hence influence the transport of wastes.

The wave modelling was carried out by MSL, with the details given in their report contained in Appendix 3. The model was tested against satellite-measured wave heights in the ocean around Stewart Island. The waves were propagated under the influence of the winds within two nested SWAN model grids, with progressively finer scale to obtain modelled wave information within North and South Arms. Three regular model grids were defined with resolutions progressively decreasing from 5 km to 100 m, with the 100 m model used within Pegasus Inlet.

3.2.2. Currents

Modelled speeds and directions of currents at the proposed farm areas are shown in Figure 14. Currents at all sites were weak, rarely exceeding 0.1 m/s (Appendix 1 and

[8] Additional technical details of this model are provided in a working manual of the document, which is attached to Appendix 2 of this report.

Table 5). These weak flows were also observed in the ADCP-measured currents for the Mid Bay site (Figure 8). To provide context for the current speeds at the farm areas in North Arm, modelled currents in the middle of South Arm are also shown (Figure 14). At South Arm, currents are comparatively weaker, rarely exceeding 0.05 m/s.

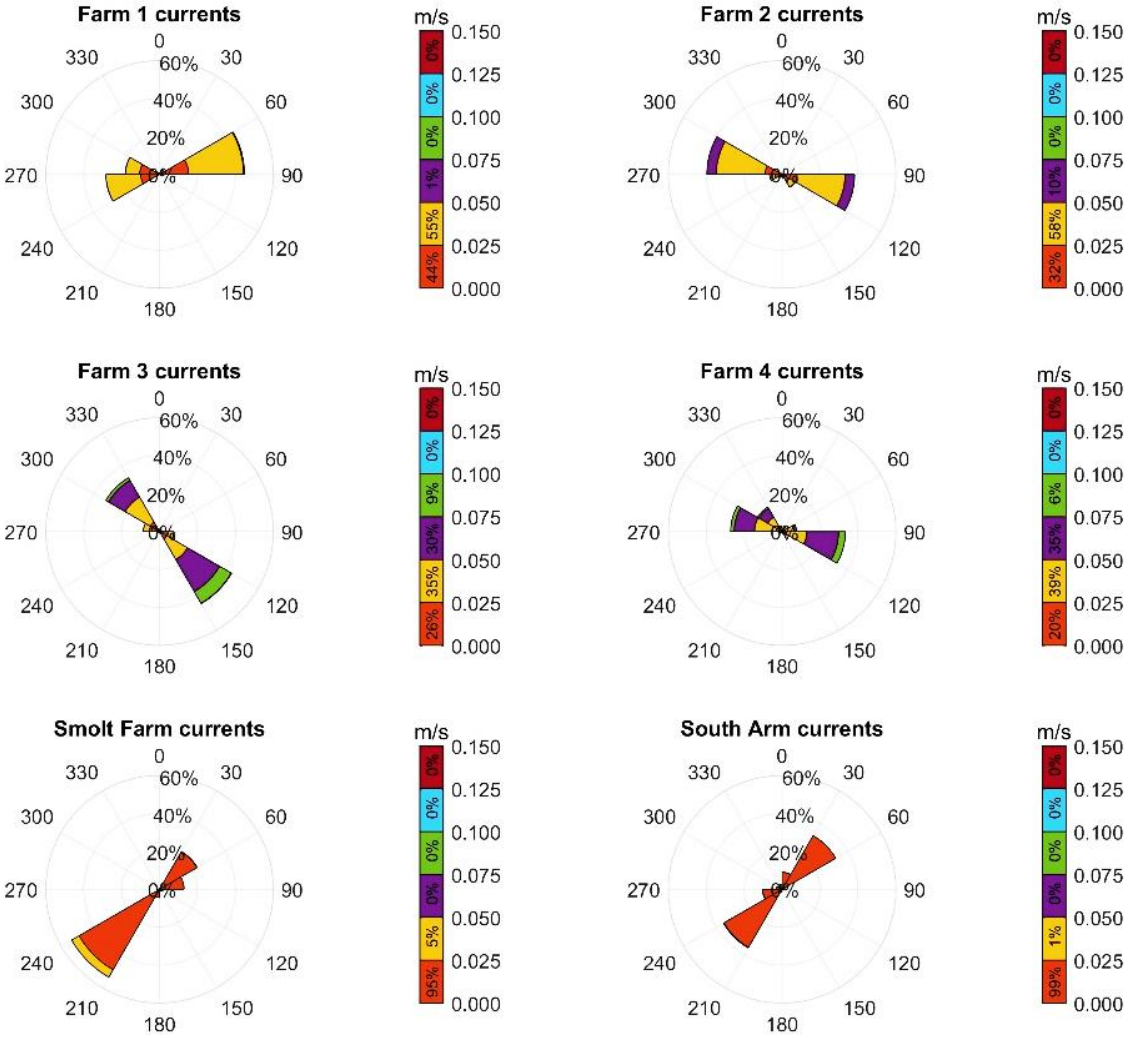

Figure 14. Current roses showing speeds and directions of depth-averaged modelled currents at proposed farm areas and mid-South Arm (for context). Locations are shown in Figure 3 and Figure 15.

Based on mean depth averaged currents[9] all of the sites considered here (Table 5) would be considered 'low-flow' sites for the purposes of managing benthic effects (from the best management practice guidelines for Marlborough salmon farms; MPI 2015). Some comparative information for other Big Glory Bay and Marlborough Sounds sites is also provided in Table 5.

[9] Assumed to be equivalent to mid-water current speeds for the purposes of determining low- or high-flow site status based on MPI (2015).

Table 5. Summary of mean and maximum modelled current speeds and depths at proposed North Arm sites, and comparative information from Big Glory Bay and the Marlborough Sounds.

Location	Site	Mean mid-water current speed (m/s)	Maximum mid-water current speed (m/s)	Model water depth[a] (m)	Source/Reference
North Arm Port Pegasus* (proposed sites)	f1 site	0.026	0.054	38	Extracted from model data for the period 23 April to 30 June 2017; model depths provided in mean sea level datum.
	f2 site	0.033	0.069	36	
	f3 Site	0.045	0.115	38	
	f4 site	0.039	0.096	42	
	Smolt site	0.016	0.039	32	
Big Glory Bay (BGB)	Unclear – old salmon farming site (inner BGB) or entrance to BGB	< 0.05-0.1		~20-30	'… low current velocities (Generally less than 5-10 cm/s depth averaged)' Roper et al. (1988): page 8. Salmon farming water right studies, Big Glory Bay, Stewart Island, DSIR.
Marlborough Sounds (Low-flow sites)	Forsyth	0.032	0.109	31	Table 10 in Keeley (2012).
	Waihinau	0.091	0.297	29	
	Ruakaka	0.035	0.142	34	
	Otanerau	0.035	0.135	38	Speeds are about 2-3 m above seabed and would generally be slightly lower than mid-water currents.
Marlborough Sounds (High-flow sites)	Clay Point	0.191	0.790	30–40	
	Te Pangu	0.194	0.632	27–31	
	Ngamahau	0.211	0.662	23–35	
	Waitata	0.176	1.267	~63	
	Kopaua	0.157	0.563	32–40	
BMP High-flow site criteria		≥ 0.1			Table 3 of *Best Management Practice Guidelines for salmon farms* (MPI 2015)
BMP Low-flow site criteria		< 0.1			

a. Note small depth differences exist between the wave and hydrodynamic model sites in Port Pegasus, due to differences in locations selected within the farm sites and in underlying grids of each model.

Modelled tidal currents and elevations typically compared well to measured tidal currents and elevations within North Arm, although 'mid bay' tidal currents appeared to be underestimated at the start of the model simulation (Appendix 2). As well as a good qualitative comparison, quantitative analysis also indicates that both the model predicted current speeds and water elevations have relatively low bias and Mean Absolute Errors (MAE) and Root Mean Square Errors (RMSE) within North Arm. The model authors (MSL) note that this suggests that 'the model is capable of reproducing the salient hydrodynamics within the study area' (Appendix 2). Based on these comparisons, the model was deemed suitable for further use in the assessment; however, it could be further validated for a Stage 3 assessment if additional information is available.

3.2.3. Connectivity

Particle tracking modelling results are used to (a) estimate the residence time of water in North Arm and, (b) estimate the probability of water in North Arm, from farm areas, entering South Arm. Additional information on the fate of dissolved wastes is provided in Chapter 5.

In order to track and aggregate the movements of particles and to facilitate assessment of results, regions were assigned within the model boundaries. There were two sets of regions used (Figure 15); the first comprised four regions, two covering North Arm (inner region and outer region) and two covering South Arm (inner and outer). These were used to derive statistics, e.g. particle numbers or ages over time. The second set of regions separated only North Arm and South Arm, and was used to estimate the particle durations within each Arm.

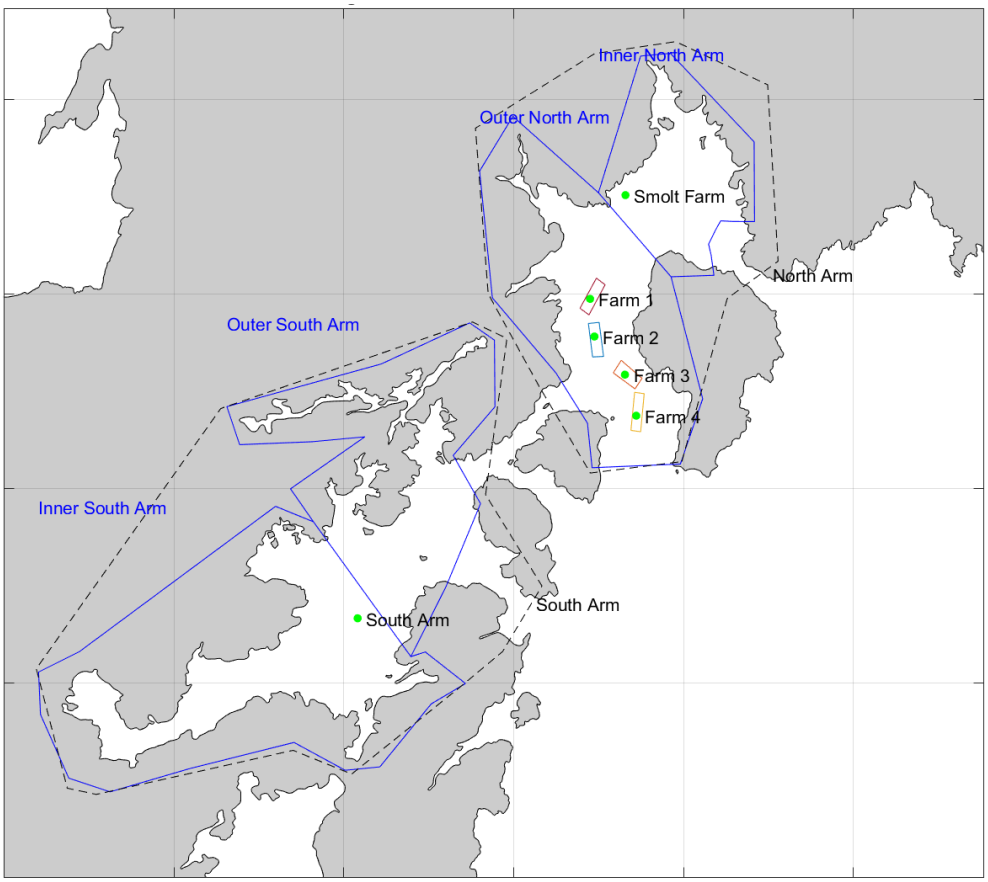

Figure 15. Green dots show the six particle release sites; the farm areas 1 to 4 (also referred to as f1–f4), the smolt farm (s1) and the release site in South Arm. Blue lines show the first set of regions used for calculating particle statistics, Inner and Outer North Arm, and Inner and Outer South Arm. The black dashed lines show the other set of regions used for estimating statistics (all of North Arm and all of South Arm).

Virtual particles were generally continuously released at the centre of each farm area at 10 m depth, as well as one large area covering South Arm. The model's particles were released (every 5 minutes) at a rate equivalent of 680 particles per day per area, giving a total of around 54,000 virtual particles released from each locations. One exception to the continuous release of particles was a one-off pulse release for estimating residence time using water parcels. In all simulations, particles released were retained for the entire 79 days of the modelling run, unless they exited the model domain at its circular outer ocean boundary (see Figure 12, Figure 13). These model runs were used for estimating connectivity, residence times and transport of dissolved wastes.

Examples of particle tracks

To show connectivity between North Arm and South Arm, a small selection of randomly chosen particle tracking examples from throughout the 79 days of the modelling run were used to show the character of the movement of parcels of water released from two of the release locations, the farm areas f1 and f4. A spatial summary of the particle tracks is shown in Figure 16. Examples of the northern-most farm site (the smolt farm, s1) and the middle grow-out areas (f2 and f3) are not provided, as the tracking patterns were similar to those tracks for f1 and f4 (respectively).

It is also useful to provide some quantification of this 'exchange' of particles over time *between* the North and South Arms, as well as *within* the North and South Arms (using the four sub-regions). We can do this by looking at how the proportion of particles (from each release site) present inside each of the four regions changed over time since they were first released (Table 6, Figure 17 and Figure 18).

Particles (or water parcels) released in inner North Arm tend to say there for a while, with a proportion exiting mostly through Whale Passage. Very few particles then enter South Arm. Those released in outer North Arm mostly exit southwards into the ocean, with a few then entering South Arm through South Passage. Particles released in South Arm spend a long time there, and those which do exit are unlikely to enter North Arm. Only around 1% of particles released from the farm sites enter South Arm and vice versa. Therefore, this results suggests there is very low physical connectivity between the waters of the two Arms.

Most particles released from f1 spend a lot of time in the north end of North Arm, and the ones that do escape tend to exit through Whale Passage (Figure 16). Of the 27 particles shown in Figure 16, only two entered South Arm with both exiting after some time. Particles released from f4 (Figure 16) spent most of their time in southern North Arm, with a few persisting for extended periods within northern North Arm, and a few escaping through Whale Passage. Most particles of the f4 released particles were lost to the ocean through Big Ship Passage and two more of the f4 released particles entered South Arm than those released from f1 (Figure 16).

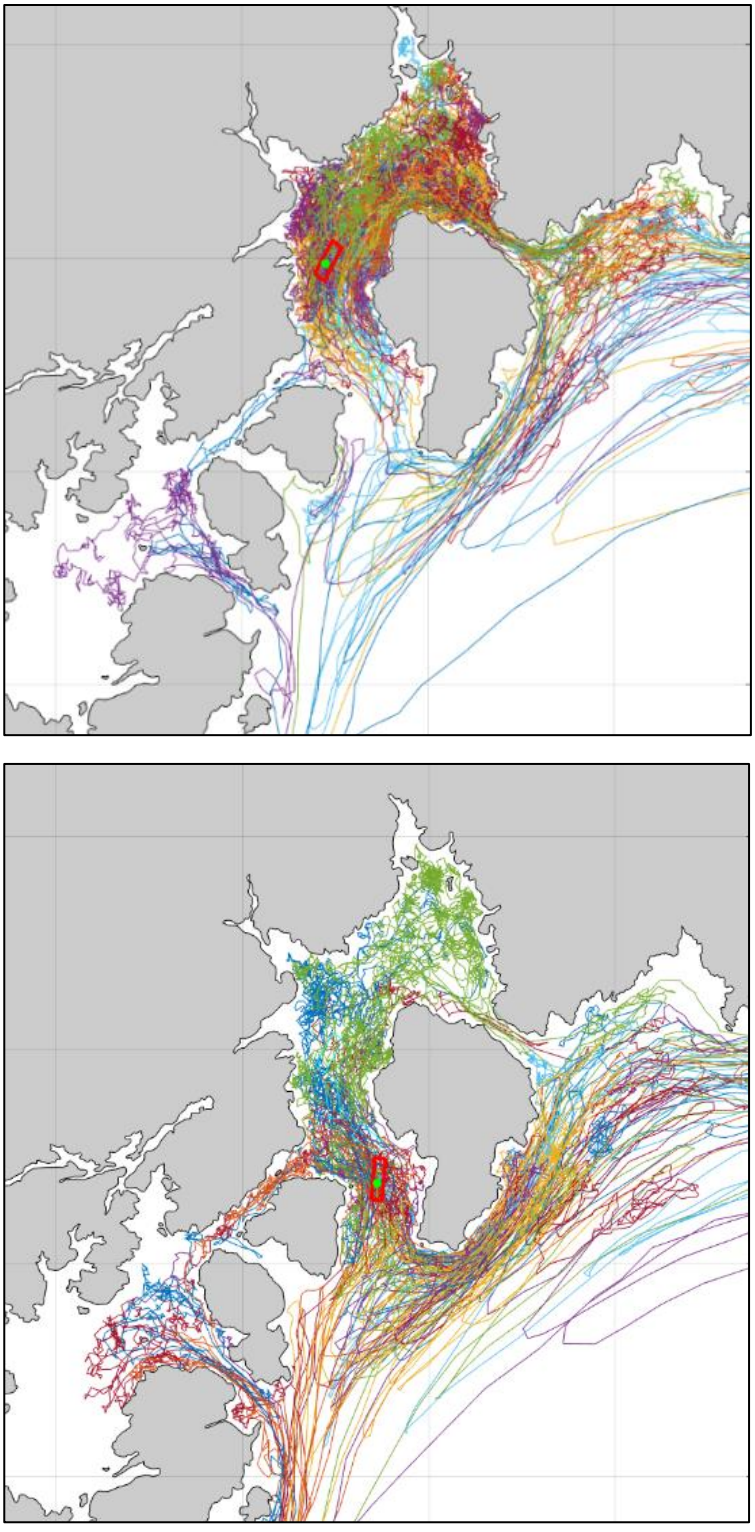

Figure 16. Examples of tracks for 27 of the particles released from Farm 1 (f1; top) and Farm 4 (f4; bottom) at different times throughout the 79 day model run.Colours correspond to different particles. The green dot shows the release location.

When looking at the sub-regions, the numbers of particles within each grew with time, but levelled out as the number entering a region approached a balance with the number exiting that region. This balance suggests the models had reached a quasi 'steady-state' and were therefore suitable for estimating mean connectivity and residence time (see following section). This balance was approached within the 79-day extent of the particle tracking for North Arm releases, though there are two clear 'peaks' starting at about 30 days, and again at about 50 days, which coincide with periods when longer residence times occurred[10] (Figure 17 and Figure 18). Variation around these peaks tended to show a slow increase of particle numbers within a region, followed by a more rapid decrease. The rapid decreases were likely due to weather or spring tide events rapidly flushing more particles out of the regions.

Typically 5–10% of particles released from each farm site are present within each of the two North Arm regions at any given time. The exception is particles released from the smolt farm (s1) sited within inner North Arm, where 12–15% of particles are typically present within each of two North Arm regions. However, while a higher percentage of particles from the smolt farm is retained within North Arm, overall this farm is likely to have much lower inputs into the environment, significantly reducing any impact it may have.

The modelled data indicate that the more exposed southern farm sites may have less impact on North Arm as a whole. Simulated particles released from the northernmost site (f1) showed proportionally more (~100% more) particles retained in the North Arm region (23%) compared to the release from southern-most site (f4; 10% total retained in North Arm) (Table 6).

[10] This could be associated with a period of lower flushing due to calm weather or weak tidal flows.

Table 6. Retention of particles in the model, shown as mean percentage of particles released which are present within each sub region in Figure 15 during last 15 days of modelling, after day 64. Note that sub regions (inner/outer) can be summed to estimate the total regional North or South Arm retention.

Release Location	Sub-region			
	Inner North Arm	Outer North Arm	Inner South Arm	Outer South Arm
Farm 1 (f1)	11%	12%	1%	<1%
Farm 2 (f2)	9%	11%	1%	1%
Farm 3 (f3)	7%	9%	1%	<1%
Farm 4 (f4)	4%	6%	1%	<1%
Smolt Farm (s1)	15%	12%	<1%	<1%
South Arm	1%	1%	8%	14%

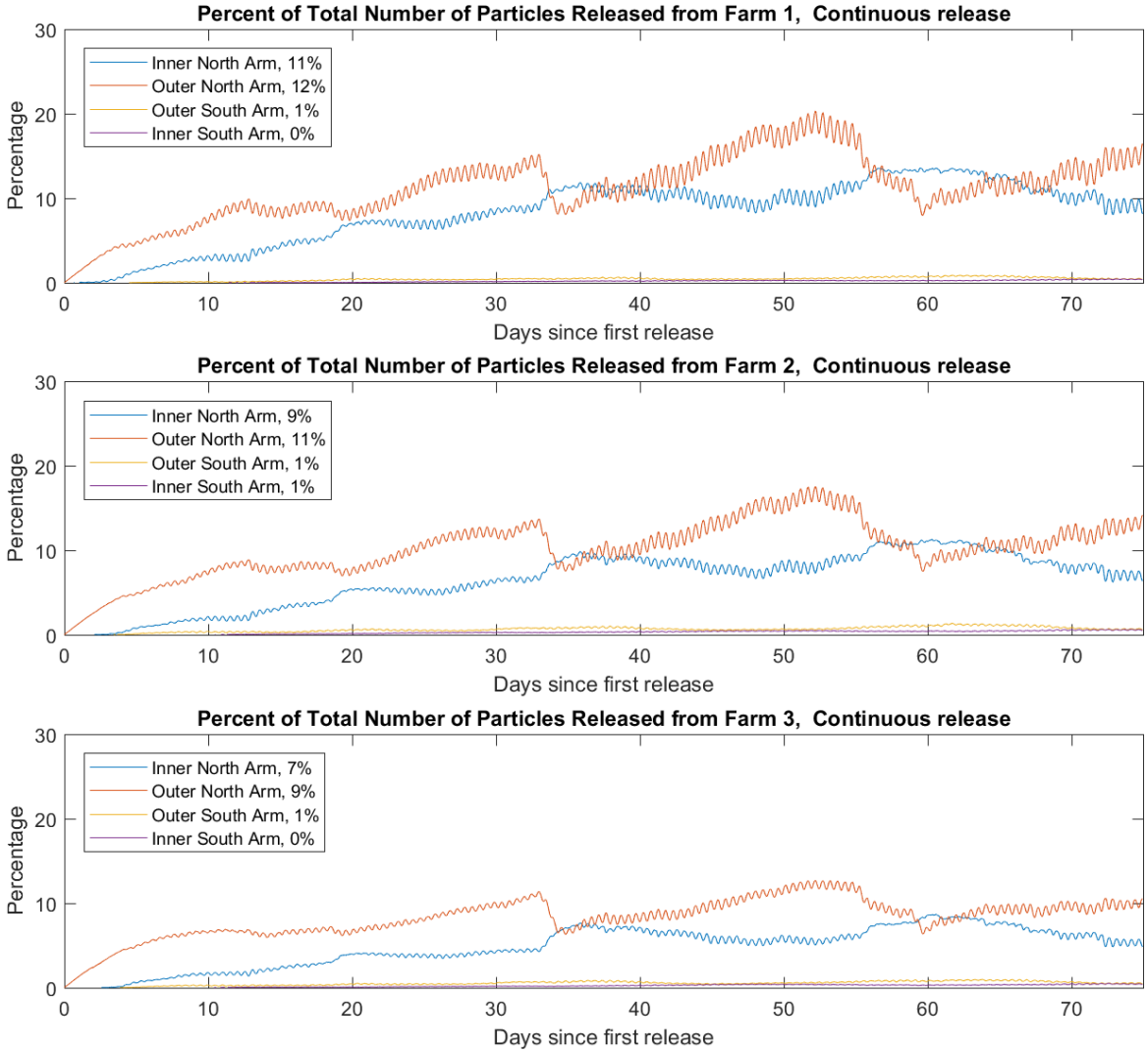

Figure 17. Percentage of total number of particles which are within each of the four regions in Figure 15 for particle releases from farms 1–3. Lines show how percentage varies with time since the first particles were released on 15 April 2017. Each coloured line is for one of the four regions as given in legend. The number in the legend gives average percentage of particles inside the region during the last 15 days.

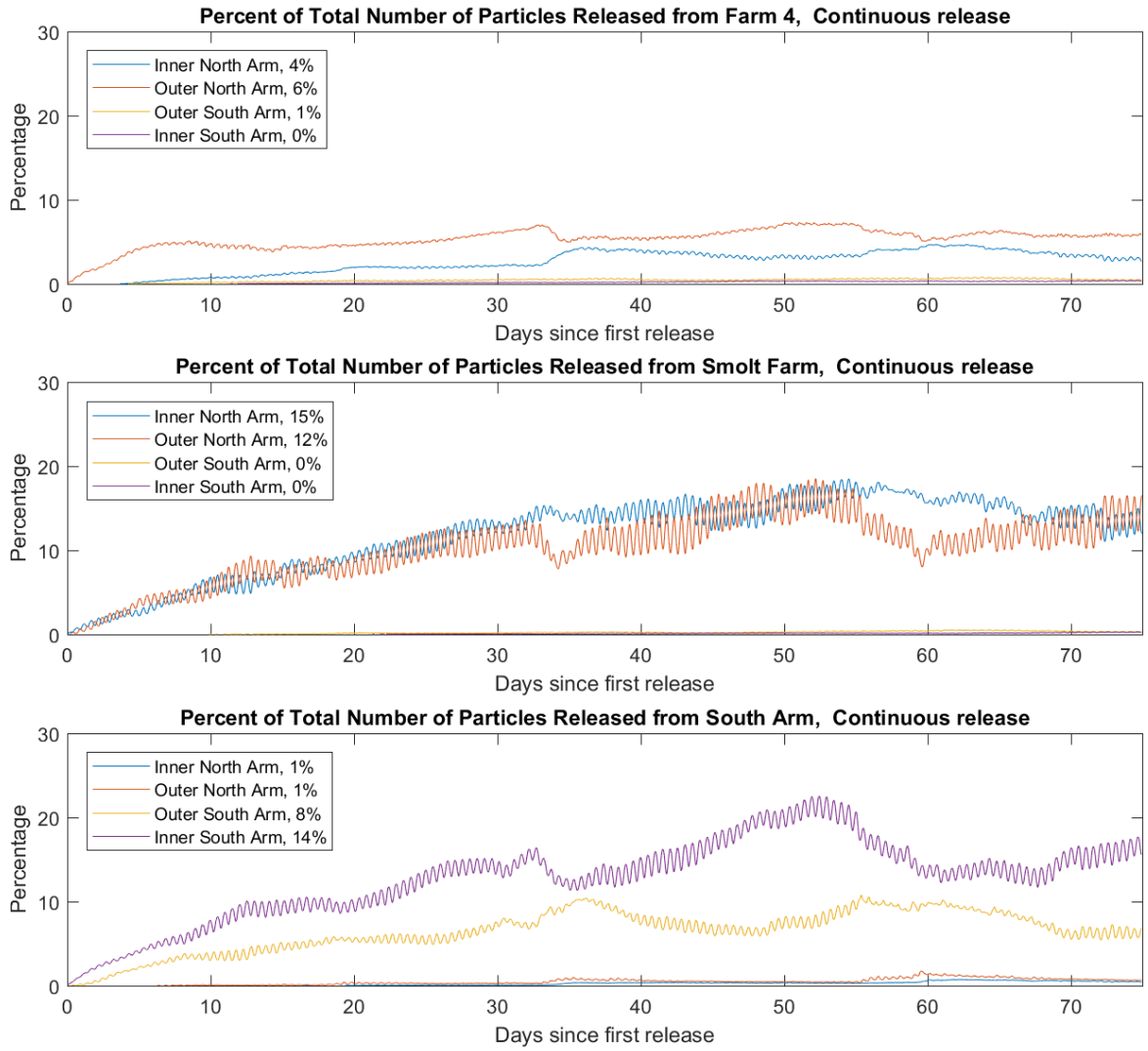

Figure 18. Percentage of total number of particles which are within each of the four regions in Figure 15, for particle releases from Farm 4 (f4), the smolt farm (s1) and South Arm. Lines show how percentage varies with time since the first particles were released on 15 April 2017. Each coloured line is for one of the four regions as given in the legend. The number in legend gives average percentage of particles inside the region during the last 15 days.

3.2.4. Residence time

The residence time for a region is a metric which describes how long water remains in an area. A region with a short residence time refers to an area in which water, or dissolved wastes from net pens, are rapidly flushed, whereas a long residence time suggests the opposite. Consequently, assessing residence time is useful for determining the potential for dissolved waste to be flushed from a given area. One way to measure residence time is to release particles and measure their 'age' (time since release). The average ages rise until they plateau at some level approaching an upper limit, indicating that the number of particles entering a region is nearing a

balance with the number of particles exiting that region. The average age at this plateau is an indication of the average time particles spent within each region and therefore gives a basic measure of residence time. There is also a more direct estimate of residence time, which assess the time a 'water parcel' typically spends within a given region. We present both approaches, as the age-based approach relates more directly to the release of dissolved wastes from finfish aquaculture. This is discussed later in our assessment of effects (Chapter 5).

Based on both methods of residence time analysis it is clear that average residence times of releases from farms f1–f4 are in the range of 14–22 days, with shorter residence times for releases from the southernmost site (f4). The smolt farm (s1), in inner North Arm has a longer 25-day residence time; however deposition from this farm would be much lower than that of production farms due to lower feed levels.

Residence time by particle age

For all farms (f1–f4 and s1) the upper limit is reached towards the end of the modelling period (Figure 19 and Figure 20). The region closer to the release sites reached a balance more quickly than those farther from the release site, thus had a lower average age (Table 7). For example, the average age of particles in South Arm was lowest for the South Arm release simulation because the particles were released within that region (Table 7). In adjacent 'non-release' regions[11] average ages were increased by the time required to travel distance between the release site and the region of interest. The ages are also affected by wind events as seen in the inner and outer North Arm average particle ages.

Table 7. Average age of particles within each region according to release location. Averages are for the last 15 days of the modelling (days 64–79) for continuous particle release.

	Region			
Release Location	**Inner North Arm (days)**	**Outer North Arm (days)**	**Inner South Arm (days)**	**Outer South Arm (days)**
Farm 1 (f1)	23	15	22	32
Farm 2 (f2)	23	14	19	29
Farm 3 (f3)	22	13	19	29
Farm 4 (f4)	24	12	18	29
Smolt Farm (s1)	21	17	30	37
South Arm	33	28	17	17

[11] Regions other than those within which particles were released.

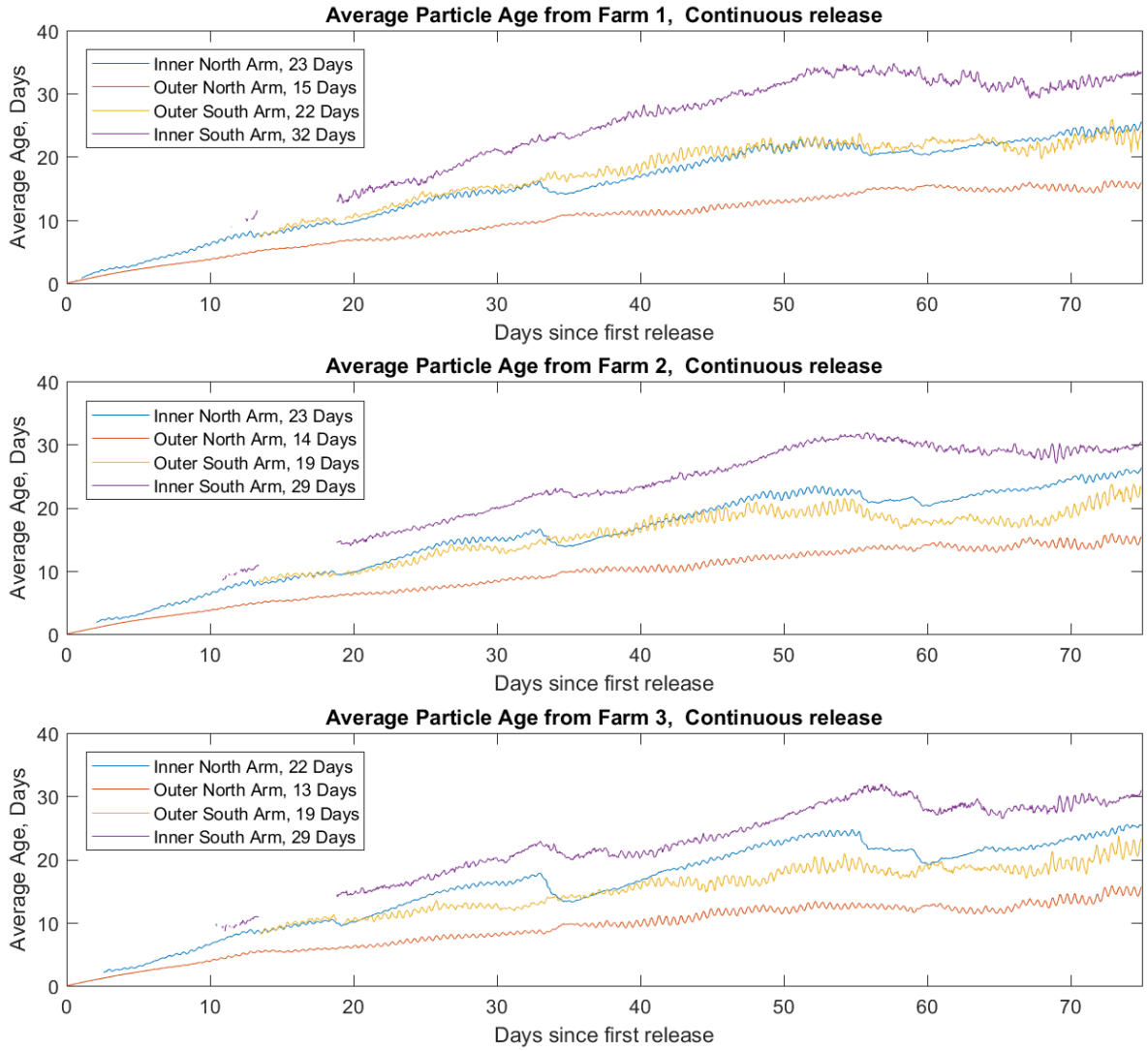

Figure 19. Average age of continuously released particles which are within each of the four regions in Figure 15 for particle releases from farms 1–3 (f1–f3). Lines show how age, the number of days since a particle was first released, varies with time since the first particles were released on 15 April 2017. Each coloured line is for one of the four regions as given in legend. Number in legend gives average age of particles inside the region during the last 15 days.

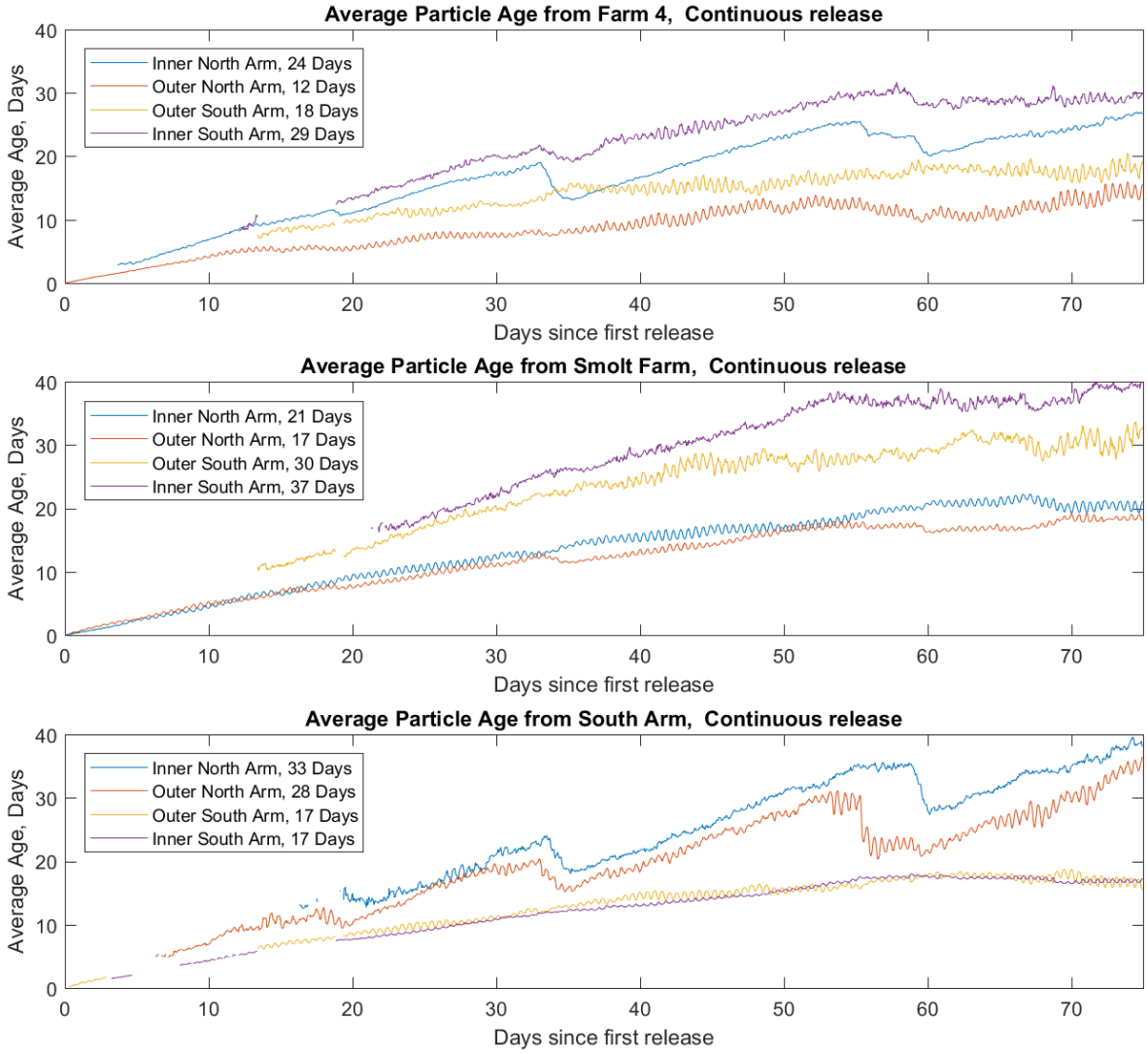

Figure 20. Average age of continuously released particles which are within each of the four regions in Figure 15 for particle releases from Farm 4 (f4), the smolt farm (s1) and South Arm. Lines show how age and the number of days since a particle was first released, varies with time since the first particles were released on 15 April 2017. Each coloured line is for one of the four regions, as given in legend. Number in legend gives average age of particles inside the region during the last 15 days.

Residence time using water parcels

The 'water parcel' approach to estimating residence time uses a pulsed release of 50,000 particles released at the start of the model run. It is then calculated by simply adding up how long each particle spends within each of the arms, and could include multiple entries or exits from the either North or South Arm due to oscillating tidal flows. Figure 21 shows the average duration of particles inside each of the arms, according to the release site using this approach.

Mean residence times and percentile values are also summarised in Table 8, to give an indication of the 'spread' of particle residence times. For example, 10% of particles released from f1, spend less than 6 days within North Arm, while 90% spend less than 54 days. The median value is 15 days. Thus, there is a wide range of times that particles spend within the Arm. Particles released within South Arm have similar values to those released in North Arm from f1, with 10% of South Arm releases spending less than 6 days within South Arm, while 90% spend less than 49 days and the median value is 16 days. For all release sites the median values are smaller than the mean values (Figure 21). This indicates a distribution for particle residence times which is skewed towards smaller values, with a long tail of larger values.

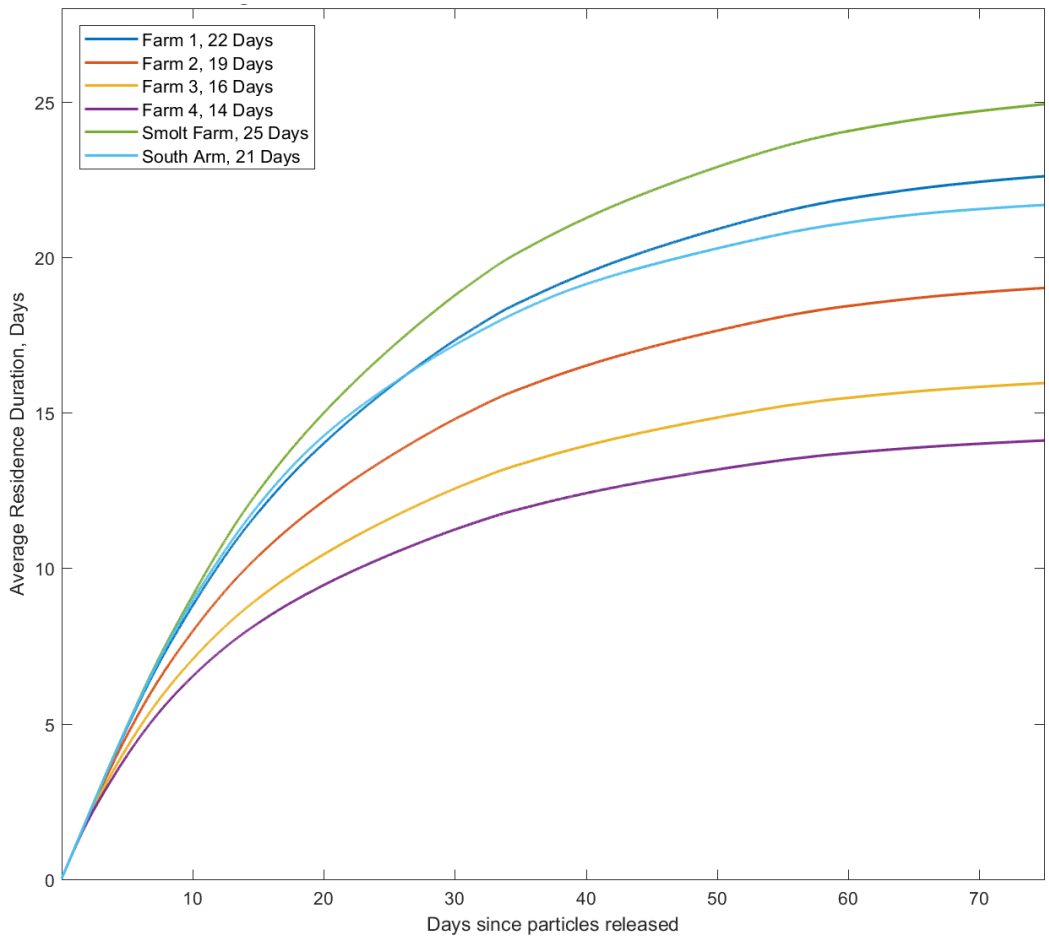

Figure 21. Average time pulse-released particles spend inside the arm within which they were released, i.e. North Arm (all except light blue) and South Arm (light blue). Colours correspond to release site. In this example 50,000 particles were released from each location in a single pulse as the start of the modelling period. Numbers in legend indicate the average of the durations shown by the curve over the last 15 days of the modelling period (i.e. day 64–79) after they somewhat plateau; thus indicating a typical residence time for particles released from each location.

Table 8. Residence time statistics for continuously released particles within North and South Arm, calculated from the time that particles spend within the Arms. The means match the values in the legend of Figure 21. Like the means, the percentile values given are the averages of these values over the last 15 days of the model run (days 64–79).

Release site	Mean residence time (days)	10% percentile (days)	50% percentile, or median (days)	90% percentile (days)
Farm 1 (f1)	22	6	15	54
Farm 2 (f2)	19	3	12	48
Farm 3 (f3)	16	2	9	41
Farm 4 (f4)	14	2	8	37
Smolt Farm (s1)	25	7	18	56
South Arm	21	6	16	49

3.2.5. Wave modelling

Wave modelling was undertaken to determine the likely wave action experienced at each of the farm areas, given that high wave action would be a limiting factor for placement of farm structures. The wave modelling also provides broader information on the wave climate within North Arm of Pegasus Inlet, which can indicate the relative importance of waves in re-suspending material in different areas of the Inlet. Thirty-eight years of wave modelling was carried out by MSL, with the full details provided in the appended report (Appendix 3).

As well as the model validation undertaken by MSL at offshore locations, we also undertook a local comparison of the model with measured waves. Results showed that the maximum measured significant wave height recorded by the wave sensor (1.9 m) over one month during at the West 2016 ADCP deployment (Section 3.1.3) was similar to that given by the hindcast (1.76 m). This suggests wave heights are potentially underestimated in the model hindcast, given that it is unlikely a one-month deployment to measure wave heights exceeded a 38-year period. Although this is not a thorough validation of the model in the area of interest, the modelled heights are adequate for this initial assessment of the region. However, further validation would be recommended if a Stage 3 assessment collects additional data, particularly if model estimates are required for engineering of structures.

Wave heights

A regional overview of modelled waves (Figure 22) shows that maximum significant wave heights vary between the North and South arms of Port Pegasus, with higher wave heights in North Arm. However, in the inner part of North Arm and all of South Arm, maximum significant wave heights are mostly under 1 m (Figure 22). Maximum significant wave height rapidly increases from 1 to 6 m from inner North Arm to the southern entrance to North Arm, respectively.

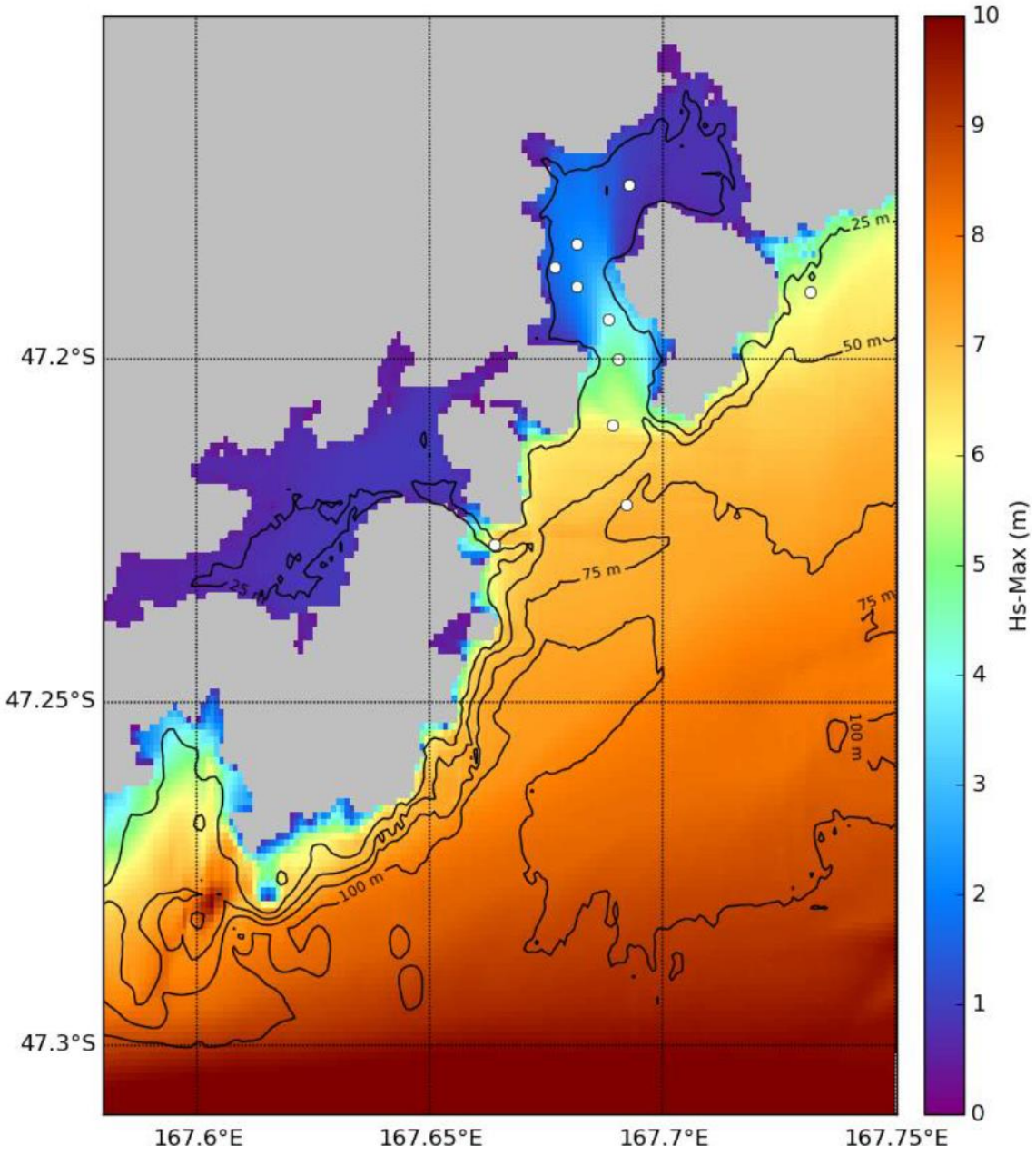

Figure 22. Maximum significant wave height (Hs-Max) in and around Port Pegasus, calculated from the 38-year hindcast. White dots show the sites of interest. Figure supplied by MetOcean Solutions Ltd. It should be emphasised that the maximum wave height at any location will be larger than Hs-Max at that location.

Within North Arm, model results indicate that mean wave heights at the farm areas were all under 1 m. At the most exposed farm area (f4) the average significant wave height was 0.91 m, decreasing to 0.41 m at the more sheltered northernmost grow-out area (f1). Nearer to the smolt farm area (Site 06), average significant wave height was only 0.23 m.

Maximum significant wave heights followed a similar pattern. Thus, the largest significant wave height decreases rapidly for sites progressively further north from f4 (Farm 4) as they benefited from the shelter provided by Pearl Island. In the inner part of North Arm and all of South Arm, the maximum significant wave heights are mostly under 1 m (as gauged from site 09), while at the entrance to North Arm the maximum significant wave height is up to 6 m.

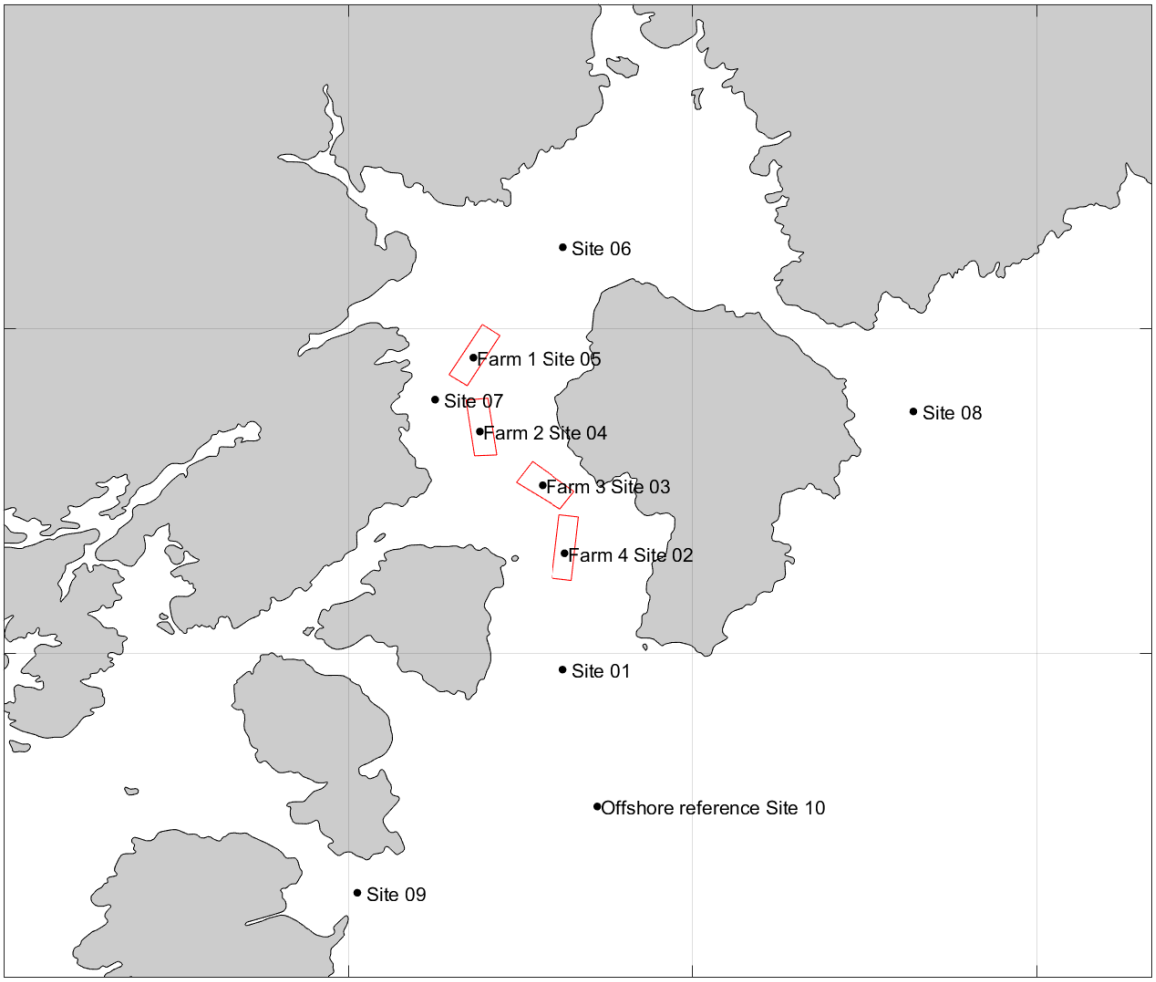

Figure 23. Locations from which wave statistics were generated in and around the study area. Sites 02–05 correspond to Farms 1–4. Site 10 was used a reference site for offshore wave conditions.

Table 9. Summary of wave statistics from a 38-year model hindcast for Port Pegasus for each location (locations shown in Figure 23).

Existing site label	MetOcean site name	Water depth (m)	Mean significant wave height (m)	Maximum significant wave height (m)
	Site 01	41	1.21	5.99
Farm 4 (f4)	Site 02	38	0.91	4.78
Farm 3 (f3)	Site 03	34	0.74	3.96
Farm 2 (f2)	Site 04	32	0.44	2.24
Farm 1 (f1)	Site 05	35	0.41	2.18
Mid Bay 2017 ADCP	Site 06	42	0.23	0.96
West 2016 ADCP	Site 07	33	0.33	1.76
	Site 08	34	1.21	5.79
	Site 09	28	0.93	6.58
Offshore reference	Site 10	77	1.43	7.07

Based on the potential for large waves at f3 and f4 (maximum significant wave heights of 3.96 m and 4.78 m respectively), they will likely represent challenging conditions for the placement of moored structures, such as salmon farms, in the area. We are unaware of any existing farms in New Zealand that would be exposed to this level of wave energy. However 'fortress' net pens may be considered for this site which are advertised by the manufacturer (Huon Aquaculture) as:

> …designed for, and now tested in, some of the toughest Australian conditions at Storm Bay, Tasmania and Providence Bay, New South Wales.
>
> These sites are high energy, exposed sites, frequently receiving storms swells and gale force winds. Modelling by Aquastructures AS, Norway show the Fortress Pens are capable of withstanding these tough conditions and Farming these pens at these locations over the last few years have shown them to be able to withstand storm events.[12]

However, no specific details are available that could allow direct comparison of Storm and Providence bays to the outer North Arm areas considered here at this time[13].

Nicoll et al. (2011) simulated and measured the response of similar circular finfish pens to hurricane-induced waves of significant wave height of 4.3 m and a dominant period of 8.5 s at a salmon farm site in Nova Scotia, Canada. They conclude that modelling and measured results 'compare favourably and demonstrate the viability of

[12] https://www.huonaqua.com.au/huons-fortress-pens/ (accessed 21/9/2017)
[13] We have made an enquiry into the conditions at the Storm Bay and Providence Bay sites, but have not yet received the details on the wave climate at those sites.

this type of analysis for mitigating risk in aquaculture systems.' Consequently, it appears that structures could be engineered for such a region.

It should be emphasised that the maximum wave height at any location will be larger than the modelled maximum *significant* wave height at that location. More detailed analysis for extreme values would be needed to estimate the maximum wave heights likely to be experienced at each of the sites of interest.

Wave direction

As would be expected at sites within North Arm, large waves arrived from southerly directions, travelling northwards into the inlet. Wave direction at a given site can be captured on a rose plot (e.g. Figure 24 for Site 02) as shown for f4 (the most exposed farm area) where around 90% of significant wave heights are under 1.8 m.

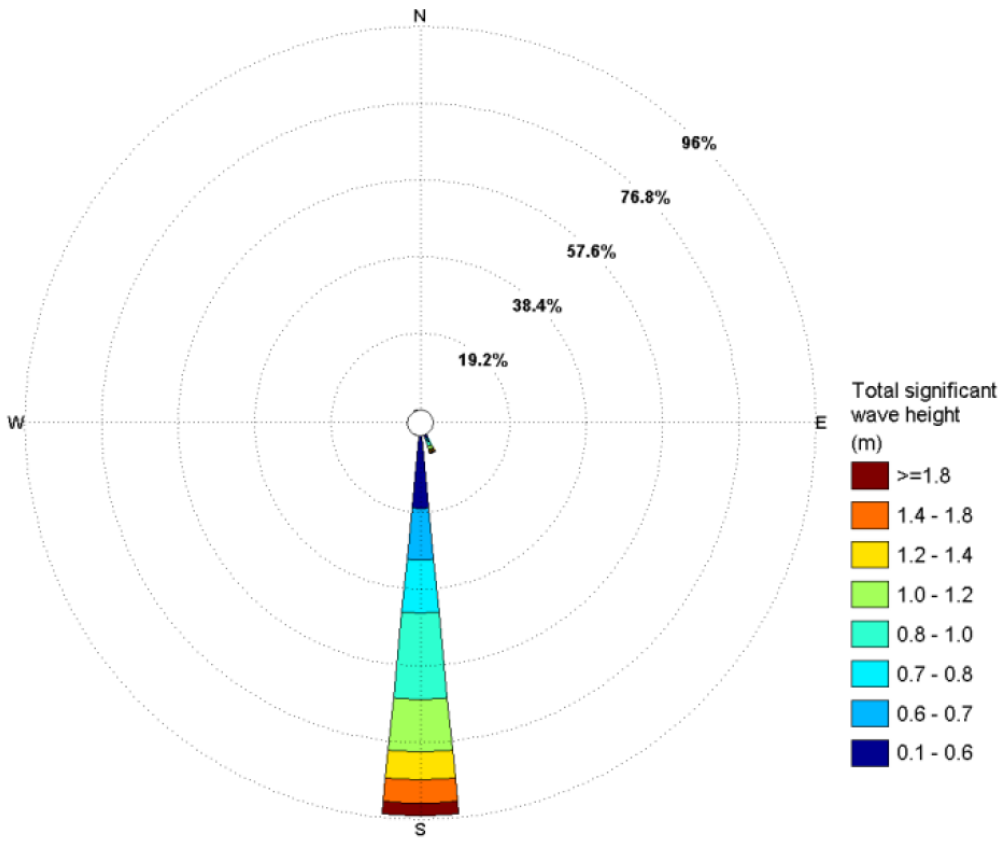

Figure 24. Rose plot for the total (annual) significant wave height at Site 02, corresponding to Farm 4. Sectors indicate the direction from which waves approach. Rose plots for all sites are provided in the MetOcean Solutions full report (Appendix 3).

Near bottom wave-induced currents

Waves generate orbital currents through the water column which decrease with depth but can penetrate to the seabed. These wave-induced currents may re-suspend material deposited from a marine farm on the seabed. The degree to which that may occur depends on the cohesiveness of the deposited material with the existing bottom sediments, with critical resuspension velocities estimated to be between 0.09 m/s and 0.15 m/s in the Marlborough Sounds (e.g. Keeley et al. 2013). Re-suspension of deposited material enables tidal and wind currents to spread the material over a wider area.

It is beyond the scope of this assessment to carry out modelling of any additional dispersion of deposited material assisted by waves. However, it is useful to estimate the size of the wave-induced near seabed orbital velocities (hereafter, 'seabed velocities') and the frequency with which they occur. This will help to determine whether seabed velocities might have a significant influence on farm-related deposits. The water depths of c. 30–40 m depths at the main farm areas, and wave attenuation with depth will significantly reduce the size of the seabed velocities at these sites.

The seabed velocities calculated from the model[14] show that 'sea waves' (defined as those with periods less than 9 seconds) induce peak velocities less than 0.06 m/s at the bottom for 90% of the time (Table 10 and Figure 25). The shorter wavelengths of these sea waves means they do not penetrate as far down the water column. The probabilities for both sea wave and swell wave induced seabed velocities are summarised in Table 10. Note that this information is not representative of the proportion of time that peak currents occur as they will only occur for a proportion of the time the wave passes

Swell waves (those with periods more than 9 seconds) at Farms 1 and 2 appear to induce peak velocities greater than 0.09 m/s about 10% of the time (Figure 25). At the outer two farm areas (Farms 3 and 4) the velocities were higher; greater than 0.09 m/s about 60% of the time (Figure 25). Consequently it is only the outer two sites that could potentially have wave-induced currents strong enough to regularly affect sediments under net-pens.

Wave-induced peak benthic currents are different to mean mid-water tidal currents used to define 'high-flow' and 'low-flow' aquaculture sites (MPI 2015), with wave events creating episodic currents for short periods (e.g. in the order of seconds per

[14] The peak near seabed orbital velocities were calculated using linear wave theory and the significant wave height, and peak wave periods of the wave or swell given in the 38-year hindcast. The peak periods are the periods at which the sea or swell wave spectrum peaks. The significant wave height may lie above the wave height corresponding to the peak period. Thus, the near seabed velocities calculated from significant wave height and peak wave periods may not accurately represent the near seabed velocity using a more representative wave height. However, they will be similar, a more accurate estimate would involve recalculating peak seabed orbital velocity statistics from 38 years of hindcast spectra, which was beyond the time available for this assessment.

wave period) unlike peak tidal currents that can persist for hours over a twelve hour tidal period. Of relevance to salmon waste dispersion is that peak wave currents are short lived and are able to penetrate to the seabed, whereas longer periods of high tidal currents allow boundary layers to form, shielding the seabed from higher currents. Resuspended material can also be affected by vertical components of wave-induced currents that, unlike tidal currents, can act to further disperse material. Consequently, there are many differences between tidal and wave driven currents. It is outside of the scope of this assessment to conduct further analysis; however if a Stage 3 assessment is undertaken we would recommend a more direct comparison between wave and tidal currents is undertaken. Although the dispersive effects of wave-induced currents are likely to be different to tidal currents, the net effect of high energy waves seems likely to result in a mitigated (but not presently quantifiable) impact on the seabed under farms based on overseas experience (as discussed in Fletcher et al. 2017).

The length of time between wave events with strong seabed velocities will alter the influence they have on material dispersion. At f1 and f2 (the inner grow-out areas), the typical time (90% probability; Table 10) between 'high velocity' (> 0.1 m/s) events is 8–10 days or fewer (Figure 26). At the two outermost grow-out areas (f3 and f4), the high velocity events are much more frequent (less than 2–3 days between events; Figure 26). The frequency of these events at the outer sites suggest wave-induced currents could affect the dispersion of wastes at the seabed. Similarly, the high frequency of the wave events at these sites may also present constraints on operations (e.g. vessel access).

Table 10. Summary of peak near bottom wave induced velocity statistics with statistics given for both sea waves, and the more deeply penetrating swell waves. Values in body of table are the peak velocities in m/s. The peak velocity is less than the given values 10%, 50% or 90% of the time. For example the table indicates peak currents are below 0.1 m/s only 10% of the time, or could be interpreted to be greater than 0.1 m/s 90% of time. However, peak currents will only be induced for a fraction of the time shown (e.g. 10% to 50% of the time) and will depend on the wave period and height, which has not been calculated for this assessment. Water depths given are depths from the wave model grid.

			Sea waves, periods < 9 sec.			**Swell waves, periods > 9 sec.**		
	Wave site	**Water depth**	**10%**	**50% Median**	**90%**	**10%**	**50% Median**	**90%**
Farm 1	Site 05	35 m	0.00	0.00	0.00	0.03	0.03	0.05
Farm 2	Site 04	32 m	0.00	0.00	0.01	0.06	0.05	0.06
Farm 3	Site 03	34 m	0.02	0.03	0.03	0.10	0.11	0.08
Farm 4	Site 02	38 m	0.04	0.06	0.07	0.10	0.17	0.19

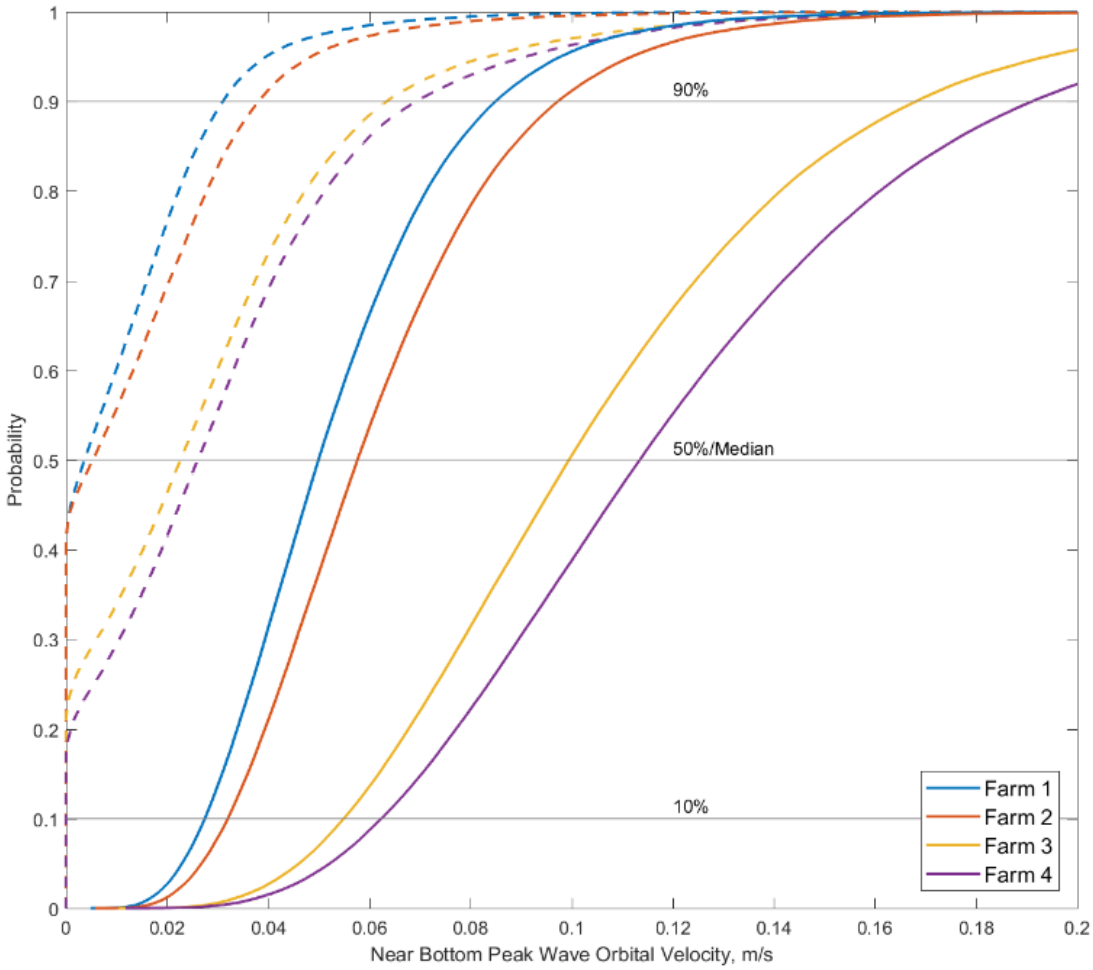

Figure 25. Cumulative probability of peak velocities generated by swell (solid lines) and sea waves (dashed lines) near the seabed at the four grow-out areas (f1–f4).

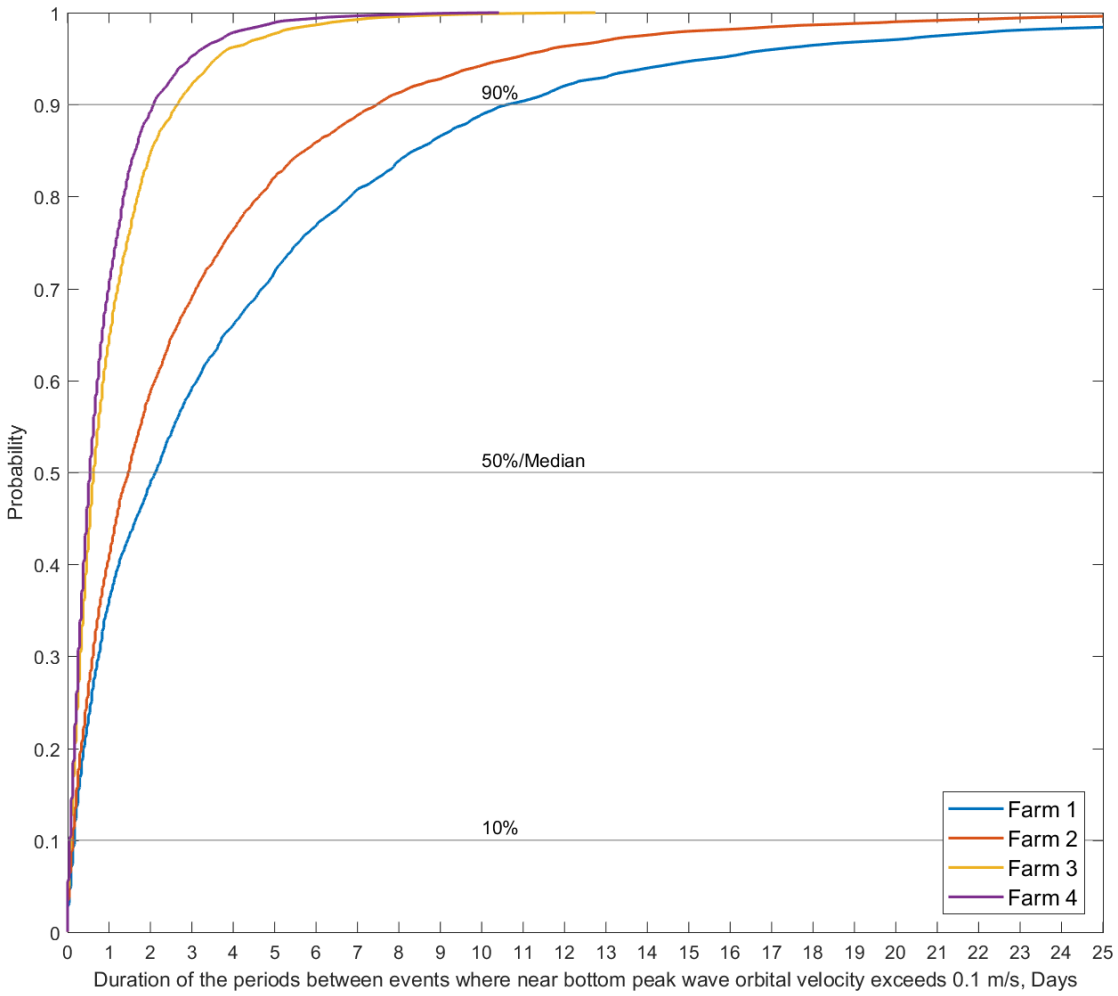

Figure 26. Cumulative probability for time periods between high velocity (> 0.1 m/s) events near the seabed at the four grow-out sites (f1–f4). Plot combines both sea and swell wave-induced seabed velocities.

4. BIOLOGICAL AND CHEMICAL MEASUREMENTS

In planning for this assessment it was clear that no measurements of pelagic biological and chemical properties existed for Port Pegasus. Consequently, initial measurements of biological and chemical properties potentially relevant to finfish aquaculture were included in our pelagic survey. The purpose of collecting these data was to provide initial baseline information on water quality, which could allow an assessment of the potential magnitude of effects and comparisons with other sites.

'Snapshots' of water column characteristics were obtained from 14 sampling sites across the North and South Arms of Port Pegasus, on three occasions (Figure 27).

On the first two occasions (30 March and 3 April 2017), the following biologically relevant data on the pelagic environment were measured[15] through the water column profile using a CTD[16]:

- chlorophyll-*a* fluorescence (a proxy for phytoplankton biomass)
- photosynthetically active radiation (PAR), to indicate light penetration
- dissolved oxygen
- turbidity.

In addition, water samples were collected on 3 April 2017 at the 14 sites for analysis of nutrients, total suspended solids (TSS) and extracted chlorophyll-*a*. Samples were collected from the top 15 m of the water column using a tube sampler, and from 3-5 m depth intervals at the deepest site (Station 5; Figure 27). A near-bottom water sample was collected also collected using a van Dorn sampler at all sites.

On the third sampling occasion (10 May 2017), repeat CTD casts were carried out at all sites, as well as the collection of 15 m depth-integrated samples for phytoplankton community characterisation.

[15] In addition to temperature and salinity, which are presented in Section 3.1.1
[16] With additional sensors.

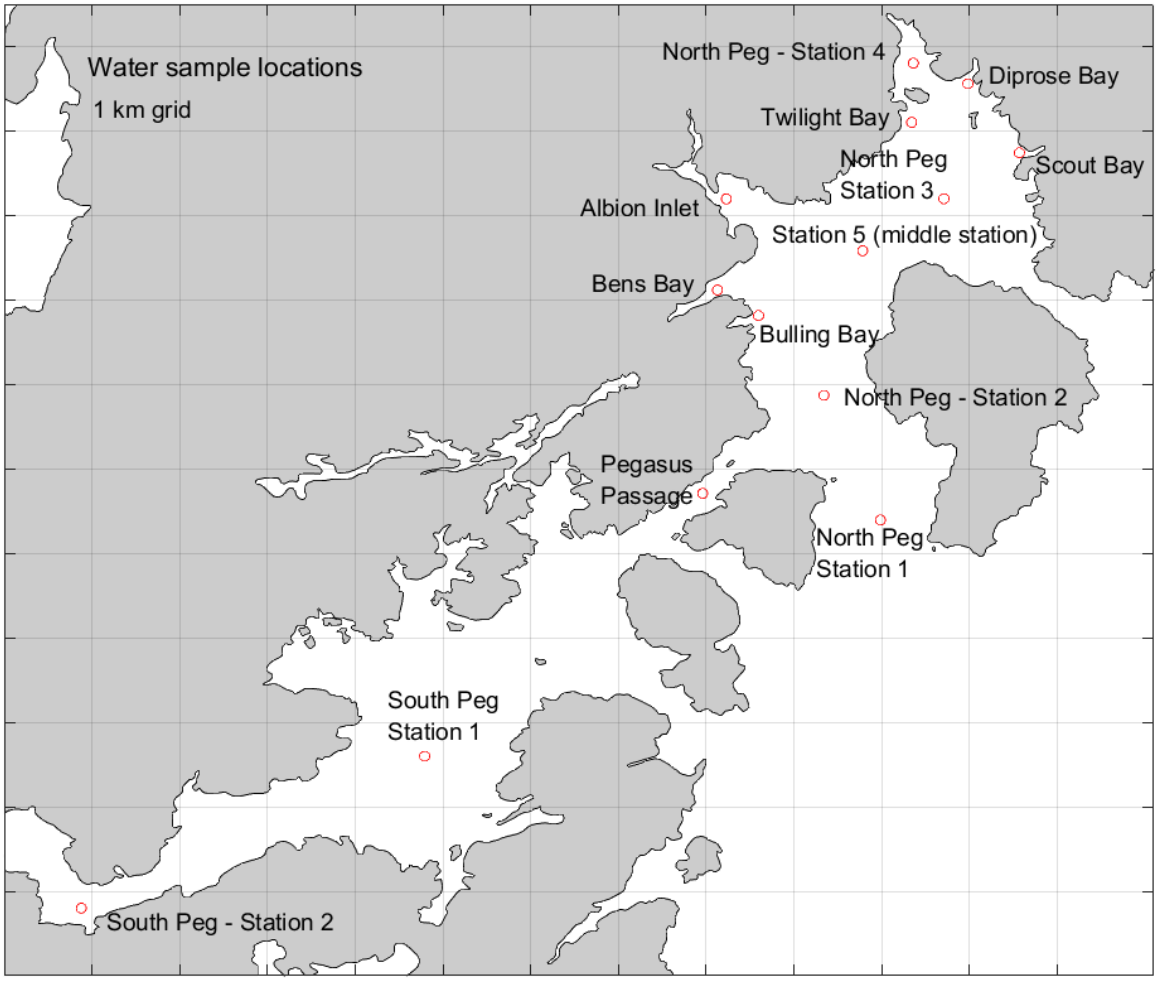

Figure 27. Water quality sampling locations throughout the North and South Arms of Port Pegasus.

4.1. Phytoplankton

4.1.1. Biomass

Mid-water chlorophyll-*a* fluorescence values were higher (> 1 mg/m^3) on 30 March and 3 April 2017, than on 10 May 2017 (maximum 0.6 mg/m^3). This was also reflected in lower turbidity and higher light penetration (photosynthetically active radiation: PAR) on 10 May 2017.

During the first CTD surveys of the North Arm (30 March and 3 April 2017) higher chlorophyll-*a* fluorescence was measured on the western side of North Arm and in Ben's Bay (Figure 28). This was associated with visibly red-discoloured water. This was believed to be caused by a localised bloom of the photosynthetic ciliate *Mesodinium rubrum*; however deterioration of samples that were collected meant this

could not be confirmed. Chlorophyll-*a* fluorescence was spatially more uniform at sites throughout the North Arm on 10 May 2017 (Figure 28).

Although only two measurements of extracted chlorophyll-*a* were undertaken in the South Arm (Figure 27), chlorophyll-*a* appeared to be substantially higher (mean of 1.5 mg/m^3; Table 11) compared to North Arm (mean of 0.4 mg/m^3; Table 11 and Figure 29). This was also consistent in the fluorescence measurements between the arms, which were about three times higher in South Arm, compared to North Arm (Table 11). The South Arm also had higher levels of turbidity (as measured by the CTD back scatter sensor: Figure 29, Appendix 5), presumably due to the higher phytoplankton biomass in this area.

Water column profile measurements taken in the centre of North Arm showed higher biomass in the surface waters (Figure 30). This did not appear to be associated with any major nutrient variations except for total nitrogen and phosphorus which also appeared slightly elevated at the surface (Figure 30).

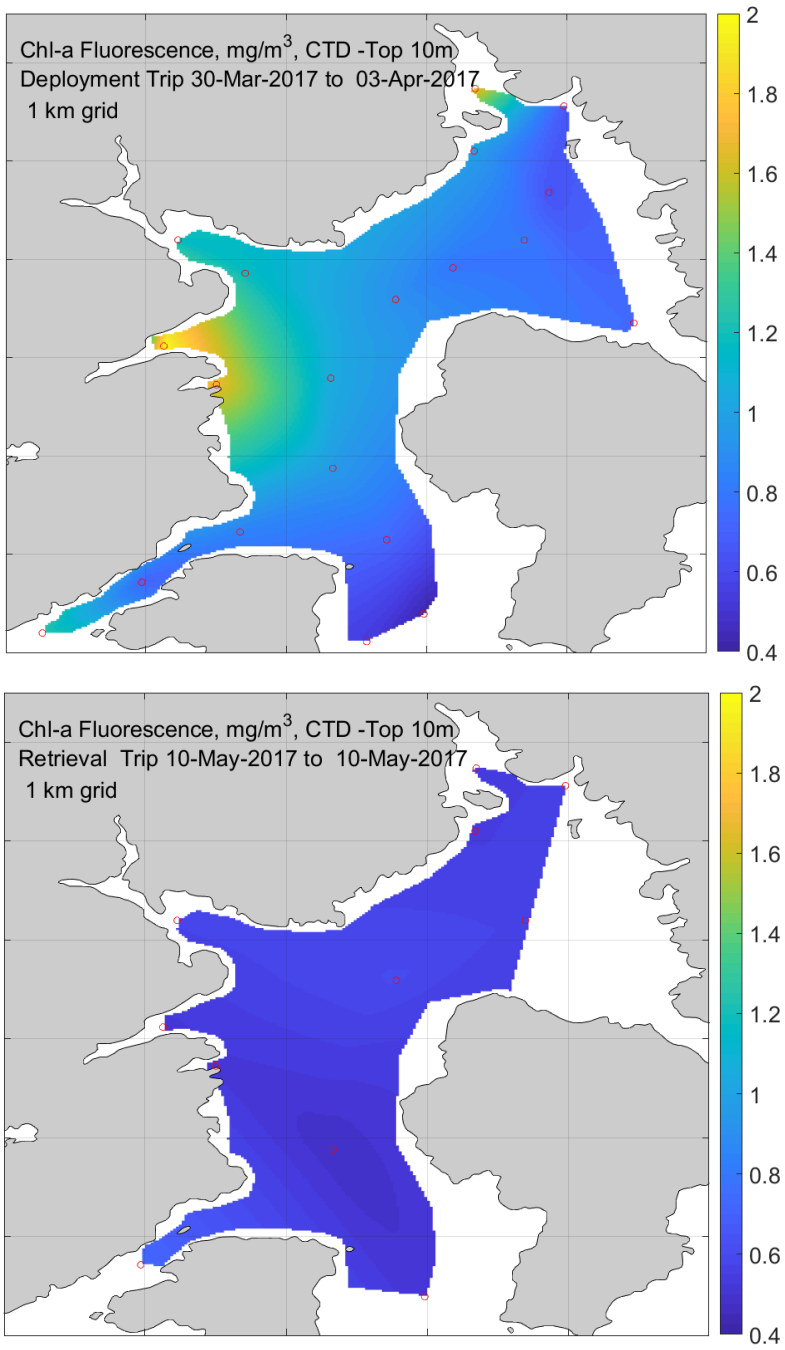

Figure 28. Mean chlorophyll-*a* concentration estimates (mg/m^3) determined by fluorometry in the top 10 m of the water column from North Arm Port Pegasus on 30 March and 3 April 2017 (top) and 10 May 2017 (bottom). Note that fluorometric measurements presented here were approximately twice as high as more accurate lab-derived extracted chlorophyll-*a* measurements (Table 11), consequently values presented here are likely overestimated.

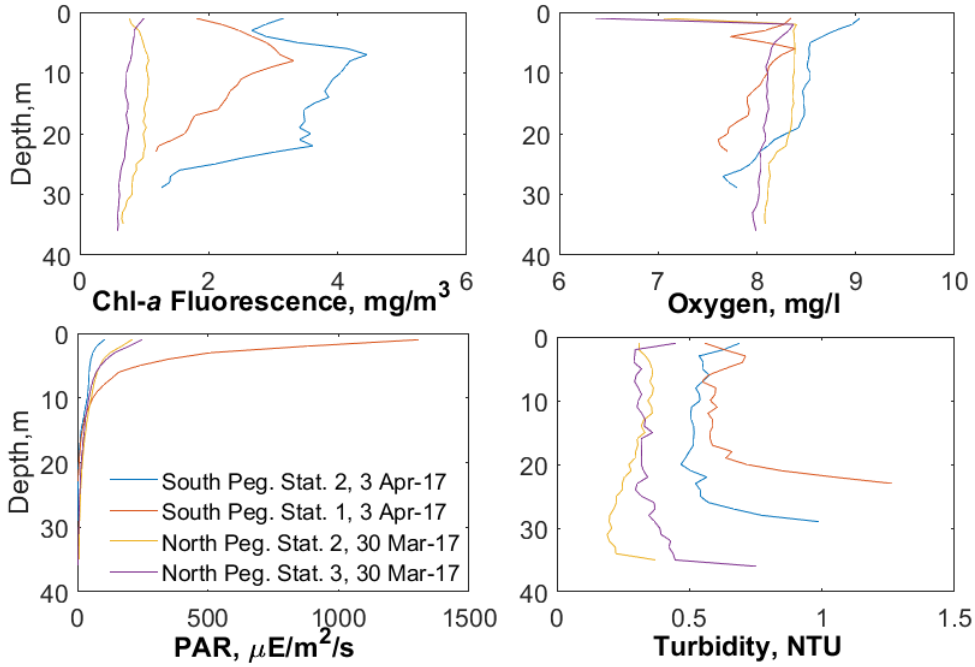

Figure 29. Profiles of CTD derived measurements of from selected sites in the North Arm and South Arm for the dates shown. Site locations as shown in Figure 27. PAR = photosynthetically active radiation, a measure of light intensity in the range of 400 to 700 nm.

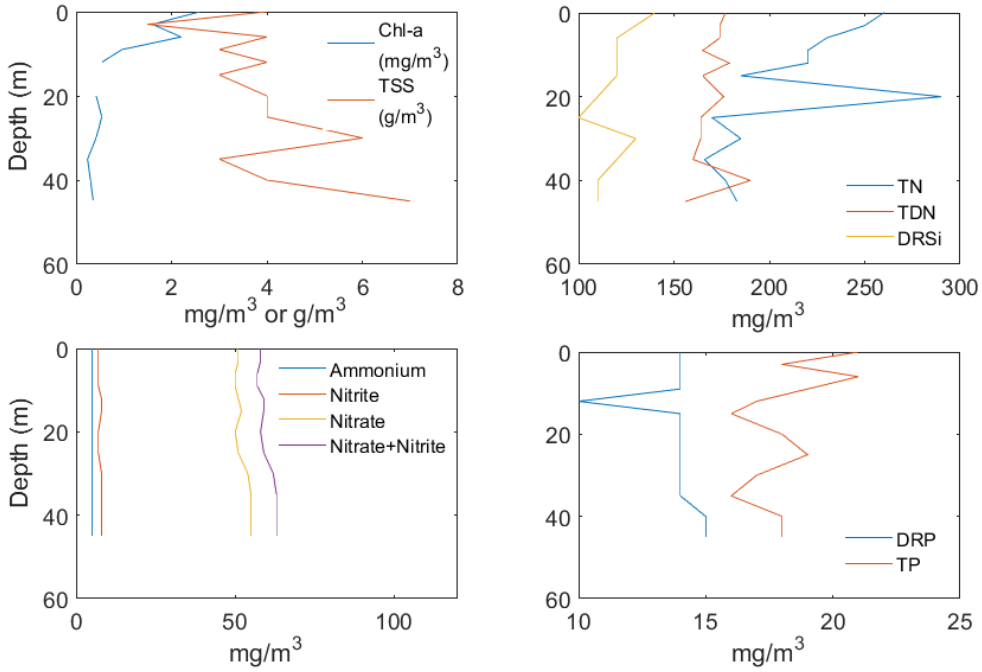

Figure 30. Profile of water quality parameters at North Arm–site 5 (middle station) from 30 March 2017. Units for all nitrogen analytes expressed in mg-N/m^3. Abbreviations are: Chl-*a* = chlorophyll-*a*, TN = total nitrogen, TDN = total dissolved nitrogen, PN = particulate nitrogen, TP = total phosphorus, DRP = dissolved reactive phosphorus, DRSi = dissolved reactive silicate, TSS = total suspended solids.

Table 11. Mean chlorophyll-*a* (chl-*a*) measurements from lab-derived extracted chl-*a* samples of 15 m integrated samples and chl-*a* estimated from *in situ* fluorescence from 3 April 2017. A subset of the same five chl-*a* fluorescence sites as the extracted measurements is labelled as 'for comparison'. Comparison of these values shows that fluorescence estimates of chl-*a* are about twice as high as more accurate lab extracted measurements, consequently fluorescence values presented here are likely to be overestimated.

Region	Mean extracted chl-*a* ± SE (mg/m^3) [sample size]	Mean chl-*a* fluorescence ± SE for comparison (mg/m^3) [sample size]	All mean chl-*a* fluorescence ± SE (mg/m^3) [sample size]
North Arm	0.40 ± 0.13 [5]	1.18 ± 0.46 [5]	0.75 ± 0.28 [15]
South Arm	1.50 ± 0.40 [2]	2.58 ± 0.43 [2]	2.58 ± 0.43 [2]

Regional / historical context

Extracted chlorophyll-*a* concentrations in Port Pegasus fall within the range of previous observations made in other regions around Stewart Island including Big Glory Bay (BGB), Patterson Inlet and Foveaux Strait (Table 12). Most recently, concentrations of chlorophyll-*a* in BGB, from July 2014 to June 2015, were also described in the monitoring reports by Stenton-Dozey et al. (2015) and ADS (2016). Stenton-Dozey et al.'s observations showed that concentrations were lowest in winter (0.2–1.2 mg/m^3) and highest in spring (1.1–2.4 mg/m^3). ADS presented similar results, but detected higher chlorophyll-*a* concentrations (up to 5.3 mg/m^3; Table 12).

Between July 1999 and July 2000, Key (2001) measured chlorophyll-*a* concentrations monthly at nine stations along a transect from inner BGB to Foveaux Strait. Minimum and maximum chlorophyll-*a* concentrations of 0.1–5.3 mg/m^3 were observed over this period with slightly higher concentrations (by about 0.2 mg/m^3) in spring in BGB, although this trend was reversed in mid-summer. Her study concluded that there had been no significant change in chlorophyll-*a* concentrations in BGB over the preceding decade.

In an older study, Bradford et al. (1991) measured chlorophyll-*a* concentrations that ranged from < 1 mg/m^3 to > 10 mg/m^3 in offshore waters in Foveaux Strait and around Stewart Island (Table 12).

Table 12. Mean and ranges of extracted chlorophyll-*a* concentrations in Port Pegasus with estimates from Big Glory Bay, Patterson Inlet and Foveaux Strait. SE = standard error, SD = standard deviation.

		Chl-*a* (mg/m^3)	
Sampling year / reference	**Region**	**Mean**	**Range**
2017 / current study	Port Pegasus North Arm	0.4	0.2-0.9
	Port Pegasus South Arm	1.5	1.1-1.9
2015 / Stenton-Dozey et al. (2015)	Big Glory Bay	1.1	0.2 - 2.4
2016 / ADS (2016)	Big Glory Bay	1.4	0.2 - 5.1
2001 / Key (2001)	Big Glory Bay	0.6	0.1 – 5.3
	Patterson Inlet	0.6	0.1 – 2.3
	Foveaux Strait	0.5	0.1 – 2.8
1988 / Pridmore and Rutherford (1992)	Patterson Inlet	0.9	± 0.1 (SE)
	Big Glory Bay	1.1	± 0.2 (SE)
1989 / Pridmore and Rutherford (1992)	Patterson Inlet	2.1	± 0.2 (SE)
	Big Glory Bay	9.0	± 1.0 (SE)
1980 / Bradford et al. (1991)	Foveaux Strait	2.2	± 0.7 (SD)
1979 / Bradford et al. (1991)	Foveaux Strait	2.5	± 0.6 (SD)
1978 / Bradford et al. (1991)	Foveaux Strait	5.3	± 2.4 (SD)
1977 / Bradford et al. (1991)	Foveaux Strait	1.7	± 0.5 (SD)

4.1.2. Phytoplankton community analysis

On the day of phytoplankton sampling (10 May 2017), phytoplankton cell numbers were low at most sites in the North Arm of Port Pegasus, but were substantially higher at the South Arm sites (Table 13). The relative difference between the two regions was consistent with the CTD fluorescence chlorophyll-*a* estimates (Table 11). The phytoplankton flora in the samples was dominated by a mix of common diatoms and flagellate taxa in both arms. Several diatom genera (*Chaetoceros* spp., *Nitzschia* spp. and *Pseudo-nitzschia* spp.) were especially numerous at the South Arm sites and these were undoubtedly responsible for the higher chlorophyll concentrations in this region. *Chrysochromulina* spp. were present at nearly all sites in both arms but were particularly numerous (32,000 cells/L) at Site 12 in the South Arm.

Some *Chrysochromulina* species have been responsible for mortalities of sea-pen salmon in Scandinavia (Dahl et al. 1989), though not to our knowledge in New Zealand. *Chrysochromulina* species belong to a large and diverse group known as the Prymnesiophytes which are globally common and important to ocean productivity. Finding a representative of this group in this type of location is not unusual, and it does not signify any inherent problem with respect to the suitability of this location for

fish farming. However, salmon farms in Big Glory Bay and elsewhere in New Zealand have, on occasion, been seriously affected by harmful algal blooms (Mackenzie 1991; Mackenzie et al. 2011). It is therefore recommended that a routine harmful phytoplankton monitoring programme be developed in Port Pegasus if salmon farms were to become established.

Table 13. Phytoplankton cells numbers (cells/litre) in the 0–15 m water column, at various sampling locations in the North and South Arms of Port Pegasus 10 May 2017. Table entries are coloured from dark blue, light blue, white, light red to dark red to indicate a gradient from low to high counts of cells. Table continued over page.

Sites	Bens Bay	Bulling Bay	Albion Inlet	Twilight Bay	Diprose Bay	Scout Bay	Nth Arm CTD 1	Nth Arm CTD 3	Nth Arm CTD 5	Nth Arm CTD 7	Nth Arm CTD 9	Sth Arm CTD 10	Sth Arm CTD 11	Sth Arm CTD 12
Diatoms														
Asterionellopsis sp.											600			
Bacteriastrum sp.	600		200											
Chaetoceros spp.	400	1000	1200	200	4200		600		1400	800	800	62000	272000	155000
Cylindrotheca sp.											200			1000
Guinardia sp.												400	600	1000
Leptocylindricus spp.													12000	2000
Navicula spp.	200	400	200	200								200		200
Nitzschia spp.	1000	1000	1000	1000	2400	600	200		600	1200	1400	4000	69000	59000
Paralia sp.				1600			800	1000						
Pleurosigma sp.														
Pseudo-nitzschia spp.	400	600	1200		1000	1200			800	600	1400	4000	44000	21000
Rhizosolenia sp.													2400	
Skeletonema costatum										1200				
Thalassionema spp.		800				600			400	400		200		
Thalassiosira spp.		400	800	200	200	400		400	200		200	600	1000	1000
Dinoflagellates														
cf. *Azadinum* sp.													3000	400
Dinophysis acuminata			200	200										400
Dinophysis acuta														400
Ceratium spp.													800	2000
Cochlodinium sp.													400	200
Gymnodinium spp.	400	200	200		200			600		400		1800	1200	3400
Gyrodinium spp.						200		200				400	400	800
Heterocapsa spp.	600		200		200	400	200	200		200		600	800	4800
Katodinium sp.										200	600		400	600
Peridinium sp.				200	200	200		600		200	600		2200	1000
Protoperidinium spp.		400		200	200								200	200
Scrippsiella spp.			200				200	200			200	200	600	200

Table 12, continued.

Sites	Bens Bay	Bulling Bay	Albion Inlet	Twilight Bay	Diprose Bay	Scout Bay	Nth Arm CTD 1	Nth Arm CTD 3	Nth Arm CTD 5	Nth Arm CTD 7	Nth Arm CTD 9	Sth Arm CTD 10	Sth Arm CTD 11	Sth Arm CTD 12
Prymnesiophytes														
Chrysochromulina spp.	600	800	400	200	200	2200	4800	8200	2400	2600		3200		32000
Raphidophytes														
Fibrocapsa japonica														200
Chrysophytes														
Dictyocha spp.			200					200	200					400
Prasinophytes												200		
Pyramimonas sp.														
Cryptomonads														
Cryptomonas sp.		800			200		2000	1000	1200			4200	800	7800
Other														
Unidentified	600	1800	200	800	1000	200	1800	1200	1000	1600		1200	2000	2600
Mesodinium rubrum						400					200	200	600	

4.2. Nutrients

4.2.1. Nitrogen

Ammonium-N (NH^{+}_{4}-N) was undetectable (< 10 mg/m^3) in all but one sample (South Pegasus Station 3-deep; 25 mg/m^3) throughout the North and South Arms of Port Pegasus in March (Table 14). Nitrate-N (NO^{-3}-N) concentrations were higher in the upper water column (0–15 m) of the North Arm, than in the South Arm (Table 14 and Figure 31).

The mean concentrations of nitrate observed in the North Arm (48.4 mg-N/m^3) were typical of New Zealand coastal waters in autumn. In mid-winter, prior to the spring bloom, it is expected that nitrate would exceed these values, while in mid-summer markedly lower concentrations would be expected. For example, summer concentrations of nitrate (1.0–3.4 mg-N/m^3) were recorded in Patterson Inlet and Big Glory Bay (BGB) (Pridmore and Rutherford 1992; Table 15).

The levels of total dissolved and particulate nitrogen in Port Pegasus were comparable to concentrations observed by Pridmore and Rutherford in BGB in 1988 and somewhat lower than observed in 1989 (Table 15).

Table 14. Mean concentrations of nitrogen nutrients (mg/m^3) in the water column (0–15 m) at sampling stations in the North (11 sites) and South Arms of Port Pegasus (3 sites), 3 April 2017. Note that dissolved inorganic nitrogen (DIN) is marked with ***** as it has been derived from nitrate (NO^{-3}-N), nitrite (NO^{-2}-N) and a nominal ammonium (NH^{+4}-N) value set at half the detection limit (5 mg/m^3). Other abbreviations are: TN = total nitrogen, TDN = total dissolved nitrogen, PN = particulate nitrogen. Means have been calculated by specifying concentrations at half the detection limit where lab results were below detection, all raw data can be found in Appendix 6.

Location	TN	TDN	PN	NH^{+4}-N	NO^{-3}-N	NO^{-2}-N	DIN*
North Arm	214.9	170.8	44.1	<10	48.4	6.9	60.3
South Arm	191	164.7	26.3	<10	20.3	2.7	28

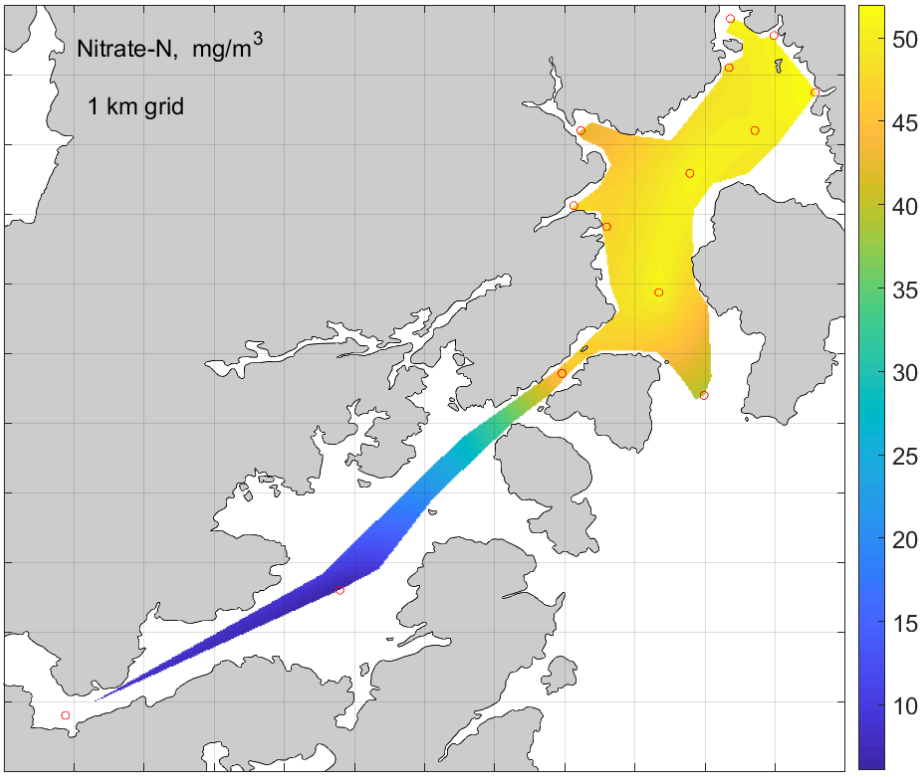

Figure 31. Nitrate-N concentrations (mg/m^3) in the North and South Arms of Port Pegasus 30 March 2017.

Table 15. Mean (±SE) summer nitrogen concentrations (mg/m^3) in Paterson Inlet and Big Glory Bay 24 February 1988 and 11–12 January 1989 (from Pridmore and Rutherford 1992). nd = not detectable.

	Urea-N	NH^+_4-N	NO^-_3-N	PN
1988				
Patterson Inlet	2.3 ± 1.2	16.4 ± 3.6	nd	35.2 ± 2.9
Big Glory Bay	1.9 ± 1.8	26.1 ± 4.2	1.0 ± 0.2	42.5 ± 4.3
1989				
Patterson Inlet	3.0 ± 1.0	7.9 ± 1.3	3.4 ± 1.0	63.1 ± 1.2
Big Glory Bay	5.2 ± 1.0	2.3 ± 0.3	1.3 ± 0.4	90.4 ± 10.7

Regional / historical context

In addition to the studies of Pridmore and Rutherford (1992; Table 15) there have been a number of other water quality assessments of BGB that provide useful data for comparison with the Port Pegasus observations (Table 16). Between July 1999 and July 2000, Key (2001) measured inorganic nitrogen concentrations monthly at nine stations on a transect from inner BGB to Foveaux Strait. Nitrate concentrations were usually the same or lower in BGB than in more open waters. She observed that

NH^{+4}-N concentrations at the same location could change substantially over short time periods (e.g. 30.7–466.0 mg/m^3 over 4 days; Table 16). This latter value was exceptional. In general NH^{+4}-N concentrations were higher in BGB than those observed in Foveaux Strait and Patterson Inlet at this time (especially from April to July). It is conceivable that the elevated NH^{+4}-N concentrations may have been associated with salmon farm discharge, especially during winter when rates of phytoplankton nutrient assimilation were minimal. Key (2001) concluded that total oxidised nitrogen (nitrate + nitrite) concentrations had not changed significantly over the previous decade in BGB and Patterson Inlet.

O'Callaghan (1998) observed variations in nitrate and nitrite of 3.8–54.9 mg-N/m^3 and 1.3–12.6 mg-N/m^3, respectively, over tidal cycles in spring and summer at the entrance to Big Glory Bay. These results are consistent with more recent sampling by ADS (2016), who measured mean nitrate concentrations of 43 mg-N/m^3 over the period February to August 2016. These concentrations were similar to what was observed in Port Pegasus (Table 16).

Although their observations did not extend as far south as Port Pegasus, Bradford et al. (1991) found that the surface distribution of nitrate concentrations (as well as salinity, temperature and chlorophyll-*a*) in the Foveaux Strait/Stewart Island region were highly variable over four successive summers (February 1977 to February 1980). Nitrate-N ranged from < 10 to 60 mg/m^3 and higher concentrations were observed associated with cooler higher salinity waters intruding into the region from the south.

Table 16. A summary comparing inorganic nutrient (mg/m^3) concentration observed in this study with those in Big Glory Bay from academic studies and monitoring reports. nd = not determined.

	NH^{+4}-N	**NO^{-3}-N**	**DRP**
This study	< 10	20.3–48.4	9.7–12.7
O'Callaghan 1998	nd	1–55	14–17
Key 2001	31–466	< 1–102	< 1–35
ADS (2016) Feb-Aug 2016	26–81 (mean ≈ 44)	20–90 (mean = 43)	9–26 (mean = 18)
Bradford et al. 1991	nd	< 10–60	nd

4.2.2. Phosphorus and silica

Dissolved reactive phosphorus (DRP) and dissolved reactive silicate (DRSi) concentrations were appreciably lower at the South Arm sites compared to those in the North Arm (Table 17). The higher concentrations of DRP in North Arm were within

typical ranges observed for Queen Charlotte (mean 14 mg/m^3) and Pelorus Sound (13 mg/m^3) in Marlborough (Marlborough District Council [MDC] State of the Environment [SOE] monitoring data; see e.g. Broekhuizen 2013 for Pelorus Sound).

Concentrations of DRSi in North Arm were similar to other more oceanic-influenced coastal waters such as Queen Charlotte Sound (127 mg/m^3), but were substantially lower than regions more heavily impacted by freshwater runoff, such as Pelorus Sound (337 mg/m^3).

Table 17. Mean concentrations of phosphorus and silicate nutrients (mg/m^3) in the water column (0-15 m) at sampling stations in the North (11 sites) and South Arms of Port Pegasus (3 sites) 3 April 2017. Means have been calculated by specifying the half the detection limit for where lab results were below detection, all raw data can be found in Appendix 6. Abbreviations are: TP = total phosphorus, DRP = dissolved reactive phosphorus, DRSi = dissolved reactive silicate.

Locations	TP	DRP	DRSi
North Arm	17.8	12.7	114.3
South Arm	16	9.7	60

4.2.3. Nutrient molar ratios

Molar ratios of dissolved inorganic nitrogen (DIN) and phosphorus (DRP) in the upper and lower water column within the North Arm ranged from 10.2 to 11.0 (Table 18). In the South Arm, the DIN/DRP ratios were significantly lower (5.7–7.6; Table 18). As the ratios are less than a Redfield ratio of 16:1 (a typical ratio of N:P in marine phytoplankton), this indicates that nitrogen was likely limiting growth at the time of sampling though available nitrogen was not exhausted. Nitrogen is almost invariably the major limiting nutrient for phytoplankton growth in coastal waters worldwide, so this result is not unusual.

The relatively higher ratio values in the North Arm are typical of coastal waters elsewhere in New Zealand during winter or other times when phytoplankton productivity is low. The lower values in the South Arm were more typical of periods when phytoplankton production is higher in spring and summer. For example, in Queen Charlotte Sound winter and summer DIN/DRP ratios average 10.6 and 6.1, respectively (MDC SOE data[17]), which are close to the ratios observed in Port Pegasus. The lower DIN/DRP ratio in South Arm is likely attributable to the draw-

[17] Ratio analyses performed by the author.

down of inorganic nitrate relative to phosphorus by the higher phytoplankton biomass that existed in this inlet at this time.

Molar ratios of DRSi to DIN were lower than the Redfield ratio for diatoms (Table 18), as were DRSi/DRP ratios, although they are also typical of other New Zealand coastal waters that are not significantly impacted by freshwater inputs. The Redfield ratio for diatoms refers to a typical nutrient stoichiometry for this group, which require silicate for growth and is not the case for other phytoplankton groups (e.g. dinoflagellates). Transient reductions of DRSi concentrations due to uptake by diatoms blooms are not uncommon for typically fast-growing diatom species, but it tends to be rapidly regenerated or resupplied in most situations.

Table 18. Molar ratios of macronutrients in upper (0–15 m) and lower water column (deep) of the main arms of north and south Pegasus Bay and minor embayments in the North Arm, 30 March 2017.

	DIN/DRP	Tot-N/Tot-P	DRSi/DIN	DRSi/DRP
North Pegasus transect (0–15 m)	10.9	7.7	0.5	5.1
North Pegasus deep	11.0	8.6	0.4	3.9
North Pegasus bays (0–15 m)	10.2	7.3	0.5	5.2
South Pegasus (0–15 m)	5.7	3.9	0.7	3.7
South Pegasus deep	7.6	5.2	0.6	4.2

cf. Redfield ratio for diatoms Si:N:P = 15:16:1 (Redfield 1934).

4.3. Dissolved oxygen

Dissolved oxygen (DO) concentrations were high (close to 100% saturation) throughout the water column at all stations in the North Arm of Port Pegasus (Table 19). This is indicative of the dynamic, well-mixed nature of the water column in the inlet. By comparison, Stenton-Dozey et al. (2015) measured oxygen levels as low as 4.7 mg/L (July 2014) and as high as 12.5 mg/L (June 2015) in Big Glory Bay. They observed that in the spring DO changed little with depth, but in winter near-surface waters and deeper waters were below and above saturation levels (respectively). In the summer this pattern was reversed and DO concentrations were saturated towards the surface. The authors did not did not suggest any reasons for the observed patterns of water column DO, but it is assumed they are due to natural seasonal variations.

Aquadynamic Solutions (ADS 2016) reported dissolved oxygen concentrations from six stations (July 2015–August 2016) in Big Glory Bay ranging from 6.8–12.4 mg/L

and made the comment that: ‘There is no indication that fish or mussel farming activities are having any adverse impacts on oxygen levels in the bay.’

Table 19. Dissolved oxygen concentrations parameters (mg/L and % saturation) through the water column CTD profiling stations in the North Arm of Port Pegasus on 30 March 2017.

Station & depth	Maximum		Minimum		Near-bottom	
	mg/L	% satn	mg/L	% satn	mg/L	% satn
CTD-1 (43.8 m)	10.6	102.9	7.8	91.9	8.1	95.0
CTD-2 (38.4 m)	10.7	102.9	8.1	95.2	8.1	95.5
CTD-3 (34.7 m)	9.7	99.9	8.0	92.6	8.1	95.3
CTD-4 (38.1 m)	9.7	100.8	8.1	90.5	8.1	95.1
CTD-5 (48.2 m)	9.8	101.8	8.1	92.2	8.1	95.9
CTD-6 (40.4 m)	9.6	99.6	8.1	89.0	8.2	96.3
CTD-7 (38.2 m)	9.6	101.1	8.1	89.5	8.2	96.0
CTD-8 (35.6 m)	9.5	98.7	7.9	88.7	8.2	96.9
CTD-9 (18.0 m)	9.6	99.8	7.9	95.9	7.9	92.9

4.4. Summary

Although synoptic sampling of the water column in North and South Arms showed an environment predominantly influenced by southern oceanic seawater (low temperature, high salinity; see Section 3.1.1), the North and South Arms had comparatively different nutrient and phytoplankton characteristics due to their different morphologies and water exchange dynamics. The nutrient environment in the North Arm at the time of sampling was consistent with water frequently refreshed by exchange with adjacent coastal waters, whereas the South Arm appeared to have comparatively less exchange.

At the time sampling was carried out, the high nutrient/low phytoplankton biomass condition in the North Arm probably reflected the conditions in the wider ocean environment. These conditions are typical for this time of year when phytoplankton production is declining because of a shorter day length and less solar irradiation and subsequently higher nutrient concentrations are available (especially of nitrate). In the relatively more enclosed waters in the South Arm, a higher phytoplankton biomass and consequently, lower dissolved nutrients regime, had apparently persisted until later in the season.

The phytoplankton flora was dominated by a mix of diatoms and flagellate taxa common throughout New Zealand’s coastal waters. The occurrence of a potentially ichthyotoxic (fish-killing) species in the phytoplankton community is not unusual.

5. ASSESSING POTENTIAL PELAGIC CHANGES FROM AQUACULTURE

Given the limited time-series available on annual or multi-annual variation in the water column properties of North Arm, we have used a two-pronged approach to our assessment:

1. Firstly, we estimate an initial production level, using information from a comparable farming site in Big Glory Bay (BGB).
2. Secondly, we estimate potential pelagic changes from high levels of salmon production. To do this, we apply quantitative methods and modelling to extend the initial analysis from (1) to consider the maximum potential pelagic effects that could result from the largest production scenario/s considered (6,000 tpa max.).

5.1. Parallels with existing aquaculture

In order to place the proposal in the context of existing salmon activities which have been monitored previously, we began our assessment with a search for potential comparative sites. The highest production scenario (scenario 1a; refer Table 1 on page 6) considered in this report is 6,000 tpa for North Arm (feed input of about 10,000 tpa excluding smolt feed). Although this level of production is consistent with the 'high-flow' salmon farming sites in Tory Channel (Marlborough Sounds), the extremely high current speeds observed in Tory Channel means it is not a suitable environment for comparison[18]. Consequently, we have focused our analysis on BGB, which has a similar latitude, a lower production level and a more comparable low-flow environment[19].

5.1.1. BGB production and history

Big Glory Bay is located on the eastern side of Stewart Island, north of Port Pegasus. The embayment has a similar surface area to North Arm (Figure 32) and a similar low-flow regime (typically less than 0.05–0.1 m/s; Rutherford et al. 1988). Thus it represents a useful context for considering the potential effects of finfish aquaculture in North Arm.

Big Glory Bay has a long history of salmon farming (about 30 years). Production levels for BGB of 3,000 tpa were initially predicted based on nitrogen emissions, and an estimate of 3,400 tpa to prevent oxygen issues (Rutherford et al. 1988). In recent years site production has been about 3,500 tpa (Jaco Swart, Sanford Farm manager pers. comm.).

[18] This is due to the lower current speeds observed and modelled in North Arm.
[19] Note there were very few data available on water quality changes associated with low-flow farms in the Marlborough Sounds to allow comparison with those sites.

Although BGB salmon production is about half that of the highest production scenario considered in this report, there are similarities between the North Arm and BGB areas (e.g. latitude, area, tidal range etc.). Consequently, we consider BGB as a suitable 'yardstick' for considering an initial limit for North Arm. However, there are also likely to be some hydrological differences (e.g. flushing times, depths and number of entrances) and the potential mitigating effects of mussel farming in BGB, so a perfect comparison is not possible.

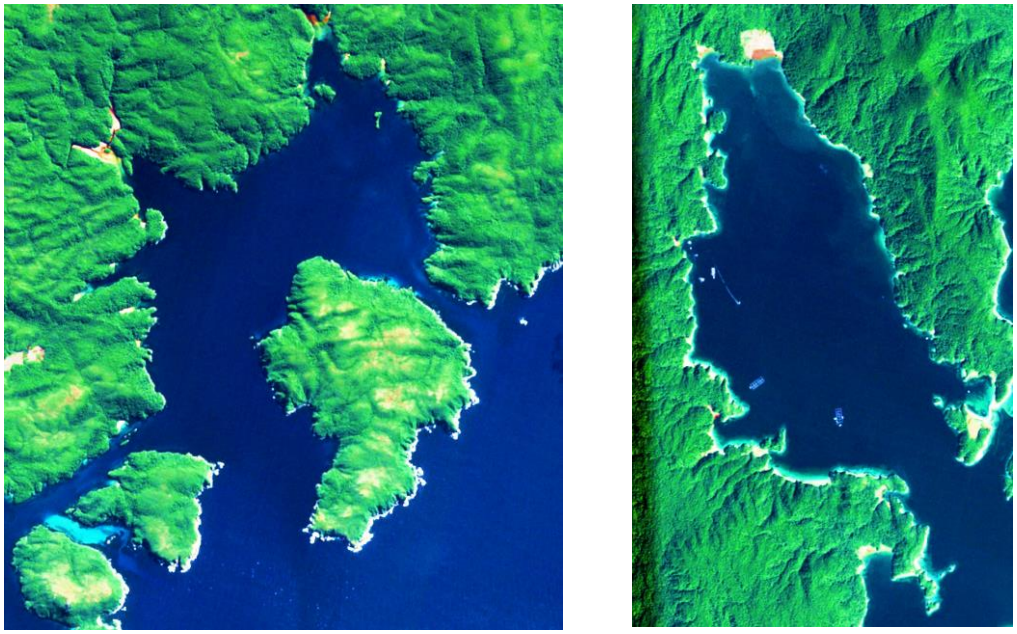

Figure 32. Sentinel 2 satellite images at the same spatial scale showing similarities between North Arm (left) and Big Glory Bay (right). Note that Big Glory Bay has been rotated 90 degrees clockwise to aid comparison. Source: European Space Agency.

We also recognise that no two locations will have identical responses in their pelagic environments to finfish aquaculture. For instance, the large biomass of green-lipped mussels (GLM; *Perna canaliculus*) in BGB could act to suppress phytoplankton response to new nutrients in that region. Similarly the water in BGB appears to be more tannin-coloured than Port Pegasus and hence some additional attenuation of light is possible, which could act to reduce phytoplankton growth. This tannin material was also implicated in potentially binding iron which could also help support blooms (MacKenzie 1991). Mussels also process non-phytoplankton material and have also been known to increase observed chlorophyll-*a* concentration in summer conditions by increasing the availability of dissolved nitrogen (Ogilvie et al. 2003). Consequently, there are differences between the regions which could both act to increase, or supress, a phytoplankton response. However, for the purposes of our assessment we consider the regions comparable.

Harmful algal bloom event in Big Glory Bay

In January 1989, a large fish-killing harmful algal bloom (HAB) occurred during a period of calm summer weather in BGB (MacKenzie 1991). This HAB event appeared to be associated with an out-of-bay sourced intrusion of high nitrogen (N) water which also may have transported algal cells into BGB. However, it is likely that the contribution from salmon waste nutrients led to an increased bloom intensity (e.g. Pridmore and Rutherford 1991). The event inflicted substantial losses on the cultured salmon (Chang et al. 1990), but MacKenzie (1991) noted that:

> Despite the mass mortalities within the sea cages, there was little evidence of effects on other flora and fauna. Scuba and shoreline observations revealed an abundance of fish (including wild salmon) and healthy invertebrate life; shellfish seemed to be unaffected. It appeared that these species could either avoid dense concentrations of the algae or were adapted to resist their effects. Throughout the duration of the bloom there were only rare accounts of the death of other species besides salmon and without the presence of the sea cages the event would probably have gone unnoticed.

Since this early HAB event, salmon farming has continued in BGB without significant HAB issues reoccurring. Based on previous studies and recent water quality monitoring information from BGB (ADS 2016; Stenton-Dozey et al. 2015), it appears that the BGB farm has operated below a pelagic 'carrying capacity' for finfish aquaculture for the area with a recent report noting:

> In the five month data set, chl-*a* levels were lowest in the autumn/winter months and highest spring (September and October 2014), indicative of phytoplankton blooms coincident with warmer water and longer daylight. In previous years, distinct seasonal patterns were evident simultaneously at all six stations across the bay which suggests that variations in chl-*a* are driven by natural processes (or other large-scale factors) unrelated to the presence of the marine farms. (Stenton-Dozey et al. 2015)

5.2. Assessment of initial production levels in North Arm; comparison to aquaculture effects observed in Big Glory Bay

To draw meaningful parallels between effects of salmon farming in BGB, we used some of the models discussed earlier in the report consider two questions:

- What is the difference in residence times in North Arm, compared to in Big Glory Bay?

- What are the cumulative changes in nitrogen concentrations in North Arm?

5.2.1. Differences in the residence times of North Arm compared to Big Glory Bay

In order to improve our knowledge of the relative differences between North Arm and BGB, we have calculated and compared the modelled relative residence time characteristics between the two areas. For North Arm, the hydrodynamic model results in Section 3 was used, and for BGB, the 'box model' used by Pridmore and Rutherford (1992). Determining the differences in residence time characteristics will provide context for qualitatively assessing the potential for pelagic effects from salmon aquaculture in North Arm relative to BGB.

The three-dimensional hydrodynamic model approach to determining residence time (Section 3) is different[20] to the drogue approach adopted by Pridmore and Rutherford (1992), although it is relevant that both approaches include wind. Consequently, we also make a comparison using basic tidal-prism-based residence time estimate which ignores the effect of wind-driven currents.

For the tidal-prism estimates of residence time, Rutherford et al. (1988) note that the tidal-prism is about 10% of the volume of BGB and therefore the tidal residence time for BGB is about 5 days. However, when considering the results of their drogue studies they estimate a more likely residence time is about 10 –13 days under light winds. The tidal residence time for North Arm is about 8 days[21] (i.e. about 60% longer than BGB). Using the North Arm particle model with all farm sites (f1 to f4 and s1; Figure 3)[22] operating at scenario 1a production levels, we estimate the residence time of salmon farm wastes is about 18 days (Figure 33). This period is about 40% to 80% longer than the BGB range estimate of 10–13 days (Pridmore and Rutherford 1992).

[20] The 3-D hydrodynamic model has the advantages of being able to accommodate the complex flows that result from multiple entrances such as those in North Arm. This model can also provide information on the potential connectivity to the nearby South Arm of Port Pegasus.

[21] Note that the tidal prism volume of North Arm is estimated to be 20.23 x 10^6 m^3, assuming a tidal range of 1.8 m; the total volume is 321.87 x 10^6 m^3.

[22] Note that the smolt site (f5) is not included in our calculations, as it represented less than 2% of the total feed inputs under the production scenarios considered (Table 1).

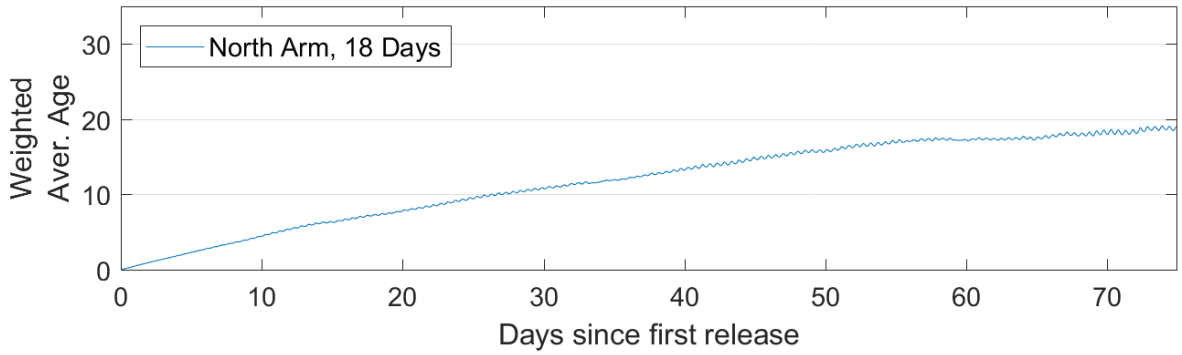

Figure 33. Average age of modelled particles released in the North Arm of Port Pegasus over a 75-day period from 15 April to 26 June 2017, assuming feed-weighted release of aged particles across all potential farm sites. This result suggests the mean residence time of released farm wastes is about 18 days.

5.2.2. Initial production estimate

Both residence time estimates suggest that the residence times in North Arm are considerably longer than in BGB. Because the relative differences in the residence times between North Arm and BGB were reasonably consistent between the tidal prism estimates (60% longer in North Arm) and the other residence time estimates (40% to 80% longer), we can be reasonably confident in the relative differences between the two regions. The results imply that nutrients released from salmon farming in North Arm would be retained about 60% longer than they are in than BGB. Assuming nutrient retention is the limiting constraint for pelagic effects, we can infer that initial production levels for North Arm would be about 60% lower, at 2,200 tpa based on BGB production of 3,500 tpa[23].

Given that BGB sits within the larger system that is Patterson Inlet, one could argue that there is potential for greater retention of nutrients than in North Arm which is bounded only by the southern ocean. However, with only limited information available on the wider circulation of BGB, it is difficult to quantify what the effect Patterson Inlet has on the retention of salmon-derived wastes, but one would expect it would potentially increase the retention time. Consequently, we note that 2,200 tpa is probably a lower bound estimate for a production limit in North Arm. Considering these geographical differences, it is possible that a slightly higher production level could be achieved without substantial risk of adverse pelagic effects (e.g. the 2,540 tpa estimated as a minimum economic break-even point [Clough and Pambudi 2017]).

[23] 3,500 tpa / 1.6 = 2,187 tpa

5.2.3. Summary

BGB has a current salmon production of 3,500 tpa, which appears to have limited wide-scale pelagic effects in the BGB region. North Arm appears to have a longer residence time than BGB (i.e. it is more poorly flushed than BGB) and it will therefore have higher levels of nutrient retention from finfish aquaculture than BGB. Based on these findings, we estimate an initial production scenario (IPS) to be about 2,200 tpa, or about two-thirds of the current stable BGB production.

5.3. Estimate of potential effects from higher production scenarios

Critical production limits of up to 9,650 tpa had been estimated for BGB (Rutherford et al. 1988)[24], but the realisation of levels anywhere near this level of production has not eventuated in the region. As such, there is no applicable parallel that can be drawn between BGB and North Arm for the higher production scenarios that are considered (e.g. up to 6,000 tpa; Table 1). Consequently, we use a modelling approach to assess the potential effects from higher production scenarios.

5.3.1. Model overview

Two models were used to assess potential effects from salmon production levels above the IPS level (2,200 tpa) determined in the previous section. Firstly we perform particle-tracking to estimate the scale of likely nitrogen changes in the area. We then apply a logistic phytoplankton model to estimate potential phytoplankton changes.

Particle tracking of nitrogen wastes

Particle tracking, described previously in Chapter 3, was used to simulate the release and transport of nitrogen (N) from salmon farming scenarios. This information is used to estimate potential cumulative effects in North Arm from proposed salmon farming scenarios (Table 1).

As in Pridmore and Rutherford (1992), we only consider N in our modelling assessment. This is because:

1. Nitrogen is the main macronutrient released from salmon farming (e.g. Buschmann et al. 2007)
2. Nitrogen is typically the limiting nutrient to phytoplankton production in marine waters around New Zealand, and has been shown to be limiting at BGB, Stewart Island (Pridmore and Rutherford 1992)[25].

[24] Based on a very high nutrient loading estimate of 258 kgN/tpa production, a critical chlorophyll-*a* concentration of 15 mg/m^3 and a low 7–9 day residence time for BGB under moderate winds.

[25] Note that the micronutrient iron (Fe) has been associated with limiting the southern ocean waters that surround Stewart Island, and chelated forms of iron were implicated by MacKenzie (1991) as a possible contributing factor to a bloom event in Big Glory Bay. Consequently, it is possible that iron may also be limiting to phytoplankton growth in North Arm. However, insufficient information is available to be able to be able to make an informed assessment of its potential role in phytoplankton growth.

Nitrogen release and transport from each of the four salmon farming scenarios (1a to 4a; Table 1) was modelled using the particle tracking hydrodynamic models described in Chapter 3. The release and transport of waste N loads from salmon farming scenarios were modelled through the use of neutrally buoyant passive particles within a hydrodynamic model. The model was run over a period of 75 days, with each particle released within the net pen area. The nitrogen load of released particles equated to the estimated salmon N emissions that would be released for each production scenario. While the modelling approach differed from the approach of Pridmore and Rutherford (1992) for BGB, the outputs were similar to that of a box model, because the N load was averaged over North Arm.

Net annual salmon N emissions are estimated to be 68.3 kg N/t fish production; see Table 20 for the assumptions and calculations on which this was based. This emission estimate is lower than Rutherford et al. (1988) used in BGB; who cited N emissions of 100 kg N/t fish production (cited within as Weston 1986). The higher emission rate from Rutherford et al. (1988) is consistent with our summer estimate. This is because N emissions are proportional to feed, and the level of feed is typically 50% higher in the summer period (Table 20)[26].

In a southern area such as Stewart Island, low light and temperature can restrict the growth of phytoplankton in the winter, thus pelagic effects are more likely to be observed in the spring/summer. Consequently, to model a ‘summer’ feeding period we adopt the higher emission value (100 kg N/t fish production) used by Rutherford et al. (1988), as a more conservative approach[27].

[26] Our estimate of 68.3 kg/tpa production x1.5 = 102 kg/tpa production

[27] We note Rutherford et al. also consider a higher N release estimate of 258 kgN/tpa production, which was empirically derived from field measurements. This value seems much higher than is feasible under typical modern salmon farming practices and hence is not considered in our assessment.

Table 20. Mean total nitrogen (TN) and dissolved nitrogen (DN) emissions from Chinook salmon farming expressed in kg per tonne of feed and per tonne of production. The key information used to arrive at these emission levels are provided. The net DN excretion values for summer are used in the modelling for this report and hence are higher than those shown here. Values indicated with a * are based on industry-provided information and are representative of typical operations, but may vary throughout and between years. Typical summer feed levels are approximately 50% higher than mean annual feed which results in higher nitrogen emissions, these are also shown.

Description	Value
Feed conversion ratio* (FCR; wet weight fish to dry feed)	1.7*
Percentage protein in feed*	40%*
Percentage N in protein (Stead and Laird 2002)	16%
Fish N (kg/tonne of fish) (Bromley and Smart 1981)	27.20
% faeces production (Butz and Vens-Cappell 1982)	26%
% N in faeces (Penczak et al 1982)	4%
Estimated benthic N loss (e.g. Broekhuizen et al. 2015)	75%
DN emissions (kg per ton fish)	63.9
DN emissions (kg per ton feed)	37.6
TN emissions (kg per ton fish)	81.6
TN emissions (kg per ton feed)	48.0
Mean annual DN emissions (kg per ton fish)	**68.3**
Mean annual DN emissions (kg per ton feed)	**40.2**
Summer DN emission rate x summer feed levels (kg per ton fish)	**102**

Logistic phytoplankton model

Another way of assessing an effect is the approach of Rutherford et al. (1988), who considered potential changes to phytoplankton blooms (and associated chlorophyll-*a*) from salmon-derived N in BGB. In their assessment they consider a logistic modelling approach, which incorporates residence time to estimate maximum chlorophyll-*a* changes from salmon-derived N. They estimate that 'maximum chlorophyll-*a* concentrations of 15 mg/m^3 are likely if 'available' nitrogen concentrations approach 300 mg/m^3 …' (Rutherford et al. 1988). Based on this 'threshold' they arrived at a level of salmon production of 3,000 tpa for BGB.

We applied this model to North Arm for assessing potential changes under this extreme scenario. The key component of the model of Rutherford et al. (1988) is a logistic growth equation. This model relies on an equation described in Pridmore and Rutherford (1992), which requires an estimate of the potential maximum achievable chlorophyll-*a* concentration. Pridmore and Rutherford based their estimate of the

maximum chlorophyll-*a* concentration on a relationship of observed field maxima of chlorophyll-*a* to particulate nitrogen (PN) during periods of dissolved nitrogen limitation from a variety of marine and freshwater sources (Pridmore and Rutherford 1992)[28].

This maximum chlorophyll-*a* (Chl-*a*) equation estimate is presented as:

$$Chl\text{-}a = 0.0876 \times N - 0.253 \quad (1)$$

where N is the available nitrogen concentration. For the purposes of differentiating this value from other model outputs we refer to it as the maximum logistic chlorophyll-*a*.

In order to model North Arm using the same logistic approach of Pridmore and Rutherford (1992) we parameterised their model with an 18-day residence time, initial and boundary chlorophyll-*a* concentrations of 1 mg/m^3 and a maximum growth rate of 0.5 /day[29]. We do not repeat all of the detailed equations here, as they can be found in Pridmore and Rutherford (1992). Available nitrogen was also a key component of the model and was estimated to have a base of 104 mg/m^3 for North Arm (PN + DIN; Table 14) and was increased for scenario assessments based on the outcome of N modelling results.

The model was originally developed for assessing potential effects from salmon farming (e.g. Rutherford et al. 1988) and was subsequently used for comparison to the BGB bloom event of 1989 (Pridmore and Rutherford 1992). We note that logistic model presented by Pridmore and Rutherford (1992) was able to reproduce the magnitude of the 1989 event. However, the model overestimated the magnitude of chlorophyll-*a* concentrations in the preceding year (1988) and the following 27 years, during which another major bloom event has not occurred. Consequently, this model appears to be very conservative in the case of BGB (i.e. it almost always overestimates the chlorophyll-*a* response). Therefore it will not predict 'likely' phytoplankton changes for North Arm, but it is still useful for highlighting potential maximum changes in phytoplankton from salmon-farming N.

5.3.2. Particle tracking model results

The particle tracking results of releases from proposed aquaculture sites in North Arm over a 72-day period showed that the majority of particles released from the farm areas were not retained in the arm (only 19.7% retained; Figure 34). Of the 80% of particles that are not retained in North Arm, most were lost to the Southern Ocean, with about 1% of the particles transported into South Arm.

[28] Note that Pridmore and Rutherford (1992) is cited here, as their paper provides additional details on the data used to determine the maximum chlorophyll-*a* to nitrogen relationship.
[29] See Pridmore and Rutherford (1992) for a full description of the model.

This result implies there would potentially be small increases in total nitrogen (TN) transferred to the South Arm under a 'worst case' summer feeding scenario[30]. However, difficultly in reconciling the modelled and measured currents in Port Pegasus means that some uncertainty exists in this modelling-based assessment. However, given good match-ups with measured currents in North Arm and stable numbers of particles observed by day 50, we consider the North Arm N change estimates reliable (Figure 34).

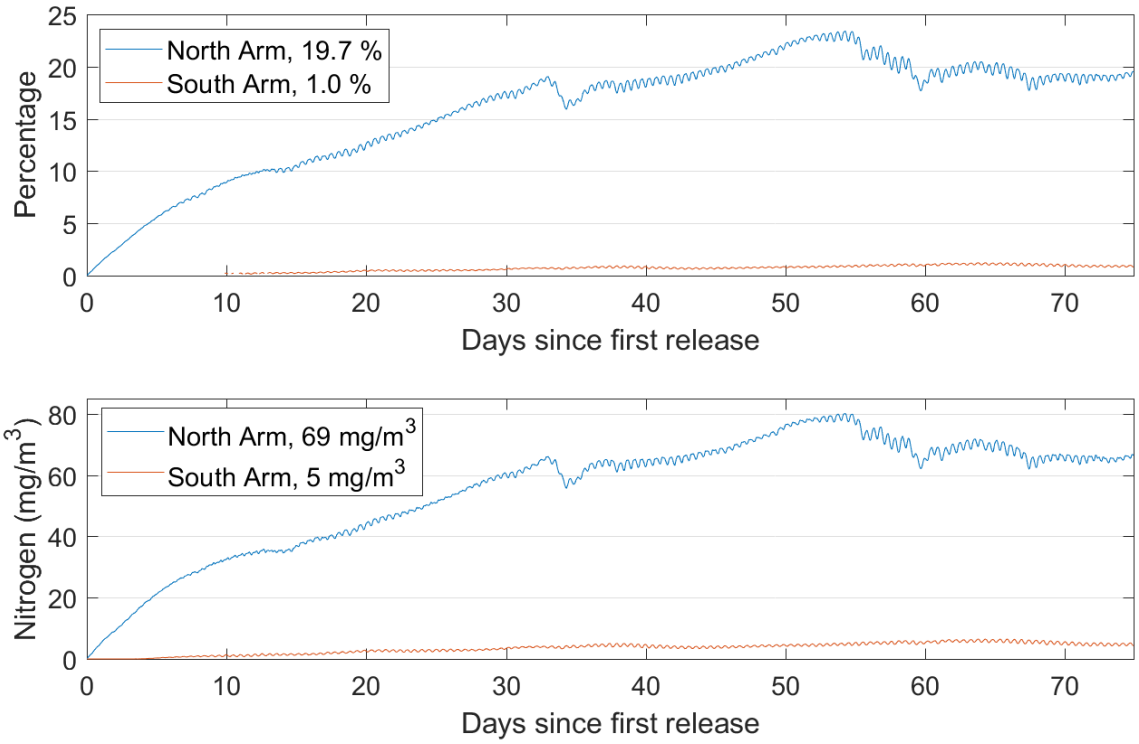

Figure 34. Total nitrogen concentration increases (bottom) and percentage of particles retained (top) estimated from particle tracking simulations. Simulations included the cumulative results of all four proposed Port Pegasus North Arm salmon farm locations. Discharges assumed 100 kg N release per t of fish production based on peak summer feeding rates under a 6,000 tpa production scenario. The model results are shown for a 72-day period which covered 15 April to June 26 2017 and results were separated into North and South Arm changes.

The maximum summer feeding scenario of 6,000 tpa production in North Arm shows a potential increase in mean[31] TN concentration of 69 mg/m^3 is possible (Figure 34).

[30] We note the model was run for an autumn period to coincide with the period of measurements, stratified summer conditions with calm weather could potentially alter the magnitude of modelled effects. Consequently while the feeding and nutrient load estimates are 'worst case', the conditions are not necessarily 'worst case'. We do not believe this change would have a large influence on our results; however, if a Stage 3 assessment is undertaken we would recommend a field survey is repeated in the summer and winter period is also modelled to address this.

[31] Mean across all of North Arm

Because we assume N is tied to the particles in the model and not degraded with time (e.g. through denitrification processes), other production scenarios can quickly be assessed as the effect will be proportional to the N load. That is, if the production is halved, the TN concentration change would also be halved. A reference table of increased TN for each scenario is provided in Table 21.

Table 21. Modelled maximum total nitrogen (TN) concentration increases under summer conditions for a range of salmon production scenarios in North Arm. The scenario-based information presented in Table 1 is shown here with an additional minimum economic break-even (EBE) scenario (Clough and Pambudi 2017) and an initial production scenario (IPS). A relative increase is based on a measured mean background TN concentration of 220 mg/m^3 (Table 14). Scenarios marked with * assume the same proportional feed input across the farms as scenario 4a.

Scenario	Salmon production (tpa)	Summer TN increase (mg/m^3)	Summer TN increase relative to 'background'
1a	6000	69	31%
2a	4478	48	22%
3a	3728	40	18%
4a	2801	29	13%
EBE*	2540	26	12%
IPS*	2200	23	10%

5.3.3. Relevance of total nitrogen increases

To assess the relevance of the modelled nitrogen increases, we consider the increase in total nitrogen as an indicator of the trophic state; secondarily, we consider the potential changes in the phytoplankton response. We note this assessment is not exhaustive, for further details of other potential effects we refer the reader to the MPI summary aquaculture effects report (MPI 2013), or the earlier finfish effects review of Forrest et al. (2007).

Trophic state assessment

It is difficult to gauge the importance of a TN change on the ecological functioning of the area. For example, no guideline values or ranges are given for TN in ANZECC (2000) and TN is not generally reflective of 'toxic' constituents[32], but is a measure of an important ecosystem-supporting nutrient. However, at high concentrations TN could be symptomatic of a degraded ecosystem. Consequently, it can be used to characterise the 'trophic state' of a system from low (oligotrophic) to moderate (mesotrophic) to high (eutrophic) nutrient states (e.g. Smith et al. 1999; Table 22).

[32] At very high concentrations, some forms of nitrogen can have toxic effect, although these are well above the concentrations considered here.

There were no year-round measurements of TN available for the North Arm region. However, the measurements collected for this assessment suggest that mean TN concentrations of 220 mg-N/m^3 for North Arm (Table 14) are typical of other NZ coastal locations for this time of year (e.g. Pelorus Sound; Gibbs et al. 1992). An additional chronic increase of up to 69 mg-N/m^3 (i.e. a 31% increase) over the summer months could therefore be significant[33].

Using the classifications presented by Smith et al. (1999) and based on the TN concentrations measured in our surveys (about 220 mg-N/m^3), North Arm would probably be described as oligotrophic. An increase in the TN concentration of 69 mg-N/m^3 suggests the system would potentially move from an oligotrophic to mesotrophic state. In reality, small coastal embayments such as North Arm are probably dynamic and hence a static trophic state assignment is probably too simplistic. Nevertheless, TN levels defining a mesotrophic state span a 90 mg-N/m^3 range (i.e. 260-350 mg-N/m^3; Table 22), and a 69 mg-N/m^3 increase is a substantial fraction of this range. Therefore, we consider this potential change in pelagic TN over the summer to be 'large'.

Table 22. Typical characteristics for different trophic states for coastal marine waters, as summarised by Smith et al. (1999) and based on the review by Håkanson (1994). TN = total nitrogen, TP= total phosphorus, Chl-*a* = chlorophyll-*a*, SD= Secchi disc depth (a measure of water clarity).

Trophic state	TN (mg/m^3)	TP (mg/m^3)	Chl-*a* (mg/m^3)	SD (m)
Oligotrophic	< 260	< 10	< 1	> 6
Mesotrophic	260–350	10–30	1–3	3–6
Eutrophic	350–400	30–40	3–5	1.5–3
Hypertrophic	> 400	> 40	> 5	< 1.5

Although the magnitude of the change in TN in summer is potentially large (as determined in the trophic state context), it is difficult to determine the relevance of this in terms of effects to the pelagic ecosystem. Consequently, we use the logistic phytoplankton modelling approach applied by Rutherford et al. (1988), which is described with additional detail in Pridmore and Rutherford (1992).

Logistic phytoplankton modelling assessment

Although a residence time term was also included in the model of Pridmore and Rutherford (1992), the maximum logistic chlorophyll-*a* concentration appears to dominate the model in North Arm. The modelled long-term maximum, which includes factors such as flushing is close to, but lower, than the logistic maximum value. For

[33] Because the denitrifying and burial processes present in the real system are not considered in our model the 69 mg/m^3 increase represents a maximum potential change over the summer.

example, the available N based on data collected for this assessment is about 104 mg N/m^3 (Table 14)[34], which suggests that a maximum chlorophyll-*a* concentration of 8.8 mg/m^3 is possible in the region (Table 23).

In order to model potential phytoplankton changes in North Arm using the same logistic 'box-model' approach of Pridmore and Rutherford (1992), we parameterised their model with an 18-day residence time, initial and boundary chlorophyll-*a* concentrations of 1 mg/m^3 and a maximum growth rate of 0.5 /day[35]. Available nitrogen was also a key component of the model and was estimated to have a base of 104 mg/m^3 for North Arm, with any previously modelled TN increases associated with salmon farming scenarios added to this value (Table 21).

The result of the application of the model to North Arm with no salmon farming gave a steady state concentration of 7.4 mg chlorophyll-*a*/m^3. Under the highest feed scenario (6,000 tpa), with an associated increase in available N of 69 mg/m^3, this increased chlorophyll-*a* by 67% to 12.3 mg chlorophyll-*a*/m^3. Potential maximum chlorophyll-*a* changes for all the modelled scenarios are presented in Table 23.

Table 23. Logistic and modelled maximum chlorophyll-*a* concentrations under bloom summer conditions for a range of salmon production scenarios in North Arm Port Pegasus. Logistic maximum and modelled maximum chlorophyll-*a* estimates are based on the model equations presented in Pridmore and Rutherford (1992). Scenarios are based information presented in Table 1, with minimum economic break-even (EBE) (Clough and Pambudi 2017), an initial production scenario (IPS) and a no farms scenario also considered. Scenarios marked with a * assume the same proportional feed input across the farms as scenario 4a.

Scenario	Salmon production (tpa)	Estimated summer available N (mg/m^3)	Logistic maximum chlorophyll-*a* concentration (mg/m^3)	Modelled maximum chlorophyll-*a* concentration, including flushing (mg/m^3)
1a	6000	173	14.7	12.2
2a	4478	152	12.9	10.8
3a	3728	144	12.2	10.2
4a	2801	133	11.3	9.4
EBE*	2540	130	11.0	9.2
IPS*	2200	126	10.6	8.9
No farms	0	104	8.8	7.4

[34] Based on dissolved inorganic nitrogen (DIN) of 60.3 mg/m^3 plus particulate nitrogen (PN) of 44.1 mg/m^3.
[35] See Pridmore and Rutherford (1992) for a full description of the model.

Such large chlorophyll-*a* concentrations produced by the model relate to rather extreme conditions and seem unlikely to be observed with regular frequency. Nevertheless, they represent an extreme example of a possible effect on phytoplankton biomass in the region. Given the potential magnitude of change possible under the largest scenario (1a), this modelling also suggests that 'large' changes to the pelagic environment are possible. However, at the lowest feed scenario (e.g. 2,200 tpa for the IPS) the potential increase in the intensity for these rare events appears to be moderate (1.5 mg/m^3 or c. 20% increase; Table 23). However, this could increase by up to c. 70% under the highest (6,000 tpa) scenario considered here (Table 23).

Assessment limitations

As with any attempt to model highly complex biophysical systems, mathematical models require numerous simplifications. In order to raise some of these known and potentially important simplifications, we list them here; however we note that it is likely that this list is not exhaustive.

Examples of potential modelling issues are:

1. The depth of modelled particle release. Although 25% of the faecal N load is assumed to be remineralised near the seabed in our models, we release all particles at the mean depth range of the net pens. A difference from the real system is possible, although considering the majority (93%) of the dissolved N is released within the net pens, this will have a minor effect on our results.
2. Lack of spatial variation information from our model. We provide averaged changes over the whole volume of North Arm. It is possible localised changes could be higher in some parts of North Arm, but, because the particle tracking approach can introduce uncertainties at the fine scale, these are not shown.
3. Biological processes are not modelled. For example, the uptake of N into phytoplankton, the potential for algal to regulate their depth, or the loss of N to the seabed through cell mortality and sinking. All of these processes can redistribute N within the water column and could potentially change the retention, loss or horizontal distribution of N within North Arm.
4. Ongoing denitrification or burial processes are not explicitly modelled, consequently mean modelled changes could be viewed as an upper estimate of potential total N change in the region.
5. It is assumed that nutrient availability and the associated phytoplankton response are the primary limiting ecological constraints for aquaculture production. However, this may not be the case. For example, other pelagic properties (e.g. dissolved oxygen or pH changes) may affect sensitive or rare benthic organisms (e.g. brachiopods, black corals and sea pens) which have been identified in the region (Fletcher et al. 2017).

Considering all these limitations, we note that the results of our analysis are uncertain, but probably overestimate the likely mean N and chlorophyll-*a* changes in the region of North Arm over a year. Given the uncertainties in the modelling, we consider our conservative 'summer-focused' assessment appropriate for assessing potential water column effects.

Summary

Based on the particle tracking of nitrogen for an initial production scenario, it appears 80% of any dissolved wastes will be lost from the area, which implies the selected locations are good locations for mitigating impacts to the North and South Arms of Port Pegasus. From this, we assess that the change in summer N in North Arm could increase by about 10% from an initial production scenario of 2,200 tpa. Following from this, the logistic phytoplankton modelling suggests this could result in an up to 20% increase in the measured chlorophyll-*a* concentration during a 'bloom event'. However, considering the BGB experience, it appears that the worst case chlorophyll-*a* changes modelled here are very unlikely to eventuate (i.e. less than 4%, or 1 year in 30).

High production scenarios predict the potential for large changes in TN, hence a conservative approach to development of the region is recommended. If maximum production scenarios of 6,000 tpa are considered for the region, a staged development from initially low production (e.g. 2,200 tpa) would be recommended to manage potential risks to the environment. Regular monitoring of the pelagic environment, particularly in the summer, should also be undertaken to measure the actual response of the pelagic change to increasing nutrient loads and compared to modelled effects considered here.

If pelagic effects are not detected, in future, it is therefore possible that the benthic environment may be the limiting constraint on finfish production in North Arm. This is typically the case in other salmon sites around New Zealand; however, the lack of suitable 'low-flow' comparison sites with the relatively high levels of production considered here, means that this cannot be determined for North Arm at this time.

6. SUMMARY AND CONCLUSIONS

A combination of instrument measurements, samples and models have helped to provide a description of the Port Pegasus pelagic environment over a March to May period in 2017. Of primary interest to potential finfish aquaculture is the North Arm region, which was the focus of this assessment.

The North Arm appears to offer low current flows which are not ideal for finfish aquaculture both from a pelagic and benthic effects perspective. However, the locations of higher production farms in Big Ship Passage (as has been included in the scenarios considered here) potentially offers a periodically high energy wave environment at proposed outer farm sites. These powerful waves may affect operations at the site and also act to reduce benthic effects from finfish aquaculture, as wave stirring can induce peak currents that are above typical resuspension thresholds (> 0.1 m/s). Based on a 38-year period wave model, 'large' wave events (i.e. inducing currents greater than 0.1 m/s at the seabed) appear to be a regular occurrence[36] at the proposed outer farm sites (farms 3 and 4). However, there are key differences between midwater tidal (used to define 'low' and 'high' flow sites) and benthic wave-driven currents. Tidally-driven currents occur daily over long time periods (hours), whereas peak wave-driven currents occurring for short periods of time (seconds) and rapidly change direction. Consequently, the magnitude of any benthic effect from wave-driven currents could not be determined for this assessment.

The hydraulic residence time of dissolved wastes is also an important consideration in determining the potential for pelagic effects. Models simulating the release of wastes from potential aquaculture sites in North Arm suggest 80% of dissolved wastes will be lost from the system. Of those that make it into North Arm, residence times were estimated to be about 18 days. Based on the residence times, there is the potential for finfish wastes to be retained longer in North Arm than estimated for the reasonably comparable BGB area. Given that the long history (30 years) of salmon farm production without significant pelagic effects in BGB, we consider that the site is probably operating within its carrying capacity. If this is correct then the longer residence time of North Arm means that an initial production limit in this area is probably lower than that of BGB. We therefore suggest an initial production of 2,200 tpa is probably a level at which the North Arm would also be within its carrying capacity. The feasibility of an initial 2,200 tpa production level would be subject to following Stage 3 aquaculture assessments and subsequent increases would be anticipated to be subject to stable and acceptable water quality results over a period of time.

[36] Waves typically occur less than weekly but no less than fortnightly.

However, we note there was a historical bloom that occurred in 1989 in BGB during a period of relatively low finfish production (c. 1,000 tpa see e.g. Mackenzie 1991; Pridmore and Rutherford 1992). Bloom events can occur naturally and waste nitrogen from salmon farming has the potential to exacerbate the intensity of these events. Our assessment of finfish production scenarios suggested that mean summer increases of up to 69 mg/m^3 in total nitrogen (i.e. about 32% above background) are possible for the largest production scenario assessed (6,000 tpa) and these means are considered to be relatively large increases. There is also potential for an associated change in the potential size and magnitude of a phytoplankton bloom, with an increase in intensity of c. 70% possible. We also consider this change to be large. However, it is very difficult to assess the ecological relevance of such rare events, which appears to have occurred only once in about 30 years in BGB and only appeared to have limited effects on the wider ecosystem (MacKenzie 1991).

Although we suggest there is potential for water quality effects at the higher production scenarios, we note that the implications of nutrient induced effects on pelagic environments are extremely complex. Consequently, it is difficult to predict what the ecological effects of new nutrients in the North Arm could be. At the ‘worst case’ end we have considered that nitrogen from finfish production contributes to phytoplankton growth. There are many potential ecosystem pathways for salmon-derived nutrients, with phytoplankton uptake being one of many possibilities. For instance, an initial increase in phytoplankton could support a larger grazer biomass of zooplankton which could act to suppress phytoplankton growth. Without surety of effects it is difficult to translate a total nitrogen change into a ‘good’, ‘bad’ or ‘significant’ ecological change, but we can say is that there is the potential for a relatively large change in the availability of nitrogen in the region if the highest finfish production scenarios are considered.

Given the uncertainty of effects, any proposed production scenarios should be staged in development from initially low production (e.g. 2,200 tpa) to manage potential risks to the environment. Regular monitoring of the pelagic environment, particularly in the summer, should also be undertaken to measure the actual response of the pelagic change to increasing nutrient loads.

7. ACKNOWLEDGEMENTS

We would like to acknowledge the significant contribution and field assistance provided by Bill and Lynn Kato (Takaroa II), Paul Creswell (MPI), Hayden Rabel (Cawthron), Marc Jary (Cawthron), Lauren Fletcher (Cawthron) and Thomas Hildebrand (Ngāi Tahu). Phytoplankton species identifications were carried out by the Cawthron Institute phytoplankton team. Deanna Elvines is also thanked for review of the report.

8. REFERENCES

ADS 2016. Big Glory Bay benthic and water quality sampling 2016. Confidential Client Report prepared for Sanford Limited by Aquadynamic Solutions. September 2016. 115 p.

ANZECC 2000. Guidelines for fresh and marine water quality volume 1: The Guidelines. Australian and New Zealand Environment and Conservation Council, Canberra, ACT, Australia.

Bradford JM, Cranfield HJ, Michael KP 1991. Variability in phytoplankton biomass in relation to the surface hydrology of southern New Zealand and possible effects on the food chain. New Zealand Journal of Marine and Freshwater Research 25: 133-144.

Broekhuizen N 2013. Review of historical water quality data from Pelorus Sound and Queen Charlotte Sound: long-term NIWA time-series and Marlborough District Council time-series. NIWA Client Report No: HAM2013 - 070. Prepared for NIWA. 104 p.

Broekhuizen N, Hadfield M, Plew D 2015. A biophysical model for the Marlborough Sounds, Part 2: Pelorus Sound. Client Report CHC2014-130. 175 p.

Bromley PJ, Smart G 1981. The effects of the major food categories on growth, composition and food conversion in rainbow trout (*Salmo gairdneri* Richardson). Aquaculture 23(1-4): 325-336.

Buschmann A, Costa-Pierce BA, Cross S, Iriarte JL, Olsen Y, Reid G 2007. Nutrient impacts of farmed Atlantic salmon (*Salmo salar*) on pelagic ecosystems and implications for carrying capacity, Report for World Wildlife Fund Salmon Aquaculture Dialogue by the Technical Working Group on Nutrients and Carrying Capacity.

Butz I, Vens-Cappell B 1982. Report of the FIFAC Workshop on Fish-Farm Effluents. Denmark. pp 113-121.

Chang FH, Anderson C, Boustead NC 1990. First record of a *Heterosigma* (Raphidophyceae) bloom with associated mortality of cage-reared salmon in Big Glory Bay, New Zealand. New Zealand Journal of Marine and Freshwater Research 24: 461-469.

Clark D, Dunmore R, Taylor D, Barter P 2015. Stewart Island site assessments. Prepared for Ministry for Primary Industries. Cawthron Report No. 2669. 49 p.

Clough P, Pambudi D, 2017. Port Pegasus salmon farm, indicative business case for new aquaculture in Southland NZIER. Final report to Ministry for Primary Industries. 22 August 2017.

Dahl E, Lindahl O, Paasche E, Throndsen J 1989. The *Chrysochromulina polylepis* bloom in Scandinavian waters during spring 1988. In: Cosper EM, Bricelj VM, Carpenter EJ (eds). Novel phytoplankton blooms. Coastal and estuarine studies Vol 35. Springer, Berlin, Heidelberg. pp 383-405.

Elvines D, Dunmore R, Knight B 2015. Port Adventure site assessment: August 2015. Prepared for Ministry for Primary Industries. Cawthron Report No. 2767. 15 p.

Elvines DM, Taylor DI, Knight B, Jary M 2016. Stage One aquaculture site assessments - Stewart Island, 2016. Prepared for Ministry for Primary Industries. Cawthron Report No. 2940. 27 p. plus appendices.

Fletcher L, Taylor D, Goodwin E, Jary M, Floerl L 2017. Pelagic biophysical assessment: Port Pegasus / Pikihatiti. Prepared for Ministry for Primary Industries. Cawthron Report No. 3047. 66 p. plus appendices.

Forrest B, Keeley N, Gillespie P, Hopkins G, Knight B, Govier D 2007. Review of the ecological effects of marine finfish aquaculture: Final report. Prepared for Ministry of Fisheries. 71 p.

Gibbs MM, Pickmere SE, Woods PH, Payne GW, James MR, Hickman RW, Illingworth J 1992. Nutrient and chlorophyll a variability at six stations associated with mussel farming in Pelorus Sound, 1984–85. New Zealand Journal of Marine and Freshwater Research 26(2): 197-211.

Keeley NB, Cromey CJ, Goodwin EO, Gibbs MT, Macleod CM 2013. Predictive depositional modelling (DEPOMOD) of the interactive effect of current flow and resuspension on ecological impacts beneath salmon farms. Aquaculture Environment Interactions 3: 275-291.

Keeley NB 2012. Supplementary document of tables – for the evidence of Nigel Brian Keeley provided in relation to benthic impacts for the New Zealand King Salmon Co. Limited. June 2012. 11 p. http://www.epa.govt.nz/Publications/11(a)%20Nigel%20Brian%20Keeley%20-%20Supplementary%20Document%20of%20Tables%20-%20v1.pdf (accessed 26 September 2017)

Key JM 2001. Growth and condition of the Greenshell mussel in Big Glory Bay, Stewart Island: relationships with environmental parameters. Master of Marine Science, Dunedin, New Zealand. University of Otago.

Håkanson L 1994. A review on effect dose sensitivity models for aquatic ecosystems. Internationale Revue der gesamten Hydrobiologie und Hydrographie 79 (4): 621-667.

MacKenzie AL 1991. Toxic and noxious phytoplankton in Big Glory Bay, Stewart Island, New Zealand. Journal of Applied Phycology 3: 19-34.

MacKenzie L, Smith KF, Rhodes LL, Brown A, Langi V, Lovell G, Preece M 2011. Mortalities of sea-cage salmon (*Oncorhynchus tshawytscha*) due to a bloom of *Pseudochattonella verruculosa* (Dictyophyceae) in Queen Charlotte Sound, New Zealand. Harmful Algae 11: 45-53.

Ministry of Primary Industries (MPI) 2013. Literature review of ecological effects of aquaculture. A collaboration between Ministry for Primary Industries, Cawthron Institute and National Institute for Water and Atmospheric Research Ltd. August 2013. Ministry for Primary Industries, Wellington, New Zealand. ISBN: 978-0-478-38817-6.

Ministry of Primary Industries (MPI) 2015. Best Management Practice guidelines for salmon farms in the Marlborough Sounds: Part 1: Benthic environmental quality standards and monitoring protocol (Version 1.0 January 2015). Prepared for the Ministry for Primary Industries by the Benthic Standards Working Group (Keeley N, Gillard M, Broekhuizen N, Ford R, Schuckard R, and Urlich S).

Nicoll RS, Steinke DM, Attia J, Roy A, Buckham BJ 2011. Simulation of a high-energy finfish aquaculture site using a finite element net model. In ASME 2011 30th International Conference on Ocean, Offshore and Arctic Engineering. American Society of Mechanical Engineers. pp 35-44.

O'Callaghan MD 1998. Exchange of nutrients from Big Glory Bay, Stewart Island. Unpublished MSc thesis, University of Otago, Dunedin, New Zealand.

Ogilvie SC, Ross AH, James MR, Schiel DR 2003. *In situ* enclosure experiments on the influence of cultured mussels (*Perna canaliculus*) on phytoplankton at times of high and low ambient nitrogen. Journal of Experimental Marine Biology and Ecology 295(1): 23-39.

Penczak T, Galicka W, Molinski M, Kusto E, Zalewski M 1982. The enrichment of a mesotrophic lake by carbon, phosphorus and nitrogen from the cage aquaculture of rainbow trout, *Salmo gairdneri.* Journal of Applied Ecology 19(2): 371-393.

Pridmore RD, Rutherford JC 1990. Factors influencing phytoplankton abundance in Big Glory Bay, Stewart Island: a modelling study. Water Quality Centre Consultancy Report No 6107. Hamilton. 30 p.

Pridmore R, Rutherford J 1992. Modelling phytoplankton abundance in a small enclosed bay used for salmon farming. Aquaculture Research 23(5): 525-542.

Redfield AC 1934. On the proportions of organic derivations in sea water and their relation to the composition of plankton. In University Press of Liverpool. James Johnstone Memorial Volume. (ed. R.J. Daniel): 177-192.

Roper D, Rutherford J, Pridmore R 1988. Salmon farming water rights studies, Big Glory Bay, Stewart Island, Water Quality Centre - DSIR Consultancy Report T7074/2 Prepared for Southland Water Catchment Board.

Rutherford JC, Pridmore RD, Roper DS 1988. Estimation of sustainable salmon Production in Big Glory Bay, Stewart Island. DSIR Consultancy Report T7074/1 prepared for MAFFish. 38 p.

Smith V, Tilman G, Nekola J 1999. Eutrophication: impacts of excess nutrient inputs on freshwater, marine, and terrestrial ecosystems. Environmental Pollution 100(1-3): 179-196.

Stead SM, Laird LM 2002. Handbook of salmon farming. Springer Praxis, Chichester, UK.

Stenton-Dozey J, Olsen L, Bradley A, Brown S 2015. Assessment of the water column and benthic environments of marine farms in Big Glory Bay, Stewart Island from July 2014 to June 2015. NIWA Client Report CHC2015-105 prepared for Sanford Ltd. 30 November 2015 (version 4) (Confidential). 99 p.

Weston DP 1986. The environmental effects of floating mariculture in Puget Sound. Washing Department of Fisheries.

9. APPENDICES

Appendix 1. Time series of ADCP current data

The following figures show the currents at 30 min intervals during the ADCP deployments at a depth cell near mid-water depth. These confirm the weak flows at Mid Bay and West Side and stronger flows within the Passages. These figures illustrate that the currents are mainly tidal at all sites.

The water levels measured at each site are shown by the red curves. These show an average tidal range around 1.8 m at all sites. During periods of neap tides the ranges are around 0.9 m, while during spring tides ranges are around 2.5 m.

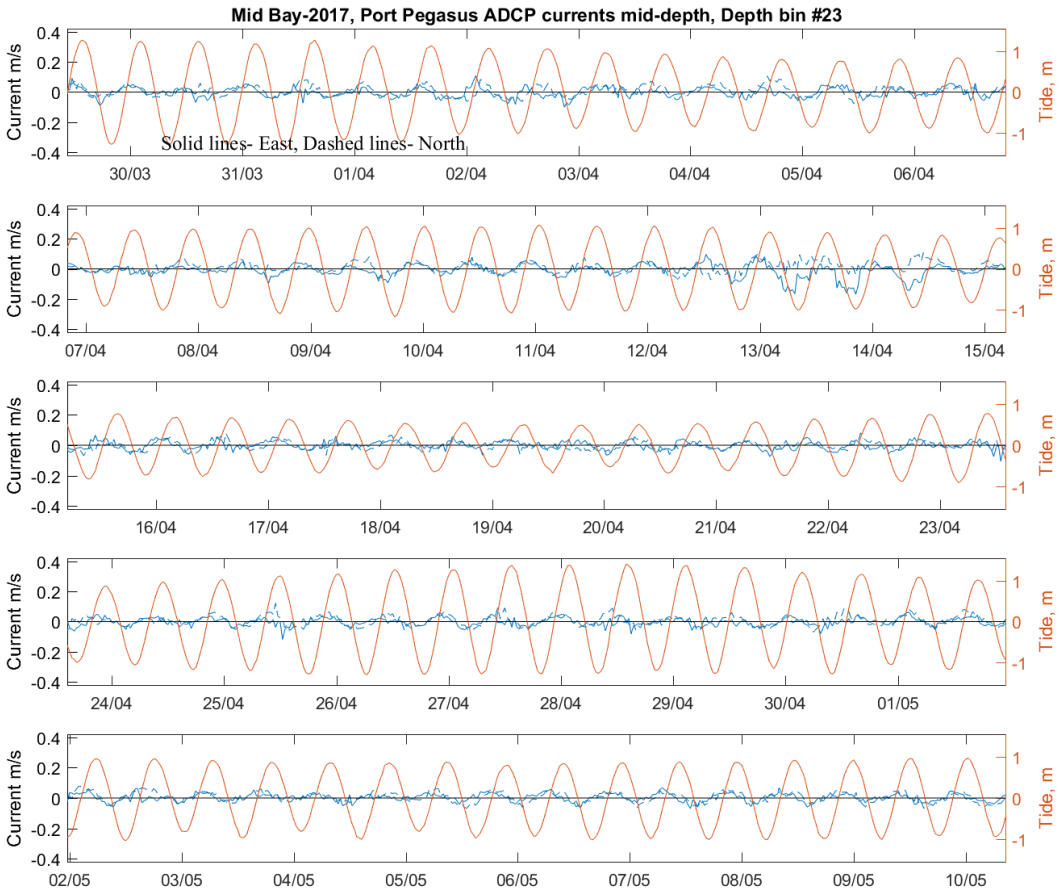

Figure A1.1. ADCP measured currents at mid-depth for Mid Bay 2017 ADCP.

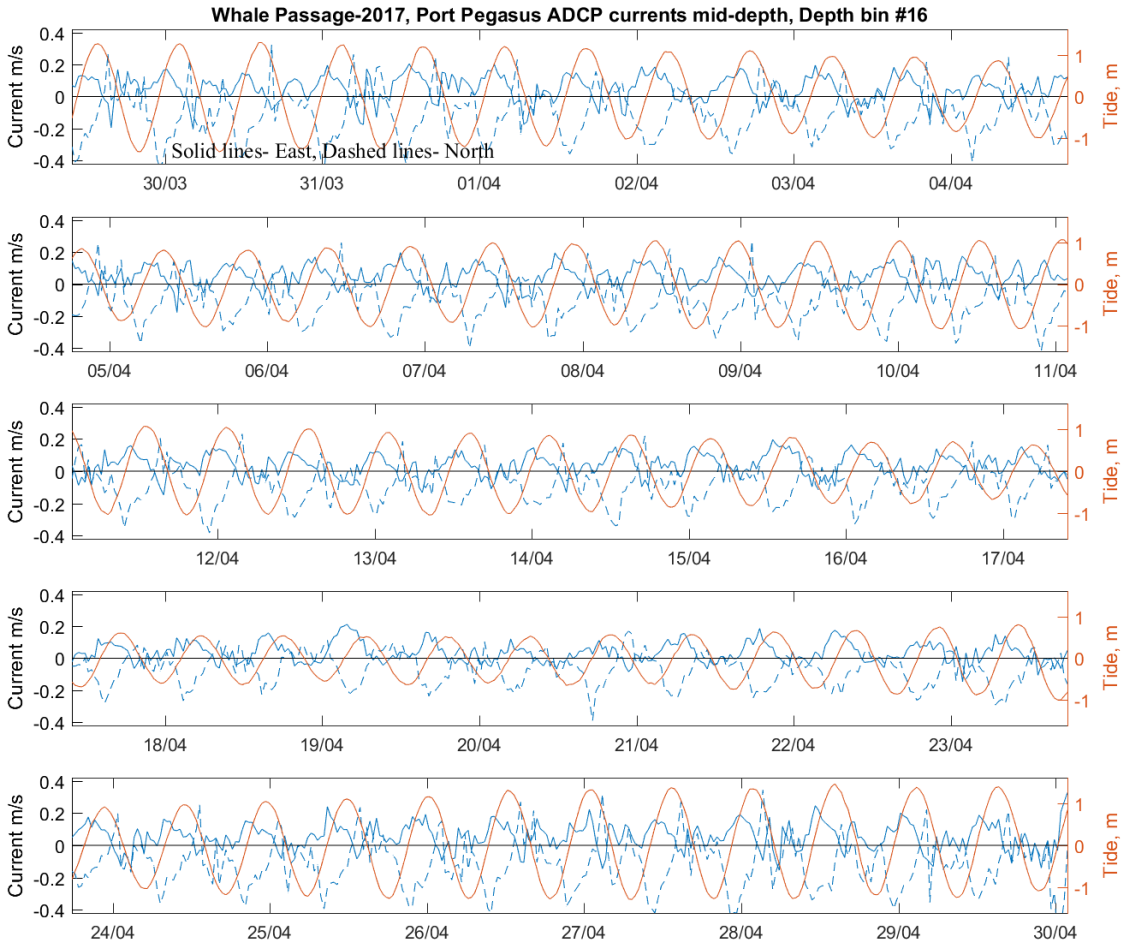

Figure A1.2. ADCP measured currents at mid-depth for Whale Passage Bay 2017 ADCP.

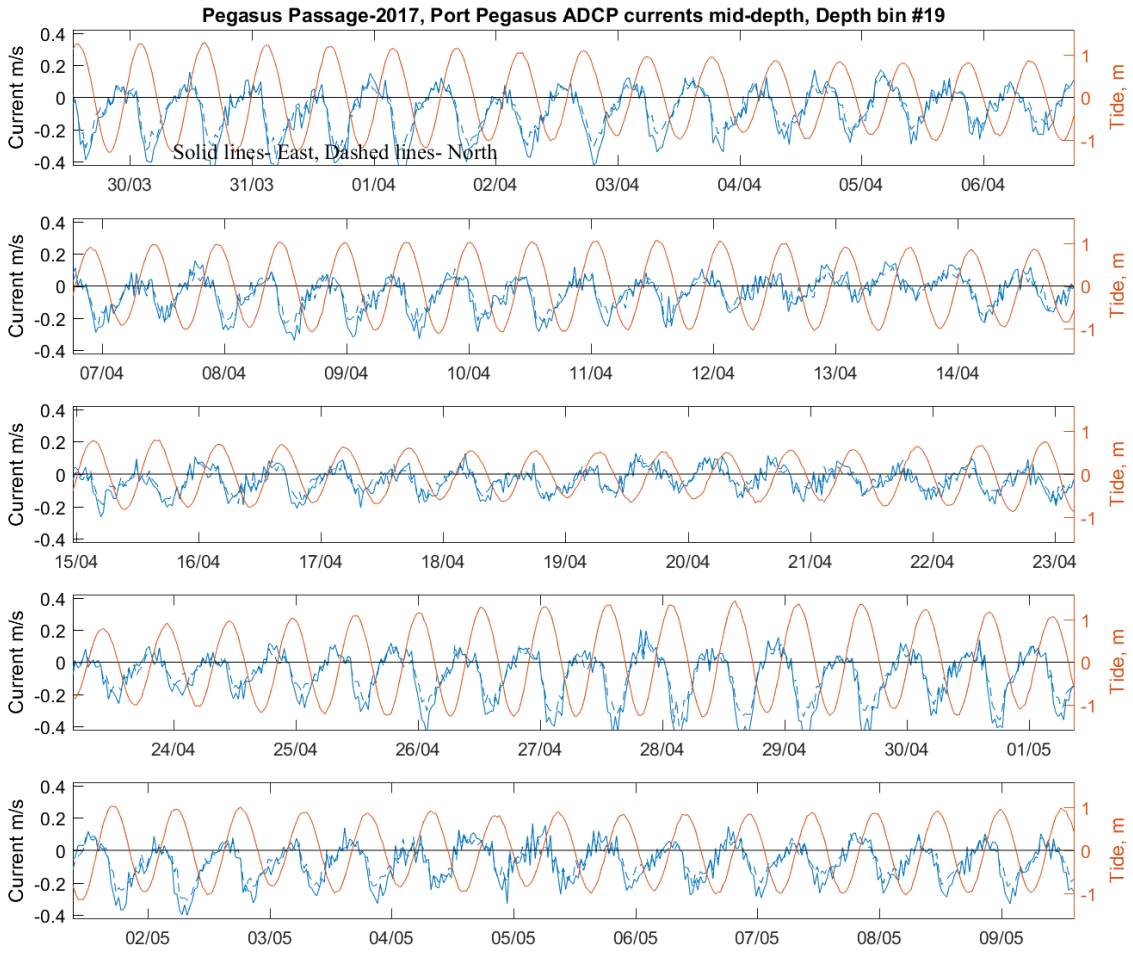

Figure A1.3. ADCP measured currents at mid-depth for Pegasus Passage 2017 ADCP.

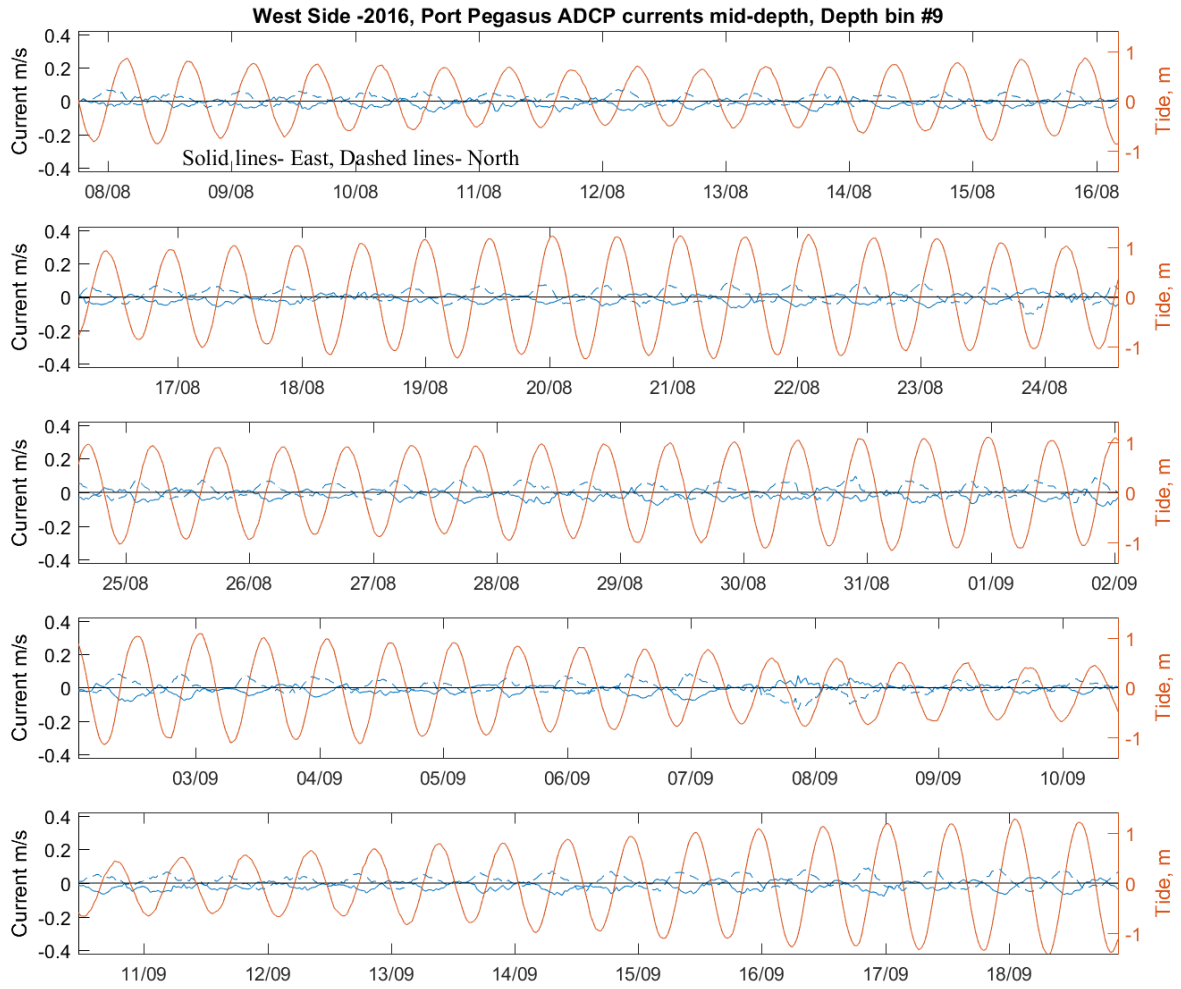

Figure A1.4. ADCP measured currents at mid-depth for West Side North Arm 2016 ADCP.

Appendix 2. MetOcean Hydrodynamic Model Report.

MetOcean Solutions

PEGASUS BAY HYDRODYNAMICS

Pegasus Bay hydrodynamics for fish farm ecological impacts

Report prepared for Cawthron

Specialists in Oceanography

MetOcean Solutions Ltd: P0330

August 2017

Report status

Version	Date	Status	Approved by
RevA	09/08/2017	Draft for internal review	Zyngfogel
RevB	14/08/2017	Draft for client review	Beamsley
RevC	27/09/2017	Draft for client review	Beamsley

It is the responsibility of the reader to verify the currency of the version number of this report.

TABLE OF CONTENTS

LIST OF FIGURES

LIST OF TABLES

1. INTRODUCTION

Cawthron have commissioned MetOcean Solutions to undertake a hydrodynamic study of Pegasus Bay, south-eastern Stuart island (Figure 1.1). The purpose of the study is to provide greater understanding of the hydrodynamics and the flushing time in the bay, particularly within Northern bay. Hydrodynamic data is intended to be used to provide the forcings required to undertake Lagrangian particle modelling to investigate connectivity between the North and South Arms of Pegasus Bay.

The report is structured as follows. Measured data used to calibrate and validate the numerical model is described in Section 2, while the numerical model itself, including boundary conditions applied, is detailed in Section 3. Results are provided in Section 4 and a brief summary in Section 5. References cited are listed in Section 6.

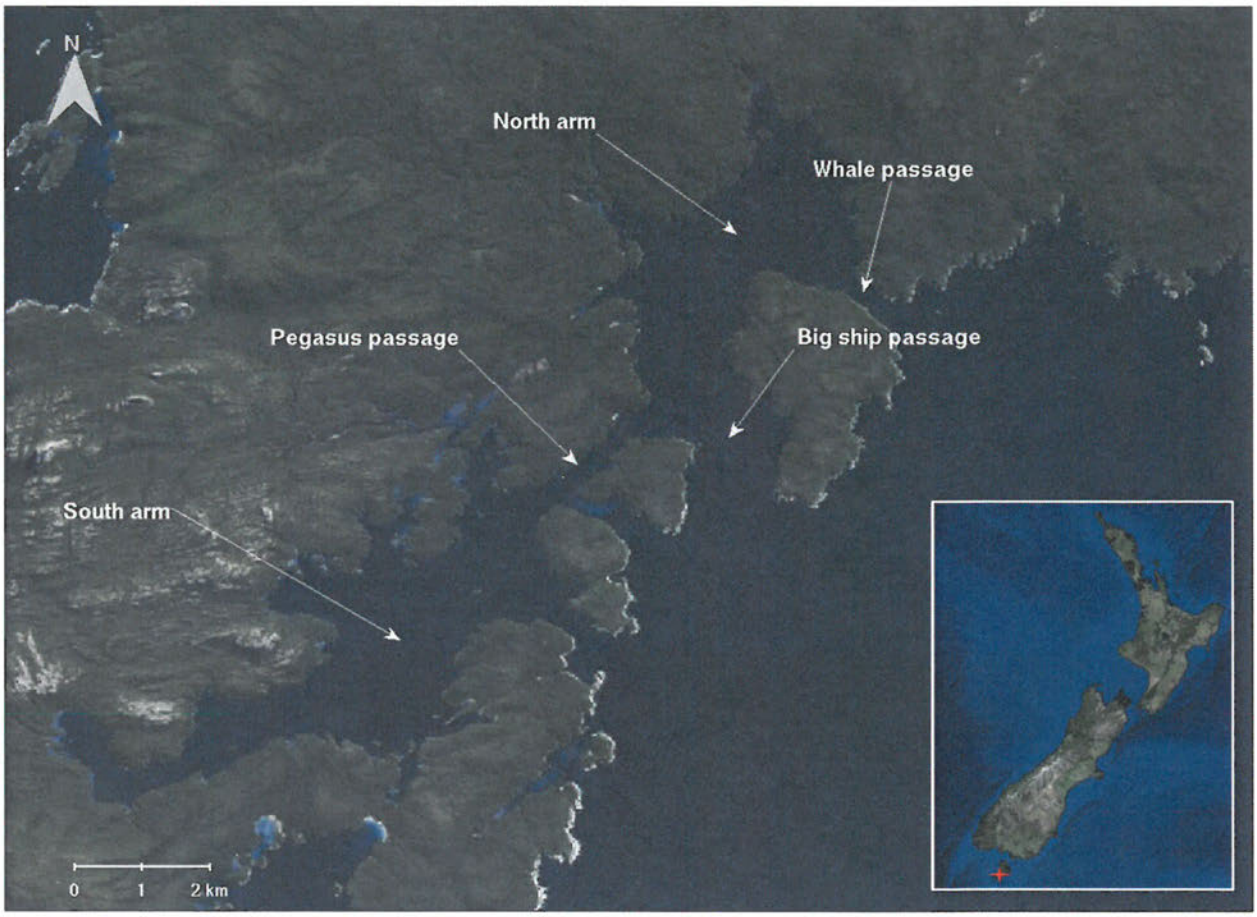

Figure 1.1 Location of Pegasus Bay South-East of Stewart Island. NZ. Pegasus Bay consists of a North and South Arm

2. FIELD MEASUREMENT CAMPAIGN

Cawthron has undertaken a field measurement campaign to assist the characterisation of the hydrodynamic regime of Pegasus Bay and provide the necessary field data for calibration of a hydrodynamic model. The campaign focused on the hydrodynamics of the north arm.

Two datasets were used in this study: one from July to August 2016 and another one from April to May 2017. They include measurements of water elevation, and velocities. Measurements were undertaken using Acoustic Doppler Current Profiler (ADCP); coordinates of the deployment sites are provided in Table 2.1 while the deployment location is shown in Figure 2.1.

Further details on instrument deployment and measured data are provided in the following sections.

Figure 2.1 Aerial photography of the North arm in Pegasus Bay. The triangles represent the positions of the four ADCP profilers used in the model validation.

Table 2.1 Duration, location coordinates and approximate water depth of Acoustic Doppler Current Profile (ADCP) deployed within Pegasus Bay. ADCP were measuring both pressure and velocities

Site	Name	Deployment duration		Deployment coordinates (WGS 84)		Depth [m]
		Start	End	Latitude	Longitude	
Mid bay	A1	29/03/17	10/05/17	-47.17462 °S	167.6928 °E	47
Pegasus passage	A2	29/03/17	09/05/17	-47.19995 °S	167.6664 °E	20
Whale passage	A3	29/03/17	30/04/17	-47.1793 °S	167.7152 °E	16
North arm West	A4	07/08/16	18/09/16	-47.1866 °S	167.6768 °E	36

2.1. Sea level pressure

Sea surface elevations were measured using the pressure sensor from the ADCP. The instruments recorded pressures continuously from the end of March to beginning of May 2017 and from the beginning of August to mid-September 2016.

2.2. Current velocities

Three ADCP (Nortek RDI) profilers were deployed in 2017 and one in 2016 at various places in the North Arm, in depth ranging from 16 to 47 m (see Figure 2.1).

For interpretation and comparison with model outputs, each bin were separated into their tidal and residual components using the tidal analysis package t-tide (Pawlowicz et al., 2002).

3. THE HYDRODYNAMIC MODEL

3.1. Model description

The 3D hydrodynamics of Pegasus Bay were modelled using the open-sourced hydrodynamic model SCHISM[1,2]. The benefit of using open-source science models is the full transparency of the code and numerical schemes, and the ability for other researchers to replicate and enhance any previous modelling efforts for a given environment.

SCHISM is a prognostic finite-element unstructured-grid model designed to simulate 3D baroclinic, 3D barotropic or 2D barotropic circulation. The barotropic mode equations employ a semi-implicit finite-element Eulerian-Lagrangian algorithm to solve the shallow-water equations, forced by relevant physical processes (atmospheric, oceanic and fluvial forcing). A detailed description of the SCHISM model formulation, governing equations and numerics, can be found in Zhang and Baptista (2008).

The SCHISM model is physically realistic, in that well-understood laws of motion and mass conservation are implemented. Therefore, water mass is generally conserved within the model, although it can be added or removed at open boundaries (e.g. through tidal motion at the ocean boundaries) and water is redistributed by incorporating aspects of the real-world systems (e.g. bathymetric information, forcing by tides and wind). The model transports water and other constituents (e.g. salt, temperature, turbulence) through the use of triangular volumes (connected 3-D polyhedrons).

The finite-element triangular grid structure used by SCHISM has resolution and scale benefits over other regular or curvilinear based hydrodynamic models. SCHISM is computationally efficient in the way it resolves the shape and complex bathymetry associated with estuaries, and the governing equations are similar to other open-source models such as Delft3D and ROMS. SCHISM has been used extensively within the scientific community[3,4] where it forms the backbone of operational systems used to nowcast and forecast estuarine water levels, storm surges, velocities, water temperature and salinity[5].

3.2. Bathymetric data

Local hydrographic fare sheets were digitized in order to ensure that all available bathymetric data was available for consideration when generating the model domains. The coverage and resolution of the digitized data is shown in Figure 3.1.

[1] http://ccrm.vims.edu/schism/
[2] http://www.ccrm.vims.edu/w/index.php/Main_Page#SCHISM_WIKI
[3] http://www.stccmop.org/knowledge_transfer/software/selfe/publications
[4] http://ccrm.vims.edu/schism/schism_pubs.html
[5] https://tidesandcurrents.noaa.gov/ofs/creofs/creofs_info.html

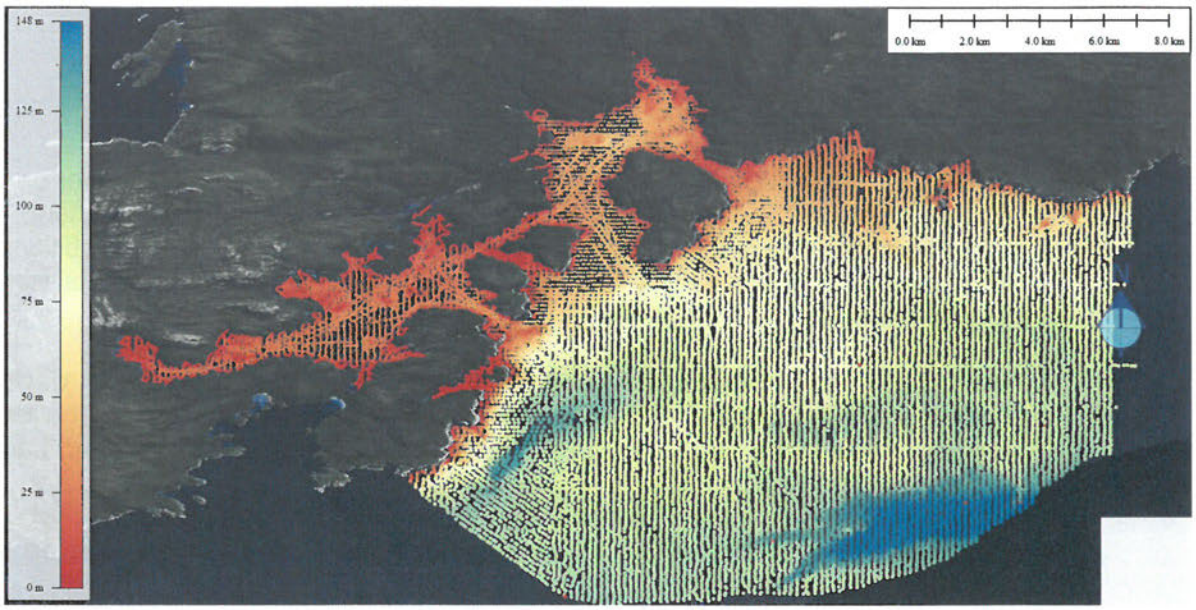

Figure 3.1 Digitized fair sheet data extent

3.3. Model domain

The model resolution was optimised to ensure replication of the salient hydrodynamic processes. The resolution ranged from 100 m at the boundary to 10 m in shallow water and near the coast, with grid refinement in the main passage (i.e. Whale passage, Pegasus passage). The triangular elements of the model domain meshes are shown in Figure 3.2 and associated bathymetries are presented in Figure 3.3.

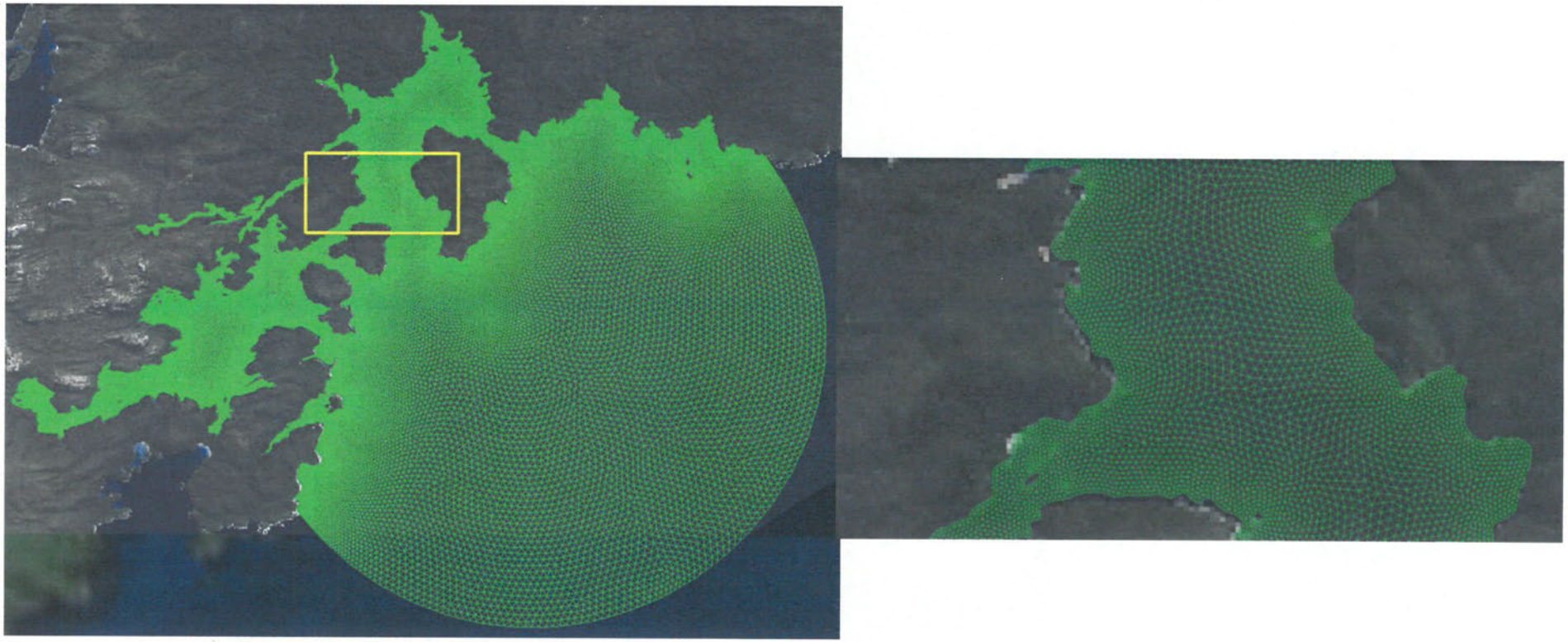

Figure 3.2 Triangular model mesh defined for Pegasus Bay. Left is the whole domain use in this study and right show zoom over the Pegasus passage and the entrance of North Arm.

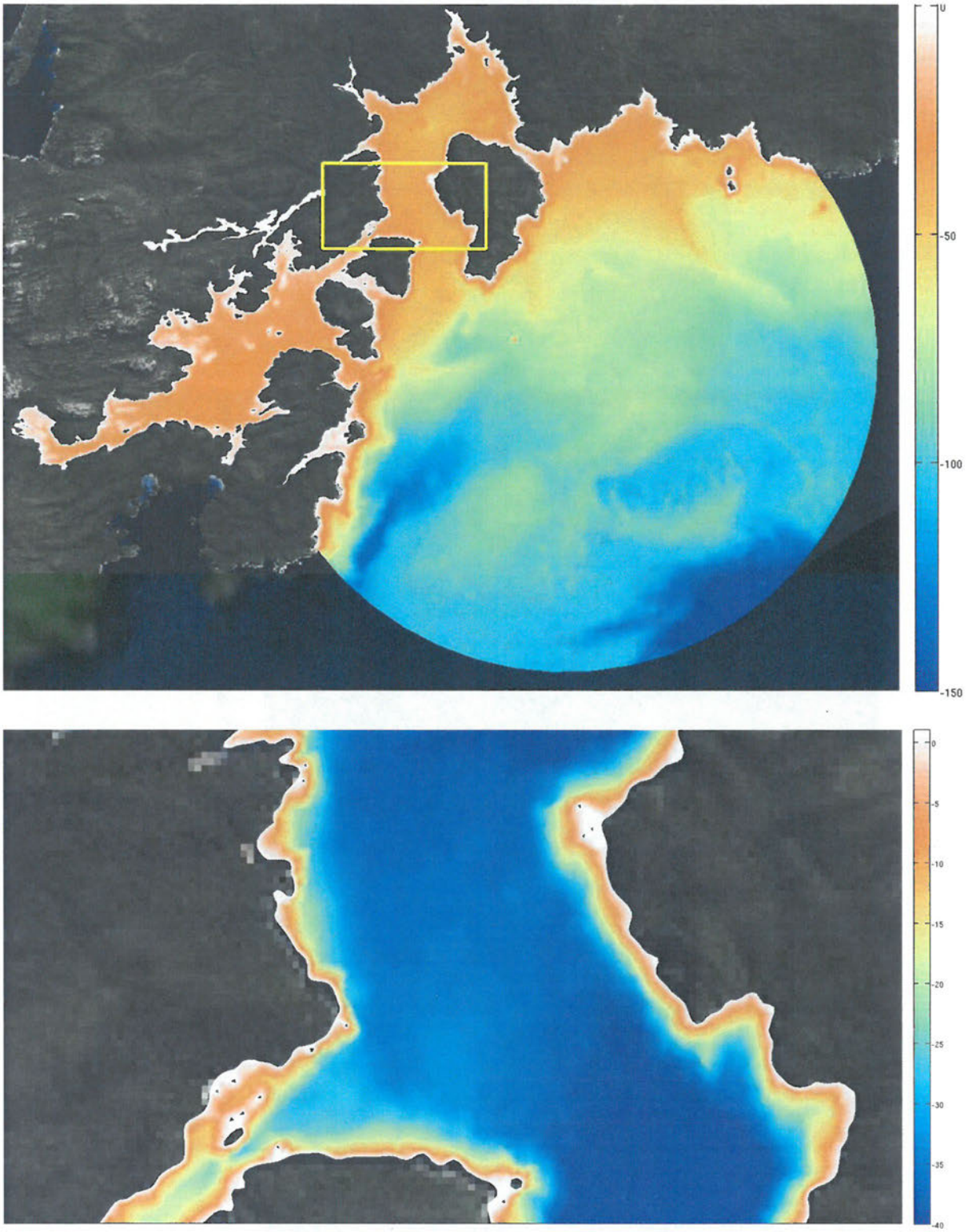

Figure 3.3 Bathymetries of model domains showing the water depth in m below mean sea level. Top shows the whole domain used in this study (colour scale covers 0-150 m depth) and bottom shows a focused area covering Pegasus passage and the entrance of North Arm (colour scale covers 0-40 m depth).

3.4. Vertical discretisation

For the 3D model simulations, the vertical discretisation of the water column consisted of the combination of 3 terrain-following sigma-coordinate layers. The model was found to validate best when using only a limited number of sigma-layers.

The terrain following S-coordinates vary according to the depth (h) following the scheme of (Song and Haidvogel 1994) :

$$\begin{aligned} z \quad &= \eta(1+\sigma) + h_c\sigma + (\tilde{h} - h_c)C(\sigma) \\ for \quad &[-1 \le \sigma \le 0] \end{aligned}$$

$$C(\sigma) = (1-\theta_b)\frac{\sinh(\theta_f \sigma)}{\sinh(\theta_f)} + \theta_b \frac{\tanh[\theta_f(\sigma + 1/2)] - \tanh(\theta_f/2)}{2\tanh(\theta_f/2)} \qquad (2.1)$$

$$for$$

$$[0 \le \theta_b \le 1;\ 0 \le \theta_f \le 20]$$

where h = $min(h,h_s)$, a 'restricted' depth, η is the sea surface elevation (metres above mean sea level, *msl*) and σ is a vector of the proportional thicknesses of the vertical layers as defined in a standard sigma-coordinate scheme.

The parameter h_c is a positive constant (set at 5 m) dictating the thickness of the bottom or surface layer that needs to be resolved. If $h<h_c$ the vertical scheme is a standard sigma-coordinate model. θ_b and θ_f are constants that control the vertical resolution near the bottom and surface, respectively.

For this study, the model was configured with increased vertical resolution at the surface and close to the seabed by setting θ_b = 0 and θ_f = 10 where the depth was greater than 5 m (Figure 3.3). This ensures that the surface cell depth is always well resolved.

3.5. Boundary conditions

3.5.1. Hydrodynamic forcing

Both residual and tidal elevations and velocities were applied to the open boundary of the 3D SCHISM model.

Tidal constituent phase and amplitudes (elevation and velocity) were extracted from the (Oregon State University Tidal Inverse Software) Pacific Ocean grid which has an horizontal resolution of ~1/12° (Egbert and Erofeeva 2002).

Residual velocities and water elevation boundary conditions for the offshore boundary were prescribed from a 2D New Zealand Regional Ocean Modelling System (ROMS) (Haidvogel et al., 2008) domain, with a resolution of 0.05°, assuming a logarithmic velocity profile.

3.5.2. Atmospheric forcing

The atmospheric forcings applied to the regional model domain were extracted from the Climate Forecast System Reanalysis (CFSR) from WRF at 8-km resolution, with its initial and lateral boundary conditions set by the Climate Forecast System Reanalysis (Saha *et al.*, 2010) from the National Centers for Environmental Prediction (NCEP).

3.6. Evaluation criteria

The predictive skill assessment of the SCHISM numerical model was based on two main evaluation criteria:

- The qualitative agreement between model and measured time-series data, and
- The quantitative agreement between model and observations at several sites within the study area. For this purpose, the following quantitative accuracy parameters were calculated from the measured X_m and hindcast, X_h data:

Mean absolute error (MAE):	$\overline{\lvert x_h - x_m \rvert}$	(Eq. 3.1)
Root Mean Square Error (RMSE):	$\sqrt{\overline{(x_h - x_m)^2}}$	(Eq. 3.2)
Mean relative absolute error (MRAE):	$\overline{\left\lvert \frac{x_h - x_m}{x_m} \right\rvert}$	(Eq. 3.3)
Bias:	$\overline{x_h - x_m}$	(Eq. 3.4)
Scatter Index (SI):	$\frac{\sqrt{\overline{(x_h - x_m)^2}}}{\overline{x_h}}$	(Eq. 3.5)

Additionally comparisons between model and measured time series and tidal constituents were used to assess the agreement between model and measured data.

4. RESULTS

4.1. Measured data

4.1.1. Water levels

Time series of measured water elevations are shown in Figure 4.1. These show that the bay is influenced by a semi-diurnal tidal component. The maximum tidal range measured over the period was 2.7 m; the minimum 1.2 m for all sites.

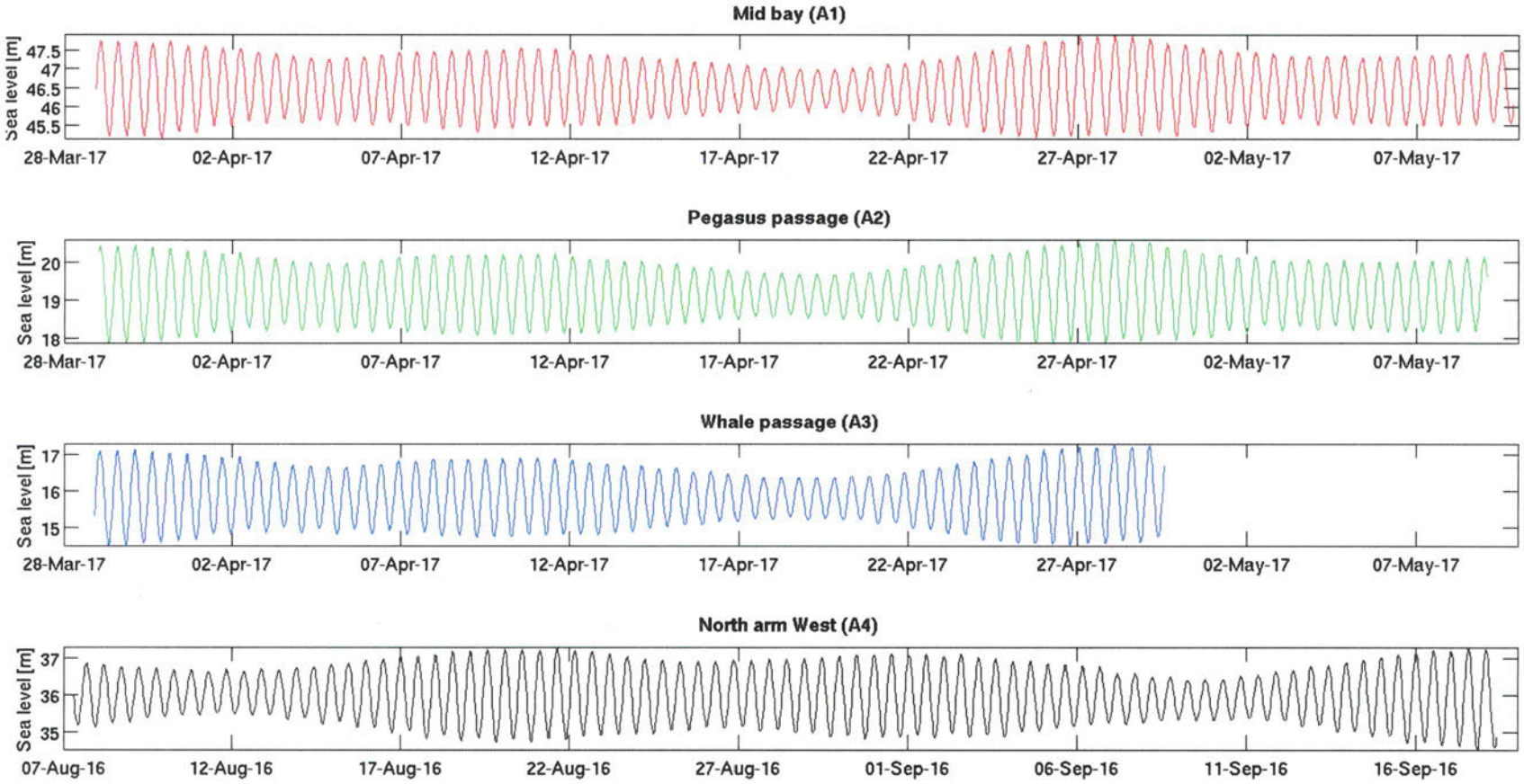

Figure 4.1 Time series of sea level measured at Mid Bay, Pegasus passage, Whale passage and North arm West using the ADCP pressure sensors (see Figure 2.1 for instruments positions). Elevations are reported as relative to seabed/water depth

4.1.2. Current velocities

Depth average tidal current roses for each for the sites (4) are presented in Figure 4.2. The strongest tidal signal is observed at Pegasus Passage with velocities reaching 0.35 $m.s^{-1}$ during spring tide. The lowest tidal flow is observed at the mid bay site with tidal flows of the order 0.04 $m.s^{-1}$.

Time series of the residual vertical velocity profiles and corresponding wind speeds are given in Figure 4.3. Within the measurement period residual current velocities vary from 0.2 $m.s^{-1}$ at site A1 to 0.4 $m.s^{-1}$ in the Whale passage (site A3, Figure 3.2).

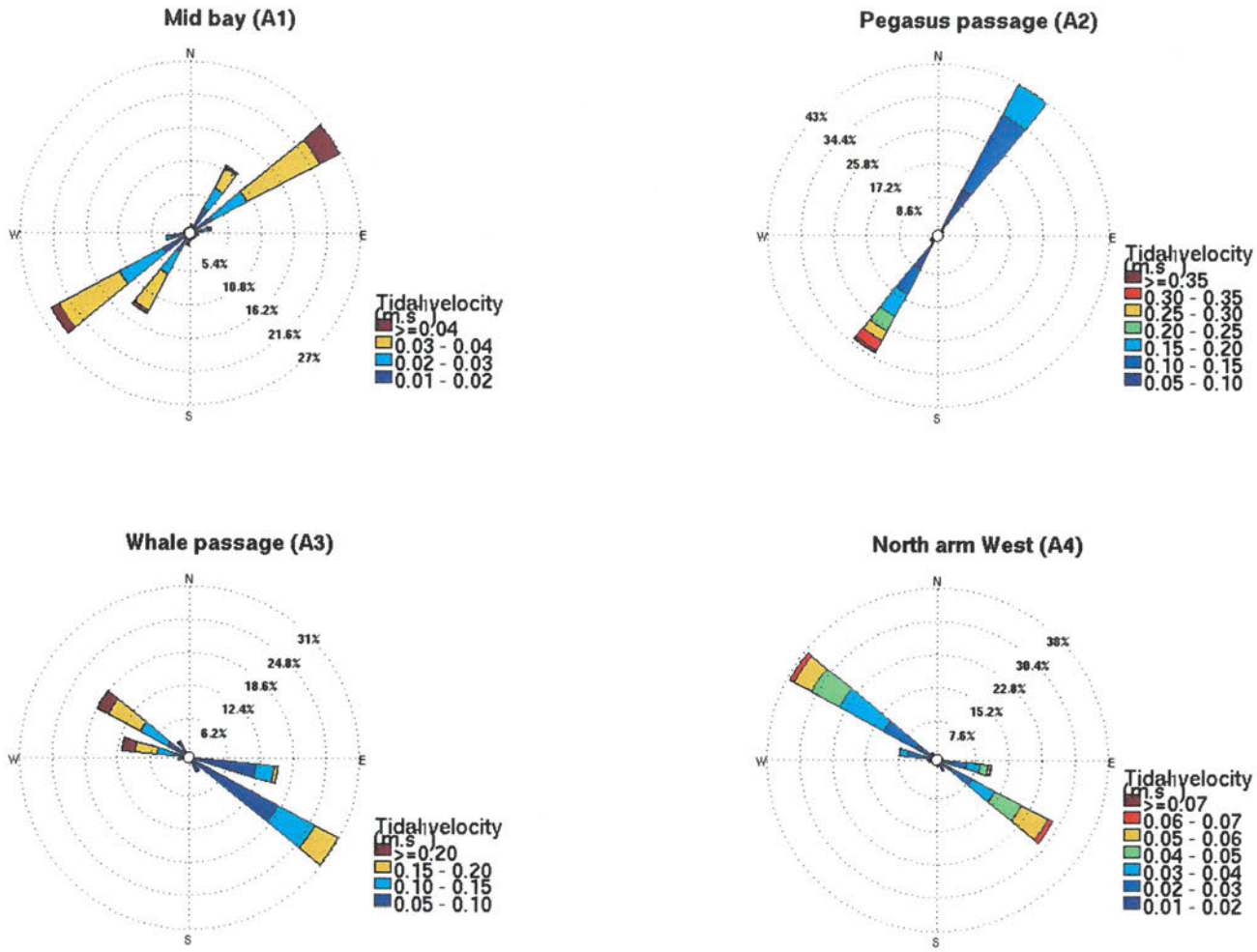

Figure 4.2 Current roses of the depth average tidal velocities at the four locations. Note directions are reported in the "going to" convention.

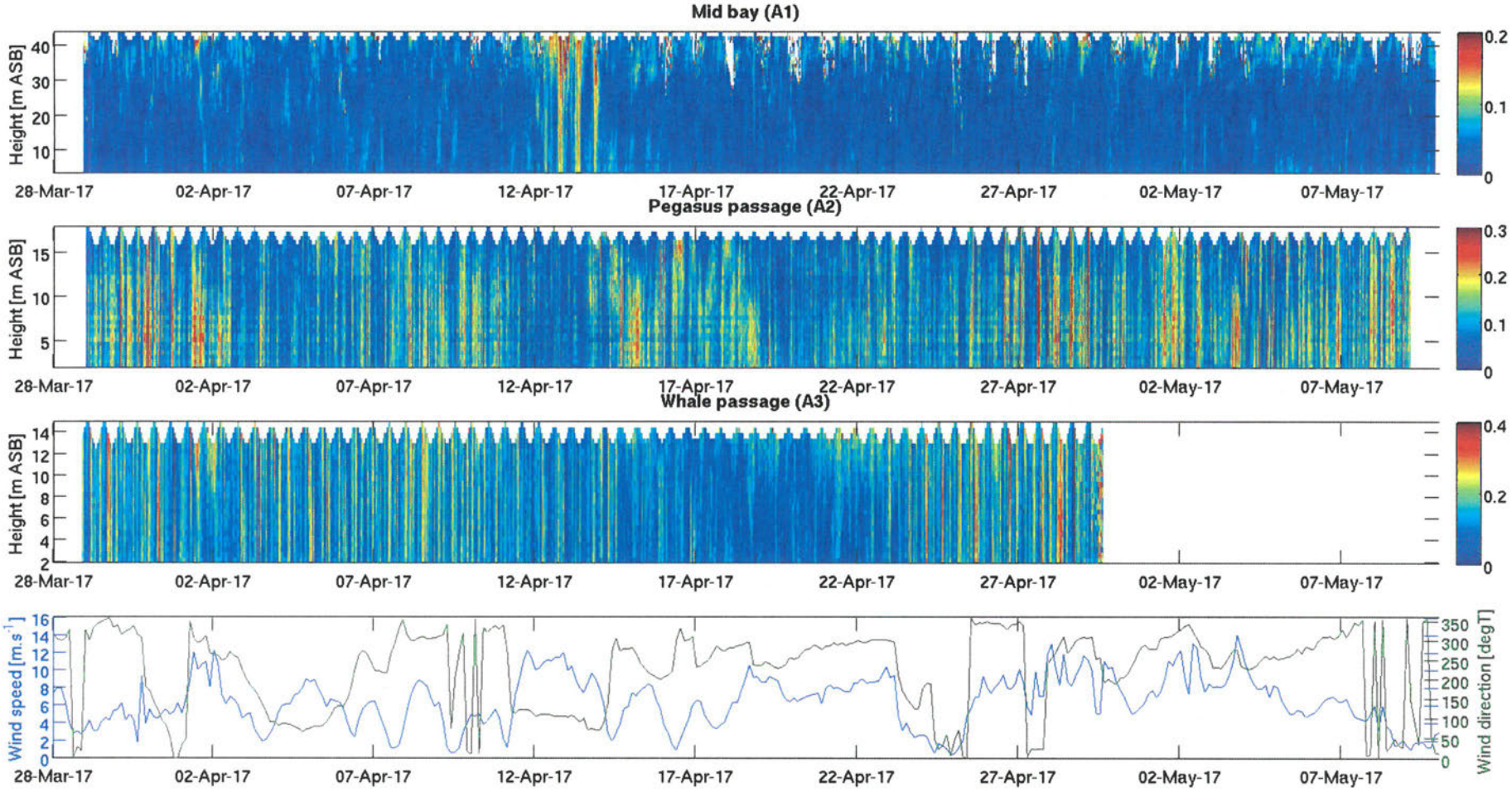

Figure 4.3 Time-series of winds near Pegasus Bay and measured residual velocity profiles Above Sea Bed (ASB) in $m.s^{-1}$ for the three ADCP deployed in 2017. Note, wind direction shows the wind coming from.

4.2. Model Validation

For this study, the *T-Tide* package in MATLAB (Pawlowicz et al., 2002) was used to decompose the measured and modelled time series of water elevation and flows into a sum of sinusoids at specifics frequencies corresponding to the tidal constituents (harmonics analysis).

A comparison of the measured and model predicted water elevation during April 2017 is given in Figure 4.4. Tidal constituents were extracted from the measured velocities measured within north arm west and used to re-create the tidal velocities of April 2017. Comparisons show that the model successfully reproduces the propagation of the tidal wave inside the bay, with good agreement between both amplitudes and phases of the principal tidal constituents at all sites (Table 4.1 to Table 4.4).

The predicted and modelled depth average tidal velocities are compared in Figure 4.5 and tidal direction in Figure 4.6. In general, the measured and modelled velocities are in agreement. The model reproduces correctly the phase and amplitude of tidal flows in the north arm.

Flow characteristics within Pegasus Passage are complicated due to the complex bathymetry within the passage. This resulted in the calibration and validation of the hydrodynamic model being problematic. There is a slight shift in phase between the measured and modelled tidal flow and the amplitude are smaller. It is likely that the difference between the model and measured data are due to small scale processes of such narrow channels and poorly defined bathymetry within the model domain.

Overall, the comparisons indicate that the model reproduces the measured velocities and water elevations to a reasonable degree. In particular, the model appears to robustly replicate the tidal dynamics in the north arm, which makes it fit for the present purpose.

The quantitative agreement between model and observations at several sites within the study area are provided in Table 4.5. Analysis indicates that both the model predicted current speeds and water elevations have relatively low bias and Mean Absolute Errors (MAE) and Root Mean Square Errors (RMSE), suggesting that the model is capable of reproducing the salient hydrodynamics within the study area.

Table 4.1 Comparison of measured and modelled constituents at mid bay (see Figure 2.1).

Tidal constituent	Amplitude [m]		Phase [deg]	
	Measured	Modelled	Measured	Modelled
M2	0.86	0.85	30.38	28.61
S2	0.16	0.18	47.39	42.76
N2	0.22	0.20	20.50	6.47
K2	0.07	0.06	35.78	34.20
K1	0.02	0.03	319.98	329.54
O1	0.04	0.03	256.64	248.38
P1	0.01	0.02	338.14	278.37
Q1	0.01	0.02	248.08	241.66
MF	0.03	0.03	128.32	248.86
MM	0.03	0.02	46.17	317.46
M4	0.02	0.02	246.19	250.35
MS4	0.01	0.01	272.11	261.53
MN4	0.01	0.01	229.35	195.86

Table 4.2 Comparison of measured and modelled constituents at Pegasus passage site (see Figure 2.1).

Tidal constituent	Amplitude [m]		Phase [deg]	
	Measured	Modelled	Measured	Modelled
M2	0.87	0.84	30.20	28.68
S2	0.17	0.18	46.81	42.86
N2	0.22	0.20	19.74	6.85
K2	0.07	0.05	32.76	33.78
K1	0.02	0.03	306.80	325.05
O1	0.04	0.04	256.74	248.92
P1	0.00	0.02	309.38	276.87
Q1	0.01	0.02	239.51	240.45
MF	0.03	0.02	128.87	243.04
MM	0.03	0.02	36.94	337.28
M4	0.02	0.02	251.02	250.01
MS4	0.01	0.01	284.15	262.17
MN4	0.01	0.01	237.58	196.71

Table 4.3 Comparison of measured and modelled constituents at Whale passage site (see Figure 2.1

Tidal constituent	Amplitude [m]		Phase [deg]	
	Measured	Modelled	Measured	Modelled
M2	0.87	0.85	29.50	28.75
S2	0.19	0.18	38.43	42.91
N2	0.21	0.20	16.31	6.38
K2	0.03	0.06	59.92	34.08
K1	0.02	0.03	312.66	330.47
O1	0.04	0.03	256.57	248.88
P1	0.00	0.02	329.54	277.14
Q1	0.01	0.02	238.46	240.70
MF	0.03	0.03	126.17	248.62
MM	0.03	0.02	38.72	308.58
M4	0.01	0.02	244.76	251.86
MS4	0.01	0.01	286.56	261.37
MN4	0.01	0.01	233.63	194.97

Table 4.4 Comparison of measured and modelled constituents at North arm West site (see Figure 2.1

Tidal constituent	Amplitude [m]		Phase [deg]	
	Measured	Modelled	Measured	Modelled
M2	0.90	0.84	29.41	28.55
S2	0.18	0.18	34.05	42.62
N2	0.19	0.20	17.24	6.48
K2	0.06	0.05	44.40	33.84
K1	0.02	0.03	297.10	327.31
O1	0.04	0.03	242.16	248.49
P1	0.01	0.02	290.47	277.59
Q1	0.01	0.02	258.93	240.84
MF	0.01	0.03	116.14	246.09
MM	0.01	0.02	43.33	326.39
M4	0.02	0.02	258.86	250.13
MS4	0.01	0.01	298.31	261.55
MN4	0.01	0.01	214.81	196.17

Table 4.5 Comparison between measured and SCHISM hindcast hydrodynamic data. Accuracy measures for current speed and water elevation at several sites within Pegasus Bay.

Sites	Parameters	MAE (m)	RMSE (m)	MRAE	Bias
Mid bay (A1)	Current speed ($m.s^{-1}$)	0.01	0.01	0.32	-0.01
	Elevation (m)	0.05	0.06	0.28	-0.00
Pegasus passage (A2)	Current speed ($m.s^{-1}$)	0.08	0.10	1.01	-0.04
	Elevation (m)	0.05	0.06	0.24	-0.00
Whale passage (A3)	Current speed ($m.s^{-1}$)	0.03	0.03	0.42	0.00
	Elevation (m)	0.05	0.07	0.27	0.00
North arm West (A4)	Current speed ($m.s^{-1}$)	0.01	0.01	0.48	-0.00
	Elevation (m)	0.06	0.08	0.34	-0.00

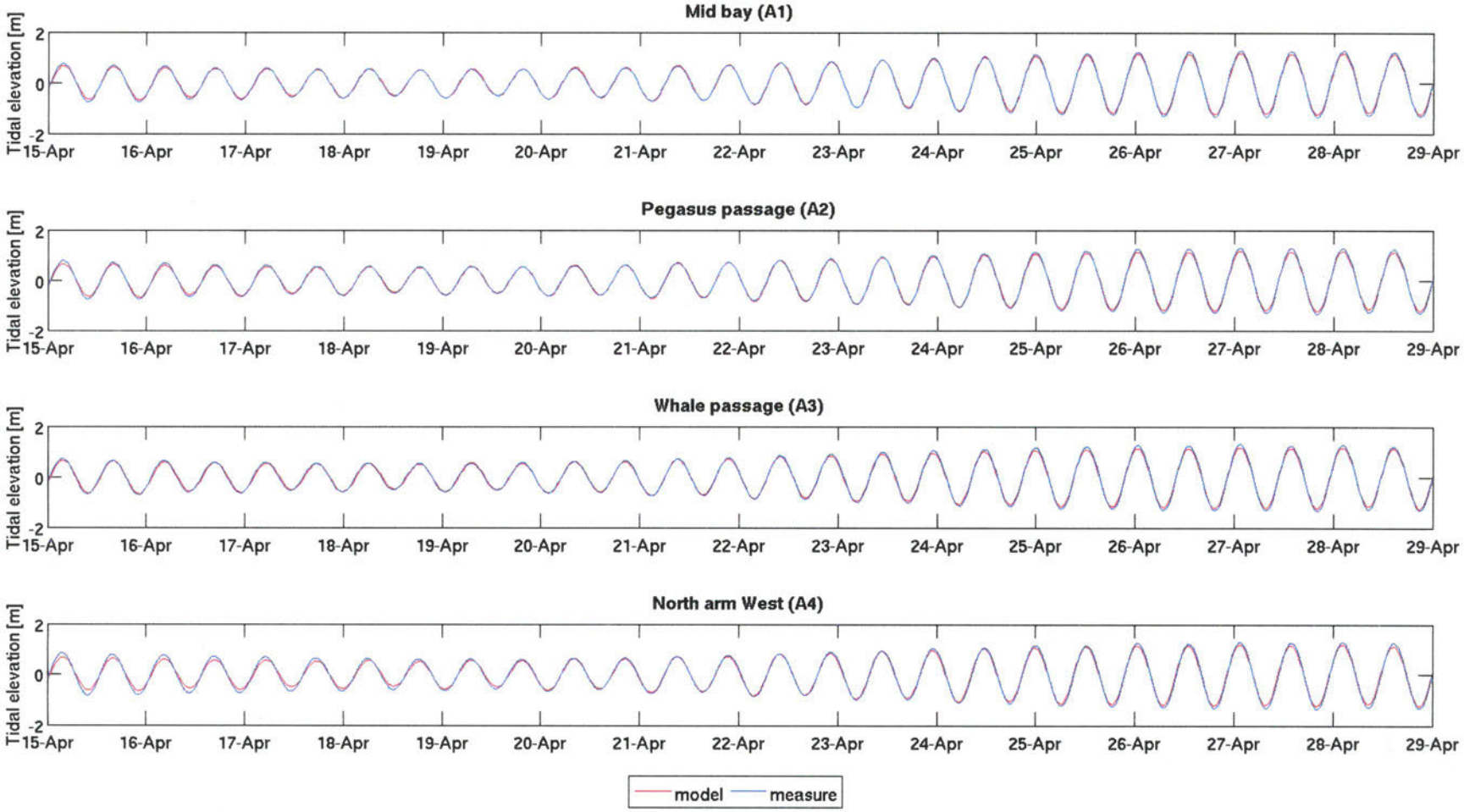

Figure 4.4 Comparison of modelled (red) and measured (blue) tidal water levels in April 2017 measured at four sites: Mid bay; Pegasus passage; Whale passage and North Arm West. Note that the tidal constituents were extracted from the flow at north arm West and used to re-create the tidal flow of April 2017

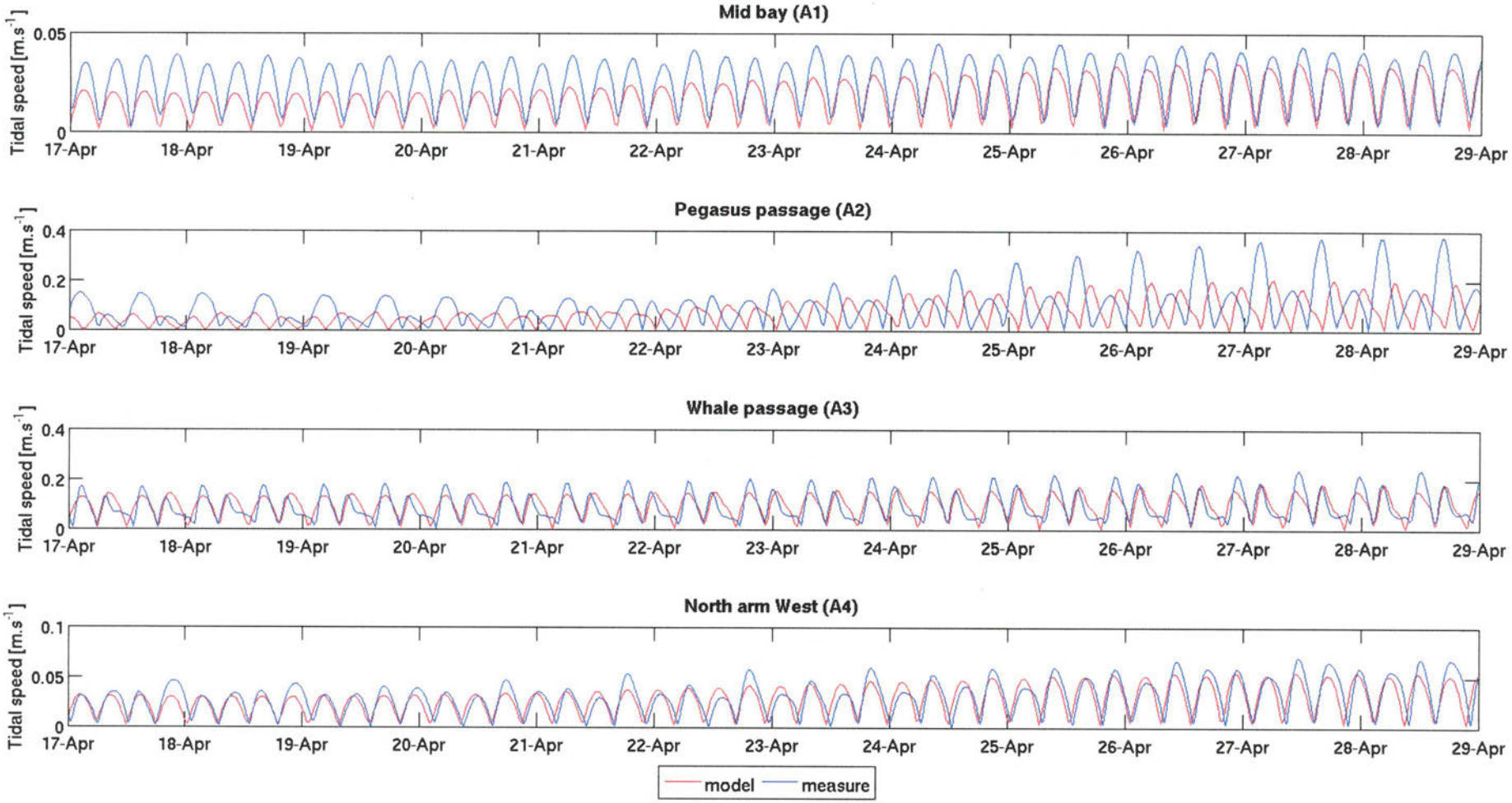

Figure 4.5 Comparison of measured and modelled depth-averaged tidal speed during the validation period at four sites: Mid bay; Pegasus passage; Whale passage and North Arm West. (see Figure 2.1 for position).

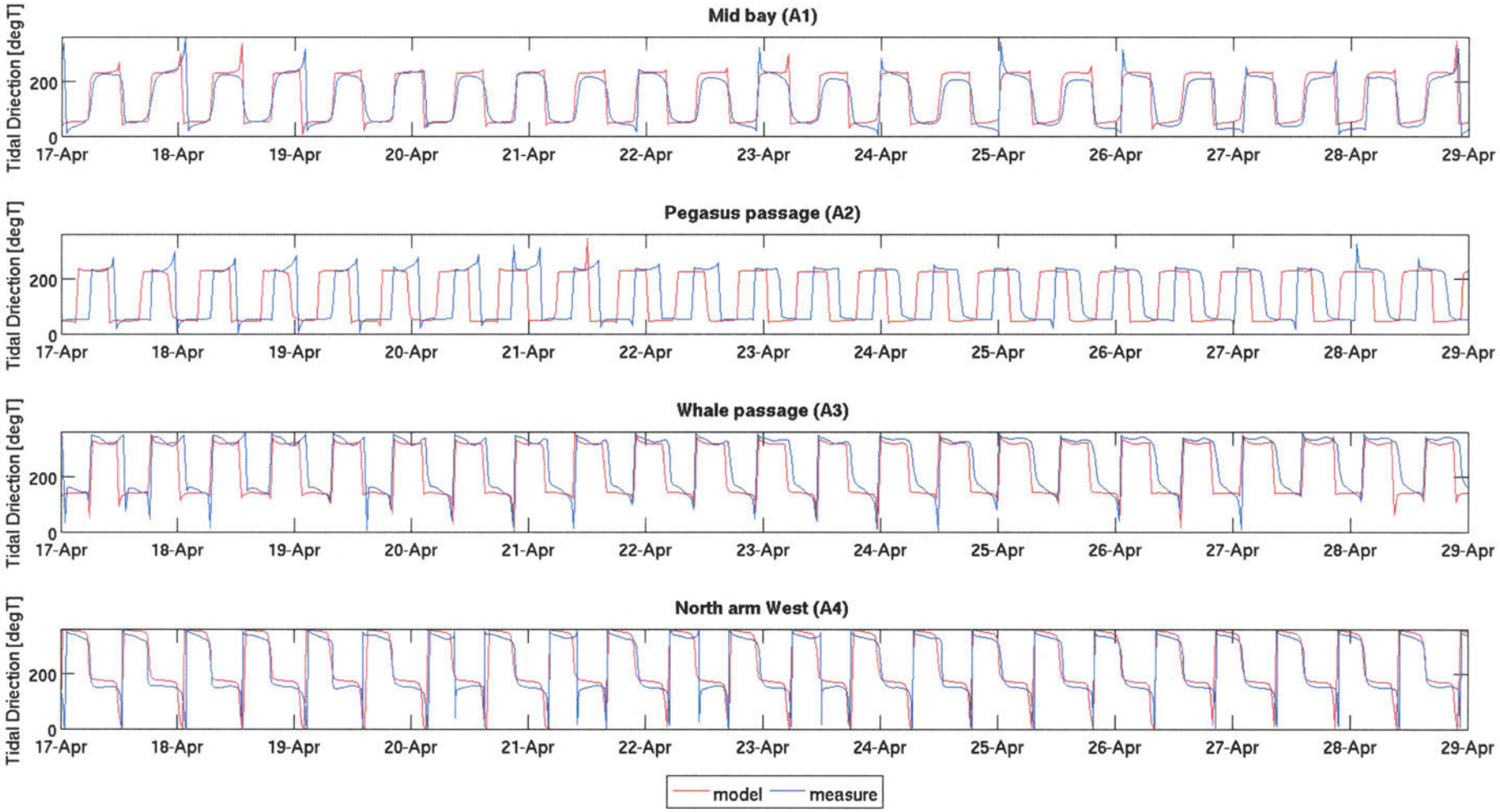

Figure 4.6 Comparison of measured and modelled depth-averaged tidal direction during the validation period at four sites: Mid bay; Pegasus passage; Whale passage and North Arm West. (see Figure 2.1 for position).

4.3. Model current velocities

The flood and ebb spatial distribution of current velocities within both the North and South Arms of Pegasus Bay at a Spring tidal stage are provided in Figure 4.7 and Figure 4.8 respectively. Not surprisingly, strong current velocities are expected within all of the main channels and passes. In general the North Arm of Pegasus Bay has slightly stronger current velocities.

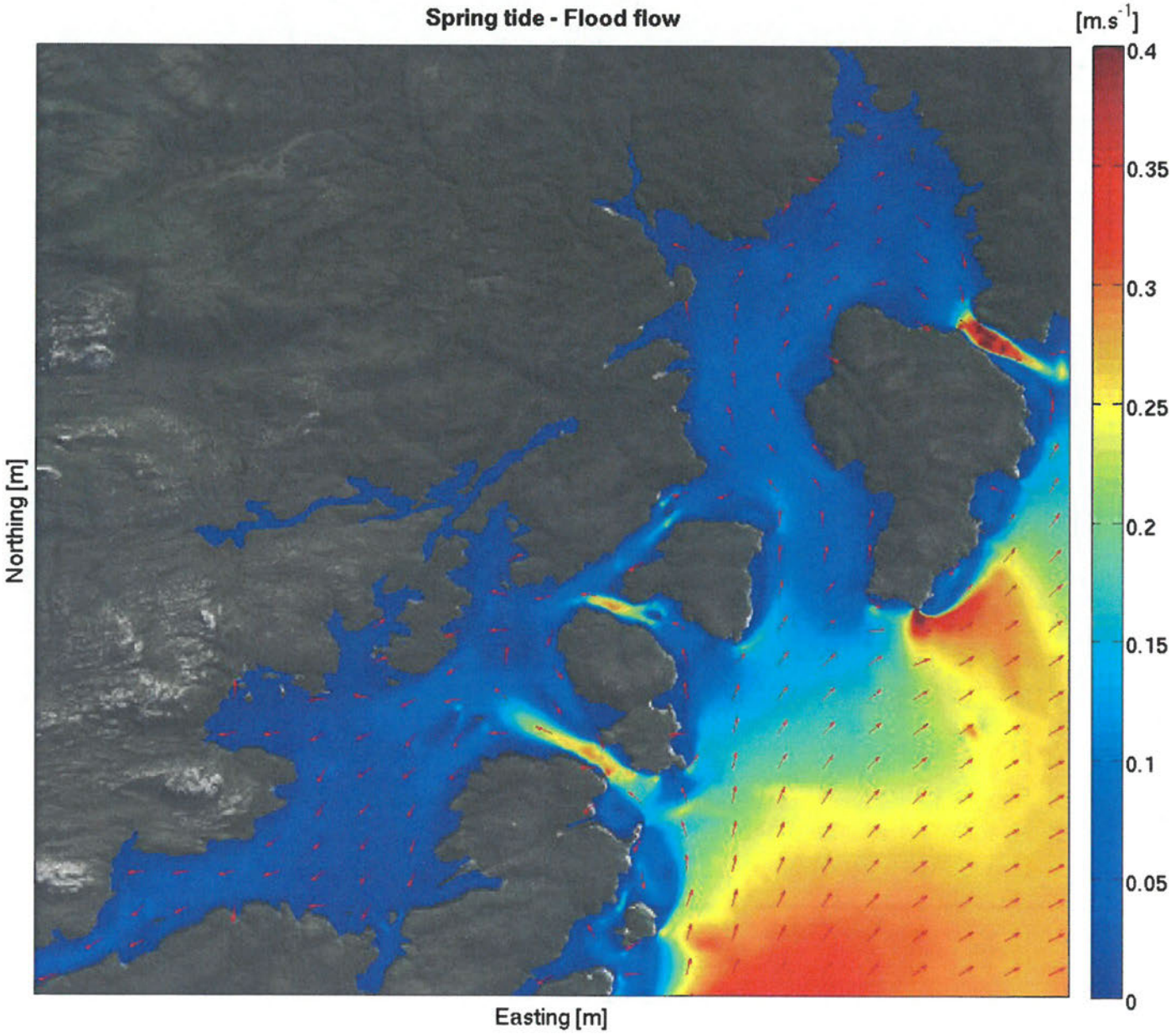

Figure 4.7 Snapshot of peak flood depth average total velocity in $m.s^{-1}$ during a spring tide in Pegasus Bay

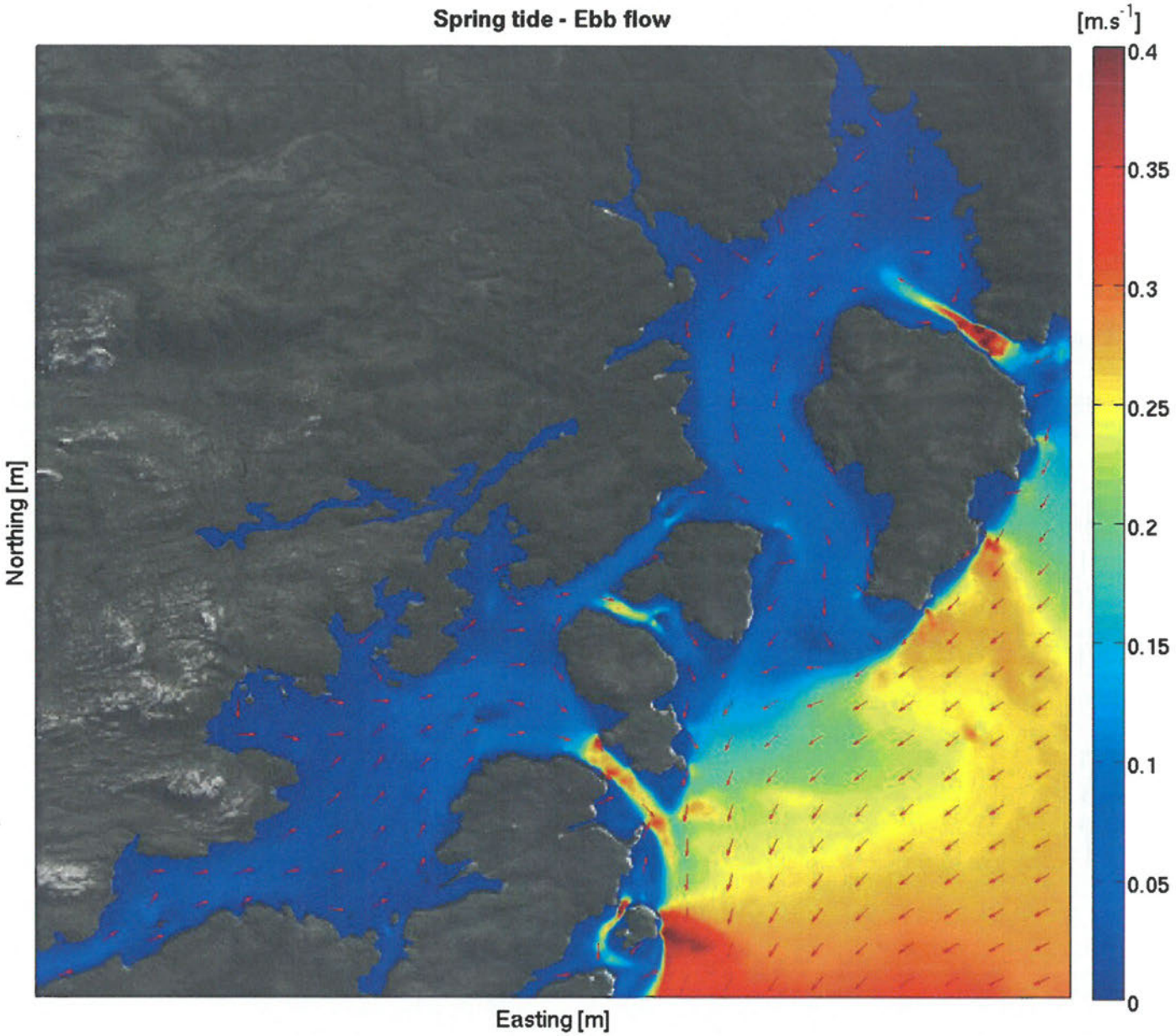

Figure 4.8 Snapshot of peak ebb depth average total velocity in $m.s^{-1}$ during a spring tide in Pegasus Bay.

5. SUMMARY

A high resolution hydrodynamic SCHISM model of Pegasus Bay, Stewart Island has been developed to examine the connectivity between the North and South Arms of Pegasus Bay.

The hydrodynamic model has been successfully calibrated and validated against measurements at 4 sites within Pegasus Bay (Figure 3.2), with 3 months hindcast data supplied. Calibration and validation in Pegasus Passage was complicated due to the complex bathymetry within the passage. Here, differences between the model and measured data are attributed to small scale processes occurring within the narrow channels which are likely to be relatively poorly defined within the model domain.

Hydrodynamic flow fields produced as part of the hindcast are suitable to use as to examine connectivity between the North and South Arms of Pegasus Bay.

REFERENCES

Egbert, G. D., and S. Y. Erofeeva. 2002. Efficient inverse modeling of barotropic ocean tides. Journal of Atmospheric and Oceanic Technology 19(2):183–204.

Saha, S., S. Moorthi, H.-L. Pan, X. Wu, J. Wang, S. Nadiga, P. Tripp, R. Kistler, J. Woollen, D. Behringer, H. Liu, D. Stokes, R. Grumbine, G. Gayno, J. Wang, Y.-T. Hou, H.-Y. Chuang, H.-M. H. Juang, J. Sela, M. Iredell, R. Treadon, D. Kleist, P. Van Delst, D. Keyser, J. Derber, M. Ek, J. Meng, H. Wei, R. Yang, S. Lord, H. Van Den Dool, A. Kumar, W. Wang, C. Long, M. Chelliah, Y. Xue, B. Huang, J.-K. Schemm, W. Ebisuzaki, R. Lin, P. Xie, M. Chen, S. Zhou, W. Higgins, C.-Z. Zou, Q. Liu, Y. Chen, Y. Han, L. Cucurull, R. W. Reynolds, G. Rutledge, and M. Goldberg. 2010. The NCEP Climate Forecast System Reanalysis. Bulletin of the American Meteorological Society 91(8):1015–1057.

Song, Y., and D. Haidvogel. 1994. A semi-implicit ocean circulation model using ageneralized topography-following coordinate system 115:228–244.

Zhang, Y. L., and A. M. Baptista. 2008. A semi-implicit Eulerian-Lagrangian finite element model for cross-scale ocean circulation. Ocean Modelling 21:71–96.

Appendix 3. MetOcean Wave Modelling Report.

METOCEAN
SOLUTIONS

STEWART ISLAND WAVE HINDCAST

Spectral wave modelling of Pegasus Bay

Report prepared for
Cawthron

Specialists in
Oceanography and
Meteorology

MetOcean Solutions Ltd: Report P0330-01

August 2016

Report status

Version	Date	Status	Approved by
RevA	07/08/2017	Draft for internal review	Guedes
RevB	09/08/2017	Draft for client review	Beamsley
RevC	10/08/2017	Updated draft	Guedes
RevD	14/08/2017	Updated draft or client review	Beamsley
RevE	27/09/2017	Updated draft or client review	Beamsley

It is the responsibility of the reader to verify the currency of the version number of this report.

TABLE OF CONTENTS

LIST OF FIGURES

LIST OF TABLES

1. INTRODUCTION

Cawthron have commissioned MetOcean Solutions to undertake a desktop metocean study of Pegasus Bay, Stewart Island. Pegasus Bay is situated near the south east corner of Stewart Island and consists of a North and South Arm.

An overview of the annual/seasonal metocean conditions at each location of interest is required to provide an initial characterisation of the environment from a marine operability perspective and determine extreme weather conditions.

Note that the standard oceanographic directional conventions are applied in this report, with wave directions reported in the 'coming from' directional reference frame.

Details of the numerical model used to characterise the historical wave climate, including the post-processing techniques and model validation are provided in Section 2, while results are presented in Section 3. Cited references are provided in the final section.

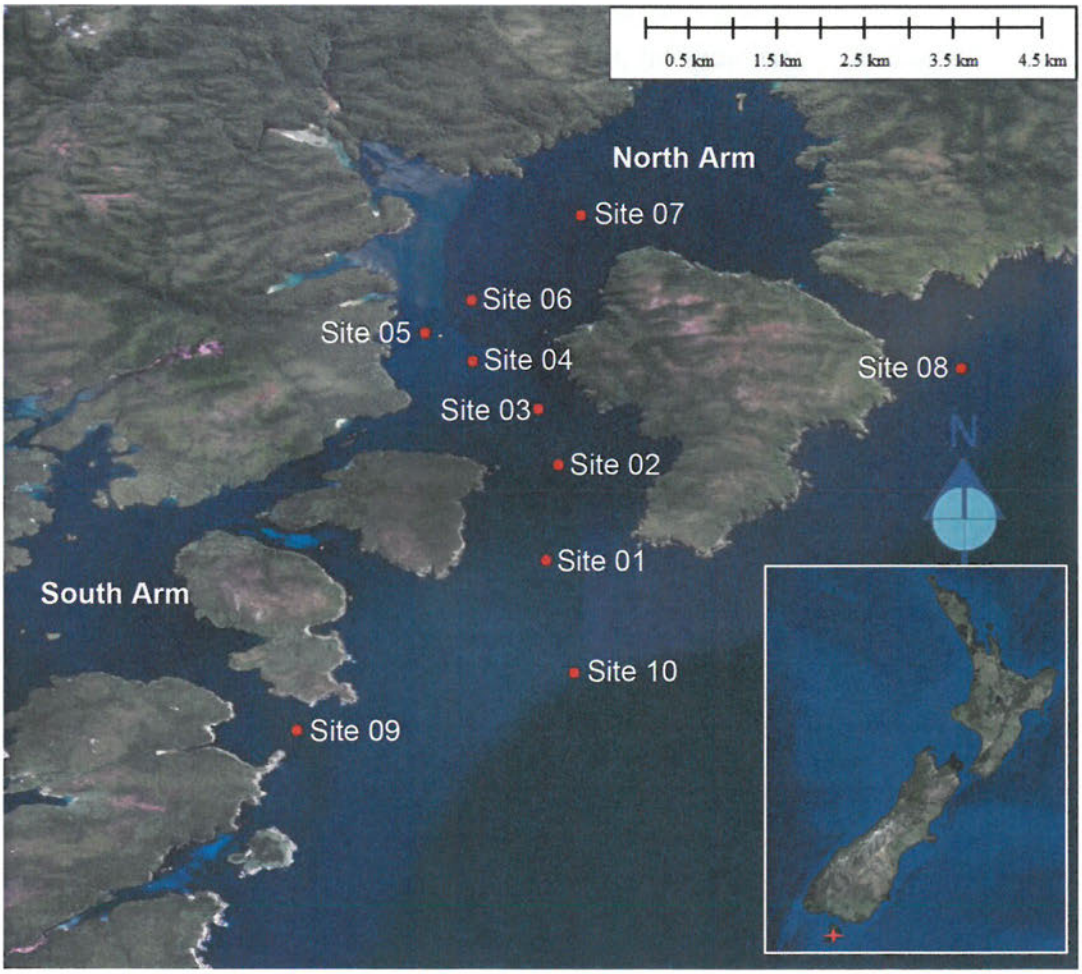

Figure 1.1. Location of Pegasus Bay on the south east corner of Stewart Island, NZ. Pegasus Bay consists of a North and South Arm. Output sites are also shown

2. WAVE HINDCAST

2.1. Model description

The wave hindcast was run over a 38-year period (1979–2016) using a modified version of SWAN[1] (Simulating WAves Nearshore). SWAN is a third generation ocean wave propagation model which solves the spectral action density balance equation (Booij *et al.*, 1999). The model simulates the growth, refraction and decay of each frequency-direction component of the complete sea state, providing a realistic description of the wave field as it changes in time and space. Physical processes that are modelled include the generation of waves by surface wind, dissipation by white-capping, resonant nonlinear interaction between the wave components, bottom friction and depth limited breaking dissipation. A detailed description of the model equations, parameterisations and numerical schemes can be found in Holthuijsen et al. (2007) and in the SWAN documentation[2].

2.2. Model setup

SWAN was run in the non-stationary mode with all third generation physics included in the model. The source term parameterisations of *Westhuysen et al.* (2007) were employed and the *Collins* (1972) scheme was used for bottom friction with the default coefficient of 0.015. The spectra were discretised with 36 directional bins (10° directional resolution) and up to 35 logarithimic frequencies f between 0.0412 and 1.0521 Hz with resolution $\Delta f = 0.1f$ (Table 2.1).

A downscale nesting approach was employed to resolve the nearshore region around Army Bay. Three regular nests were defined with resolutions progressively increasing from 5 km to 100 m (Table 2.1). The South of New Zealand 5 km parent nest extended all the way south of Auckland Island to account for sheltering effects from the islands and surrounding shallow shelf (Figure 2.1). The Stewart Island 1 km nest (Figure 2.2) provided appropriate downscaling and detailed boundary conditions to run the high-resolution domain around Pegasus Bay (Figure 2.3). Full spectral boundaries to the parent SWAN nest were prescribed from a global implementation of WAVEWATCH III (WW3) spectral wave model (*Tolman*, 1991) run at 0.5° resolution using the source term parameterisatios of *Ardhuin et al.* (2010).

2.3. Model data sources

The two child SWAN nests were run with wind fields specified from the MetOcean Solutions New Zealand Reanalysis. The dataset was constructed by running WRF at 8-km resolution, with its initial and lateral boundary conditions set by the Climate Forecast System Reanalysis (*Saha et al.*, 2010) from the National Centers for Environmental Prediction (NCEP). The parent SWAN nest was forced from CFSR winds. Model depths were constructed from a combination of the global GEBCO dataset (*Weatherall et al.*, 2015) and Electronic Nautical Charts (ENC).

Time-series of wave parameters were extracted from the child domain at 10 locations (Table 2.2) as shown in Figure 2.3 and Figure 1.1.

[1] Modified from SWAN version of the 40.91 release
[2] http://swanmodel.sourceforge.net/online_doc/online_doc.htm

Table 2.1. Extents, resolution and frequency range defined for the four SWAN nests. Each child domain was run off spectral wave boundaries provided by domain immediate above in the table. Spectral boundaries to run the NZN parent nest were prescribed from the 0.5° global WW3 wave model.

	Longitude (degree)			Latitude (degree)			Frequencies (Hz)	
Domain	x_{min}	x_{max}	dx	y_{min}	y_{max}	Res	f_{min}	f_{max}
South NZ	164	171	0.05	-51.5	-46	0.05	0.0412	0.7186
Stewart Island	167.0	168.5	0.01	-47.5	-46.5	0.01	0.0412	0.7186
Pegasus Bay	167.58	167.75	0.001	-47.31	-47.15	0.001	0.0412	1.0521

Table 2.2. Coordinates and model depth for the 10 sites were frequency-direction wave spectra were output.

Site	Longitude (degree)	Latitude (degree)	Depth (m)
Site 01	167.689252	-47.209640	41
Site 02	167.690444	-47.200005	38
Site 03	167.688414	-47.194246	34
Site 04	167.681666	-47.189457	32
Site 05	167.681537	-47.183293	35
Site 06	167.692783	-47.174617	42
Site 07	167.676803	-47.186572	33
Site 08	167.731548	-47.190093	34
Site 09	167.663790	-47.227046	28
Site 10	167.692091	-47.221178	77

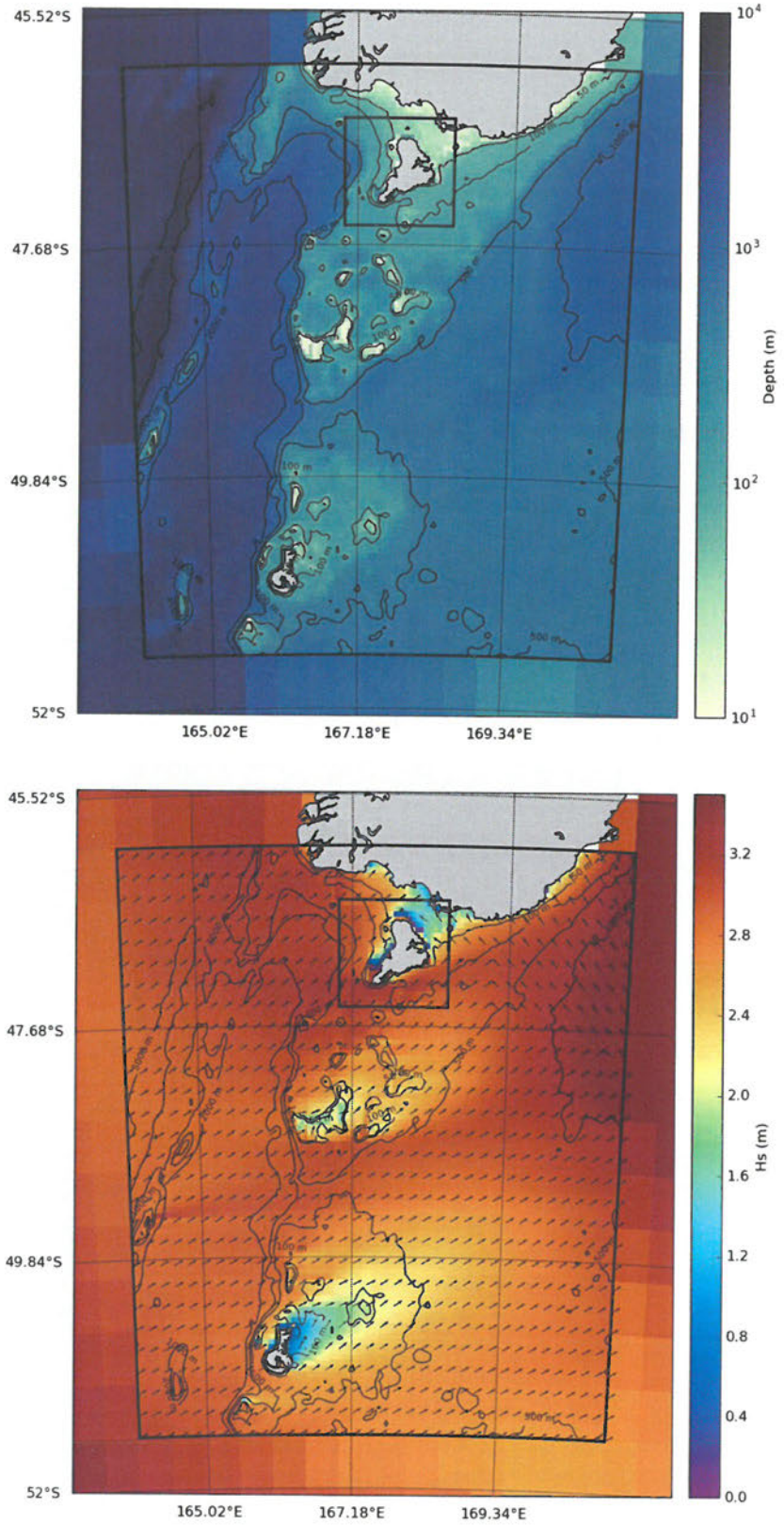

Figure 2.1. Snapshots of (top) model depths and (bottom) significant wave height *Hs* from the SNZ 5 km SWAN parent domain on 01 January 2000, shown within the area delimited by the outer rectangle. Arrows show the mean wave direction at the peak wave frequency *Dpm*. Model data from the 0.5° global wave model are shown outside of this area. Extension of Stewart Island child nest is shown by the inner rectangle.

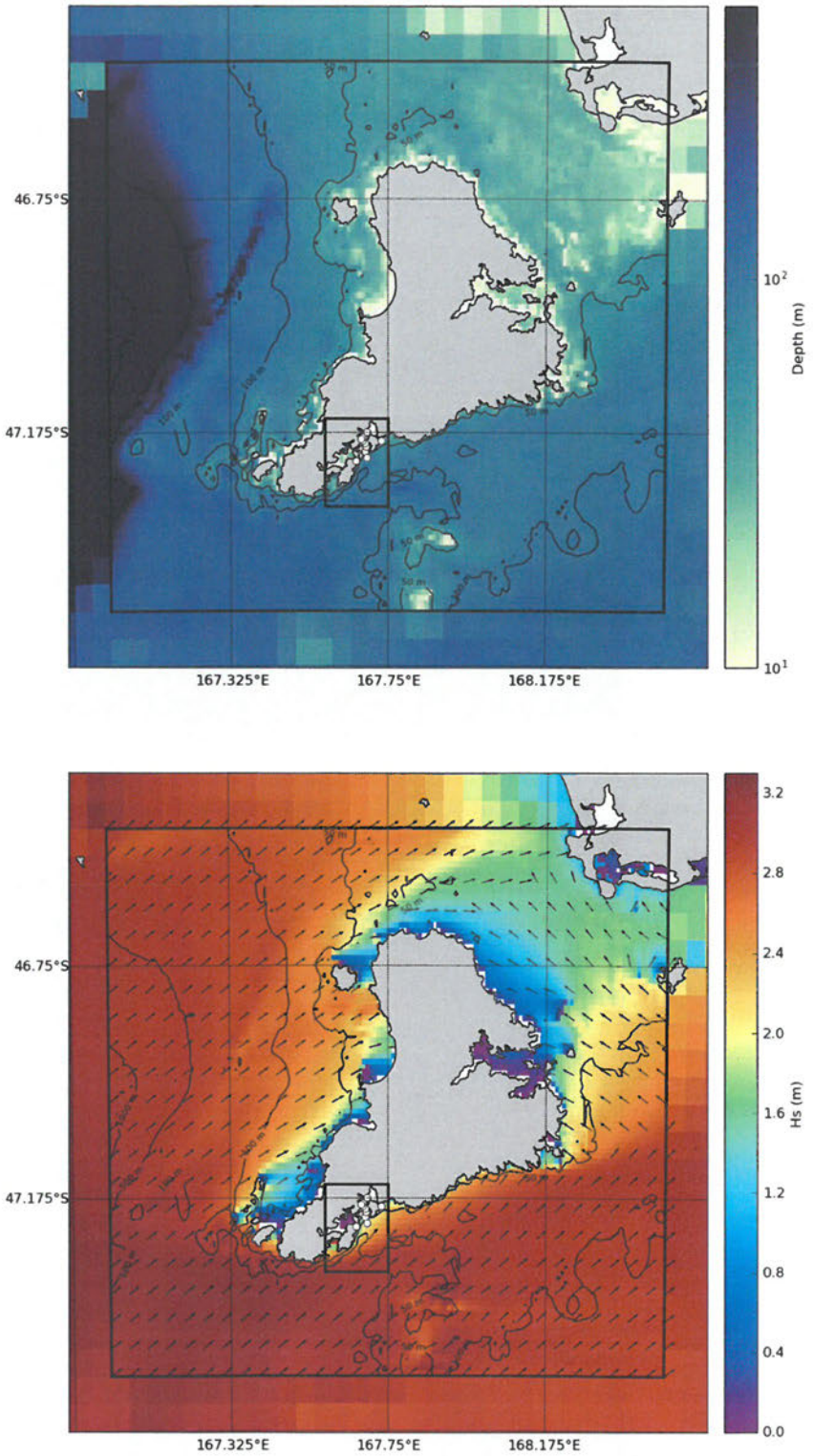

Figure 2.2. Snapshots of (top) model depths and (bottom) significant wave height *Hs* from the Stewart Islands 1 km SWAN parent domain on 01 January 2000, shown within the area delimited by the outer rectangle. Arrows show the mean wave direction at the peak wave frequency *Dpm*. Model data from the 5 km SZN wave model are shown outside of this area. Extension of Pegasus Bay child nest is shown by the inner rectangle.

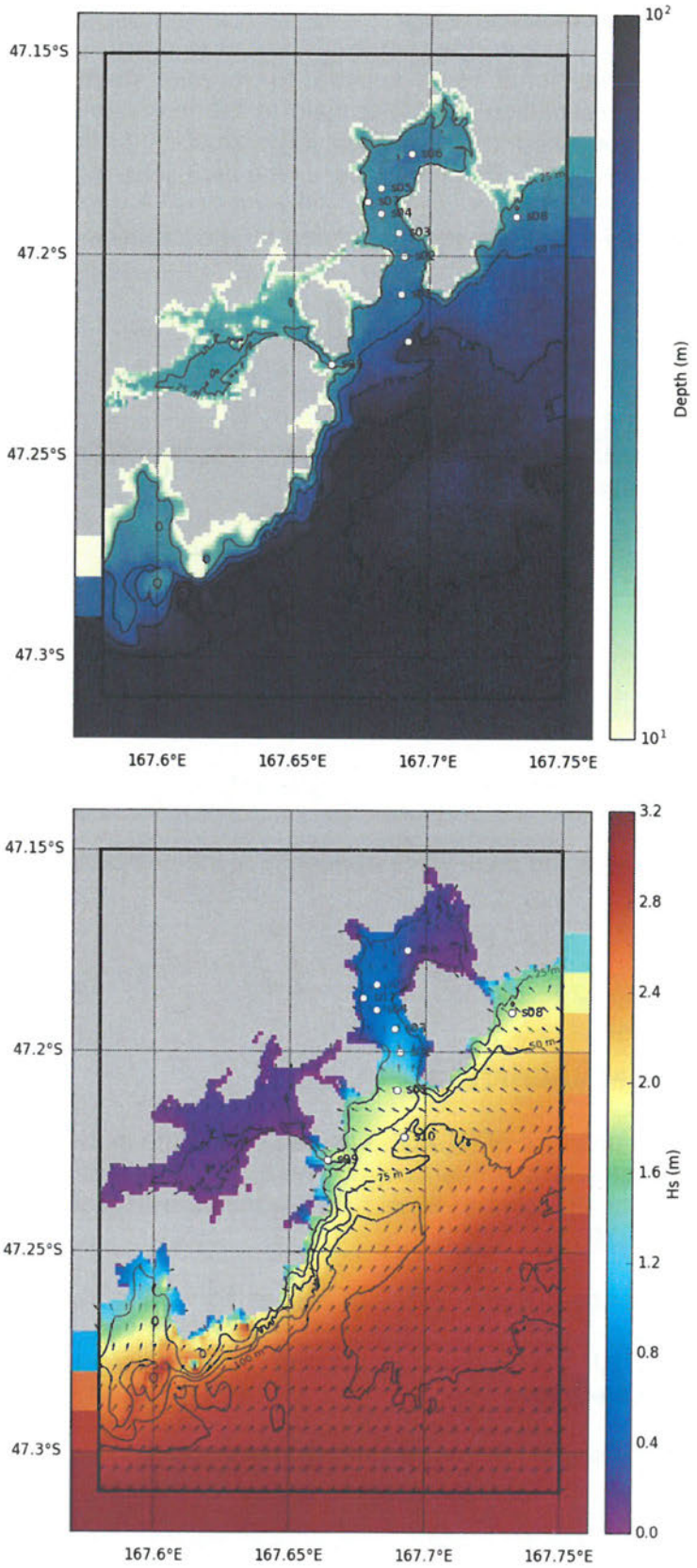

Figure 2.3. Snapshots of (top) model depths and (bottom) significant wave height *Hs* from the Pegasus 1 km SWAN parent domain on 01 January 2000, shown within the area delimited by the outer rectangle. Arrows show the mean wave direction at the peak wave frequency *Dpm*. White circles show the output sites in Table 2.2

2.4. Post-processing

Two-dimensional wave spectra $E(f,\theta)$ were output at hourly intervals from the highest resolution SWAN domain at the ten sites in Table 2.2. The spectra were post-processed to calculate wave parameters for the total wave field as well as the sea and swell components (assuming an 8 second period split).

Spectral moments were calculated for the total and partitioned spectra as:

$$m_x = \iint f^x E(f,\theta) df\, d\theta, \tag{2.1}$$

where θ is the wave direction and x is an integer. The significant wave height *Hs*, the mean direction at the peak wave frequency *Dpm* and the peak wave period *Tp* were defined as:

$$H_s = 4\sqrt{m_0}, \tag{2.2}$$

$$Dpm = \tan^{-1}\frac{\int_{-\pi}^{\pi} E(f_p,\theta)\sin\theta\, d\theta}{\int_{-\pi}^{\pi} E(f_p,\theta)\cos\theta\, d\theta}, \tag{2.3}$$

$$T_p = 1/f_p, \tag{2.4}$$

where f_p is the peak wave frequency of the one-dimensional spectra:

$$E(f) = \int_{-\pi}^{\pi} E(f,\theta) d\theta. \tag{2.5}$$

2.5. Model validation

In the absence of in-situ measured wave data in the area, the model was validated against satellite observations. The data consists of a multi-platform global altimeter data, quality-controlled and homogenised as described in *Queffeulou and Croize-Fillon* (2017).

Model and altimeter *Hs* were collocated withing the area of the 5 km SNZ SWAN domain (Figure 2.4; Table 2.1), within 0.05° by 0.05° squares, over the period 2012–2016. the following accuracy measures were calculated for each pair of collocated data:

Mean Absolute Error (MAE):

$$MAE = \sum_{i=1}^{N} \overline{M_i - O_i} \tag{2.9}$$

Root Mean Square Error (RMSE):

$$RMSE = \sqrt{\frac{1}{N}\sum_{i=1}^{N}(M_i - O_i)^2} \quad (2.10)$$

Mean Relative Absolute Error (MRAE):

$$MRAE = \frac{1}{N}\sum_{i=1}^{N}\left|\frac{M_i - O_i}{O_i}\right| \quad (2.11)$$

Bias:

$$Bias = \frac{1}{N}\sum_{i=1}^{N} M_i - O_i \quad (2.12)$$

Scatter Index (SI):

$$SI = \frac{\sqrt{\frac{1}{n}\sum_{i=1}^{N}\left((M_i - \bar{M}) - (O_i - \bar{O})\right)^2}}{\bar{O}} \quad (2.13)$$

where M_i and O_i are the modelled and observed *Hs*, *N* is the number of collocations and overbar denotes the mean value. The Scatter Index presents the percentage of RMSE difference with respect to mean observation or it gives the percentage of expected error for the parameter, so reltatively smaller numbers are desirable. With respect to RMSE, smaller values also indicate better agreement between measured and modelled values.

The accuracy measures are presented in Table 2.3.

There was good agreement overall between modelled and observed *Hs* over the area South of New Zealand. Error measures were relatively low particularly when the wave height range in the region is considered. A positive overall bias of 8 cm was observed with a Root Mean Square Error of 53 cm, and low Mean Relative Absolute Error and Scatter Index of 11 and 14% respectively. Gridded validation (Figure 2.5) shows that the model tended to overpredicted *Hs* towards the western side of the domain presumably due to excess south-west swell wave energy generated in the global wave model over the Southern Ocean. Overall model and satellite altimeter *Hs* agree well over the entire wave height range (Figure 2.6).

Table 2.3. Accuracy measures of the hindcast significant wave height *Hs* against satellite altimeter data.

Bias	RMSE	MAE	MRAE	SI
0.08 m	0.53 m	0.40 m	0.11	0.14

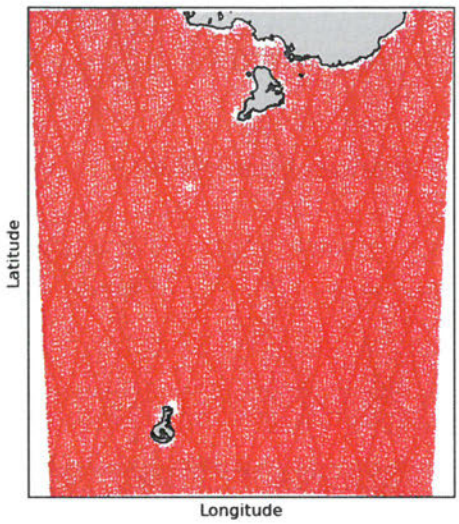

Figure 2.4. Collocations of model and altimeter data during 2012–2016 used for the model validation over the SNZ SWAN domain. Red-dots denote the collocated data used to perform the analysis.

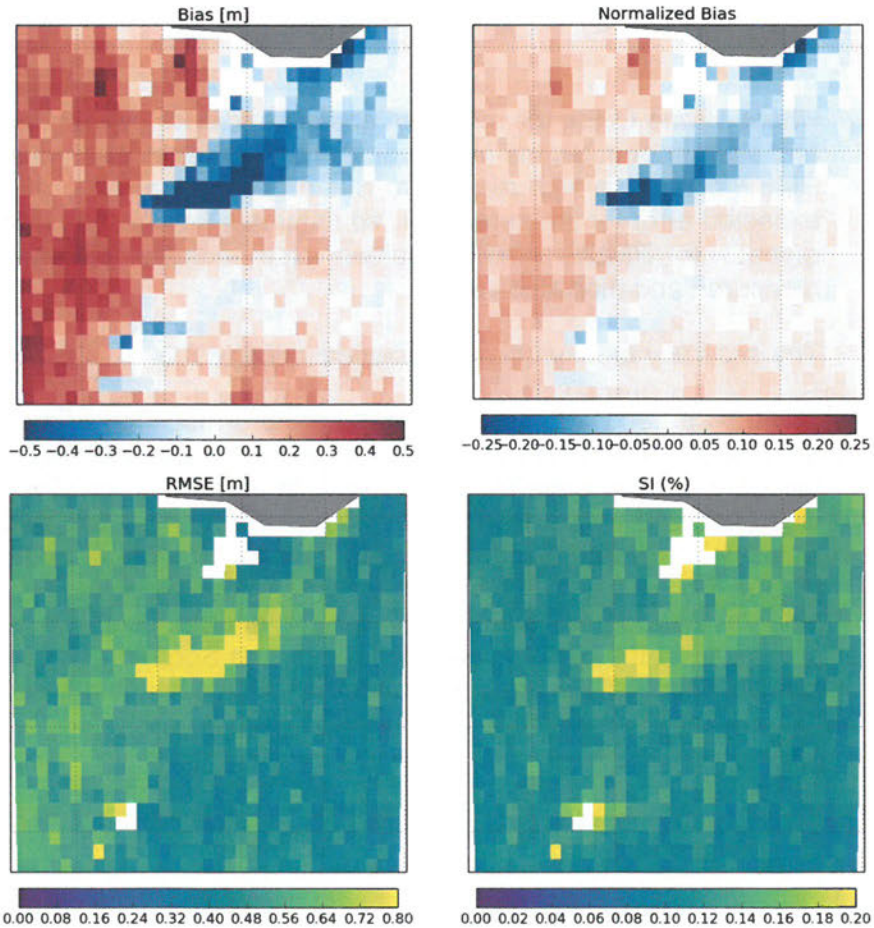

Figure 2.5. Gridded accuracy statistics within the area of the SNZ SWAN domain. Model and satellite altimeters H_s were collocated within 0.05° by 0.05° squares over the 2012–2016 period. The Scatter Index presents the percentage of RMSE difference with respect to mean observation so smaller numbers are desirable. With respect to RMSE, smaller values also indicate better agreement between measured and modelled values.

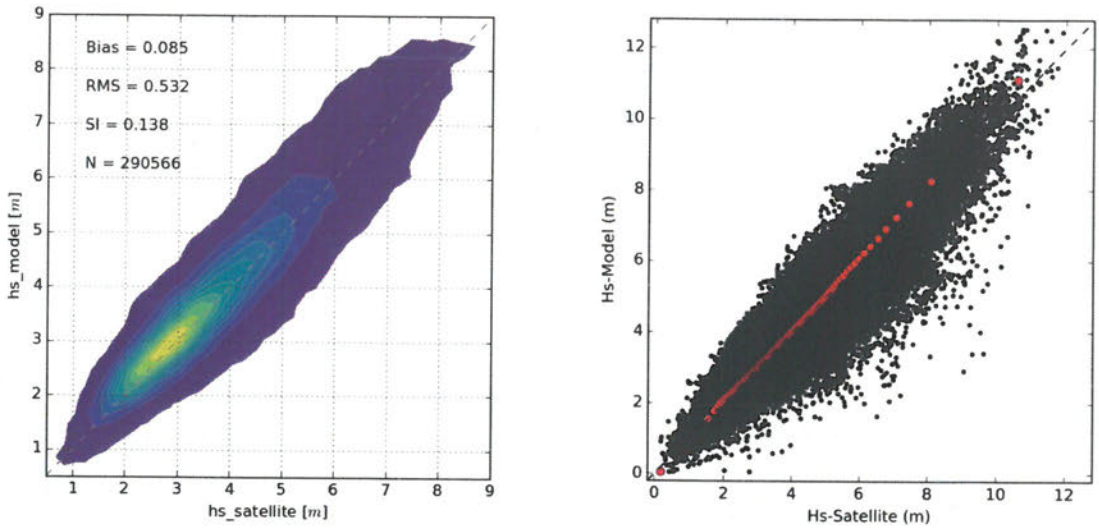

Figure 2.6. Scatter density (left) and scatter diagram (right) comparing *Hs* from model and satellite altimeters over the years 2012–2016. Hot colours on the left indicate higher density of datapoints. Red circles on the right show the quantile-quantile at 1-percentile increments.

3. RESULTS

3.1. Summary gridded statistics

Summary statistics were calculated over the Pegasus Bay 100 m SWAN domain from the entire hindcast period. Mean and maximum gridded significant wave height for the 38-year period are presented below in Figure 3.1 and Figure 3.2.

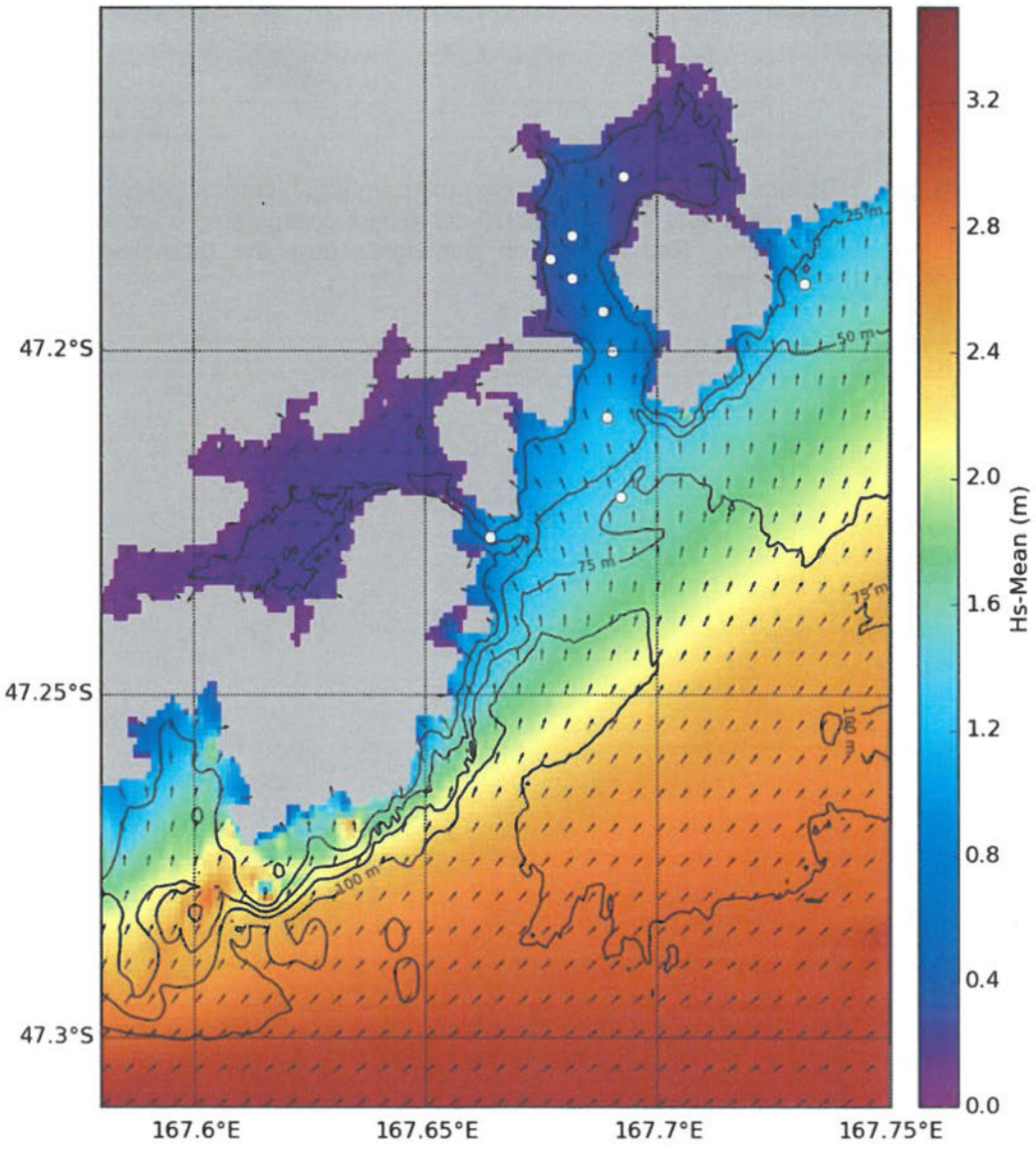

Figure 3.1. Mean significant wave height *Hs* over the Pegasus Bay 100 m SWAN domain calculated from the 38-year hindcast. Arrows represent the vector-average mean direction at the peak wave frequency. White circles show the output sites in Table 2.2.

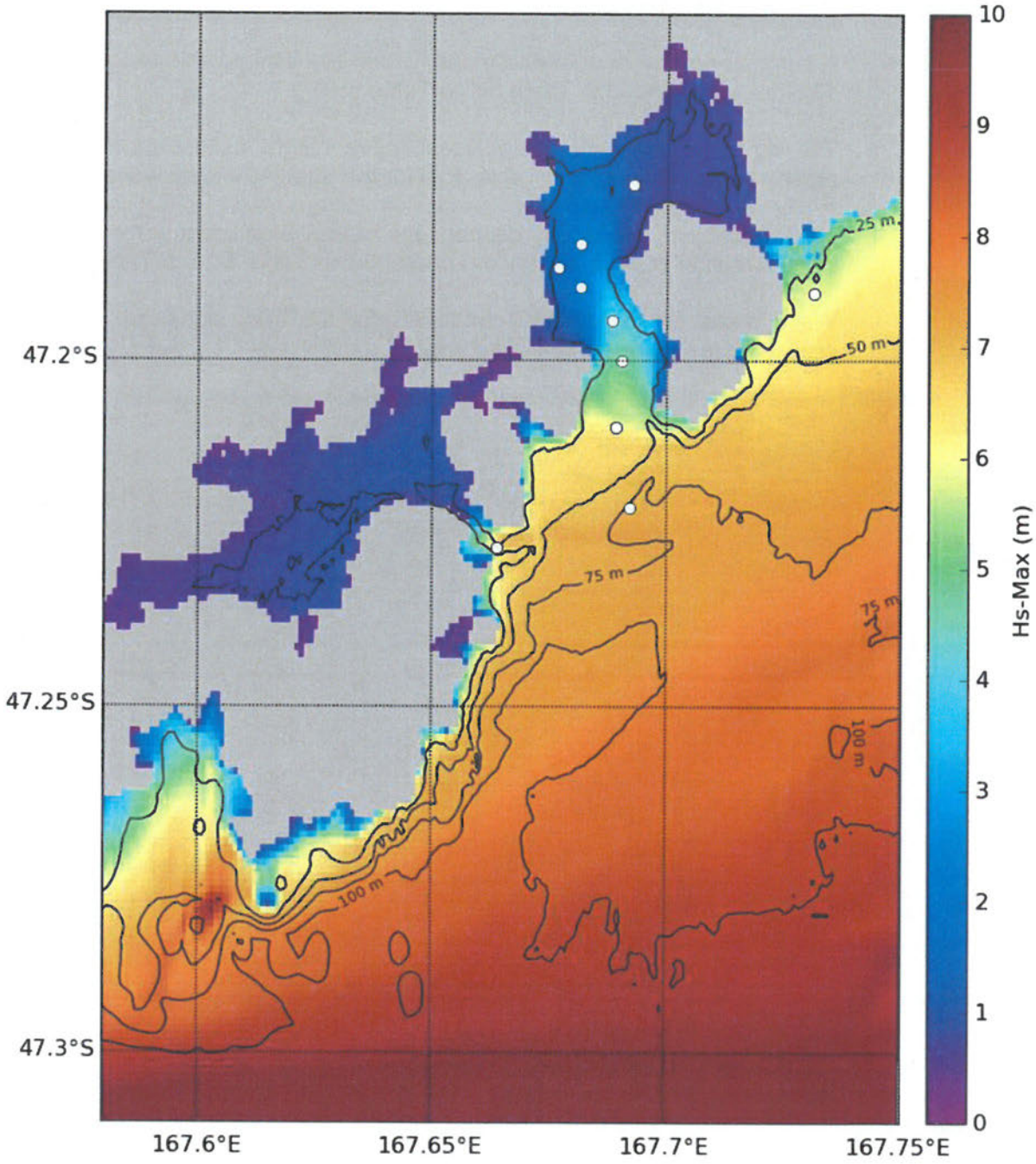

Figure 3.2. Maximum significant wave height Hs over the Pegasus Bay 100 m SWAN domain calculated from the 38-year hindcast. White circles show the output sites in Table 2.2.

3.2. Site wave statistics

A summary of the annual and monthly total significant wave height statistics at the 10 sites are provided in Table 3.1 to Table 3.10.

The monthly and annual significant wave height exceedance probabilities are presented in Table 3.11 to Table 3.20 for the total significant wave height.

The annual joint probability distributions of total significant wave height and mean wave direction at peak energy are presented in Table 3.21 to Table 3.30.

Wave roses for the annual conditions for the total significant wave height are presented in Figure 3.3 to Figure 3.12.

Table 3.1 Annual and monthly total significant wave height statistics at Site 01.

	Significant wave height (m)								
	min	mean	std	p10	p50	p90	p95	p99	max
January	0.25	1.02	0.40	0.63	0.93	1.50	1.76	2.48	5.07
February	0.36	1.07	0.40	0.67	0.98	1.55	1.85	2.58	3.95
March	0.39	1.17	0.40	0.75	1.10	1.67	1.90	2.53	4.20
April	0.41	1.24	0.47	0.75	1.15	1.83	2.12	2.70	5.63
May	0.45	1.35	0.53	0.83	1.24	2.02	2.40	3.21	5.45
June	0.46	1.41	0.55	0.84	1.31	2.08	2.46	3.30	5.99
July	0.39	1.37	0.54	0.80	1.26	2.08	2.41	3.20	5.57
August	0.39	1.37	0.53	0.82	1.27	2.04	2.38	3.19	4.97
September	0.43	1.27	0.48	0.74	1.18	1.89	2.16	2.91	4.52
October	0.41	1.17	0.40	0.75	1.10	1.69	1.93	2.44	3.98
November	0.36	1.09	0.39	0.68	1.02	1.57	1.82	2.40	3.99
December	0.39	1.00	0.35	0.62	0.94	1.47	1.70	2.17	3.68
All	0.25	1.21	0.48	0.72	1.12	1.81	2.12	2.86	5.99

Table 3.2 Annual and monthly total significant wave height statistics at Site 02.

	Significant wave height (m)								
	min	mean	std	p10	p50	p90	p95	p99	max
January	0.18	0.77	0.32	0.47	0.70	1.15	1.37	1.90	4.24
February	0.28	0.81	0.31	0.50	0.75	1.20	1.39	1.86	3.18
March	0.29	0.89	0.33	0.55	0.82	1.30	1.52	2.03	3.40
April	0.29	0.94	0.38	0.55	0.87	1.41	1.65	2.23	4.78
May	0.31	1.03	0.45	0.59	0.93	1.58	1.94	2.69	4.39
June	0.30	1.04	0.45	0.56	0.96	1.60	1.93	2.62	3.99
July	0.26	0.99	0.41	0.56	0.91	1.51	1.79	2.42	3.61
August	0.24	0.96	0.42	0.55	0.88	1.48	1.77	2.41	4.06
September	0.24	0.94	0.39	0.55	0.86	1.45	1.70	2.33	3.58
October	0.32	0.91	0.34	0.55	0.85	1.35	1.57	2.06	3.35
November	0.23	0.86	0.34	0.50	0.79	1.29	1.50	1.98	3.05
December	0.21	0.75	0.29	0.44	0.69	1.12	1.30	1.77	2.91
All	0.18	0.91	0.39	0.52	0.83	1.38	1.64	2.26	4.78

Table 3.3 Annual and monthly total significant wave height statistics at Site 03.

	Significant wave height (m)								
	min	mean	std	p10	p50	p90	p95	p99	max
January	0.15	0.63	0.26	0.38	0.57	0.94	1.11	1.54	3.55
February	0.22	0.66	0.25	0.40	0.61	0.97	1.14	1.55	2.62
March	0.22	0.72	0.27	0.44	0.67	1.07	1.23	1.68	2.77
April	0.23	0.77	0.31	0.44	0.71	1.16	1.34	1.82	3.96
May	0.24	0.84	0.37	0.48	0.75	1.29	1.59	2.20	3.63
June	0.24	0.85	0.38	0.45	0.78	1.31	1.58	2.17	3.30
July	0.20	0.80	0.34	0.45	0.74	1.24	1.47	2.00	3.01
August	0.19	0.78	0.35	0.44	0.71	1.22	1.46	1.98	3.44
September	0.19	0.77	0.32	0.45	0.70	1.18	1.39	1.90	3.02
October	0.24	0.74	0.28	0.45	0.69	1.10	1.28	1.68	2.66
November	0.18	0.70	0.28	0.41	0.65	1.05	1.23	1.62	2.48
December	0.15	0.61	0.24	0.36	0.56	0.91	1.06	1.44	2.47
All	0.15	0.74	0.32	0.42	0.67	1.13	1.34	1.85	3.96

Table 3.4 Annual and monthly total significant wave height statistics at Site 04.

	Significant wave height (m)								
	min	mean	std	p10	p50	p90	p95	p99	max
January	0.11	0.37	0.15	0.23	0.35	0.54	0.63	0.87	2.03
February	0.11	0.39	0.15	0.24	0.36	0.56	0.67	0.98	1.46
March	0.12	0.42	0.15	0.26	0.39	0.60	0.69	0.94	1.64
April	0.15	0.45	0.17	0.27	0.42	0.66	0.77	1.02	2.22
May	0.14	0.49	0.20	0.30	0.45	0.72	0.87	1.23	2.24
June	0.14	0.50	0.21	0.29	0.46	0.74	0.89	1.26	1.91
July	0.12	0.48	0.19	0.29	0.44	0.72	0.84	1.15	1.72
August	0.11	0.47	0.20	0.29	0.43	0.70	0.85	1.17	2.10
September	0.13	0.46	0.17	0.29	0.43	0.67	0.79	1.06	1.88
October	0.13	0.43	0.15	0.28	0.41	0.61	0.70	0.92	1.67
November	0.12	0.40	0.15	0.25	0.38	0.58	0.67	0.88	1.56
December	0.10	0.36	0.13	0.22	0.34	0.53	0.61	0.82	1.52
All	0.10	0.44	0.18	0.26	0.40	0.64	0.76	1.06	2.24

Table 3.5 Annual and monthly total significant wave height statistics at Site 05.

	Significant wave height (m)								
	min	mean	std	p10	p50	p90	p95	p99	max
January	0.10	0.36	0.15	0.21	0.33	0.52	0.60	0.85	2.01
February	0.11	0.37	0.15	0.22	0.34	0.53	0.64	0.94	1.44
March	0.12	0.40	0.15	0.24	0.37	0.58	0.67	0.93	1.54
April	0.13	0.43	0.17	0.25	0.39	0.63	0.74	1.00	2.18
May	0.13	0.47	0.20	0.28	0.42	0.70	0.86	1.22	2.15
June	0.13	0.47	0.21	0.27	0.43	0.72	0.86	1.24	1.83
July	0.11	0.45	0.19	0.27	0.41	0.69	0.81	1.12	1.71
August	0.11	0.45	0.19	0.26	0.40	0.67	0.81	1.12	2.06
September	0.12	0.43	0.17	0.26	0.40	0.64	0.76	1.03	1.82
October	0.12	0.41	0.15	0.26	0.39	0.59	0.68	0.92	1.63
November	0.11	0.39	0.15	0.23	0.36	0.57	0.66	0.88	1.48
December	0.08	0.35	0.13	0.21	0.32	0.51	0.59	0.80	1.47
All	0.08	0.41	0.17	0.24	0.38	0.62	0.73	1.03	2.18

Table 3.6 Annual and monthly total significant wave height statistics at Site 06.

	Significant wave height (m)								
	min	mean	std	p10	p50	p90	p95	p99	max
January	0.04	0.22	0.11	0.10	0.19	0.36	0.41	0.52	0.96
February	0.04	0.21	0.10	0.10	0.19	0.35	0.40	0.49	0.76
March	0.04	0.22	0.11	0.10	0.20	0.37	0.42	0.52	0.80
April	0.04	0.23	0.11	0.11	0.21	0.38	0.44	0.55	0.85
May	0.04	0.26	0.13	0.12	0.23	0.43	0.50	0.66	0.96
June	0.03	0.25	0.13	0.12	0.22	0.42	0.49	0.64	0.80
July	0.05	0.24	0.11	0.12	0.21	0.40	0.46	0.59	0.82
August	0.04	0.24	0.11	0.11	0.21	0.39	0.45	0.58	0.95
September	0.04	0.24	0.11	0.12	0.23	0.40	0.46	0.58	0.82
October	0.04	0.24	0.11	0.12	0.23	0.39	0.44	0.55	0.78
November	0.04	0.24	0.11	0.11	0.22	0.39	0.43	0.52	0.75
December	0.03	0.21	0.10	0.10	0.19	0.34	0.39	0.49	0.64
All	0.03	0.23	0.11	0.11	0.21	0.39	0.44	0.57	0.96

Table 3.7 Annual and monthly total significant wave height statistics at Site 07.

	Significant wave height (m)								
	min	mean	std	p10	p50	p90	p95	p99	max
January	0.08	0.29	0.12	0.17	0.27	0.42	0.48	0.68	1.54
February	0.08	0.30	0.12	0.18	0.27	0.43	0.52	0.77	1.28
March	0.09	0.32	0.12	0.20	0.30	0.46	0.53	0.72	1.37
April	0.12	0.34	0.13	0.21	0.31	0.50	0.59	0.78	1.67
May	0.11	0.37	0.15	0.23	0.34	0.55	0.66	0.95	1.76
June	0.11	0.38	0.16	0.23	0.35	0.57	0.68	0.99	1.67
July	0.09	0.37	0.15	0.22	0.33	0.56	0.66	0.92	1.48
August	0.09	0.37	0.15	0.23	0.33	0.55	0.66	0.93	1.66
September	0.10	0.35	0.13	0.22	0.33	0.51	0.60	0.84	1.48
October	0.10	0.33	0.11	0.21	0.31	0.46	0.53	0.70	1.36
November	0.10	0.31	0.11	0.19	0.28	0.44	0.51	0.67	1.27
December	0.09	0.28	0.10	0.17	0.26	0.41	0.48	0.64	1.20
All	0.08	0.33	0.14	0.20	0.31	0.49	0.58	0.83	1.76

Table 3.8 Annual and monthly total significant wave height statistics at Site 08.

	Significant wave height (m)								
	min	mean	std	p10	p50	p90	p95	p99	max
January	0.23	1.02	0.41	0.61	0.94	1.52	1.78	2.46	4.91
February	0.37	1.07	0.41	0.66	0.99	1.57	1.85	2.56	3.87
March	0.36	1.17	0.40	0.73	1.10	1.68	1.93	2.50	4.07
April	0.36	1.24	0.47	0.73	1.16	1.85	2.12	2.69	5.41
May	0.40	1.36	0.54	0.81	1.24	2.04	2.42	3.19	5.24
June	0.43	1.41	0.55	0.82	1.32	2.09	2.46	3.27	5.79
July	0.36	1.37	0.54	0.78	1.26	2.08	2.41	3.16	5.44
August	0.36	1.36	0.53	0.80	1.27	2.04	2.38	3.17	4.80
September	0.41	1.26	0.49	0.72	1.19	1.90	2.17	2.88	4.43
October	0.38	1.18	0.41	0.73	1.11	1.71	1.96	2.47	3.87
November	0.36	1.10	0.40	0.66	1.03	1.60	1.84	2.41	3.85
December	0.35	1.00	0.37	0.60	0.94	1.48	1.71	2.17	3.56
All	0.23	1.21	0.49	0.70	1.12	1.82	2.13	2.84	5.79

Table 3.9 Annual and monthly total significant wave height statistics at Site 09.

	Significant wave height (m)								
	min	mean	std	p10	p50	p90	p95	p99	max
January	0.25	0.77	0.38	0.44	0.67	1.17	1.46	2.35	4.19
February	0.20	0.82	0.41	0.47	0.70	1.30	1.60	2.44	4.29
March	0.29	0.88	0.38	0.52	0.80	1.33	1.56	2.31	3.79
April	0.31	0.93	0.44	0.54	0.81	1.42	1.74	2.61	5.58
May	0.32	1.00	0.44	0.58	0.89	1.56	1.84	2.66	4.67
June	0.27	1.09	0.51	0.59	0.98	1.69	2.01	2.93	6.58
July	0.29	1.11	0.58	0.60	0.94	1.81	2.23	3.29	6.39
August	0.27	1.16	0.56	0.61	1.02	1.88	2.23	3.19	4.99
September	0.34	0.99	0.47	0.54	0.87	1.57	1.90	2.64	4.38
October	0.27	0.85	0.36	0.51	0.76	1.30	1.52	2.22	3.53
November	0.25	0.77	0.31	0.46	0.71	1.15	1.31	1.78	4.02
December	0.26	0.77	0.34	0.44	0.69	1.20	1.48	1.95	2.83
All	0.20	0.93	0.46	0.51	0.81	1.48	1.79	2.68	6.58

Table 3.10 Annual and monthly total significant wave height statistics at Site 10.

	Significant wave height (m)								
	min	mean	std	p10	p50	p90	p95	p99	max
January	0.33	1.21	0.45	0.78	1.11	1.75	2.06	2.83	5.58
February	0.46	1.28	0.45	0.83	1.19	1.81	2.12	2.90	4.64
March	0.46	1.38	0.44	0.92	1.31	1.93	2.22	2.91	4.55
April	0.53	1.45	0.52	0.92	1.35	2.11	2.43	3.13	6.21
May	0.58	1.58	0.59	1.00	1.46	2.32	2.74	3.60	5.88
June	0.55	1.64	0.61	1.00	1.54	2.38	2.81	3.67	7.07
July	0.51	1.60	0.61	0.97	1.47	2.40	2.81	3.65	6.39
August	0.50	1.61	0.60	0.99	1.50	2.35	2.75	3.67	5.34
September	0.54	1.49	0.54	0.90	1.40	2.19	2.50	3.29	4.85
October	0.51	1.38	0.45	0.90	1.30	1.96	2.24	2.87	4.34
November	0.44	1.30	0.43	0.85	1.22	1.82	2.08	2.76	4.29
December	0.47	1.20	0.39	0.78	1.13	1.72	1.98	2.46	3.90
All	0.33	1.43	0.54	0.88	1.32	2.09	2.44	3.27	7.07

Table 3.11 Monthly and annual wave height exceedance probabilities (%) at Site 01.

Hs (m)	Exceedance (%)												
	January	February	March	April	May	June	July	August	September	October	November	December	Year
>0.00	100.00	100.00	100.00	100.00	100.00	100.00	100.00	100.00	100.00	100.00	100.00	100.00	100.00
>0.50	97.80	98.93	99.62	99.77	99.92	99.76	99.65	99.77	99.72	99.63	98.97	98.37	99.33
>1.00	41.58	47.84	62.07	66.67	74.17	78.71	75.10	76.77	67.44	61.46	52.86	42.26	62.31
>1.50	10.08	11.39	16.18	22.21	29.07	34.24	31.07	31.28	24.71	16.88	12.66	8.97	20.77
>2.00	2.56	3.31	3.86	6.54	10.31	11.65	11.79	10.87	7.65	4.01	2.99	1.78	6.46
>2.50	0.96	1.16	1.08	1.84	4.03	4.59	4.15	4.05	2.37	0.88	0.75	0.23	2.18
>3.00	0.35	0.37	0.14	0.51	1.55	1.83	1.43	1.48	0.69	0.22	0.22	0.02	0.74
>3.50	0.17	0.12	0.06	0.25	0.57	0.70	0.60	0.60	0.20	0.08	0.09	0.01	0.29
>4.00	0.01	0.00	0.00	0.03	0.04	0.00	0.00	0.02	0.00	0.00	0.00	0.00	0.01
>4.50	0.06	0.00	0.00	0.10	0.14	0.12	0.05	0.07	0.01	0.00	0.00	0.00	0.05
>5.00	0.02	0.00	0.00	0.07	0.04	0.05	0.03	0.00	0.00	0.00	0.00	0.00	0.02
>5.50	0.00	0.00	0.00	0.02	0.00	0.03	0.01	0.00	0.00	0.00	0.00	0.00	0.00

Table 3.12 Monthly and annual wave height exceedance probabilities (%) at Site 02.

Hs (m)	Exceedance (%)												
	January	February	March	April	May	June	July	August	September	October	November	December	Year
>0.00	100.00	100.00	100.00	100.00	100.00	100.00	100.00	100.00	100.00	100.00	100.00	100.00	100.00
>0.50	85.15	89.54	94.16	94.06	95.99	94.76	94.40	94.09	94.21	95.12	89.94	82.60	92.01
>1.00	16.28	20.14	29.09	34.59	41.40	45.92	39.25	35.74	34.41	31.60	26.83	16.10	30.98
>1.50	3.22	3.53	5.25	7.66	12.03	12.91	10.29	9.57	8.85	6.40	5.05	2.56	7.29
>2.00	0.77	0.54	1.16	2.08	4.38	4.39	2.86	2.90	2.09	1.22	0.95	0.47	1.99
>2.50	0.21	0.08	0.13	0.45	1.57	1.47	0.82	0.87	0.59	0.25	0.14	0.02	0.55
>3.00	0.09	0.04	0.02	0.18	0.51	0.33	0.17	0.36	0.08	0.06	0.01	0.00	0.16
>3.50	0.07	0.00	0.00	0.05	0.16	0.05	0.01	0.11	0.01	0.00	0.00	0.00	0.04
>4.00	0.04	0.00	0.00	0.03	0.04	0.00	0.00	0.02	0.00	0.00	0.00	0.00	0.01
>4.50	0.00	0.00	0.00	0.02	0.00	0.00	0.00	0.00	0.00	0.00	0.00	0.00	0.00

Table 3.13 Monthly and annual wave height exceedance probabilities (%) at Site 03.

Hs (m)	Exceedance (%)												
	January	February	March	April	May	June	July	August	September	October	November	December	Year
>0.00	100.00	100.00	100.00	100.00	100.00	100.00	100.00	100.00	100.00	100.00	100.00	100.00	100.00
>0.50	66.28	71.43	81.34	82.77	88.00	84.91	84.28	82.35	83.45	83.10	76.14	63.97	79.03
>1.00	7.74	8.66	13.18	17.26	23.32	25.48	21.74	19.32	18.15	14.87	12.12	6.61	15.73
>1.50	1.19	1.23	1.91	3.19	6.17	6.11	4.45	4.41	3.32	2.00	1.76	0.83	3.06
>2.00	0.26	0.08	0.19	0.51	1.72	1.68	1.00	0.98	0.68	0.31	0.17	0.04	0.64
>2.50	0.09	0.01	0.02	0.17	0.45	0.31	0.17	0.37	0.08	0.06	0.00	0.00	0.15
>3.00	0.07	0.00	0.00	0.05	0.15	0.05	0.00	0.05	0.00	0.00	0.00	0.00	0.03
>3.50	0.02	0.00	0.00	0.03	0.01	0.00	0.00	0.00	0.00	0.00	0.00	0.00	0.01

Table 3.14 Monthly and annual wave height exceedance probabilities (%) at Site 04.

Hs (m)	Exceedance (%)												
	January	February	March	April	May	June	July	August	September	October	November	December	Year
>0.00	100.00	100.00	100.00	100.00	100.00	100.00	100.00	100.00	100.00	100.00	100.00	100.00	100.00
>0.50	14.63	15.58	23.69	28.86	36.61	39.33	35.89	33.45	31.25	25.01	20.25	13.42	26.54
>1.00	0.57	0.87	0.65	1.10	2.84	2.94	2.25	2.25	1.51	0.66	0.42	0.16	1.35
>1.50	0.11	0.00	0.03	0.12	0.36	0.31	0.18	0.30	0.09	0.05	0.03	0.01	0.13
>2.00	0.02	0.00	0.00	0.02	0.05	0.00	0.00	0.03	0.00	0.00	0.00	0.00	0.01

Table 3.15 Monthly and annual wave height exceedance probabilities (%) at Site 05.

Hs (m)	Exceedance (%)												
	January	February	March	April	May	June	July	August	September	October	November	December	Year
>0.00	100.00	100.00	100.00	100.00	100.00	100.00	100.00	100.00	100.00	100.00	100.00	100.00	100.00
>0.50	12.04	12.78	19.74	24.21	31.06	34.68	30.63	27.89	25.63	20.83	17.63	10.96	22.38
>1.00	0.51	0.60	0.58	1.01	2.66	2.77	1.85	1.98	1.30	0.63	0.46	0.16	1.21
>1.50	0.08	0.00	0.01	0.12	0.35	0.23	0.11	0.28	0.08	0.04	0.00	0.00	0.11
>2.00	0.01	0.00	0.00	0.02	0.04	0.00	0.00	0.03	0.00	0.00	0.00	0.00	0.01

Table 3.16 Monthly and annual wave height exceedance probabilities (%) at Site 06.

Hs (m)	Exceedance (%)												
	January	February	March	April	May	June	July	August	September	October	November	December	Year
>0.00	100	100	100	100	100	100	100	100	100	100	100	100	100
>0.50	1.38	0.83	1.46	2.21	4.98	4.57	3.16	2.57	2.85	2.11	1.54	0.81	2.38

Table 3.17 Monthly and annual wave height exceedance probabilities (%) at Site 07.

Hs (m)	Exceedance (%)												
	January	February	March	April	May	June	July	August	September	October	November	December	Year
>0.00	100.00	100.00	100.00	100.00	100.00	100.00	100.00	100.00	100.00	100.00	100.00	100.00	100.00
>0.50	4.14	5.56	6.65	9.86	13.73	16.15	14.87	13.55	10.70	6.73	5.44	3.77	9.28
>1.00	0.26	0.20	0.10	0.31	0.76	0.93	0.67	0.64	0.29	0.11	0.15	0.02	0.37
>1.50	0.02	0.00	0.00	0.05	0.08	0.03	0.00	0.05	0.00	0.00	0.00	0.00	0.02

Table 3.18 Monthly and annual wave height exceedance probabilities (%) at Site 08.

Hs (m)	Exceedance (%)												
	January	February	March	April	May	June	July	August	September	October	November	December	Year
>0.00	100.00	100.00	100.00	100.00	100.00	100.00	100.00	100.00	100.00	100.00	100.00	100.00	100.00
>0.50	97.03	98.26	99.27	99.26	99.70	99.41	99.49	99.60	99.39	99.32	98.14	96.80	98.81
>1.00	42.40	48.44	61.82	66.18	73.65	78.45	74.56	75.56	67.16	62.28	53.83	43.03	62.34
>1.50	10.63	12.23	16.82	22.93	29.98	35.08	31.50	31.21	25.25	17.98	13.68	9.39	21.43
>2.00	2.78	3.36	4.04	6.80	10.69	11.98	11.76	10.94	7.76	4.39	3.30	1.84	6.65
>2.50	0.92	1.11	0.99	1.88	4.18	4.62	3.88	3.95	2.39	0.89	0.80	0.27	2.16
>3.00	0.31	0.34	0.13	0.47	1.53	1.80	1.35	1.34	0.61	0.21	0.20	0.02	0.69
>3.50	0.15	0.10	0.05	0.24	0.55	0.65	0.54	0.53	0.14	0.07	0.07	0.01	0.26
>4.00	0.08	0.00	0.01	0.12	0.23	0.20	0.19	0.23	0.05	0.00	0.00	0.00	0.09
>4.50	0.05	0.00	0.00	0.08	0.11	0.09	0.04	0.04	0.00	0.00	0.00	0.00	0.03
>5.00	0.00	0.00	0.00	0.05	0.04	0.04	0.02	0.00	0.00	0.00	0.00	0.00	0.01
>5.50	0.00	0.00	0.00	0.00	0.00	0.03	0.00	0.00	0.00	0.00	0.00	0.00	0.00

Table 3.19 Monthly and annual wave height exceedance probabilities (%) at Site 09.

Hs (m)	Exceedance (%)												
	January	February	March	April	May	June	July	August	September	October	November	December	Year
>0.00	100.00	100.00	100.00	100.00	100.00	100.00	100.00	100.00	100.00	100.00	100.00	100.00	100.00
>0.50	79.82	85.40	92.50	94.03	96.73	95.29	96.86	96.51	94.12	91.13	85.60	80.50	90.73
>1.00	17.94	21.38	27.63	30.15	39.12	48.18	44.15	51.43	37.15	24.01	17.73	18.83	31.53
>1.50	4.52	6.17	6.07	8.48	11.53	15.35	16.53	20.83	11.79	5.31	2.50	4.77	9.51
>2.00	1.90	1.93	1.74	3.11	3.43	5.10	7.38	7.86	4.08	1.52	0.62	0.79	3.30
>2.50	0.76	0.91	0.69	1.21	1.49	2.39	3.43	3.21	1.50	0.51	0.29	0.13	1.38
>3.00	0.23	0.36	0.24	0.45	0.33	0.83	1.73	1.35	0.53	0.12	0.18	0.00	0.53
>3.50	0.08	0.13	0.02	0.18	0.09	0.25	0.57	0.46	0.16	0.01	0.07	0.00	0.17
>4.00	0.02	0.04	0.00	0.07	0.04	0.12	0.31	0.12	0.09	0.00	0.00	0.00	0.07
>4.50	0.00	0.00	0.00	0.06	0.02	0.11	0.13	0.05	0.00	0.00	0.00	0.00	0.03
>5.00	0.00	0.00	0.00	0.04	0.00	0.09	0.09	0.00	0.00	0.00	0.00	0.00	0.02
>5.50	0.00	0.00	0.00	0.01	0.00	0.06	0.04	0.00	0.00	0.00	0.00	0.00	0.01
>6.00	0.00	0.00	0.00	0.00	0.00	0.04	0.02	0.00	0.00	0.00	0.00	0.00	0.01
>6.50	0.00	0.00	0.00	0.00	0.00	0.01	0.00	0.00	0.00	0.00	0.00	0.00	0.00

Table 3.20 Monthly and annual wave height exceedance probabilities (%) at Site 10.

Hs (m)	Exceedance (%)												
	January	February	March	April	May	June	July	August	September	October	November	December	Year
>0.00	100.00	100.00	100.00	100.00	100.00	100.00	100.00	100.00	100.00	100.00	100.00	100.00	100.00
>0.50	99.66	99.92	99.97	100.00	100.00	100.00	100.00	99.98	100.00	100.00	99.96	99.95	99.95
>1.00	64.23	72.82	83.21	83.94	90.14	90.10	88.26	89.30	83.06	81.90	75.44	66.12	80.74
>1.50	18.08	22.45	31.36	36.70	46.22	53.41	47.62	49.98	41.06	31.50	25.05	18.26	35.19
>2.00	5.67	6.52	8.40	12.95	17.25	19.95	20.07	19.79	15.11	9.01	6.16	4.72	12.16
>2.50	1.86	2.05	2.61	4.34	7.59	8.39	8.28	7.71	4.99	2.59	1.87	0.89	4.44
>3.00	0.72	0.84	0.79	1.39	3.03	3.61	3.64	3.24	2.06	0.69	0.53	0.12	1.73
>3.50	0.28	0.34	0.16	0.56	1.23	1.43	1.32	1.32	0.49	0.18	0.18	0.02	0.63
>4.00	0.12	0.13	0.05	0.24	0.51	0.57	0.57	0.60	0.22	0.04	0.07	0.00	0.26
>4.50	0.08	0.02	0.00	0.12	0.22	0.22	0.23	0.26	0.05	0.00	0.00	0.00	0.10
>5.00	0.06	0.00	0.00	0.10	0.13	0.11	0.08	0.03	0.00	0.00	0.00	0.00	0.04
>5.50	0.02	0.00	0.00	0.07	0.04	0.07	0.04	0.00	0.00	0.00	0.00	0.00	0.02
>6.00	0.00	0.00	0.00	0.03	0.00	0.05	0.02	0.00	0.00	0.00	0.00	0.00	0.01
>6.50	0.00	0.00	0.00	0.00	0.00	0.03	0.00	0.00	0.00	0.00	0.00	0.00	0.00
>7.00	0.00	0.00	0.00	0.00	0.00	0.01	0.00	0.00	0.00	0.00	0.00	0.00	0.00

Table 3.21 Annual joint probability distribution (in %) of the wave height and peak wave direction at Site 01.

Hs (m)	Wave direction (degT)								
	337.5 -22.5 (N)	22.5 -67.5 (NE)	67.5 -112.5 (E)	112.5 -157.5 (SE)	157.5 -202.5 (S)	202.5 -247.5 (SW)	247.5 -292.5 (W)	292.5 -337.5 (NW)	Total
> 0.00 <= 0.50	0	0	0	0.4	6.3	0	0	0	6.7
> 0.50 <= 1.00	0.3	0	0.9	40.1	329	0	0	0	370.3
> 1.00 <= 1.50	0	0	0.7	75.6	339.1	0	0	0	415.4
> 1.50 <= 2.00	0	0	0.3	43.4	99.4	0	0	0	143.1
> 2.00 <= 2.50	0	0	0.3	14.5	28	0	0	0	42.8
> 2.50 <= 3.00	0	0	0	5.7	8.7	0	0	0	14.4
> 3.00 <= 3.50	0	0	0	1.7	2.7	0	0	0	4.4
> 3.50 <= 4.00	0	0	0	0.8	1	0	0	0	1.8
> 4.00 <= 4.50	0	0	0	0.3	0.3	0	0	0	0.6
> 4.50 <= 5.00	0	0	0	0.1	0.2	0	0	0	0.3
> 5.00 <= 5.50	0	0	0	0.1	0	0	0	0	0.1
Total	0.3	0	2.2	182.7	814.7	0	0	0	1000

Table 3.22 Annual joint probability distribution (in %) of the wave height and peak wave direction at Site 02.

Hs (m)	Wave direction (degT)								
	337.5 -22.5 (N)	22.5 -67.5 (NE)	67.5 -112.5 (E)	112.5 -157.5 (SE)	157.5 -202.5 (S)	202.5 -247.5 (SW)	247.5 -292.5 (W)	292.5 -337.5 (NW)	Total
> 0.00 <= 0.50	0.1	0	0	0.2	79.7	0	0	0.1	80.1
> 0.50 <= 1.00	0.4	0	0	1.8	607.5	0	0	0.5	610.2
> 1.00 <= 1.50	0	0	0	0.7	236.2	0	0	0	236.9
> 1.50 <= 2.00	0	0	0	0.1	52.9	0	0	0	53
> 2.00 <= 2.50	0	0	0	0	14.3	0	0	0	14.3
> 2.50 <= 3.00	0	0	0	0	4	0	0	0	4
> 3.00 <= 3.50	0	0	0	0	1.2	0	0	0	1.2
> 3.50 <= 4.00	0	0	0	0	0.3	0	0	0	0.3
> 4.00 <= 4.50	0	0	0	0	0.1	0	0	0	0.1
Total	0.5	0	0	2.8	996.2	0	0	0.6	1000

Table 3.23 Annual joint probability distribution (in %) of the wave height and peak wave direction at Site 03.

Hs (m)	Wave direction (degT)								
	337.5 -22.5 (N)	22.5 -67.5 (NE)	67.5 -112.5 (E)	112.5 -157.5 (SE)	157.5 -202.5 (S)	202.5 -247.5 (SW)	247.5 -292.5 (W)	292.5 -337.5 (NW)	Total
> 0.00 <= 0.50	0.3	0	0	0.1	208.9	0	0	0.3	209.6
> 0.50 <= 1.00	0.7	0	0	0.2	631.4	0	0	0.7	633
> 1.00 <= 1.50	0	0	0	0	126.7	0	0	0	126.7
> 1.50 <= 2.00	0	0	0	0	24.2	0	0	0	24.2
> 2.00 <= 2.50	0	0	0	0	4.9	0	0	0	4.9
> 2.50 <= 3.00	0	0	0	0	1.1	0	0	0	1.1
> 3.00 <= 3.50	0	0	0	0	0.3	0	0	0	0.3
> 3.50 <= 4.00	0	0	0	0	0.1	0	0	0	0.1
Total	1	0	0	0.3	997.6	0	0	1	1000

Table 3.24 Annual joint probability distribution (in %) of the wave height and peak wave direction at Site 04.

Hs (m)	Wave direction (degT)								
	337.5 -22.5 (N)	22.5 -67.5 (NE)	67.5 -112.5 (E)	112.5 -157.5 (SE)	157.5 -202.5 (S)	202.5 -247.5 (SW)	247.5 -292.5 (W)	292.5 -337.5 (NW)	Total
> 0.00 <= 0.50	7.1	0.1	0	718.5	8.4	0	0	0.5	734.6
> 0.50 <= 1.00	2.2	0	0	238.8	10.8	0	0	0	251.8
> 1.00 <= 1.50	0	0	0	10.7	1.5	0	0	0	12.2
> 1.50 <= 2.00	0	0	0	1.2	0.1	0	0	0	1.3
> 2.00 <= 2.50	0	0	0	0.1	0	0	0	0	0.1
Total	9.3	0.1	0	969.3	20.8	0	0	0.5	1000

Table 3.25 Annual joint probability distribution (in %) of the wave height and peak wave direction at Site 05.

Hs (m)	Wave direction (degT)								
	337.5 -22.5 (N)	22.5 -67.5 (NE)	67.5 -112.5 (E)	112.5 -157.5 (SE)	157.5 -202.5 (S)	202.5 -247.5 (SW)	247.5 -292.5 (W)	292.5 -337.5 (NW)	Total
> 0.00 <= 0.50	5.2	0.8	0.1	2.5	765.6	0	0	2	776.2
> 0.50 <= 1.00	1	0.4	0	0.8	209.3	0	0	0.1	211.6
> 1.00 <= 1.50	0	0	0	0	11	0	0	0	11
> 1.50 <= 2.00	0	0	0	0	1	0	0	0	1
> 2.00 <= 2.50	0	0	0	0	0.1	0	0	0	0.1
Total	6.2	1.2	0.1	3.3	987	0	0	2.1	1000

Table 3.26 Annual joint probability distribution (in %) of the wave height and peak wave direction at Site 06.

Hs (m)	Wave direction (degT)								
	337.5 -22.5 (N)	22.5 -67.5 (NE)	67.5 -112.5 (E)	112.5 -157.5 (SE)	157.5 -202.5 (S)	202.5 -247.5 (SW)	247.5 -292.5 (W)	292.5 -337.5 (NW)	Total
> 0.00 <= 0.50	12.9	17.8	19.9	1.1	694	40.3	149.5	40.7	976.2
> 0.50 <= 1.00	0	0	0.1	0.1	10.1	8.6	4.1	0.9	23.9
Total	12.9	17.8	20	1.2	704.1	48.9	153.6	41.6	1000

Table 3.27 Annual joint probability distribution (in %) of the wave height and peak wave direction at Site 07.

Hs (m)	Wave direction (degT)								
	337.5 -22.5 (N)	22.5 -67.5 (NE)	67.5 -112.5 (E)	112.5 -157.5 (SE)	157.5 -202.5 (S)	202.5 -247.5 (SW)	247.5 -292.5 (W)	292.5 -337.5 (NW)	Total
> 0.00 <= 0.50	8.5	2	0.2	896.3	0	0	0	0.1	907.1
> 0.50 <= 1.00	0.6	0.6	0.1	87.8	0	0	0	0	89.1
> 1.00 <= 1.50	0	0	0	3.5	0	0	0	0	3.5
> 1.50 <= 2.00	0	0	0	0.2	0	0	0	0	0.2
Total	9.1	2.6	0.3	987.8	0	0	0	0.1	1000

Table 3.28 Annual joint probability distribution (in %) of the wave height and peak wave direction at Site 08.

Hs (m)	Wave direction (degT)								
	337.5 -22.5 (N)	22.5 -67.5 (NE)	67.5 -112.5 (E)	112.5 -157.5 (SE)	157.5 -202.5 (S)	202.5 -247.5 (SW)	247.5 -292.5 (W)	292.5 -337.5 (NW)	Total
> 0.00 <= 0.50	0	0	0	0.5	11.4	0	0	0	11.9
> 0.50 <= 1.00	0	0	0.1	34.2	330.4	0	0	0	364.7
> 1.00 <= 1.50	0	0	0	63.7	345.4	0	0	0	409.1
> 1.50 <= 2.00	0	0	0	37.8	110	0	0	0	147.8
> 2.00 <= 2.50	0	0	0	12.7	32.2	0	0	0	44.9
> 2.50 <= 3.00	0	0	0	4.9	9.8	0	0	0	14.7
> 3.00 <= 3.50	0	0	0	1.5	2.8	0	0	0	4.3
> 3.50 <= 4.00	0	0	0	0.7	1	0	0	0	1.7
> 4.00 <= 4.50	0	0	0	0.2	0.3	0	0	0	0.5
> 4.50 <= 5.00	0	0	0	0.1	0.1	0	0	0	0.2
> 5.00 <= 5.50	0	0	0	0.1	0	0	0	0	0.1
Total	0	0	0.1	156.4	843.4	0	0	0	1000

Table 3.29 Annual joint probability distribution (in %) of the wave height and peak wave direction at Site 09.

Hs (m)	Wave direction (degT)								
	337.5 -22.5 (N)	22.5 -67.5 (NE)	67.5 -112.5 (E)	112.5 -157.5 (SE)	157.5 -202.5 (S)	202.5 -247.5 (SW)	247.5 -292.5 (W)	292.5 -337.5 (NW)	Total
> 0.00 <= 0.50	0	0	3.5	89.2	0	0	0	0.1	92.8
> 0.50 <= 1.00	0	0	71.7	520	0.3	0	0	0	592
> 1.00 <= 1.50	0	0	75	145	0.2	0	0	0	220.2
> 1.50 <= 2.00	0	0	31.6	30.6	0	0	0	0	62.2
> 2.00 <= 2.50	0	0	11.4	7.8	0	0	0	0	19.2
> 2.50 <= 3.00	0	0	5.2	3.3	0	0	0	0	8.5
> 3.00 <= 3.50	0	0	2.3	1.3	0	0	0	0	3.6
> 3.50 <= 4.00	0	0	0.6	0.4	0	0	0	0	1
> 4.00 <= 4.50	0	0	0.3	0.1	0	0	0	0	0.4
> 4.50 <= 5.00	0	0	0.1	0	0	0	0	0	0.1
> 5.00 <= 5.50	0	0	0.1	0	0	0	0	0	0.1
Total	0	0	201.8	797.7	0.5	0	0	0.1	1000

Table 3.30 Annual joint probability distribution (in %) of the wave height and peak wave direction at Site 10.

Hs (m)	Wave direction (degT)								
	337.5 -22.5 (N)	22.5 -67.5 (NE)	67.5 -112.5 (E)	112.5 -157.5 (SE)	157.5 -202.5 (S)	202.5 -247.5 (SW)	247.5 -292.5 (W)	292.5 -337.5 (NW)	Total
> 0.00 <= 0.50	0	0	0	0.1	0.4	0	0	0	0.5
> 0.50 <= 1.00	0.2	0	5.6	15.2	171.1	0	0	0	192.1
> 1.00 <= 1.50	0	0	20.8	57.1	377.5	0.1	0	0	455.5
> 1.50 <= 2.00	0	0	17.2	45.7	167.4	0	0	0	230.3
> 2.00 <= 2.50	0	0	8.4	18.7	50.1	0	0	0	77.2
> 2.50 <= 3.00	0	0	3.3	6.3	17.5	0	0	0	27.1
> 3.00 <= 3.50	0	0	1.9	3	6.1	0	0	0	11
> 3.50 <= 4.00	0	0	0.6	0.9	2.1	0	0	0	3.6
> 4.00 <= 4.50	0	0	0.2	0.5	0.9	0	0	0	1.6
> 4.50 <= 5.00	0	0	0.1	0.2	0.3	0	0	0	0.6
> 5.00 <= 5.50	0	0	0	0	0.1	0	0	0	0.1
> 5.50 <= 6.00	0	0	0	0.1	0	0	0	0	0.1
Total	0.2	0	58.1	147.8	793.5	0.1	0	0	1000

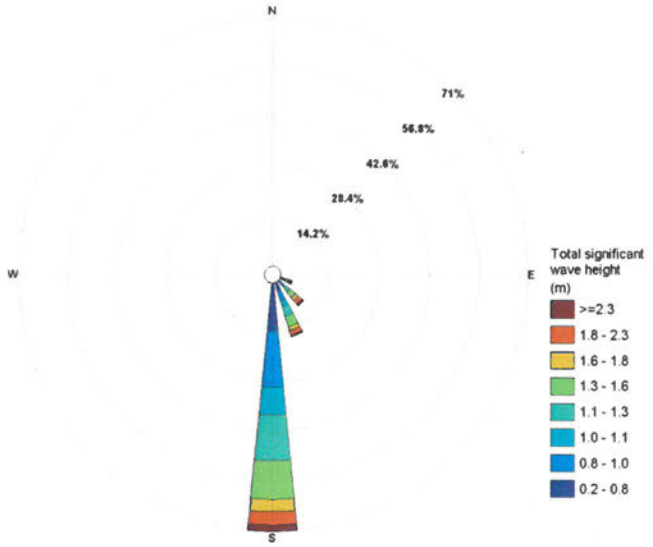

Figure 3.3 Annual wave rose plot for the total significant wave height at Site 01. Sectors indicate the direction from which waves approach.

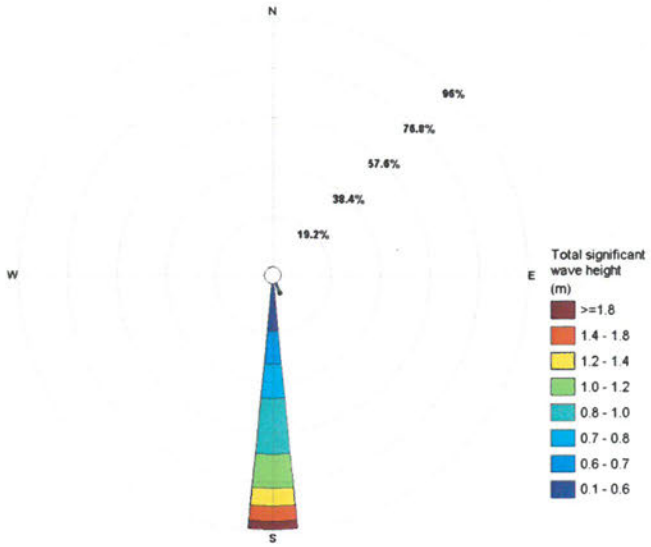

Figure 3.4 Annual wave rose plot for the total significant wave height at Site 02. Sectors indicate the direction from which waves approach.

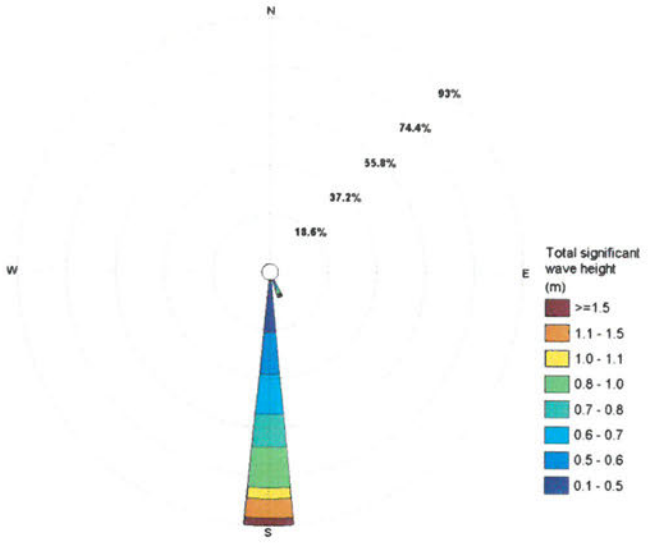

Figure 3.5 Annual wave rose plot for the total significant wave height at Site 03. Sectors indicate the direction from which waves approach.

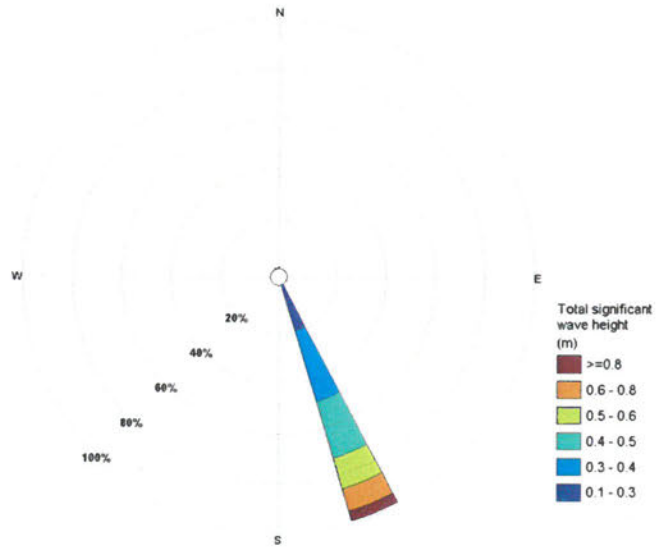

Figure 3.6 Annual wave rose plot for the total significant wave height at Site 04. Sectors indicate the direction from which waves approach.

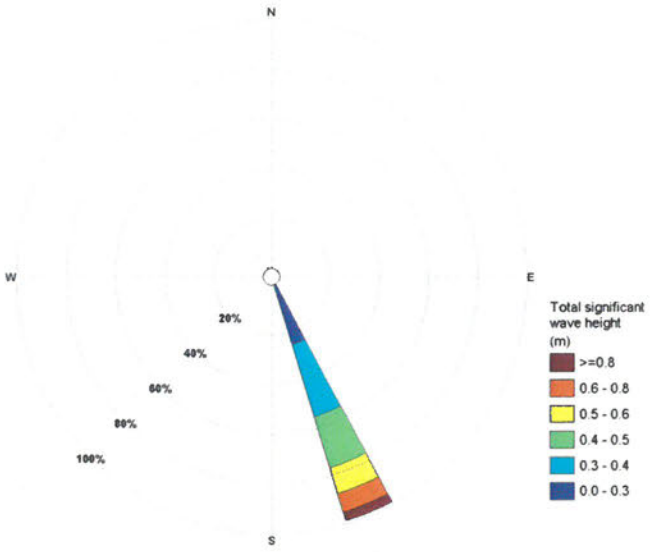

Figure 3.7 Annual wave rose plot for the total significant wave height at Site 05. Sectors indicate the direction from which waves approach.

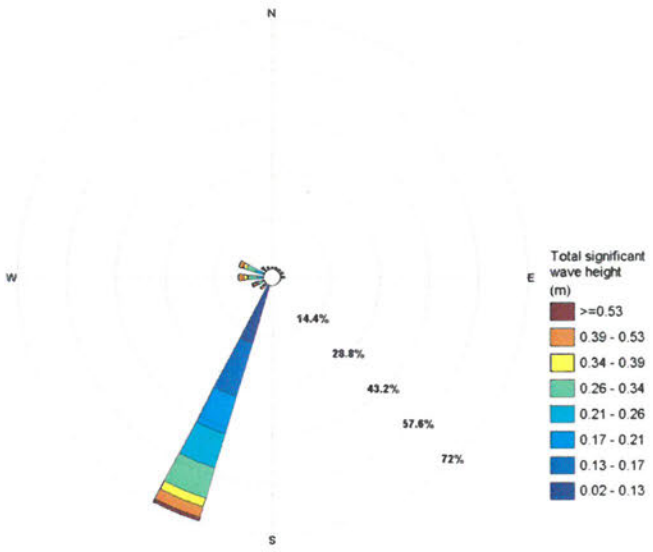

Figure 3.8 Annual wave rose plot for the total significant wave height at Site 06. Sectors indicate the direction from which waves approach.

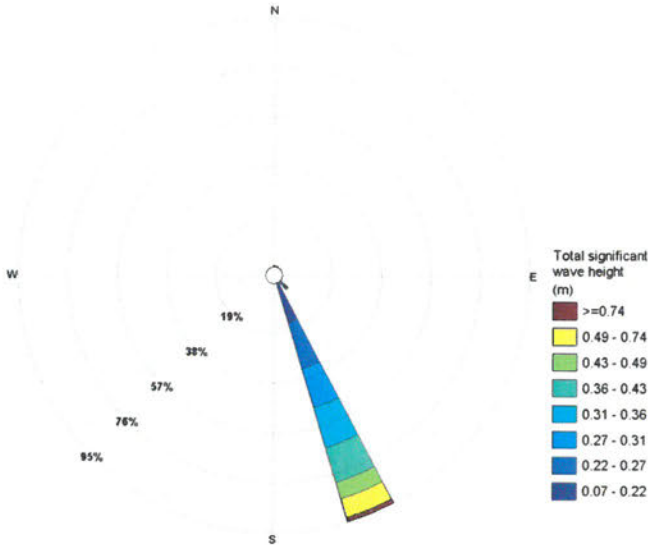

Figure 3.9 Annual wave rose plot for the total significant wave height at Site 07. Sectors indicate the direction from which waves approach.

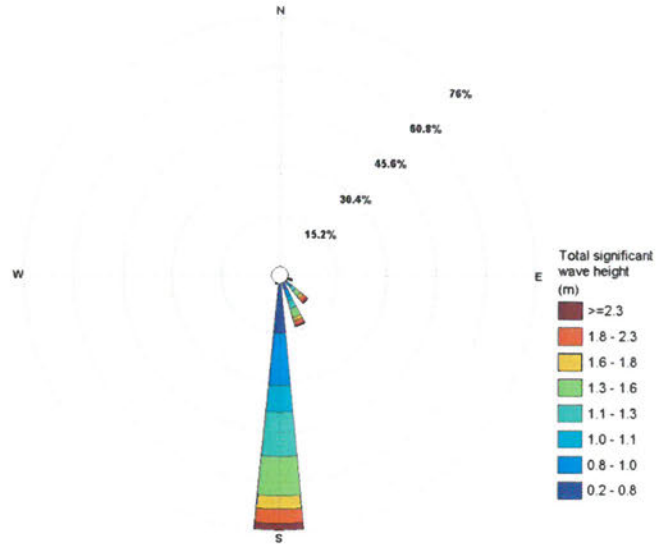

Figure 3.10 Annual wave rose plot for the total significant wave height at Site 08. Sectors indicate the direction from which waves approach.

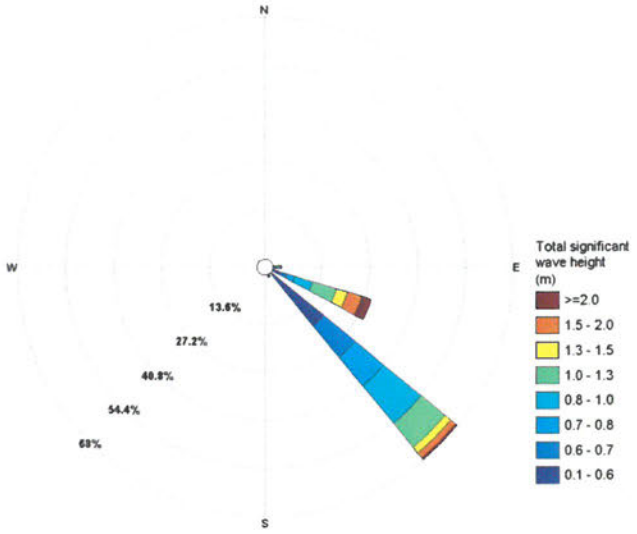

Figure 3.11 Annual wave rose plot for the total significant wave height at Site 09. Sectors indicate the direction from which waves approach.

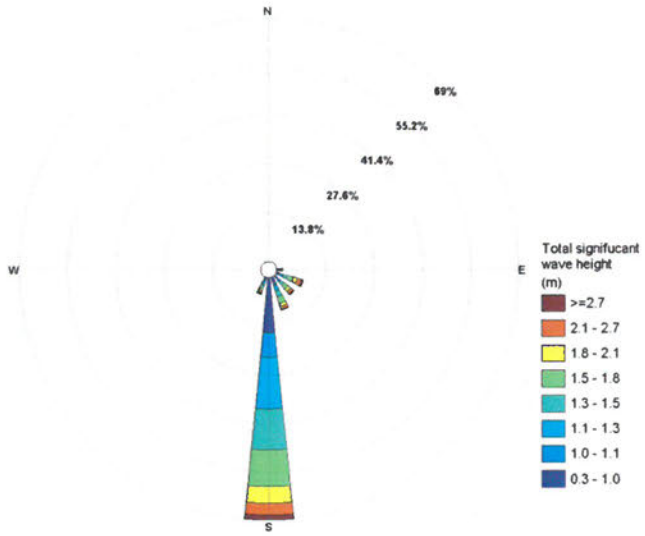

Figure 3.12 Annual wave rose plot for the total significant wave height at Site 10. Sectors indicate the direction from which waves approach.

4. REFERENCES

Ardhuin, F., W., Rogers, E., Babanin, A. V., Filipot, J. -F., Magne, R., Roland, A., van der Westhuysen, A. J., Queffeulou, P., Lee, B., Aouf, L. and Collard, F. (2010). Semiempirical Dissipation Source Functions for Ocean Waves. Part I: Definition, Calibration, and Validation, Journal of Physical Oceanography, 40(9), 1917-1941, doi:10.1175/2010JPO4324.1.

Booij, N., Ris, R. C. and Holthuijsen, L. H. (1999). A third-generation wave model for coastal regions, Part I, Model description and validation, Journal of Geophysical Research C4, 104, 7649-7666.

Collins, J. I. (1972). Prediction of Shallow Water Spectra. Journal of Geophysical Research 77, 2693-2707.

Holthuijsen, L. H., Booij, N., Ris, R. C., Haagsma, I. J., Kieftenburg, A. T. M. M., Kriezi, E. E., Zijlema, M., van der Westhuysen, A. J. (2007). SWAN cycle III version 40.51, Technical Documentation. Delft, 2600 GA Delft The Netherlands.

Queffeulou, P. and Croize-Fillon, D (2017). Global altimeter SWH data set - February 2017. Technical Report, IFREMER.

Saha, S., Moorthi, S., Pan, H. -L., Wu, X., Wang, J., Nadiga, S., Tripp, P., Kistler, R., Woollen, J., Behringer, D., Liu, H., Stokes, D., Grumbine, R., Gayno, G., Wang, J., Hou, Y. -T., Chuang, H. -Y., Juang, H. -M. H., Sela, J., Iredell, M., Treadon, R., Kleist, D., Van Delst, P., Keyser, D., Derber, J., Ek, M., Meng, J., Wei, H., Yang, R., Lord, S., Van Den Dool, H., Kumar, A., Wang, W., Long, C., Chelliah, M., Xue, Y., Huang, B., Schemm, J. -K., Ebisuzaki, W., Lin, R., Xie, P., Chen, M., Zhou, S., Higgins, W., Zou, C.-Z., Liu, Q., Chen, Y., Han, Y., Cucurull, L., Reynolds, R. W., Rutledge, G., Goldberg, M. (2010). The NCEP Climate Forecast System Reanalysis. Bull. Am. Meteorol. Soc. 91, 1015–1057. doi:10.1175/2010BAMS3001.1

Tolman, H. L. (1991). A third-generation model for wind waves on slowly varying, un-steady and inhomogeneous depths and currents. Journal of Physical Oceanography 21, 782–797.

van der Westhuysen, A. J., Zijlema, M., Battjes, J.A. (2007). Saturation-based whitecapping dissipation in SWAN for deep and shallow water. Coastal Engineering, 54, 151–170.

Weatherall, P., Marks, K. M., Jakobsson, M., Schmitt, T., Tani, S., Arndt, J. E., Rovere, M., Chayes, D., Ferrini, V. and Wigley, R. (2015). A new digital bathymetric model of the world's oceans, Earth and Space Science, 2, 331–345, doi:10.1002/2015EA000107.

Appendix 4. MetOcean Particle Tracking ERCore Manual.

ERCore Technical Description

MetOcean Solutions Ltd.

March 11, 2016

1 Introduction

ERCore is a Lagrangian particle tracking model for simulating the dispersion and fate of material in the oceanic or atmospheric environment. It solves equations describing the movement and modification of discrete particles in response to the environment. The ambient flow of water or wind advects the particles with spatially and temporally varying fields. Turbulent diffusion is included with a random walk approach and the presence of a boundary such as a shoreline or the air-sea interface can be specified. A simulated particle can represent any material with additional physical, chemical or biological processes added as required to simulate active modifications that may occur as it moves within the water or air. Examples of active particles include sediment, oil, plankton and even persons lost at sea.

This document describes the mathematical and numerical formulation of the model. Also included are descriptions of the various extensions that can be applied to the particles to allow them to simulate different materials.

2 Numerical formulation

2.1 Equations of motion

The coordinate system is defined with z positive upwards. The nominal 0 level for z is Mean Sea Level, however any consistent vertical reference can be used. The change of position x, y, z of a particle at time t is governed by:

$$\frac{dx}{dt} = U(x,y,z,t) + \tilde{u} + u_p \tag{1}$$

$$\frac{dy}{dt} = V(x,y,z,t) + \tilde{v} + v_p \tag{2}$$

$$\frac{dz}{dt} = W(x,y,z,t) + \tilde{w} + w_p \tag{3}$$

where U, V, W is the ambient flow and $\tilde{u}, \tilde{v}, \tilde{w}$ are a turbulent flow component. u_p, v_p, w_p are any additional motions that are properties of the particle's interaction with the surrounding water or air such as sinking, floating, drifting or swimming.

Each particle has a weighting and age attribute attached to it. The weight value can represent any measure of quantity depending on the application, for example mass, volume or number. The generic equation describing the rate of change of weighting, N is:

$$\frac{dN}{dt} = f(P,U,V,W,S,T,D,H) \tag{4}$$

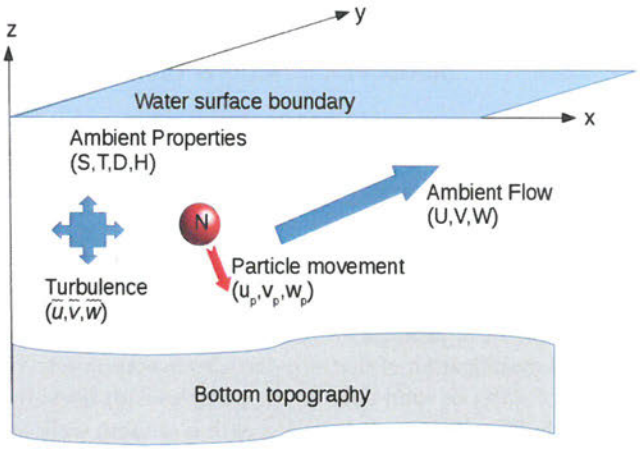

Figure 1: Schematic of physical processes acting on a particle in the model.

where P are properties of the particle itself and S, T, D, H are salinity, temperature, density and humidity of water or air. Note that for a given process and medium only some of the ambient properties will be relevant. The age is a simple measure of time since a particle was released. Any number of other attributes can also be attached to a particle which describe its physical, chemical or biological state.

2.2 Turbulent diffusion

The turbulent component of the velocity is given by:

$$\int_t^{t+\Delta t} \tilde{u} dt = \sqrt{6K_h \Delta t} H(-1, 1) \tag{5}$$

$$\int_t^{t+\Delta t} \tilde{v} dt = \sqrt{6K_h \Delta t} H(-1, 1) \tag{6}$$

$$\int_t^{t+\Delta t} \tilde{w} dt = \sqrt{6K_v \Delta t} H(-1, 1) \tag{7}$$

where K_h and K_v are horizontal and vertical eddy diffusion coefficients and H is a number sampled from a uniform distribution between -1 and 1. The eddy diffusion coefficients can be provided as known values, either constant or as a spatially (and temporally) varying field.

2.3 Coordinate system

The model solves all equations in standard SI units. However the horizontal coordinates can also be configured as geographical longitude and latitude. In this case

a map factor is applied to any horizontal differences as:

$$d\lambda = \frac{360dx}{C * cos\theta} \tag{8}$$

$$d\theta = \frac{360dy}{C} \tag{9}$$

where λ and θ are the longitude and latitude respectively. C is the circumference of the earth.

2.4 Numerical solution

The equations of motion for each particle are integrated with a constant time step, Δt. A Runge-Kutta scheme is used for the ambient flow component, with default order 4 (which can be reduced for computational speed by user configuration). The turbulent and particle components of motion are added with a simple first order integration.

2.5 Forcing fields

The ambient flow U, V, W is provided as input data which can be constant or as spatially and temporally varying fields. For variable fields, the value at the particle position for a given time is determined by simple multilinear interpolation. Any number of additional fields which can influence the particle can also be prescribed and are likewise interpolated to provide the local ambient conditions for the particle at each timestep.

2.6 Boundaries

Boundaries can be specified in 4 ways:

1. A shoreline vector
2. A spatially varying field (such as ocean depth)
3. A constant level
4. A bounding box

In each case an intersection algorithm is applied at each time-step to determine whether the particle crosses the boundary. Firstly the particle motion vector for the time-step is calculated, then an intersect test is made between that vector and the boundaries.

Shorelines are defined as line segments, each of which is tested for intersection with the motion vector in the horizontal plane. Shorelines are assumed to exist at a z-level of zero, and any horizontal intersection will relocate the particle at that level.

For variable boundaries such as the sea bottom, the z-coordinate at the start and end of the motion vector are first interpolated. The straight line between these two z-coordinates is then used for the intersection test with the motion vector in the vertical plane; the horizontal position of an intersect is then the fractional displacement in the horizontal direction.

If an intersection occurs, the particle is placed at the intersection point. The particle's subsequent action at the following time-step depends on whether the boundary is sticky. If the boundary is non-sticky the particle is free to move away from the boundary if its vector of motion carries it away, otherwise it remains at its intersection location. In the case of a bounding box, the particle is removed from the simulation.

2.7 Particle release and tracking

Particle releases are specified to be a particular location and the following options are available:

1. Instantaneaous release of total material M_{tot}: All n particles added at a given time.
$$N = \frac{N_tot}{n} \tag{10}$$
2. Continuous release, with flux of material F: Particles are added continuously, at a rate of n_{rel} every timestep Δt_{rel}.
$$N = \frac{F}{\Delta t_{rel} n_{rel}} \tag{11}$$
3. Staged release of total material N_{tot} added over time.
$$N = \frac{N_{tot}}{\Delta t_{rel}} \tag{12}$$

Multiple releases can be specified and subsequently tracked. A status code on each particle flags its state, for example whether it has been released and is mobile, stuck to a boundary or has been removed. The particle location and statuses are output at user specified intervals.

3 Particle Processes

3.1 Biota

Processes currently included that affect biota are:

1. Mortality in response to age, temperature or salinity
2. Spawning to become a subsequent life stage
3. Diurnal vertical migration

Often, the weight property will represent number of organisms that each particle represents.

Mortality is modelled with a simple die-off rate:

$$\frac{dW}{dt} = -rW \tag{13}$$

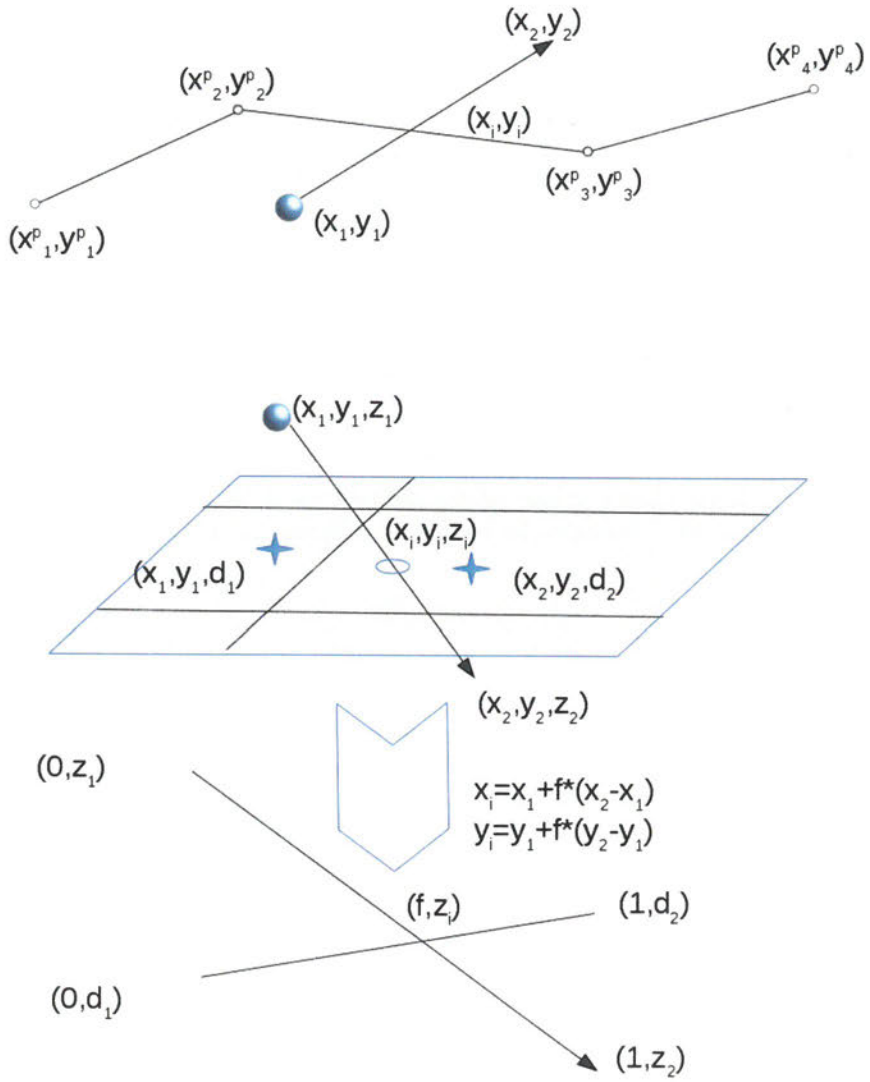

Figure 2: Illustration of boundary crossing tests for shoreline (top) and variable surface (bottom).

where r is the mortality rate. The mortality rate, can either be specified as a constant value or as a function of temperature and/or salinity:

$$r = \frac{T - T_L^{high} + T_{tol}}{T_{tol}} \in [0, 1] \tag{14}$$

$$r = \frac{T_L^{low} + T_{tol} - T}{T_{tol}} \in [0, 1] \tag{15}$$

where T_L is the lethal temperature and T_{tol} is a tolerance which describes the temperature range over which effects start to be felt. Exactly analogous equations exist for salinity. When the particle weight drops below a prescribed number, the particle is removed from the simulation.

Diurnal vertical migration is determined by:

$$w_p = w_m(t) \tag{16}$$

$$z \in [-z_{day}, -z_{night}] \tag{17}$$

where w_m is a vertical migration constant which is positive (up) after the sun sets, and negative down after sun rise.

Spawning occurs when biota either mature to their next life stage or release offspring. In the first case the relevant class of the biota simply changes. In the latter a new particle is created at the existing position, which its weight determined by a spawning ratio that describes the number of offspring the parent particle creates.

4 Tests

4.1 Comparison with GNOME

GNOME is the NOAA oil spill model (`http://response.restoration.noaa.gov/gnome`), which follows the same essential methodology as ERCore. GNOME simulates particle motion in a temporally and spatially variable horizontal field. To verify that ERCore and GNOME produce the same trajectories in the absence of turbulent diffusion, both models were run with a single particle in an identical two-dimensional flow field. The figure below shows that both models produce identical particle tracks in a complex flow field.

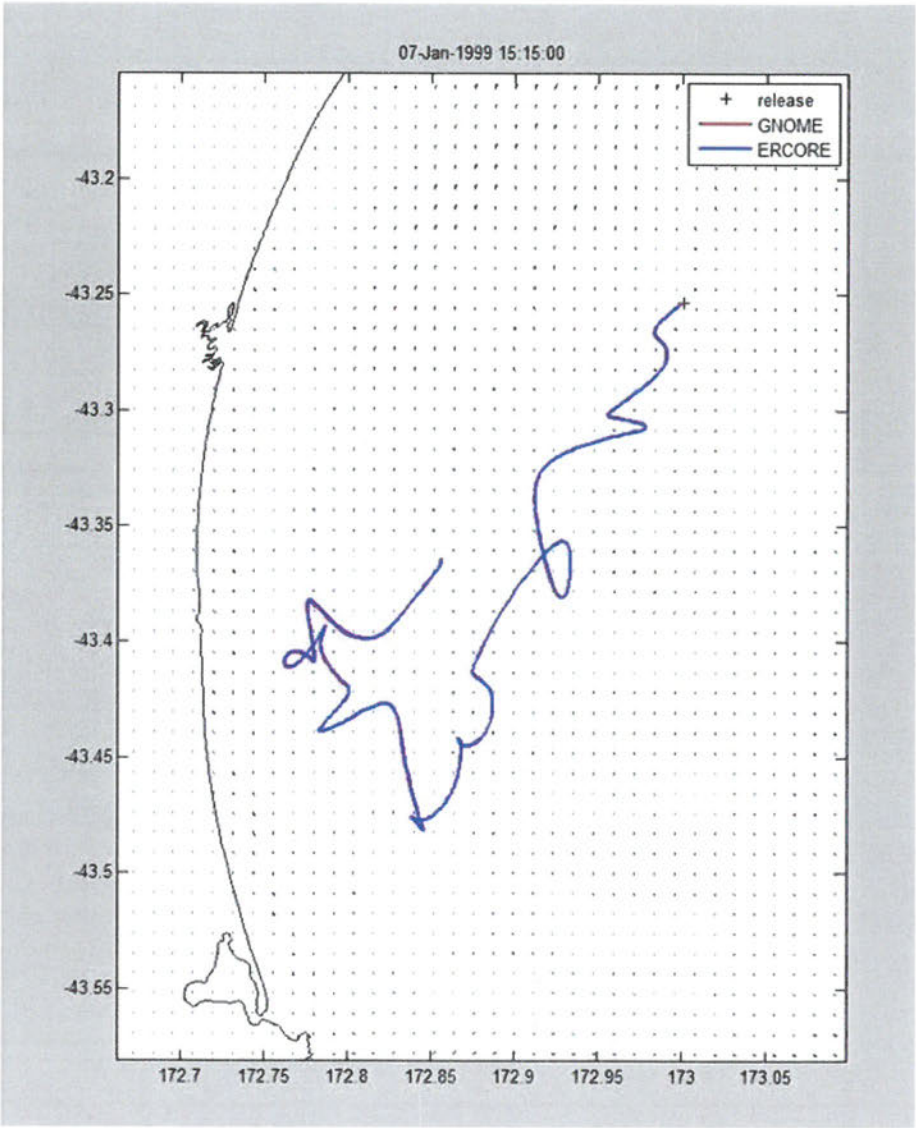

Figure 3: Single particle trajectories from GNOME and ERCore for an identical flow field in the absence of diffusion

Appendix 5. Additional CTD Maps.

Upper water column water property maps

The following figures A5.1 to A5.5 show water properties averaged over the upper 10 m of the water column based on CTD profiles made though areas of North Arm. For the first trip, these measurements were spread over 5 days. Despite this, most measured water properties show remarkably little variation across North Arm. Across North Arm upper water column temperatures varied by less than 0.25°C. Upper water column salinities varied by less than 0.1 units over most of North Arm, (Figure A5.2). There were slightly lower salinities in inlets to the north inlet and Albion Inlet, most likely due to river flows creating a thin fresher layer within these inlets. Figure A5.4 showed a 0.5 mg/l variation in oxygen concentrations across North Arm. Figure A5.5 showed upper water column turbidity was also near uniform across North Arm. Thus, oxygen and turbidity were consistent with generally near uniform temperature and salinity observed across the Arm.

Fluorescence in Figure A5.3 is also near uniform over the eastern part of North Arm, but shows significantly higher values within Bens Bay, indicating localized higher productivity. This high productivity was not seen within Bens Bay during the second trip, which showed low variation in fluorescence across all of North Arm (data for second trip not shown).

It should be noted again that the CTD measured water properties are only representative of the times they were made. Water properties may vary significant over the year, and may or may not be as uniform as indicated by most of the measured water properties.

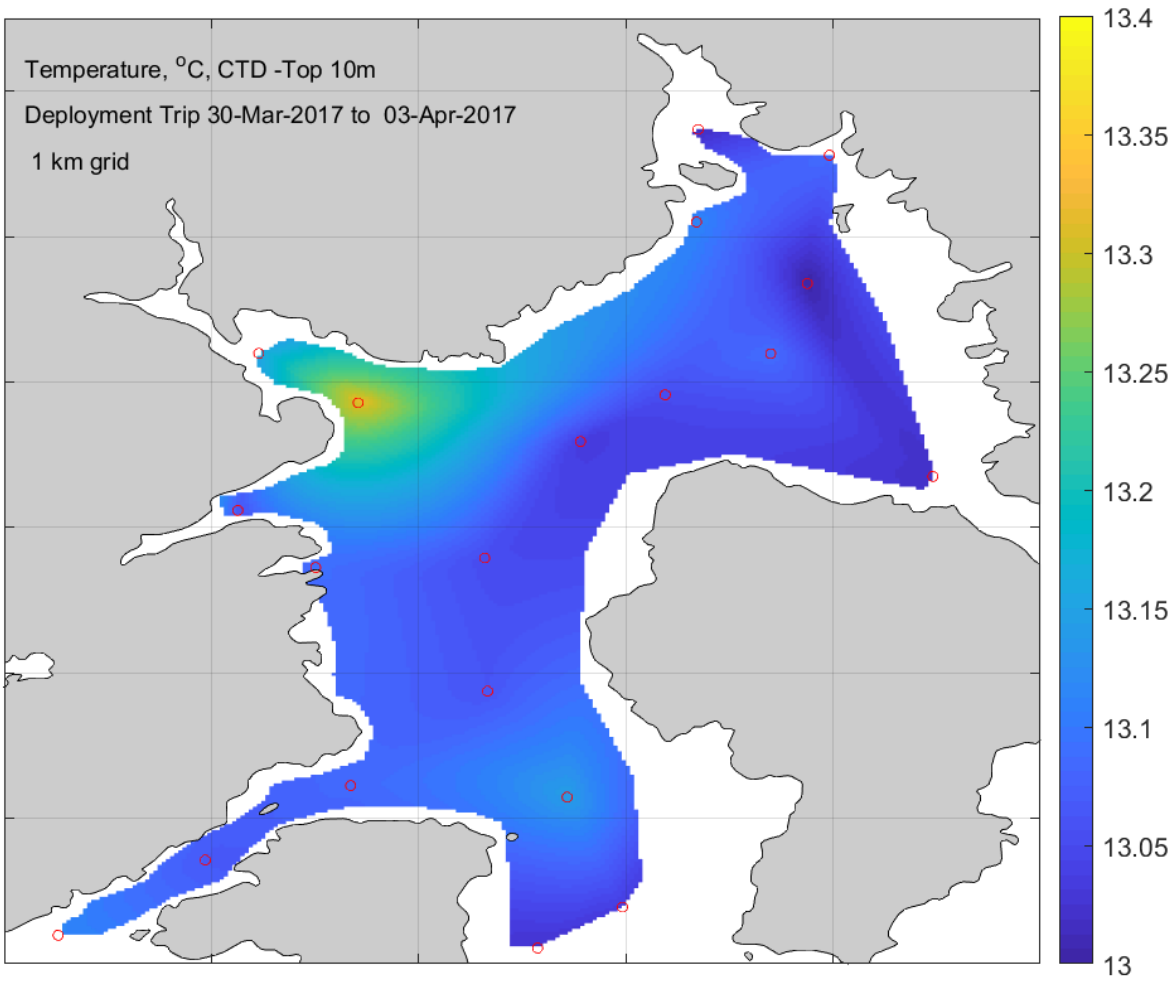

Figure A5.1. Water temperature averaged over top 10 m of North Arm Port Pegasus over the period 30 March to 3 April 2017. The location for the CTD profiles are given by red circles.

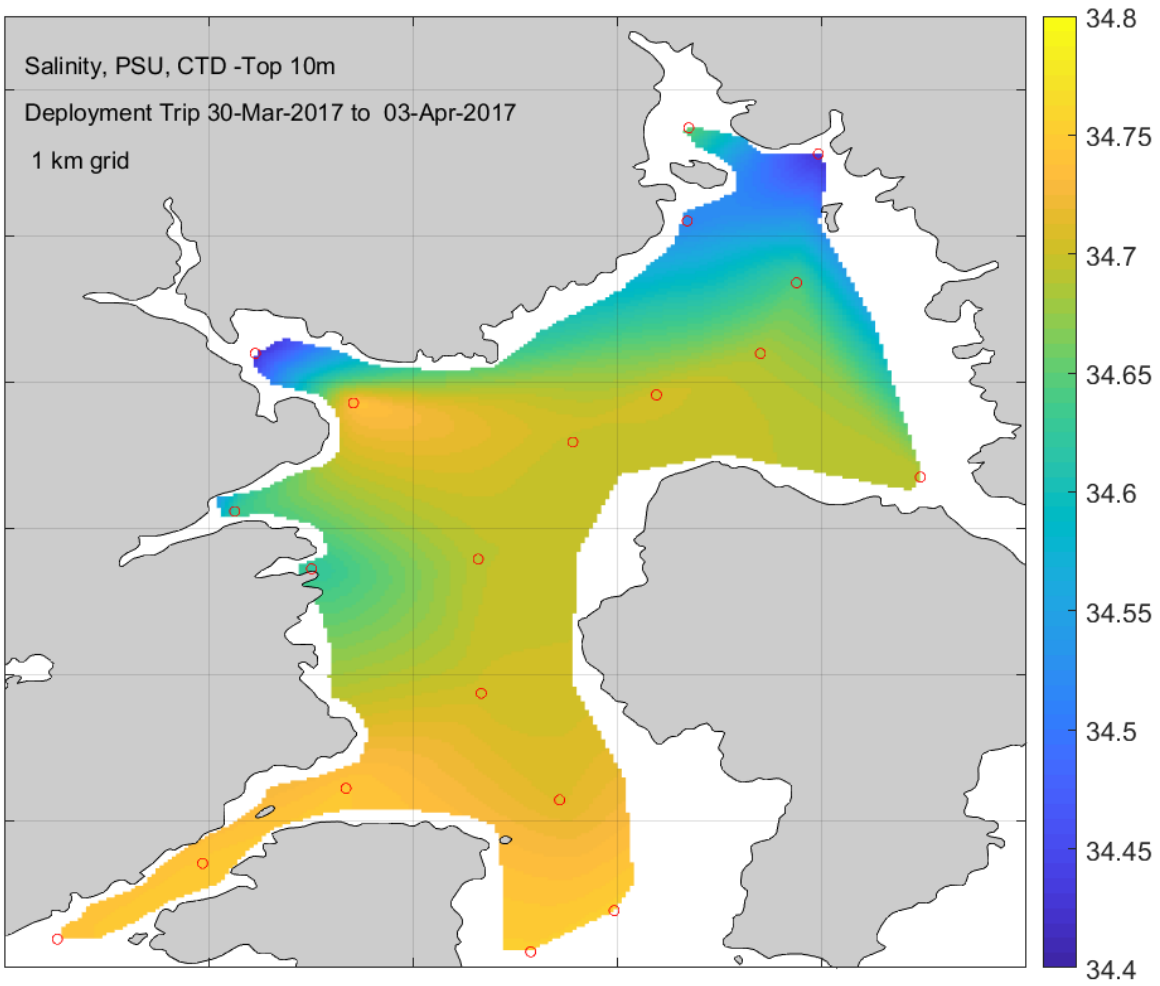

Figure A5.2. Salinity averaged over top 10 m of North Arm Port Pegasus over the period 30 March to 3 April 2017. The location for the CTD profiles are given by red circles.

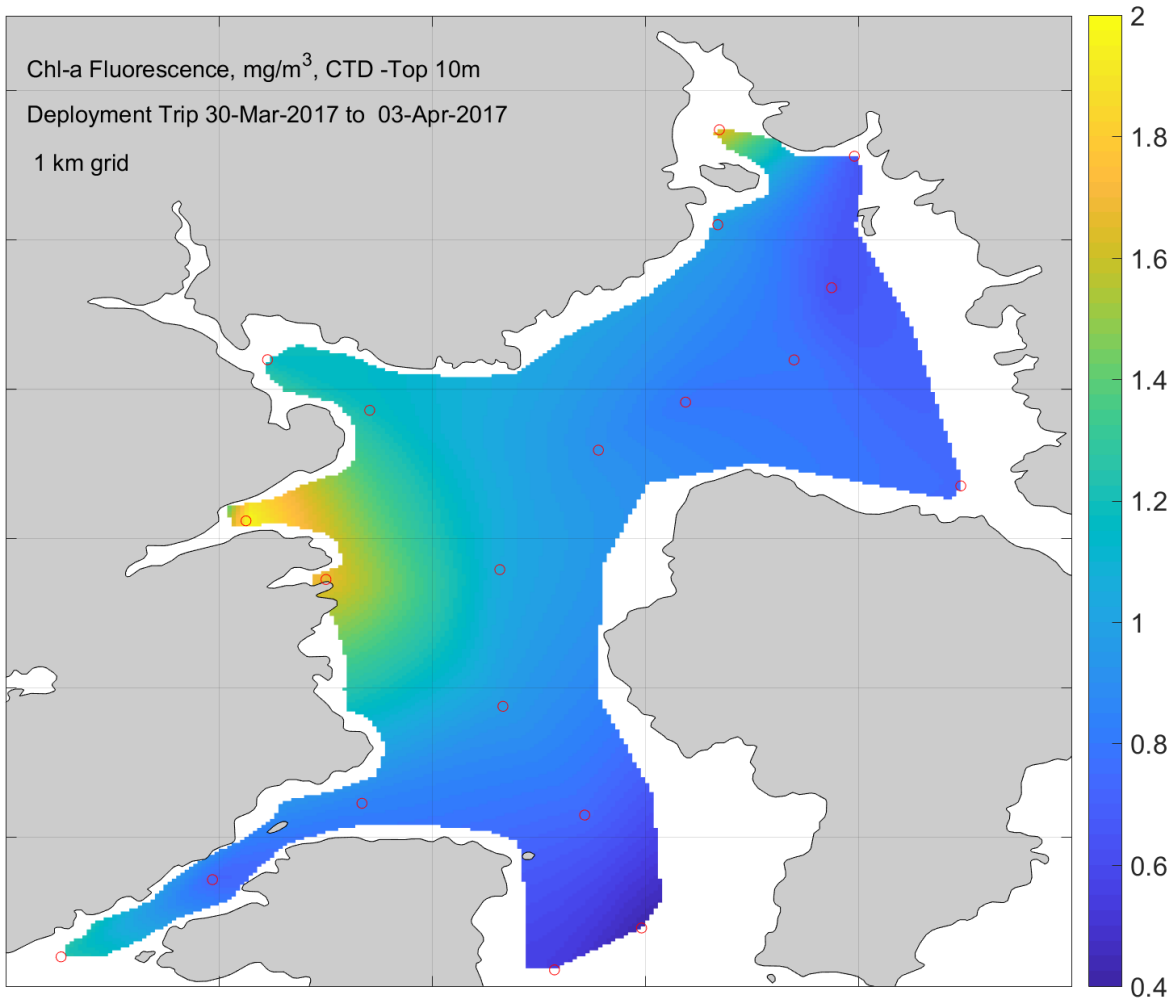

Figure A5.3. Chlorophyll-*a* fluorescence (mg/m^3) averaged over top 10 m of North Arm Port Pegasus over the period 30 March to 3 April 2017. The location for the CTD profiles are given by red circles.

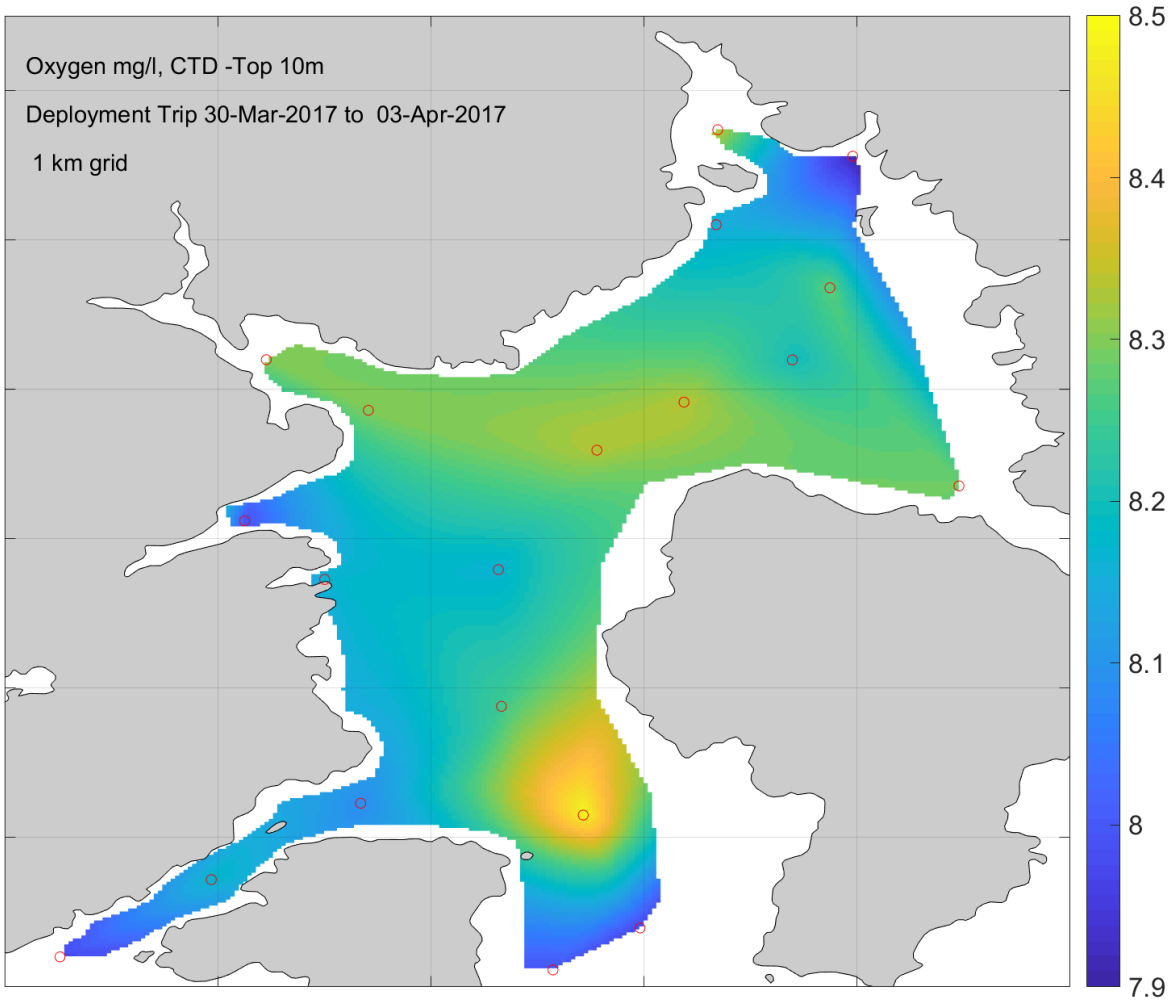

Figure A5.4. Dissolved Oxygen averaged over top 10 m of North Arm Port Pegasus over the period 30 March to 3 April 2017. The location for the CTD profiles are given by red circles.

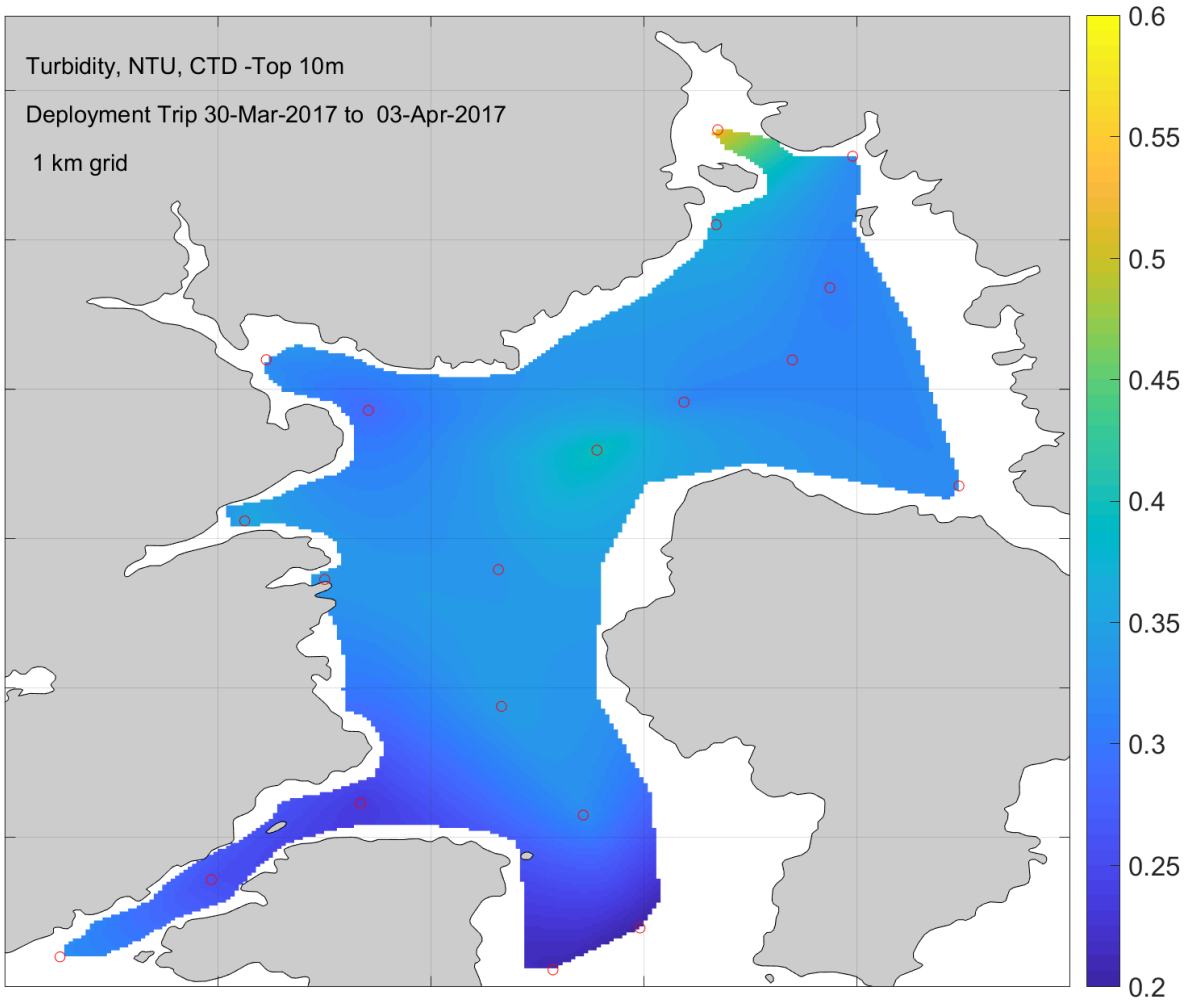

Figure A5.5. Turbidity averaged over top 10 m of North Arm Port Pegasus over the period 30 March to 3 April 2017. The location for the CTD profiles are given by red circles.

Appendix 6. Raw Laboratory Results.

Hill Laboratories
TRIED, TESTED AND TRUSTED

R J Hill Laboratories Limited
1 Clyde Street Hamilton 3216
Private Bag 3205
Hamilton 3240 New Zealand

T 0508 HILL LAB (44 555 22)
T +64 7 858 2000
E mail@hill-labs.co.nz
W www.hill-laboratories.com

ANALYSIS REPORT

Client:	Cawthron Institute (Nelson)	**Lab No:**	1759258	SPv1
Contact:	Ben Knight	**Date Received:**	15-Apr-2017	
	C/- Cawthron Institute (Nelson)	**Date Reported:**	12-May-2017	
	Private Bag 2	**Quote No:**	84458	
	Nelson Mail Centre	**Order No:**		
	Nelson 7042	**Client Reference:**	16528	
		Submitted By:	Ben Knight	

Sample Type: Saline

Sample Name:		North Peg - Station 1, 15m Surf integrated	North Peg - Station 1, Deep	North Peg - Station 2, 15m Surf integrated	North Peg - Station 2, Deep	North Peg - Station 3, 15m Surf integrated
Lab Number:		1759258.1	1759258.2	1759258.3	1759258.4	1759258.5
Total Suspended Solids*	g/m³	12	< 3	7	4	5
Total Nitrogen	g/m³	0.24	0.197 #1	0.26	0.162 #1	0.23
Total Dissolved Nitrogen	g/m³	0.22	0.22 #1	0.176	0.165 #1	0.181
Total Ammoniacal-N*	g/m³	< 0.010	< 0.010	< 0.010	< 0.010	< 0.010
Nitrite-N	g/m³	0.006	0.007	0.007	0.007	0.007
Nitrate-N	g/m³	0.039	0.075	0.051	0.062	0.050
Nitrate-N + Nitrite-N	g/m³	0.044	0.081	0.058	0.069	0.058
Dissolved Reactive Phosphorus*	g/m³	0.010	0.012	0.011	0.013	0.012
Total Phosphorus*	g/m³	0.012	0.017	0.018	0.018	0.017
Reactive Silica	g/m³ as SiO_2	< 0.10	< 0.10	0.16	< 0.10	0.15

Sample Name:		North Peg - Station 3, Deep	North Peg - Station 4, 15m Surf integrated	North Peg - Station 4, Deep	Station 5 (middle station), 0 m	Station 5 (middle station), 3 m
Lab Number:		1759258.6	1759258.7	1759258.8	1759258.9	1759258.10
Total Suspended Solids*	g/m³	4	4	< 3	4	< 3
Total Nitrogen	g/m³	0.194	0.21	0.174 #1	0.26	0.25
Total Dissolved Nitrogen	g/m³	0.177	0.171	0.189 #1	0.177	0.174
Total Ammoniacal-N*	g/m³	< 0.010	< 0.010	< 0.010	< 0.010	< 0.010
Nitrite-N	g/m³	0.008	0.007	0.008	0.007	0.007
Nitrate-N	g/m³	0.056	0.051	0.056	0.051	0.051
Nitrate-N + Nitrite-N	g/m³	0.064	0.058	0.064	0.058	0.058
Dissolved Reactive Phosphorus*	g/m³	0.014	0.014	0.016	0.014	0.014
Total Phosphorus*	g/m³	0.018	0.020	0.021	0.021	0.018
Reactive Silica	g/m³ as SiO_2	0.14	0.14	0.15	0.14	0.13

Sample Name:		Station 5 (middle station), 6 m	Station 5 (middle station), 9 m	Station 5 (middle station), 12 m	Station 5 (middle station), 15 m	Station 5 (middle station), 20 m
Lab Number:		1759258.11	1759258.12	1759258.13	1759258.14	1759258.15
Total Suspended Solids*	g/m³	4	3	4	3	4
Total Nitrogen	g/m³	0.23	0.22	0.22	0.185	0.29
Total Dissolved Nitrogen	g/m³	0.174	0.165	0.179	0.165	0.176
Total Ammoniacal-N*	g/m³	< 0.010	< 0.010	< 0.010	< 0.010	< 0.010
Nitrite-N	g/m³	0.007	0.007	0.008	0.008	0.007
Nitrate-N	g/m³	0.050	0.050	0.051	0.052	0.050
Nitrate-N + Nitrite-N	g/m³	0.057	0.057	0.059	0.059	0.058
Dissolved Reactive Phosphorus*	g/m³	0.014	0.014	0.010	0.014	0.014
Total Phosphorus*	g/m³	0.021	0.019	0.017	0.016	0.018
Reactive Silica	g/m³ as SiO_2	0.12	0.12	0.12	0.12	0.11

Sample Type: Saline						
Sample Name:		Station 5 (middle station), 25 m	Station 5 (middle station), 30 m	Station 5 (middle station), 35 m	Station 5 (middle station), 40 m	Station 5 (middle station), 45 m
Lab Number:		1759258.16	1759258.17	1759258.18	1759258.19	1759258.20
Total Suspended Solids*	g/m³	4	6	3	4	7
Total Nitrogen	g/m³	0.170	0.185	0.166	0.177 #1	0.183
Total Dissolved Nitrogen	g/m³	0.164	0.164	0.160	0.190 #1	0.156
Total Ammoniacal-N*	g/m³	< 0.010	< 0.010	< 0.010	< 0.010	< 0.010
Nitrite-N	g/m³	0.007	0.008	0.008	0.008	0.008
Nitrate-N	g/m³	0.051	0.054	0.055	0.055	0.055
Nitrate-N + Nitrite-N	g/m³	0.059	0.062	0.063	0.063	0.063
Dissolved Reactive Phosphorus*	g/m³	0.014	0.014	0.014	0.015	0.015
Total Phosphorus*	g/m³	0.019	0.017	0.016	0.018	0.018
Reactive Silica	g/m³ as SiO_2	0.10	0.13	0.12	0.11	0.11

Sample Name:		Bens Bay, Surf integrated	Bulling Bay, Surf integrated	Albion Inlet, Surf integrated	Twilight Bay, Surf integrated	Diprose Bay, Surf integrated
Lab Number:		1759258.21	1759258.22	1759258.23	1759258.24	1759258.25
Total Suspended Solids*	g/m³	18	5	< 3	< 3	< 3
Total Nitrogen	g/m³	0.21	0.23	0.166	0.22	0.176
Total Dissolved Nitrogen	g/m³	0.155	0.162	0.154	0.163	0.161
Total Ammoniacal-N*	g/m³	< 0.010	< 0.010	< 0.010	< 0.010	< 0.010
Nitrite-N	g/m³	0.007	0.007	0.006	0.007	0.007
Nitrate-N	g/m³	0.049	0.047	0.042	0.049	0.051
Nitrate-N + Nitrite-N	g/m³	0.055	0.054	0.048	0.056	0.059
Dissolved Reactive Phosphorus*	g/m³	0.014	0.013	0.011	0.014	0.013
Total Phosphorus*	g/m³	0.021	0.019	0.017	0.017	0.017
Reactive Silica	g/m³ as SiO_2	0.11	0.12	0.13	0.14	0.14

Sample Name:		Scout Bay, Surf integrated	South Peg - Station 1, Surf integrated	South Peg - Station 1, Deep	South Peg - Station 2, Surf integrated	South Peg - Station 2, Deep
Lab Number:		1759258.26	1759258.27	1759258.28	1759258.29	1759258.30
Total Suspended Solids*	g/m³	< 3	< 3	< 3	6	3
Total Nitrogen	g/m³	0.194	0.158	0.20	0.23	0.176 #1
Total Dissolved Nitrogen	g/m³	0.163	0.147	0.154	0.153	0.186 #1
Total Ammoniacal-N*	g/m³	< 0.010	< 0.010	< 0.010	< 0.010	< 0.010
Nitrite-N	g/m³	0.008	0.006	0.006	< 0.002	0.003
Nitrate-N	g/m³	0.052	0.046	0.047	0.006	0.023
Nitrate-N + Nitrite-N	g/m³	0.060	0.052	0.053	0.007	0.027
Dissolved Reactive Phosphorus*	g/m³	0.014	0.013	0.013	0.007	0.011
Total Phosphorus*	g/m³	0.019	0.016	0.017	0.015	0.016
Reactive Silica	g/m³ as SiO_2	0.15	0.11	< 0.10	< 0.10	0.14

Sample Name:		South Peg - Station 3, Surf integrated	South Peg - Station 3, Deep			
Lab Number:		1759258.31	1759258.32			
Total Suspended Solids*	g/m³	5	6	-	-	-
Total Nitrogen	g/m³	0.185 #1	0.185	-	-	-
Total Dissolved Nitrogen	g/m³	0.194 #1	0.150	-	-	-
Total Ammoniacal-N*	g/m³	< 0.010	0.025	-	-	-
Nitrite-N	g/m³	< 0.002	0.002	-	-	-
Nitrate-N	g/m³	0.009	0.015	-	-	-
Nitrate-N + Nitrite-N	g/m³	0.010	0.018	-	-	-
Dissolved Reactive Phosphorus*	g/m³	0.009	0.014	-	-	-
Total Phosphorus*	g/m³	0.017	0.024	-	-	-
Reactive Silica	g/m³ as SiO_2	< 0.10	0.11	-	-	-

Analyst's Comments

#1 It has been noted that the result for Total Dissolved Nitrogen was greater than that for Total Nitrogen, but within the analytical variation of these methods.

SUMMARY OF METHODS

The following table(s) gives a brief description of the methods used to conduct the analyses for this job. The detection limits given below are those attainable in a relatively clean matrix. Detection limits may be higher for individual samples should insufficient sample be available, or if the matrix requires that dilutions be performed during analysis.

Sample Type: Saline

Test	Method Description	Default Detection Limit	Sample No
Total Nitrogen Digestion	Caustic persulphate digestion. APHA 4500-N C 22nd ed. 2012.	-	1-32
Total Dissolved Nitrogen Digestion*	Filtered sample, caustic persulphate digestion. APHA 4500-N C 22nd ed. 2012.	-	1-32
Total Phosphorus Digestion*	Acid persulphate digestion.	-	1-32
Total Suspended Solids*	Saline sample. Filtration using Whatman 934 AH, Advantec GC-50 or equivalent filters (nominal pore size 1.2 - 1.5µm), gravimetric determination. Analysed at Hill Laboratories - Chemistry; 101c Waterloo Road, Christchurch. APHA 2540 D 22nd ed. 2012.	3 g/m^3	1-32
Total Nitrogen	Alkaline persulphate digestion, automated Cd reduction/sulphanilamide colorimetry. APHA 4500-N C & 4500-$NO3^-$ I 22nd ed. 2012 (modified).	0.010 g/m^3	1-32
Total Dissolved Nitrogen	Filtered sample. Alkaline persulphate digestion, automated Cd reduction/sulphanilamide colorimetry. APHA 4500-N C & 4500-NO3- I 22nd ed. 2012 (modified).	0.010 g/m^3	1-32
Total Ammoniacal-N*	Saline, filtered sample. Phenol/hypochlorite colorimetry. Discrete Analyser. (NH_4-N = NH_4+-N + NH_3-N). APHA 4500-NH_3 F (modified from manual analysis) 22nd ed. 2012.	0.010 g/m^3	1-32
Nitrite-N	Saline sample. Automated Azo dye colorimetry, Flow injection analyser. APHA 4500-NO_3^- I 22nd ed. 2012 (modified).	0.002 g/m^3	1-32
Nitrate-N	Calculation: (Nitrate-N + Nitrite-N) - NO2N. In-House.	0.0010 g/m^3	1-32
Nitrate-N + Nitrite-N	Saline sample. Total oxidised nitrogen. Automated cadmium reduction, Flow injection analyser. APHA 4500-NO_3^- I 22nd ed. 2012 (modified).	0.002 g/m^3	1-32
Dissolved Reactive Phosphorus*	Filtered sample. Molybdenum blue colorimetry. Discrete Analyser. APHA 4500-P E (modified from manual analysis) 22nd ed. 2012.	0.004 g/m^3	1-32
Total Phosphorus*	Total phosphorus digestion, ascorbic acid colorimetry. Discrete Analyser. APHA 4500-P B & E (modified from manual analysis) 22nd ed. 2012. Also modified to include the use of a reductant to eliminate interference from arsenic present in the sample. NWASCA, Water & soil Miscellaneous Publication No. 38, 1982.	0.004 g/m^3	1-32
Reactive Silica	Filtered sample. Heteropoly blue colorimetry. Discrete analyser. APHA 4500-SiO_2 F (modified from flow injection analysis) 22nd ed. 2012.	0.10 g/m^3 as SiO_2	1-32

These samples were collected by yourselves (or your agent) and analysed as received at the laboratory.

Samples are held at the laboratory after reporting for a length of time depending on the preservation used and the stability of the analytes being tested. Once the storage period is completed the samples are discarded unless otherwise advised by the client.

Carole Rodgers-Carroll BA, NZCS
Client Services Manager - Environmental